UAB
Universitat Autònoma de Barcelona

RGD-Targeted Nanoliposomes and Extracellular Vesicles for Enhanced Enzyme Replacement Therapy in Fabry Disease

Marc Miquel Moltó Abad

RGD-Targeted Nanoliposomes and Extracellular Vesicles for Enhanced Enzyme Replacement Therapy in Fabry Disease

PhD Thesis presented by

Marc Miquel Moltó Abad

To obtain the degree of

PhD for the Universitat Autònoma de Barcelona (UAB)

PhD thesis carried out in the Clinical Biochemistry, Drug Delivery & Therapy (CB-DDT) Group, at Vall d'Hebron Research Institute (VHIR)

PhD program of Biochemistry, Molecular Biology and Biomedicine of Universitat Autònoma de Barcelona (UAB), April 24th 2025

Director and Tutor:

Dr. Ibane Abasolo Olaortua

PhD candidate:

Marc Miquel Moltó Abad

Acknowledgements

Després d'aquesta llarga aventura, és hora d'aturar-se un moment, respirar i mirar enrere per reflexionar sobre fins on hem estat capaços d'arribar. Només d'aquesta manera podem valorar el que hem aconseguit, saber realment del que som capaços i entendre que aquest camí recorregut no és fruit d'un sol esforç, sinó d'un procés col·lectiu. Cal parar i mirar enrere per agrair a totes aquelles persones que m'han acompanyat durant aquesta aventura, perquè, sense elles, no hauria estat possible arribar al capítol final d'aquesta etapa anomenada "tesi". Ara és el moment d'escriure una de les seccions més importants d'aquesta tesi: els agraïments.

Primer de tot, m'agradaria donar les gràcies a la meva directora de tesi, la Dra. **Ibane Abasolo** per la seva guia, paciència i constant recolzament durant tot aquest període. Ibane, muchas gracias por la oportunidad de hacer el doctorado y por tu acogida desde el primer día. Ha sido un verdadero honor ser tu estudiante de doctorado, y gracias por contar conmigo siempre y por ayudarme a crecer tanto como científico como persona. Gracias también por esos momentos con cerveza en mano, en los que pudimos hablar de todo y desconectar cuando más lo necesitaba. Eskerrik asko.

Vull expressar també el meu agraïment a una persona que ha estat el meu mentor des de l'inici del meu camí en el món de les malalties lisosomals, el Dr. **Guillem Pintos**. Guillem, moltíssimes gràcies per tots els teus consells i per haver apostat per mi en el seu dia, quan el meu futur era incert. He gaudit molt de les cerveses i les discussions científiques que hem compartit durant tots els congressos en què hem coincidit. La teva visió i expertesa clínica sobre la malaltia de Fabry, així com altres malalties lisosomals, m'han ajudat a entendre les necessitats reals dels pacients afectats per aquestes malalties i a orientar la investigació de la meva tesi.

Agrair també al grup de *Clinical Biochemistry, Drug Delivery & Therapy* (CB-DDT) del VHIR, on he realitzat la meva formació com a doctorand, per la seva acollida, afecte i estima que m'han demostrat al llarg de tots aquests anys. Hauria d'escriure una altre tesi sencera només per agrair-vos tot el que heu fet per mi durant tots aquests anys. Vull agrair al Dr. **Simo Schwartz** i a la Dra. **Roser Ferrer** la confiança depositada en mi un cop finalitzada la meva beca de doctorat. Simo i Roser, moltíssimes gràcies pel vostre recolzament i per comptar amb mi, així com per haver-me donat l'oportunitat de continuar en el grup malgrat haver finalitzat la meva beca pre-doctoral. Heu sabut veure en mi la persona que realment soc.

Gràcies també al personal tècnic del grup com **Laura**, **Sandra**, **Belén** i **Àngels** per ajudar-me i animar-me en moments difícils, tant personals com relacionats amb la tesi, i per les vostres bromes que feien més passables els dies dolents. Heu estat sempre tant en els bons com en els mals moments, donant-me un cop de mà, recolzant-me i tranquil·litzant-me. També heu hagut d'aguantar moltes de les meves bromes, que sé que no es fàcil.

Laura, gràcies per ajudar-me en les nostres lluites contra l'agregòmetre, per ensenyar-me a treballar correctament en un laboratori i per defensar-me sempre (malgrat que jo no tingués la raó) en les divertides discussions que teníem en els moments per fer cafè amb la resta del personal del grup. Sempre has estat com un oracle per mi quan tenia algun dubte sobre on estava el material de laboratori que necessitava o com treballar d'una manera correcte i de qualitat.

Sandra, gracias por marcar siempre los sagrados tiempos del desayuno y por ser la dueña y señora de la radio, trayendo la música en nuestro ambiente laboral (siempre con Cadena 100 y sin mucho margen para cambiar de emisora). Aunque siempre nos estábamos picando, siempre nos hemos demostrado ese aprecio mutuo. Todo lo que sé sobre cultivos te lo debo a ti.

Belén, la nostra estimada técnica *in vivo*, gràcies per aguantar totes les meves bromes i per tots els moments que hem viscut a l'estabulari. Sempre m'has ajudat a preparar tot el material necessari per als experiments *in vivo.* Gràcies per la companyia i per fer més amenes les nostres estones amb els ratolins, i per ajudar-me quan més ho necessitava.

Àngels, gràcies per ser de les úniques persones que s'ha rigut amb les meves bromes dolentes i per ser sempre la persona més alegre del laboratori. Durant l'últim *sprint* de la tesi, m'has ajudat a tirar endavant i no m'has deixat caure mai. Sempre tenies les paraules adequades per a cada moment.

Gràcies també al personal postdoctoral del grup com **Vanessa**, **Diana**, **Fernanda** i **Quim** per la seva predisposició a ajudar i aguantar-me durant tot aquest temps. Gràcies també per tot el vostre suport durant els últims dies de redacció de tesi, quan jo dubtava de tot i vosaltres m'animàveu amb el vostre optimisme.

Vane, has sido un gran apoyo para mí durante todo este tiempo, y sé que estas líneas de agradecimiento se quedarán cortas, pero intentaré expresarlo lo mejor que pueda. Gracias por ayudarme durante todo este tiempo con tu criterio y tu gran capacidad organizativa en los experimentos, tanto *in vitro* como *in vivo*. Has sido, y serás siempre, un referente para mí, tanto a nivel personal como científico. Todo lo que he aprendido en el estabulario de experimentos *in vivo*, te lo debo a ti y a **Ana Boullosa.** Me habéis convertido en una máquina de la administración intravenosa. También me has visto en mis mejores y peores momentos de la tesis, y siempre has estado ahí para levantarme cuando mis ánimos estaban por los suelos. Con tu apoyo y ayuda constante, he podido sacar adelante esta tesis.

Diana, has sido como una hermana mayor para mí durante todo este tiempo. Día a día me has recordado lo que valía y de lo que era capaz. Al igual que Vanessa, me has acompañado en los momentos más difíciles de esta tesis, y siempre has estado ahí para levantarme y ayudarme a seguir adelante en este camino tan duro. Gracias por todos tus consejos y por todo tu apoyo durante este tiempo. Has sido una fuente de inspiración y toda una referente para mí. Estos últimos días de redacción han sido frenéticos, pero con tu ayuda he conseguido llegar a la meta.

Fernanda, al igual que Vanessa y Diana, habéis sido los tres pilares que me han mantenido a flote durante estos últimos días. Mil gracias por compartir tu sabiduría conmigo y ayudarme con la tesis. Gracias a ti aprendí a usar el DLS por primera vez, y desde entonces, siempre me has dado muy buenos consejos para seguir con mis experimentos. Gracias por ser mi ChatGPT cuando me bloqueaba. También quiero agradecerte todo tu apoyo durante la recta final de la tesis. Estuviste ahí justo cuando más lo necesitaba.

Quim, moltes gràcies per tota la teva ajuda i el teu suport durant la tesi. Tot el que he après relacionat amb les EVs durant aquest temps ha estat gràcies a tu. Encara recordo quan vaig aïllar les meves primeres EVs per precipitació amb tu. Des de llavors, em vas ensenyar a fer-ho per TFF i també a fer les meves primeres SEC. Gràcies pels teus consells per sobreviure a l'aïllament d'EVs més gran que s'ha fet mai al nostre laboratori, partint de 3 L de sobrenedant. Per tot plegat, l'apartat d'aquesta tesi relacionat amb les EVs és gràcies a tu.

Vull agrair també a la comunitat pre-doc del nostre grup com **Veronica, Júlia, Vincenzo, Maria i Diego** per la seva ajuda tant durant els experiments com per suportar-me i consolar-me en els moments de dificultat. Hem viscut molt plegats i les dificultats ens han unit més que mai.

Vero, has estat la última estudiant de doctorat en unir-te a les nostres files. Hem compartit directora de tesi i, des del primer moment que vas arribar, hem tingut molt bona relació i ens hem recolzat mútuament en tot. Em vas ajudar moltíssim durant l'últim *sprint* experimental abans de posar-me a redactar la tesi. Saps que això no ho oblidaré mai i que t'ho agrairé sempre. Ets una persona que sempre ens ha alegrat els dinars amb les teves preguntes particulars i que sempre generava algun que altre debat. Et desitjo tot el millor durant la teva tesi.

Júlia, la paraula "gràcies" també es queda curta amb tu. T'estic molt agraït per tots aquests anys que hem coincidit al laboratori. Recordo quan vaig fer el meu primer WB al laboratori de Mediterrània i com vam riure en veure que, malgrat totes les dificultats, el meu primer WB va ser tot un èxit. Gràcies pel teu constant recolzament durant els últims dies d'escriptura de la tesi, i gràcies per ajudar a desfogar-me quan més ho necessitava amb els teus "com estàs?". Ets un referent com a pre-doc per a mi, no ho oblidis mai. Confia en tu i molta sort amb el que et queda de tesi.

Vince, nuestro querido pre-doc italiano. Muchísimas gracias también por todo tu apoyo y tu ayuda durante los últimos días de tesis. Te volcaste, como todos los demás, en no dejarme caer y en ayudarme a llegar a la meta…mil gracias por ello. Ahora te toca a ti demostrar de lo que eres capaz, que es muchísimo, y sacar una tesis que nos deje a todos con la boca abierta. Mucha suerte y adelante con tu tesis.

Maria, gràcies pel teu suport i per portar sempre l'optimisme i els riures durant els llargs aïllaments d'EVs. Gràcies també per enriquir el nostre vocabulari amb paraules i expressions que només tu sabies introduir. Expressions com "es molt serio", "heavy metal", "flipo" porten la teva firma personal i sempre ressonaran als nostres caps. Et desitjo molta sort en la teva tesi.

Diego, amb tu vaig viure els primers congressos d'EVs, però ens quedem amb el primer, aquell organitzat pel GEIVEX a Santiago de Compostela, on vam compartir pòster i vam fer els nostres primers contactes en aquest món de les EVs. Moltes gràcies per tots aquest moments que hem viscut plegats i per tota la teva ajuda durant aquest llarg camí. Ara et toca a tu començar a recórrer l'etapa final de la tesi. Molts ànims.

També vull aprofitar per agrair a algunes persones que han passat pel nostre grup deixant una empremta molt important en la meva trajectòria com a pre-doc: **Monserrat, Gertruda, Paula i Natalia**.

Monse, muchísimas gracias por todo lo que me has enseñado durante tu estancia con nosotros, tanto en lo personal como en lo científico. Me guiaste mucho durante mis inicios en la investigación de la *protein corona* con los nanoliposomas y me insististe en que tenía las herramientas necesarias para avanzar y que no dudara en usarlas. Siempre me diste muy buenos consejos para continuar mi investigación cuando me sentía bloqueado. Hemos compartido muchísimos momentos juntos en el estabulario, en el laboratorio, en restaurantes…e incluso en México, donde fundamos nuestro increíble "equipo México". Te admiro mucho y eres un referente para mí, tanto como científica como persona. Gracias por todo tu apoyo.

Gertru, muchas gracias por toda tu ayuda y apoyo durante esta última etapa de mi tesis. Hemos sufrido juntos los ELISAs y las actividades enzimáticas, pero siempre nos animábamos con

nuestros chistes malos y encontrábamos la forma de sacar todo adelante. Te deseo lo mejor en tu nueva etapa en el IQAC y que sigas golpeando las placas de ELISA con la misma fuerza que en el VHIR durante los lavados.

Paula, muchas gracias por todo lo que me enseñaste durante el tiempo que estuviste en nuestro grupo. Aprendí mucho de ti. Gracias por todos tus consejos, por tu ayuda en el estabulario, por escucharme cuando te hablaba de mis experimentos y por animarme cuando me sentía frustrado.

Nat, contigo empezó todo. Me enseñaste desde el primer día que llegué al grupo. Gracias a ti aprendí todos los experimentos que he realizado a lo largo de mi tesis. Todo lo que sé sobre la homogenización de tejidos, actividades enzimáticas, ensayos de eficacia *in vitro* y de internalización celular, te lo debo a ti. Gracias por todo y por tu paciencia.

Vull donar també les gràcies als diferents estudiants de màster i de grau, com **Narine, Dani i Giovanni**, que han passat pel nostre grup i han participat en el meu projecte de tesi. Narine, gràcies per encomanar-nos la teva motivació per investigar la malaltia de Fabry i per compartir els teus coneixements bioinformàtics amb nosaltres. Sempre tenies alguna cosa nova per ensenyar-nos.

Dani, el señor de los WB y el primero en poner a prueba los ELISAs para detectar la GLA. Probablemente la palabra "gracias" se queda corta contigo. Gracias por implicarte desde el primer día en el proyecto de investigación de mi tesis. Aún me saca una sonrisa recordar el día en que hicimos tu primer WB...lo empezamos a las 18:00 de la tarde, y no hace falta decir nada más para saber a qué hora acabamos. Desde ese día aprendiste que los WB se deben empezar bastante temprano. Gracias también por tus chistes malos y por formar, junto **Nil**, un tándem imparable. Siempre nos sacabas una sonrisa incluso en los peores días. Estoy muy orgulloso del científico en el que te has convertido y te deseo todo lo mejor.

Gio, llegaste a la vez que Dani y, desde el principio, ambos os implicasteis al máximo con las enfermedades lisosomales. Aprendimos juntos a usar la TFF y a aislar las EVs, y nos enfrentamos codo a codo al ExoID. Este mundo de las EVs nos ha traído buenos y malos momentos, pero juntos los hemos superado, siempre con la ayuda de un buen Aperol. Muchas gracias por tu implicación, apoyo y ayuda durante todo este tiempo. Te deseo lo mejor y mucha suerte.

Vull agrair també a la Prof. **Nora Ventosa** i al seu gran equip de l'ICMAB-CSIC, així com al grup de NANOMOL, per la síntesi dels nanoliposomes utilitzats en aquesta tesi. **Judit, Elisabet i Nora**, moltes gràcies per tot l'esforç que heu invertit. Gràcies a vosaltres, aquesta tesi es una realitat.

També vull tenir unes paraules d'agraïment per al Dr. **José Luis Corchero**. Pepe, muchas gracias por toda tu ayuda durante todo este tiempo. Gracias por tus transfecciones a gran escala, que han permitido obtener grandes cantidades de sobrenadantes para aislar las EVs. Gracias también por apoyarnos en nuestras locuras de generar ni más ni menos que 3 L de sobrenadante para que pudiéramos aislar una cantidad suficiente de EVs para nuestros experimentos. Gran parte de esta tesis también te la debo a ti.

Vull agrair també al Dr. **Francesc Canals** i al seu grup de proteòmica del VHIO per tota la seva ajuda i l'esforç invertit en els estudis proteòmics de caracterització de la protein corona. Francesc, moltes gràcies per tots els teus consells i tota la teva ajuda amb els estudis proteòmics realitzats en aquesta tesi. Gràcies per ajudar-me a entendre millor aquest complex món de la

proteòmica. La caracterització de la protein corona en els sistemes nanoliposomals utilitzats en aquesta tesi no hauria estat possible sense la vostre ajuda.

També m'agradaria agrair als serveis del VHIR, com la **Unitat d'Alta Tecnologia (UAT)** i els seus tècnics, per ensenyar-me a fer servir el citòmetre i el microscopi confocal; i al **personal d'estabulari del VHIO,** per fer-nos la vida més fàcil ajudant-nos a mantenir la nostre colònia de ratolins Fabry. També vull agrair al **Servei de Microscòpia i Difracció de Raigs X** de la UAB, especialment a en **Martí**, per ajudar-me a utilitzar el TEM i el Cryo-TEM.

Vull transmetre també el meu agraïment al Departament de Salut de la Generalitat de Catalunya per fer-me beneficiari de l'ajut provinent del Pla estratègic de recerca i innovació en salut (PERIS), concretament la subvenció per a la contractació de personal predoctoral (PIF-Salut) (ref. SLT01720000181), que m'ha permès rebre el suport necessari per realitzar la meva tesi doctoral en el grup de *Clinical Biochemistry, Drug Delivery & Therapy* (CB-DDT) del VHIR.

También quiero agradecer al Centro de Investigación Biomédica en Red de Bioingeniería, Biomateriales y Nanomedicina (CIBER-BBN) por otorgarme una beca de movilidad (ref. CB06/01/0012), que me ha permitido realizar una estancia formativa de un mes en el grupo de investigación *Molecular Treatments for Cardiac Fibrosis (FIBROHEART)* del Instituto de Biomedicina y Biotecnología de Cantabria (IBBTEC), liderado por la Dra. **Ana Victoria Villar Ramos.** Me gustaría expresar mi agradecimiento por su acogida durante mi estancia y por la confianza depositada en mí durante dicho período. También quiero aprovechar esta oportunidad para agradecer a los investigadores predoctorales de su grupo, **Jorge y Helena**, quienes me acogieron e integraron en el grupo desde mi primer día y me enseñaron a usar por primera vez el método BF + SEC para aislar EVs.

Asimismo, también quiero agradecer a los servicios de ICTS "NANBIOSIS" del CIBER-BBN, como la U20 (Functional Validation & Preclinical Research), donde pude realizar los experimentos *in vivo* que figuran en mi tesis, y la U6 (Biomaterial Processing and Nanostructuring Unit) por su ayuda en la caracterización de las EVs mediante NTA.

Vull expressar un agraïment especial al personal de la Unitat de Malalties Minoritàries de l'Hospital de la Vall d'Hebron, amb qui vaig tenir el privilegi de treballar abans de començar el doctorat i amb qui he continuat mantenint una relació d'amistat després de tots aquests anys. **Mireia, Maria, David i Ariadna,** moltes gràcies per haver-me recolzat durant tota aquesta tesi i per haver-me aportat la vostre visió clínica, que m'ha permès conèixer les necessitats reals dels pacients amb malalties lisosomals. Gràcies també pels moments que hem compartit en congressos i reunions clíniques, i per compartir els vostres coneixements i la vostra expertesa clínica amb mi.

També vull agrair als **meus amics i amigues** tot el seu recolzament durant aquests anys, especialment al grup de tota la vida, el qual anomenem **"Concilio"**. Moltes gràcies pels vostres consells, per la vostre ajuda quan més ho necessitava, per la vostre paciència i per recordar-me dia a dia el que era capaç de fer. Heu estat, sens dubte, un dels meus principals pilars durant aquesta tesi. Heu estat a l'alçada de tot i en tot moment. Aquesta tesi també es vostre.

Per últim, però no menys important, m'agradaria dedicar aquesta tesi a la **meva família**, a la meva parella **Cristina i a la seva família**. Sense tots ells no hauria arribat fins on soc ara. Han estat el meu pilar més important durant tot aquest temps. M'han ajudat a no enfonsar-me en els moments més difícils, m'han ensenyat a no rendir-me i a lluitar per allò que vull. Sense vosaltres, no estaria escrivint aquest text.

Pare, mare, ho hem aconseguit. Hem arribat plegats al lloc que creiem impossible i hem sobreviscut en el procés. Gràcies per tot el que heu fet per mi, pels vostres valors, pel vostre suport i per fer-me la persona que soc ara. Papa, tenies raó. Sabies que ho aconseguiríem fins i tot quan jo dubtava de tot. M'has ensenyat a lluitar i a no abaixar mai els braços...i aquí estic, escrivint els agraïments d'una tesi que creia impossible. Moltes gràcies per tot. Mama, sempre ho he dit i ho seguiré dient: no hi ha persona més lluitadora que tu en el món. Ets el meu referent com a persona perseverant i lluitadora. M'has ensenyat a no rendir-me, a no donar un pas enrere ni per agafar embranzida, a sempre anar de cara i ser valent. Sempre em deies que si tu no et rendies, jo no em podia rendir. Moltes gràcies, perquè tots els teus consells m'han ajudat a arribar fins aquí.

Cris, has vivido esta tesis igual o más que yo. Hemos sufrido mucho y sin tu apoyo, esta tesis no sería una realidad. Has estado cada día a mi lado, recordándome que podía con esto y más, levantándome cuando caía, haciéndome descansar cuando más lo necesitaba y soportándome en mis peores días. Siempre con la misma sonrisa, siempre con la misma buena actitud. Gracias por ser el faro que me iluminaba el camino cuando me perdía y por darme fuerzas para seguir peleando por este sueño llamado tesis. Lo hemos conseguido, hemos ganado.

Gracias a todas estas personas por haber hecho posible cumplir uno de mis sueños: realizar una tesis doctoral.

Abbreviations

#

4-MU	4-methylumbelliferone
4-MUG	4-methylumbelliferyl α-D-galactopyranoside
6-His	Hexa histidine-tag

A

AAV	Adeno-associated virus
AcOH	Acetic acid
ADAs	Anti-drug antibodies
AFC	Automatic Fraction Collector
AGAL A	Agalsidase alfa
AGC	Auto gain control
Ahsg	Alpha-2-HS-glycoprotein
Alb	Albumin
ALG	Apoptosis-Linked Gene-2
ALIX	ALG-2-interacting protein X
AM	Alpha mannosidosis
AP2	Adaptor protein 2
Apo-A1	Apolipoprotein A1
Apoa4	Apolipoprotein A4

ApoB	Apolipoprotein B
Apoc1	Apolipoprotein C1
Apoc3	Apolipoprotein C3
Apoe	Apolipoprotein E
ARSA	Sertoli lysosomal arylsulfatase A
ASM	Acid sphingomyelinase
ASMD	Acid sphingomyelinase deficiency

B

B9	Folic acid
BACE	β-Site Amyloid Precursor Protein Cleaving Enzyme
BBB	Blood brain barrier
BD	Biodistribution
BF	Benchtop filtration
BMM	Bone marrow-derived macrophages
BMP	Bis (monoacylgly cerol) phosphate

C

CARPA	Complement activation-related pseudoallergy
c(RGDfk)	Cyclo(L-arginylglycyl-L-alpha-aspartyl-D-phenylalanyl-L-lysyl)
c(RGDyK)	Cyclic arginine-glycine-aspartic acid-D-tyrosine-lysine peptide
C1qp	Complement component 1, q subcomponent, P chain

C1ra	Complement component 1, r subcomponent A
C1s2	Complement component 1, s subcomponent 2
C1sa	Complement factor subcomponent A
C3	Complement factor 3
C4bpa	Complement component 4b - binding protein alpha
C5	Complement factor 5
C57BL6	Spherical colony that was isolated from a mouseembryo
C7	Complement factor 7
C8a	Complement factor 8 alpha
C8b	Complement factor 8 beta
C8g	Complement factor 8 gamma
C9	Cluster of Differentiation 9
CD300	Cluster of Differentiation 300
CD47	Cluster of Differentiation 47
CD63	Tetraspanin and extracellular vesicle marker
CD63	Tetraspanin and extracellular vesicle marker
CD81	Cluster of Differentiation 81
CD9	Tetraspanin-29 an extracellular vesicle marker
Ces1c	Carboxylesterase 1C
CF	Concentration Factor
Cfd	Complement factor D

Cfhr1	Complement factor H-Related Protein 1
Cfhr4	Complement factor H-Related Protein 4
Cfi	Complement factor I
Chd1	Chromodomain Helicase DNA Binding Protein 1
CHO DG44	Chinese Ovary Hamster modificate
CHO	Chinese Ovary Hamster
CHOL	Cholesterol
circDYM	Circular Dynamin
circRNA	Circular ribonucleic acid
CLN2	Ceroid lipofuscinosis 2
Clu	Apolipoprotein J
C-MYC	Cellular myelocytomatosis oncogene
CNS	Central nervous system
CO_2	Carbon dioxide
Cpn1	Carboxypeptidase N subunit 1
CPP	Cell penetrating peptides
CPZ	Chlorpromazine
CQAs	Critical Quality Attributes
Cr1l	Complement receptor 1-like protein
CryoTEM	Cryo Transmission Electron Microscopy
CTNS	Cystinosin

CTs	Chaperon therapies
CXCR4	C-X-C chemokine receptor type 4

D

DAPI	4',6-diamidino-2-phenylindole, dihydrochloride
DDA	Data-dependent acquisition
DDS	Drug delivery system
DELOS-susp	Depressurization of an Expanded Liquid Organic Solution-Suspension
DFF	Direct flow filtration
DGJ	1-deoxygalactonojirimycin
DGU	Density gradient ultracentrifugation
DiOC	Dioctadecyloxycarbocyanine
DiR	1,1'-Dioctadecyl-3,3,3',3'-tetramethylindotricarbocyanine iodide
DLS	Dynamic light scattering
DMSO	Dimethyl sulfoxide
DNA	Deoxyribonucleic acid
DOPS	Dioleoylphosphatidylserine
DPPC	1,2-dipalmitoyl-sn-glycero-3-phosphocholine
DSPE	1,2-Distearoyl-sn-glycero-3-phosphoethanolamine
DTT	Dithiothreitol
Dyn	Dynasore

E

EA	Enzyme Activity
EDC	1-Ethyl-3-(3-dimethylaminopropyl)carbodiimide
EDTA	Ethylenediaminetetraacetic acid
EGFR	Epidermal Growth Factor Receptor
EIPA	5-(N-ethyl-N-isopropyl) amiloride
ELISA	Enzyme-Linked Immunosorbent Assay
ELS	Electrophoretic light scattering
ELSD	Evaporative light scattering detector
EMA	European Medicines Agency
ER	Endoplasmic reticulum
ERT	Enzyme replacement therapy
ESCRT	Endosomal sorting complex required for transport
EtOH	Ethanol
EVs	Extracellular Vesicles

F

F13a 1	Coagulation factor XIII A chain
Fab	Fragment-antigen-binding
FBS	Fetal Bovine Serum
FC	Flow cytometry isolation method

FD Fabry disease

FDA U.S. Food and Drug Administration

FFF Field-flow fractionation

Fga Fibrinogen alpha

Fgb Fibrinogen beta

Fgg Fibrinogen gamma

FLI Fluorescence Lifetime Imaging

FN1 Fibronectin 1

G

GAA Acid alpha-glucosidase

GAG Glycosaminoglycans

GALC Galactocerebrosidase

GALNS N-acetilgalactosamine-6-sulfatase

Gb3 Globotriaosylceramide

GBA Gut–brain axis

Gc Group-specific component

GCase Loaded GBA and acid β-glucosidase

GD Gaucher disease

GFP Green Fluorescent Protein

GLA Generalized lymphatic anomaly

GNeo Guanidinylated neomycin

Gpld1 Glycosylphosphatidylinositol (GPI)-specific phospholipase D1

GT Gene Therapy

H

Hba-a1 Hemoglobin Subunit Alpha 1

Hbb-bs Immunoglobulin Mus musculus (house mouse)

HCD High-energy collision dissociation

HEK293 Human Embryonic Kidney 293 cells

HEK293F Human Embryonic Kidney 293 cells, modified to grow in suspension

HMEC-1 Human Microvascular Endothelial Cells-1

HPLC High-performance liquid chromatography

Hpx Hemopexin

HRP Horseradish Peroxidase

HSCT Hematopoietic stem cell transplantation

HSP70 Heat shock protein 70

HSPs Heat shock proteins

HSR Heat shock response

I

IA Immunoaffinity isolation

IBB-UAB Institute of Biotechnology and Bioengineering de la Universitat Autònoma de Barcelona

IC21	A line of immortalized macrophages derived from mouse bone marrow
ICMAB-CSIC	Intitut de Ciència de Materials de Barcelona
IDUA	Alpha-L-iduronidase
IEP	Isoelectric Point
IgA	Immunoglobulin A
IgE	Immunoglobulin E
IgG	Immunoglobulin G
Ighg3	Immunoglobulin G3
Ighg3	Immunoglobulin G3 heavy chain
Ighm	Immunoglobulin heavy chain mu
Ighv11-2	Immunoglobulin heavy variable 11-2
Ighv1-4	Immunoglobulin heavy variable 1-4
Ighv1-59	Immunoglobulin heavy variable 1-59
Ighv1-64	Immunoglobulin heavy variable 1-64
Ighv5-9-1	Immunoglobulin heavy variable 5-9-1
Ighv8-12	Immunoglobulin heavy variable 8-12
Igkc	Immunoglobulin kappa chain constant
Igkj2	Immunoglobulin kappa joining 2
Igkv126	Immunoglobulin kappa variable 126
Igkv13-85	Immunoglobulin kappa variable 13-85
Igkv2-109	Immunoglobulin kappa variable 2-109

Igkv3-7	Immunoglobulin kappa variable 3-7
Igkv4-62	Immunoglobulin kappa variable 4-62
Igkv6-14	Immunoglobulin kappa variable 6-14
Igkv6-15	Immunoglobulin kappa variable 6-15
Igkv7-33	Immunoglobulin kappa variable 7-33
Igkv8-34	Immunoglobulin kappa variable 8-34
IgM	Immunoglobulin M
Igv1-117	Immunoglobulin heavy variable 1-117
ISSD	Infantile Sialic Acid Storage Disease
IV	intravenous route

K

KD	Krabbe disease
Kng1	Kininogen 1
KO	Knockout

L

LAL-D	Lysosolmal acid lipase deficiency
LAMP2	Lysosomal Associated Membrane Protein 2
lEVs	Large extracellular vesicles
LSDs	Lysosomal storage disorders

M

M6P Mannose-6-phosphate

M6PR Receptor mannose-6-phosphate

MAEC Mouse aortic endothelial cells

MASP Mannan-binding lectin-associated serine protease

Mb I2 Myoglobin I2

Mbl Mannose binding lectins

Mbl1 Mannose-binding lectin 1

Mbl2 Mannose-binding lectin 2

MDA-MB-231 Human breast cancer cell

MeOH Methanol

Mf Microfluidics isolation method

MFI Median fluorescence intensity

MHC Major histocompatibility complex

MKC Miristalkonium chloride

MLD Metachromatic leukodystrophy

MPa Megapascal

MPS Mucopolysaccharidoses

MPS I Mucopolysaccharidoses type I

MPS II Mucopolysaccharidoses type II

MPS IV Mucopolysaccharidoses type IV

MPS IVA Mucopolysaccharidoses type IVA

MPS VII Mucopolysaccharidoses type VII

MQ Milli-Q water

mRNA messenger Ribonucleic Acid

MSCs Mesenchymal stem cells

Mug1 Mouse immunoglobulin G1

MVBs Multivesivular bodies

MVs Microvesicles

N

NanoGLA GLA-loaded and RGD-targeted nanoliposomes

NCL Neuronal ceroid lipofuscinoses

NHS N-hydroxysuccinimide

NM Nanometer

NP Nanoparticle

NPC Niemann-Pick type C

NPC1 Intracellular cholesterol transporter 1

NPC2 Intracellular cholesterol transporter 2

NTA Nanoparticle tracking analysis

NTA Nitrilotriacetic acid

Nys Nystatin

O

ODD Orphan drug designation

P

PAGE PolyAcrylamide gel electrophoresis

PBS Phosphate-buffered saline

PC Protein corona

PD Pompe disease

PDGFR Platelet-derived growth factor receptor

PDI Polydispersity index

pDNA Plasmid DNA

PEG Polyethylene glycol

PEI Polyethyleneimine

PMT Photomultiplier tube

Pp Precipitation

Prss1 Serine protease 1

PTGFRN Prostaglandin F2 receptor negative regulator

PTMs Post-translational modifications

PVDF Polyvinylidene difluoride

Pzp Pregnancy zone protein

R

Rab Ras-associated binding

RES Reticuloendothelial system

RGD Arginylglycylaspartic acid

rh-GLA Recombinant human GLA

Rich Express high levels of the receptor

RP Reversed-phase

RT Room temperature

RVG Rabies virus glycoprotein

S

SapC Loaded saposin C

SDS Sodium dodecyl sulfate

SEC Size exclusion chromatography

Serpina3k Serine (or Cysteine) proteinase inhibitor, clade A, member 3K

sEVs Small extracellular vesicles

SGE Stable gene expression

SGSH N-sulfoglucosamine sulfohydrolase

SiRNA Small interfering ribonucleic acid

SN Supernatants

SNAREs Soluble N-ethylmaleimide-sensitive-factor attachment protein receptor

Sptlc2 Serine palmitoyltransferase long chain base subunit 2

SRT Substrate reduction therapy

SUVs Small unilamellar vesicles

T

Tf Transferrin

TFEB Transcription factor EB

TFF Tangential flow filtration

TGE Transient gene expression

Thbs1 Thrombospondin 1

TMB 3,3’,5,5’-Tetrametilbencidina

TMP Transmembrane pressure

TPP1 Tripeptidyl peptidase 1

TSG101 Tumor susceptibility gene 101

Ttr Transthyretin

U

UAB Universitat Autònoma de Barcelona

UC Ultracentrifugation

UF Ultrafiltration

V

VF Final volume

VI	Initial volume
VSV-G	Vesicular stomatitis virus glycoprotein

W

WB	Western blot
WT	Wild-type
λexc	Excitation wavelength

Research context, funding and collaborations

The present doctoral Thesis entitled: “RGD-Targeted Nanoliposomes and Extracellular Vesicles for Enhanced Enzyme Replacement Therapy in Fabry Disease”, was carried out within the Clinical Biochemistry, Drug Delivery & Therapy (CB-DDT) group at the Vall d’Hebron Research Institute (VHIR). This work was supported by the Catalan Government's Strategic Plan for Research and Innovation in Health (PERIS) predoctoral fellowship (ref. SLT01720000181). Additionally, it received financial support from the European Commission through the H2020 program (Smart-4-Fabry project, ID 720942), the Networking Research Center on Bioengineering, Biomaterials, and Nanomedicine (CIBER-BBN, intramural projects PEGLyso, EXPLORE-2/3 and F7, among others), and the Instituto de Salud Carlos III (ISCIII) grant program (MERIAN PI18/00871 and NEXT-TRY PI21/00936), co-funded by the European Regional Development Fund (ERDF).

Most of the experimental research was conducted between 2020 and 2025 at the CB-DDT group and VHIR facilities. As a member of CIBER-BBN, I had access to the FVPR/U20 of the ICTS “NANBIOSIS” platform for in vivo assays. Additionally, I carried out a one-month research stay with the Molecular Treatments for Cardiac Fibrosis (FIBROHEART) group, led by Dr. Ana Victoria Villar Ramos, at the Instituto de Biomedicina y Biotecnología de Cantabria (IBBTEC), University of Cantabria, thanks to a mobility grant from CIBER-BBN in 2023 (group reference: CB06/01/0012). During this research stay, I had the opportunity to learn one of the methodologies for extracellular vesicles isolation used in this thesis, the benchtop filtration (BF). Furthermore, a brief one-week stay was carried out at the MSC Laboratory (Matière et Systèmes Complexes) at the University of Paris Diderot, in the group led by Dr. Florence Gazeau, as part of the EVERETT project (ANR-21-F2II-0001), in order to learn additional procedures for EV production and purification.

Furthermore, additional key collaborations were developed with several institutions. Leanbio SL provided the rh-GLA enzyme. NANOMOL group from ICMAB-CSIC led by Prof. Nora Ventosa, synthetized the nanoliposomes used in this Thesis. Dr. José Luis Corchero from the Genetic and Microbiology Department at Institut de Biotecnologia i de Biomedicina (IBB-UAB) performed the cell transfections to obtain the cellular supernatants, which were used to isolate extracellular vesicles and free GLAcmycH6 and GLAH6 enzymes.

Table of Content

1. Abstract

Lysosomal storage diseases (LSDs) are rare genetic disorders resulting from mutations that impair lysosomal protein function, leading to the accumulation of undegraded substrates. Fabry disease (FD), an X-linked LSD, is caused by a deficiency in α-galactosidase A (GLA), leading to the buildup of glycosphingolipids like globotriaosylceramide (Gb3) and affecting organs such as the kidneys, heart, and nervous system. Enzyme replacement therapy (ERT) is the most common strategy for treating FD, which involves intravenous administration of recombinant GLA. While ERT improves quality of life, it has limitations such as poor enzyme stability, limited biodistribution (BD), development of neutralizing anti-drug antibodies (ADAs), and the inability to cross the blood-brain barrier (BBB).

This thesis explores nanotechnology to enhance ERT for FD. Two drug delivery systems (DDSs) were studied: nanoliposomes and extracellular vesicles (EVs). Nanoliposomes, synthetic lipid-based vesicles, were functionalized with RGD peptides to target endothelial cells and loaded with recombinant human GLA (rh-GLA), forming the RGD-targeted nanoGLA. These showed good stability, preserved enzymatic activity, and enhanced internalization via macropinocytosis and caveolae-dependent endocytosis, and M6PR-independent pathways. *In vitro*, nanoGLA targeted with RGD peptide reduced Gb3 more effectively than free enzyme and non-targeted nanoGLA, and *in vivo* studies in Fabry mice indicated better enzyme delivery to key organs, including the brain. However, RGD-targeted nanoGLA induced higher antibody levels than free enzymes.

The study also analyzed the impact of the protein corona (PC) — plasma proteins adsorbed on nanoliposomes after their intravenously administration — which can affect biodistribution and cellular uptake. Proteomic analysis revealed that PC composition was consistent across different nanoliposomal formulations, with albumin, fibrinogen, and apolipoproteins being the most abundant proteins. RGD density and the presence of rh-GLA influenced PC composition in terms of the presence of immunoglobulins and complement factors.

EVs, natural nanoscale vesicles, were also engineered to deliver GLA (EV-GLA) using CHO and HEK 293F cells. Different purification methods were compared, including precipitation (Pp), bench-top filtration followed by size exclusion chromatography (BF + SEC), or tangential flow filtration followed by size exclusion (TFF + SEC). BF + SEC and TFF + SEC outperformed Pp in terms of EV concentration and *in vitro* efficacy. EV-GLA from CHO cells showed higher enzymatic activity and *in vitro* efficacy compared to the free enzyme, with BF + SEC and TFF + SEC providing the best purity and efficacy. For HEK 293F cells, TFF + SEC was more advantageous in terms of EV concentration and GLA protein amount, though BF + SEC showed better *in vitro* efficacy. These variable results demonstrate that further investigation is required to optimize the isolation method, cell source, and GLA expression. EV-GLA from CHO cells demonstrated higher activity and *in vitro* efficacy. Targeting EVs with recombinant F7 cell penetrating peptide (rF7) by genetically modifying HEK 293F cells to express both GLA and F7-Lamp2b, enhanced uptake and effectiveness in endothelial cells.

In conclusion, integrating nanotechnology into ERT through targeted nanoliposomes and EVs shows strong potential for improving enzyme stability, biodistribution, and efficacy in treating Fabry disease and other LSDs.

2. General introduction

2.1. Lysosomal storage diseases (LSDs)

Lysosomes are spherical organelles with a single membrane found in the cytosol of the cell. They play a key role in the breakdown of large molecules like sphingolipids, glycogen, polysaccharides and foreign particles, making intracellular digestion one of their primary functions (1,2). However, lysosomes are not only digestive organelles; they also participate in immune regulation, nutrient sensing, cellular death and proliferation, and are involved in secretory pathways, contributing to the production of extracellular vesicles (EVs). This demonstrates that lysosomes are key regulators of cellular homeostasis (3–5).

Lysosomes contain active hydrolases that are capable of degrading substrates due to their luminal acidic pH, which is maintained by the V-type ATPase proton located in their membrane (6). Post-translational modifications (PTMs) of hydrolases, such as glycosylation, are critical for their proper targeting to the lysosome and for their properties, including activity, stability, conformation and solubility (7,8). One of the most common PTMs is the addition of mannose-6-phosphate (M6P). These residues act as a signal to direct the enzymes to the Golgi apparatus, where they are incorporated into secretory vesicles that transport them to the lysosomes. Alternatively, the enzymes may be secreted into the extracellular space in extracellular vesicles (9) or they may be secreted as free enzyme and endocytosed by other cells via interaction with M6P receptors (M6PR), subsequently being incorporated into their lysosomes (Fig. 2.1) (10–12).

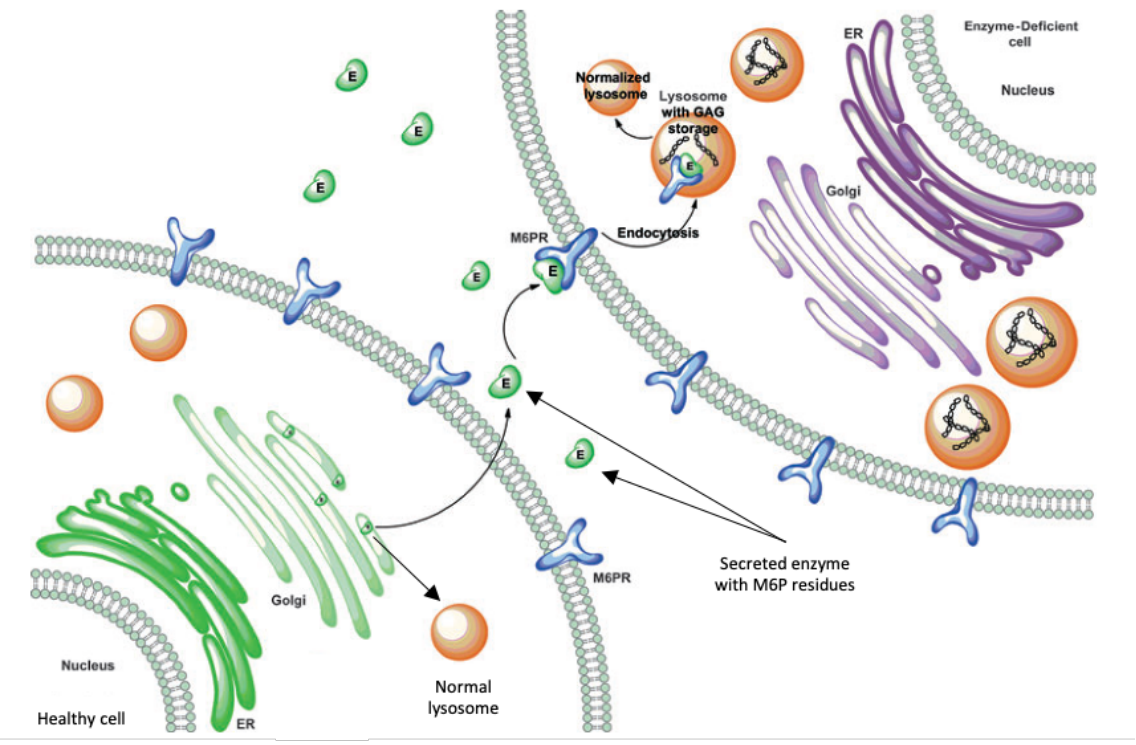

Fig. 2.1. Schematic representation of lysosomal enzymes secretion as free enzymes, which are endocytosed via M6PR and incorporated into lysosomes from enzyme-deficient cell (cross-correction). In this case, cells accumulated GAG substrate. This figure was edited from Tomanin et al. (13).

Malfunction of the lysosomes is in the origin of many pathologies, such as lysosomal storage disorders (LSDs), which are a group of rare genetic diseases, generally caused by single gene

mutations that alter the production or function of lysosomal proteins (14). Mutations in LSDs result in the deficiency or malfunction of proteins essential for the lysosomal function. These proteins include membrane proteins, enzymes and signaling proteins that enable the interaction of lysosomal hydrolases with substrates or other cellular organelles (14). The resulting dysfunction of these lysosomal enzymes leads to the accumulation of undegraded substrates in the lysosomes, triggering a pathogenic cascade with multisystemic affection (Fig. 2.2) (14,15).

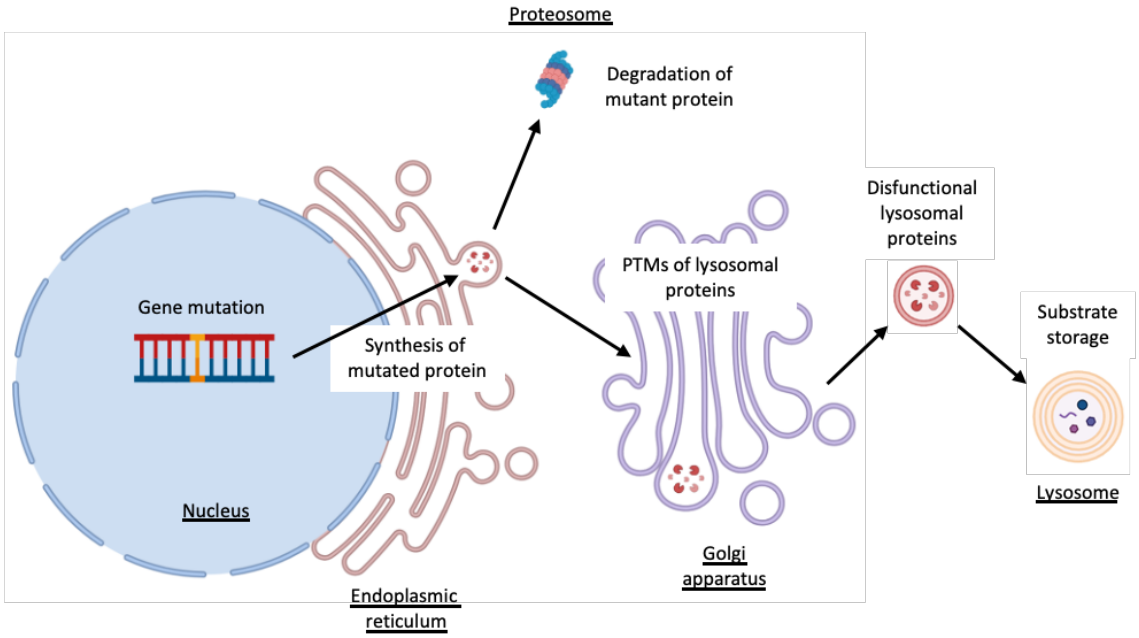

Fig. 2.2. Scheme illustrating substrate accumulation in the lysosome due to dysfunctional lysosomal proteins in lysosomal storage diseases (LSDs). Specific genetic mutations result in the synthesis of mutated lysosomal protein in the endoplasmic reticulum. The resulting dysfunctional protein can either be degraded by the proteosome or undergo post-translational modifications (PTMs) in the Golgi apparatus. It is then encapsulated into a vesicle and delivered to the lysosome. Due to malfunction of this lysosomal protein, undegraded substrates accumulate in the lysosomes, triggering the pathogenic cascade. Figure adapted from Parenti et al. (15).

There are over 70 different types of LSDs (Table 2.1). While most of these pathologies follow an autosomal recessive inheritance pattern, some are X-linked inherited, such as Hunter syndrome, Danon disorder and Fabry disease (FD) (16). Although each LSD is individually considered a rare disease, their combined incidence is estimated to be approximately 1 in 5,000 - 7,500 births (17). Ongoing advancements in newborn screening programs (18) and improved differential diagnostic methods (19) are providing new insights into the true incidence and prevalence of these diseases.

The most widely used method to classify the different LSDs is based on the accumulated substrate. Following this classification, different categories can be differentiated: mucopolysaccharidoses (e.g. Hunter and Sanfilippo syndromes), glycogen storage diseases (e.g. Pompe disease), sphingolipidoses (e.g. Fabry disease) and neuronal ceroid lipofuscinoses (NCL) (20).

The clinical presentation of LSDs can vary significantly, as not all cell types and body tissues are equally affected. This variability is influenced by factors such as the distinct biochemistry of different cell types, the expression levels of the enzymes and differences in substrate turnover rates (14). These factors contribute to the wide range of disease onset and severity seen in LSDs. The accumulation of substrates in various cells and tissues results in a diverse array of clinical

manifestations, often with overlapping symptoms across different disorders. In fact, individuals with a single disease may exhibit different symptom, age at onset, and rates of disease progression. Symptoms can appear at any age, from infancy to adulthood, making early diagnosis challenging in some cases. For instance, in FD, the most common initial symptoms in pediatric patients are neurological and gastrointestinal (21), but as the disease progresses into adulthood, kidney, cardiac and cerebrovascular complications may develop (22).

Table 2.1. Overview of the most common LSDs with their mutated genes gene, accumulated substrates and estimated incidence. Adapted from Lerussi et al. (20).

LSD group	Disease	Mutated gene	Main accumulated substrate	Estimated incidence
Sphingolipidoses	Gaucher disease (GD)	GBA	Glucosylceramide or glucocerebroside	1/30,000
	Fabry disease (FD)	GLA	Globotriaosylceramide (Gb3)	1/40,000 - 120,000
	Metachromatic leukodystrophy (MLD)	ARSA	Sulfatides	1/40,000 - 160,000
	Krabbe disease (KD)	GALC	Galactosylceramide and psychosine	1/100,000
	Niemann-Pick type C (NPC)	NPC1/NPC2	Cholesterol	1/150,000
Mucopolysaccharidoses (MPS)	MPS type I	IDUA	Heparan sulfate, dermatan sulfate	1/100,000
	MPS type IIIA	SGSH	Heparan sulfate	1/100,000
Glycogen storage diseases	Pompe disease (PD)	GAA	Glycogen	1/40,000

2.2. Current treatments for LSDs

Most of LSDs have no effective treatments and the available therapies are symptomatic and supportive to improve the life quality of the patients. However, specific therapeutical strategies have been developed to compensate the lack of function of specific lysosomal enzymes in some LSDs, such as the enzyme replacement therapy (ERT), pharmacological chaperones (17), substrate reduction therapy (SRT) (23), hematopoietic stem cell transplantation (HSCT) (24), gene therapies (*in vivo* and *ex vivo*) and regulators of autophagy and proteostasis (14) (Fig. 2.3). These therapies are summarized in Table 2.2.

2.2.1. Enzyme replacement therapy (ERT)

The first approved ERT for LSDs was a β-glucocerebrosidase enzyme called Aglucerase or Ceredase® for type 1 Gaucher disease (GD) (25). Since 1991, enzyme replacement therapy (ERT) has become the most common treatment strategy for LSDs (26,27). ERT is based on the intravenous administration of a recombinant and functional version of the impaired enzyme (Fig. 2.4). The recombinant enzyme, enriched with M6P residues, internalizes and reaches the lysosomes of the target cell primarily by interacting with M6PR, thereby compensating for the congenital enzymatic deficiency. M6PR also contains binding sites for non-M6P-containing ligands, such as insulin-like growth factor II (IGF-II) (28,29). These non-M6P binding sites facilitate the use of chimeric proteins, like IGF-II-enzymes, which can enter cells via a glycosylation-independent mechanism, although they still depend on M6PR for internalization (29,30). Furthermore, recombinant enzymes can also enter the cell via other pathways, including mannose receptor-mediated uptake, as seen with β-glucocerebrosidase (31), and uptake

mediated by low-density lipoprotein receptor-related protein 1 (LRP1), which is utilized by arylsulfatase A (32).

Table 2.2. Summary of the current therapies for LSDs.

Therapeutic approach	Description	Disease, approved treatment, and other considerations	Advantages	Disadvantages
Enzyme Replacement Therapy (ERT)	Intravenous administration of a recombinant version of the deficient enzyme to treat LSDs.	- GD: Aglucerase, Imiglucerase, Velaglucerase alfa, Taliglucerase alfa. - FD: Agalsidase alfa, Agalsidase beta, Pegunigalsidase alfa. - PD: Aglucosidase alfa, Avalglucosidase alfa-ngpt, Cipaglucosidase alfa-atga. - MPS I: Laronidase. - MPS II: Idursulfase. - MPS IV: Galsulfase. - MPS IVA: Elosulfase alfa. - MPS VII: Vestronidase alfa. - LAL-D: Sebelipase alfa. - CLN2: Cerliponase alfa. - ASMD: Olipudase alfa. - AM: Velmanase alfa.	- Effective in slowing disease progression. - Improves quality of life.	- Cannot cross the BBB. - Repeated infusions needed. - Risk of ADAs formation.
Chaperone Therapies (CTs)	Small molecules stabilize misfolded enzymes, enabling their transport to the lysosome.	- FD: Migalastat. - GD and PD: In development	- Can cross the BBB. - Oral administration. - Less immune system activation.	- Effective only in certain mutations. - Lower efficacy in some LSDs.
Substrate Reduction Therapy (SRT)	Inhibition of enzymes involved in the synthesis of accumulated substrates in the lysosome.	- GD: Miglustat and Eliglustat. - NPC: Miglustat. - PD: Miglustat. - FD: Lucerastat and Venglustat in clinical trials.	- Oral administration. - Can cross the BBB.	- Lower efficacy compared to ERT. - Potential side effects (weight loss, abdominal pain).
Hematopoietic Stem Cell Transplantation (HSCT)	Transplantation of stem cells that can produce functional enzymes.	Used for LSDs without effective treatment (e.g. MPS I, KD and MLD).	Can increase life expectancy in some cases.	- High risk of rejection and infections. - Efficacy depends on disease progression and phenotype.
Gene Therapy (GT)	Replacing or repairing the mutated gene causing the LSD via viral vectors.	- MLD: Lenmeldy - In clinical trials for various LSDs.	- Sustained enzyme production. - Can cross the BBB.	- Limited by vector size (for AAV). - Limited efficacy due to pre-existing antibodies against AAV. - Complex administration.
Proteostasis and Autophagy Regulators	Enhances the cellular stress response, improving protein folding and lysosomal function.	- NPC: Arimoclomol. - PD, GD, MPS: TFEB activation (under investigation).	- Can cross the BBB. - Helps maintain lysosomal function and reduces cell death.	- May not address all types of LSDs (e.g. complete lack of lysosomal enzyme). - Further research needed for broad application.

GD = Gaucher disease; FD = Fabry disease; PD = Pompe disease; MPS = mucopolysaccharidosis; LAL-D = Lysosolmal acid lipase deficiency; CLN2 = Ceroid lipofuscinosis 2; ASMD = Acid sphingomyelinase deficiency; AM = Alpha mannosidosis; NPC = Niemann-Pick type C; KD = Krabbe disease; MLD = Metachromatic leukodystrophy.

Barton and Neufeld described a phenomenon called cross-correction (33), which allows to a wider distribution of the ERT among cells. They reported that cells from LSD patients were able to reduce the levels of substrate accumulation when cultured with cells from healthy individuals. This occurs because some lysosomal enzymes are secreted into the extracellular space and then taken up by neighboring cells via the M6PR. Currently, different ERTs are available for clinical use in the treatment of GD, FD, Pompe disease (PD) and various types of mucopolysaccharidosis (MPS) (I, II, IVA, VI and VII) (34).

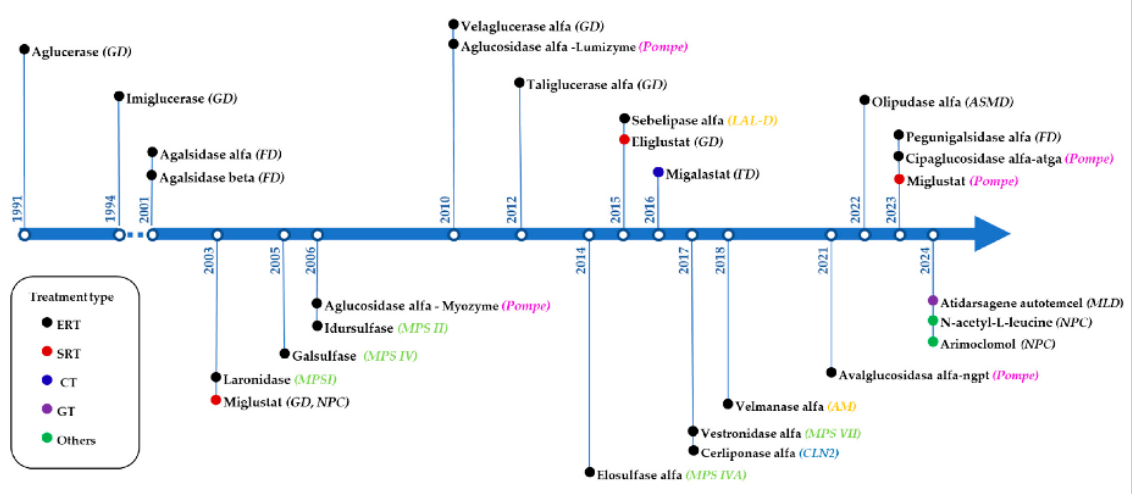

Fig. 2.3. Timeline for the approval of therapies specific to LSDs. HSCT has been excluded among different treatments for the seek of clarity. Figure extracted from Lerussi et al. (20). *GD = Gaucher disease; FD = Fabry disease; MPS = mucopolysaccharidosis; NPC = Niemann-Pick type C; LAL-D = Lysosolmal acid lipase deficiency; ASMD = Acid sphingomyelinase deficiency; CLN2 = Ceroid lipofuscinosis 2; AM = Alpha mannosidosis; MLD = Metachromatic leukodystrophy.*

ERT requires the production of large quantities of enzyme with optimal glycosylation. Therefore, strategies for obtaining high amounts of therapeutic proteins are necessary. One of the most common strategies to obtain recombinant therapeutic proteins in the pharmaceutical industry is the transfection of mammalian cells, which allow stable expression of therapeutic proteins with glycosylation patterns (35,36). The most common cell producers for recombinant human enzymes are stable cell lines as Chinese Ovary Hamster (CHO) and Human Embryonic Kidney (HEK), showing different glycosylation patterns (37,38). Additionally, therapeutic enzymes can be obtained from plant tissue culture (39). This strategy offers several advantages, such as low-cost and fast production, optimized growth conditions, the ability to perform PTMs and to produce therapeutic proteins free from bacterial toxin contaminants (40). However, there are also some drawbacks, including challenges related to regulatory compliance and the limited capacity to glycosylate enzymes, which can restrict their use (40). Examples of commercial enzymes derived from plant cells include β-glucocerebrosidase (41) and pegunigalsidase alfa (42), which are produced from tobacco plant cells to treat Gaucher disease and Fabry disease, respectively.

ERT has proven effective in slowing disease progression and improving the quality of life for patients with LSD, such as GD and FD (43). However, ERT has no impact on the neurological symptoms of LSDs due to its incapacity to cross the blood brain barrier (BBB) and faces challenges in reaching certain tissues, such as the bone, cartilage and cornea (44,45). This is mainly due to low irrigation of those organs and the enzyme sequestration by tissues wit high

expression of M6PR, such as the liver or the spleen (46). Some strategies are being studied to promote the BBB crossing by ERT in LSDs with neurological affection like MPS I and VI and metachromatic leukodystrophy (MLD).

Another important issue is that, in some LSDs, ERT requires repeated infusions of the recombinant enzyme every 2 weeks (45) due to its short half-life in the bloodstream (47,48). Additionally, there is a risk that LSD patients may develop antibodies (IgG) against the therapeutic enzyme. These anti-drug antibodies (ADAs) can directly bind to the recombinant enzyme, inhibiting its function (neutralizing antibodies) or interact with Fc receptors on immune cells, promoting its phagocytosis and subsequent elimination from systemic circulation (49). Both of these cases, as well as allergic reactions due to IgE production, have been reported in patients receiving ERT (50–52).

In recent years, new attempts to improve the stability of ERT by enhancing its half-life in blood have been developed. For example, nanoparticles such as liposomes, polyelectrolyte capsules or EVs have been explored (53). Additionally, a new generation ERT for the treatment of FD, called pegunigalsidase alfa, was recently approved in 2023 (Fig. 2.3). This recombinant enzyme is a polyethylene glycol (PEG)-covered α-galactosidase A (GLA) obtained from tobacco-derived cells. The PEG moieties improve enzyme stability and protect it from degradation and immune recognition, thereby enhancing its half-life in systemic circulation (54).

Different approaches are being explored to reach the central nervous system (CNS). One such approach, involves adding functional molecules to a recombinant enzyme to facilitate its crossing of the BBB. This is achieved by enabling the enzyme to bind to insulin or transferrin receptors on the endothelial cells of the BBB (55), allowing the recombinant enzyme to enter the CNS through transcytosis (56). An example of this strategy is Pabinafusp Alfa (IZCARGO®), a brain-targeted ERT approved in Japan (2021) for MPS II (Hunter syndrome) (57,58). Several clinical trials are being conducted to explore other brain-targeted ERTs. Here are some examples: JR-171 (J-Brain Cargo®) for MPS I (NCT04227600) and JR-441 for Sanfilippo Syndrome (MPS III) (NCT06095388) from JCR Pharmaceuticals, DNL310 (ETV:IDS) for MPS II (NCT05371613) and DNL126 (ETV:GBA) (NCT06181136) for GD type II and III from Denali Therapeutics Inc. This demonstrates important advances toward the approval of ERTs capable of crossing the BBB.

2.2.2. Chaperone therapies (CTs)

Chaperon therapies (CTs) belong to a therapeutic group called “small molecule therapies”, and is based on stabilizing the misfolded enzyme using specific chaperones to prevent enzymatic degradation and to allow its transport from the endoplasmic reticulum (ER) to the lysosome (Fig. 2.4) (34). The low pH, together with the high concentration of substrate in the lysosome, causes the release of the chaperone and allows the enzymatic degradation of the substrate.

Small molecules are a class of treatments that can cross the BBB due to their low molecular weight. They can also be administered orally, which reduces the likelihood of immune system activation compared to intravenous administration. An example of a clinically available chaperone therapy, is 1-deoxygalactonojirimycin (DGJ), also known as Migalastat, which was approved for FD in 2016 (Fig. 2.3) (20,59). Migalastat is a competitive inhibitor of GLA and has shown similar efficacy to ERT (60,61). Nevertheless, Migalastat has a significant limitation: it is only effective in specific Fabry mutation variants that do not involve a complete loss of GLA protein, known as amenable mutations (51,62).

CTs are also being investigated for other LSDs such as GD and PD (34,63,64). However, their efficacy in PD is not as high as that of Migalastat in FD. One strategy to enhance the chaperone efficacy is through administration every other day (64), since the half-life of chaperones in the blood is only a few hours, while the half-life of the enzyme is several days (34). Specifically, once the drug enters the systemic circulation, it maximizes the transport of the enzyme to the lysosome. As its concentration decreases, substrate degradation is increased, promoting the release of the chaperone at the lysosome. Additionally, co-administration of recombinant enzyme with chaperone is being investigated as a potential synergic treatment. Some studies have reported beneficial results from this combined therapy in both, *in vitro* and *in vivo* models (65–67).

New generation CTs are also being explored. New chaperones are being designed to bind to enzymatic allosteric regions, improving its stability and broadening the range of genetic variants they can target, as well as helping maintain the correct folding of the enzyme (68–70).

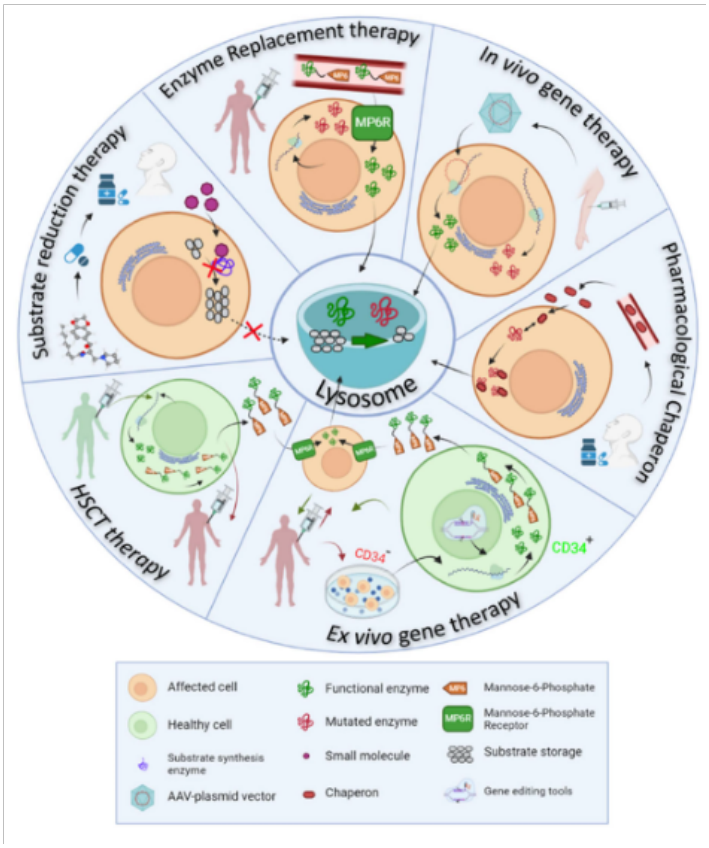

Fig. 2.4. Schematic summary of the different therapeutic approaches for LSDs. Figure extracted from Fernández-Pereira et al. (34).

2.2.3. Substrate reduction therapy (SRT)

Another example of the small molecule therapy is the substrate reduction therapy (SRT), which works inhibiting the enzymes involved in substrate synthesis, thereby reducing its accumulation in the lysosome (Fig. 2.4). Miglustat and Eliglustat are two examples of this therapy, approved for the treatment of GD in 2003 and 2015, respectively (20,71) (Fig. 2.3). Both drugs are administered orally and have the capacity to cross the BBB.

Interestingly, Miglustat can also be used for the treatment of other LSDs, such as Niemann-Pick type C (NPC) and PD (72,73). However, it has lower efficacy than ERT and may cause side effects

such as weight loss, abdominal pain and diarrhea (74). In contrast, Eliglustat shows comparable efficacy to ERT in patients with GD (75) and has fewer side effects than Miglustat. Nevertheless, Eliglustat is metabolized by cytochrome P450, which could lead to potential interactions with other drugs that share the same metabolic pathway.

Additionally, Lucerastat and Venglustat are investigational SRT drugs for FD. Both are inhibitors of glucosylceramide synthase, the enzyme responsible for synthetizing globotriaosylceramide (Gb3), the accumulated substrate in FD (76,77). However, Lucerastat is still at Phase III of clinical trials (NCT03425539) (76,78), while Venglustat is in Phase II (NCT02489344).

2.2.4. Hematopoietic stem cell transplantation (HSCT)

Before the approval of ERT, hematopoietic stem cell transplantation (HSCT) was the primary treatment for several LSDs (Fig. 2.4). It remains an effective approach for some LSDs with CNS involvement, including Krabbe disease (KD), MPS I, and MLD (34). Importantly, it has been reported that cells derived from HSCT, which have the ability to produce the functional enzyme, can reach the brain (79).

HSCT has been shown to increase life expectancy in children with MPS I (80). However, in KD and MLD, the effectiveness of HSCT depends on disease progression and phenotype (81,82). Additionally, high mortality and morbidity are associated with this strategy due to the possible rejection of donor cells and consequent infections (34).

2.2.5. Gene therapy (GT)

This therapy consists of repairing or replacing the mutated gene that causes the LSD with a healthy one using viral vectors such as adenovirus, lentivirus and adeno-associated Virus (AAV) (Fig. 2.4). In March 2024, gene therapy was approved for MLD, making it the only LSD with gene therapy as a treatment option (83). There are two main types of gene therapy: *ex vivo* gene therapy and *in vivo* gene therapy.

In *ex vivo* gene therapy, cells from the patient are extracted and modified *in vitro* to correct the genetic defect. Once modified, these cells are re-implanted into the patient (Fig. 2.4). This strategy reduces the risk of immune rejection and minimizes the chance of altering other loci in the genome, as it allows for direct homologous recombination. However, there are some limitations to this approach, such as the low percentage of re-implanted corrected cells, which sometimes requires the use of immunosuppressive drugs to improve re-implantation success.

In contrast, *in vivo* gene therapy involves the systemic administration of a viral vector containing the healthy gene (Fig. 2.4). For this reason, viral vectors that integrate their genetic material into the host genome are generally excluded, due to the difficulty in controlling transgene insertion. In this case, AAV is the most commonly used vector (84) and some serotypes are capable to cross the BBB (85). Unlike ERT, this therapy allows the sustained production of the recombinant enzyme (86), which can then be distributed throughout the body via the cross-correction effect. However, *in vivo* gene therapy also has several limitations, such as the size of AAVs, which cannot encapsulate DNA fragments larger than 5 Kb, and the reduced efficacy due to the presence of pre-existing antibodies against AAV in most of the population (87,88).

Several clinical trials using gene therapy are currently underway for different LSDs, including FD, MPS type I, II and III, KD, PD and GD, demonstrating that this therapy can be applied to different types of LSDs.

2.2.6. Proteostasis and autophagy regulators

Proteostasis refers to a sophisticated process within the cell that regulates the production, folding, transport and elimination of proteins. Presence of misfolded proteins can lead to cellular stress (89,90), which triggers a defense response known as heat shock response (HSR). The HSR promotes lysosomal homeostasis by preventing protein misfolding (91,92). Activation of the HSR leads to the production of heat shock proteins (HSPs), which are molecular chaperones associated with lysosomal function and integrity (92–95). Regulators of this process can be used as a treatments for LSDs, facilitating the transport of the enzyme to the lysosome (96).

Arimoclomol (Miplyffa) is an oral drug capable to cross the BBB (97) that it has been recently approved for Niemann-Pick type C (98) (Fig. 2.3). This treatment enhances the cellular stress response by triggering the HSR and increasing the production of HSPs, such as Hsp70, which is a critical chaperone for the correct folding and processing of NPC1 protein (95,99). This helps prevent protein misfolding and facilitates lysosomal function. As a result, arimoclomol helps maintain cellular function and prevents cell death under lysosomal stress (92,95,100–102).

Additionally, regulating autophagy can be a useful strategy to reactivate the degradation of accumulated substrates. An example of autophagy regulation is the activation of exocytosis mediated by TFEB, which has been reported to promote the degradation of accumulated substrates in PD, GD and MPS (103–105).

Unlike ERT or gene therapy, all these strategies could be used for treating different types of LSDs.

2.3. Fabry disease (FD)

Fabry disease (FD) is a rare X-linked LSD resulting from a deficiency or lack of the α-galactosidase A (GLA) enzyme from the lysosome. Its estimated incidence ranges from 1: 40,000 to 1: 120,000 live births (106).

The lack of GLA enzyme activity leads to the accumulation of neutral glycosphingolipids, mainly Gb3, within lysosomes of various cell types. Gb3 composition consists in a ceramide group linked to a sugar chain containing one glucose and two galactose units. The cells most affected by this buildup include endothelial cells, cardiomyocytes, renal cells, and nerve cells, contributing to a range of multi-systemic symptoms (Fig. 2.5) (107,108). Endothelial cells are particularly vulnerable to Gb3 accumulation, impairing several cellular functions such as metabolism, oxidative stress responses and ion transport through membrane channels. In childhood and adolescence, early signs of the disease may appear, including skin lesions like angiokeratomas, along with gastrointestinal and neuropathic pain. As the disease progresses into adulthood, more severe complications emerge, such as cardiac issues, kidney dysfunction and cerebrovascular events (stroke and ischemic attacks), leading to multi-organ pathologies and premature death in untreated patients (109–113).

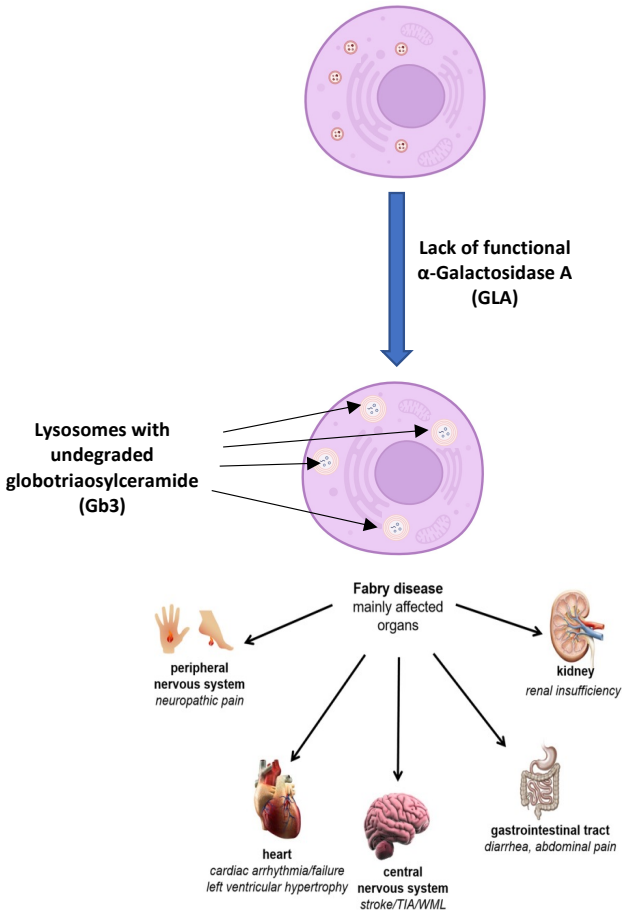

Fig. 2.5. Scheme of the physiopathology of FD. The lack of function of lysosomal GLA promotes the accumulation of undegraded substrate (mainly Gb3) triggering a multisystemic pathological cascade. Figure adapted from Lenders et al. (114).

2.3.1. Treatment options for Fabry disease

2.3.1.1 ERT options for Fabry disease

Since 2001, ERT has been the primary treatment for patients with FD, involving biweekly intravenous infusions of recombinant GLA (49,115). Three products have been authorized for this purpose: Agalsidase alfa from Shire-Takeda (Replagal®), available in Europe, produced in an undisclosed human fibroblast cell line, agalsidase beta from Sanofi-Genzyme (Fabrazyme®) approved both in Europe and the USA since 2003, produced using CHO cell cultures; and pegunigalsidase alfa (Elfabrio®) from Chiesi Global Rare Diseases, approved by FDA and EMA since 2023 (Fig. 2.3) and produced in a tobacco plant-based system called ProCellEx®.

Agalsidase alfa and beta consist of recombinant human GLA enzyme with similar biochemical characteristics, though they exhibit slight differences in glycosylation patterns and the way they are endocytosed by cells via M6PR. These variations are linked to the different cell lines used for its production (115–117). Agalsidase alfa is administered at 0.2 mg/kg and stored as a concentrated aqueous solution, while agalsidase beta is given at 1 mg/kg and stored as a freeze-dried product. In contrast, pegunigalsidase alfa is a PEGylated agalsidase alfa, which enhances the stability and pharmacokinetics of the enzyme through chemical cross-linking with short PEG molecules. Compared to other treatments, pegunigalsidase alfa offers a longer half-life, greater patient tolerance and reduced risk of ADAs generation, while still being administered biweekly at a dose of 1 mg/kg (118,119).

Studies have shown that ERT can lower Gb3 levels in both plasma and tissues, alleviate gastrointestinal symptoms and neuropathic pain, and slow disease progression by partially stabilizing heart and kidney function (43). While ERT can reduce Gb3 accumulation and improve patient quality of life, it does not fully reverse the disease, especially in its advanced stages (120). To further support FD treatment, JCR Pharmaceuticals, in collaboration with Amicus Therapeutics and GlaxoSmithKline, developed agalsidase beta biosimilar, also known as JR-051, which is a biosimilar of Fabrazyme®. A biosimilar is a biological product that is highly similar to an already approved treatment in terms of quality, efficacy, and safety. In fact, agalsidase beta biosimilar was approved for sale in Japan in 2018, demonstrating comparable efficacy and safety to the original agalsidase beta (121–123).

Extensive data on agalsidase alfa and beta have highlighted several limitations, including their inability to cross the BBB, poor enzyme stability, leading to rapid degradation and a short half-life in circulation, limited biodistribution (BD), development of neutralizing ADAs, the need for frequent intravenous administration (every two weeks) and high immunogenicity risks. Collectively, these factors contribute to reduced overall efficacy (53,113,117). While pegunigalsidase alfa improves some of these limitations by increasing enzyme stability and half-life in bloodstream and reducing immunogenicity, its posology, frequency of administration, cost, inability to cross the BBB, and efficacy in target tissues such as kidneys, remains similar to agalsidase beta (124). Furthermore, the frequent administration required for ERT is an important issue for the patients, as it is an expensive treatment (approximately 280,000 €/patient per year).

2.3.1.2 CT for Fabry disease

In contrast to ERT, migalastat (Galafold®) developed by Amicus Therapeutics, was approved as a pharmacological chaperone therapy (CT). Migalastat is especially beneficial for patients with residual GLA activity and offers some advantages over traditional ERT, including oral administration, non-immunogenic response, and potential ability to cross the BBB. However, its inefficacy in patients with a complete lack of the GLA enzyme presents a significant limitation, as it reduces the number of patients who can benefit from treatment (51,62).

2.3.1.3 Investigational SRT for Fabry disease

SRT is being developed for the treatment of FD. Lucerastat, an iminosugar that inhibits Gb3 synthesis, has shown promising results in phase I trials (NCT02930655), reducing the accumulation of glycosphingolipids, such as Gb3 (76). It is currently being evaluated in a phase III trial (MODIFY, NCT03425539) to assess its safety and efficacy (76,78). Another SRT drug, Venglustat, inhibits glucosylceramide synthase and reduces glucosylceramide synthesis (77). In a phase II trial (NCT02489344), it demonstrated long-term safety and a reduction in Gb3 levels in treated FD patients.

2.3.1.4 Clinical trials of GT for Fabry disease

Several *ex vivo* gene therapy drugs are currently being investigated in clinical trial for the treatment of FD, including Lentiviral vectors, such as AVR-RD-01 (125). Initial data from the phase I/II clinical trial (NCT02800070) exhibited no serious adverse events, and all participants showed increased GLA activity levels following intravenous infusion. Although these activity levels peaked and then declined, they did not drop to null values (126). In a subsequent study (NCT03454893), AVR-RD-01 demonstrated similar results, producing functional enzyme and

reducing Gb3 accumulation. However, its developer, Avrobio, halted clinical trials for AVR-RD-01 in 2022 (127), due to market and regulatory challenges surrounding FD treatments and inconsistent clinical trials outcomes. Meanwhile, AAV-based vectors are being tested in various phase I/II clinical trials for *in vivo* gene therapy, such as 4D-310 (NCT04519749 and NCT05629559), BBM-F101 (NCT06207552), FLT190 (NCT04040049) (128) and ST-920 (NCT04046224) (129), to assess their safety and effectiveness.

2.4. Nanomedicine: nanoparticles as drug delivery tools

The application of nanotechnology to enhance ERT could lead to more effective formulations, improving enzyme cellular uptake, enhancing BBB penetration, protecting the enzyme from degradation, and reducing immunogenic responses. These advancements have the potential to not only improve treatments for FD but also for other LSDs (27,53,130–132).

Nanotechnology, has become a powerful tool for targeting and precise delivery of therapeutic agents, enhancing traditional drug therapies and introducing the concept of drug delivery system (DDS). In DDS, a drug is encapsulated commonly in a nanocarrier and transported directly to its intended site of action. This approach opens up numerous alternative methods for drug delivery, addressing many limitations of conventional treatments. Despite significant advancements in recent years in treating various pathologies like cancer, blood disorders, immune-related conditions and metabolic diseases (133), many challenges persist with traditional therapies, such as lack of specificity, poor biodistribution, drug toxicity and severe side effects. For instance, several drugs have a narrow therapeutic window, where the optimal dose is dangerously close to the toxic dose. By modifying the drug distribution, DDS may reduce toxicity and increase therapeutic effectiveness (134). Additionally, DDS can offer benefits like protecting drugs from rapid degradation or elimination, improving solubility and enhancing drug concentrations at targeted sites, potentially reducing the required dose (135).

The most common and effective route to administrate DDS is via intravenous (i.v.) injection, as DDS typically have low absorption when are administered via extravascular routes such as oral administration. Once in the bloodstream, nanoparticles can leverage both passive and active targeting mechanisms. Passive targeting refers to the accumulation of DDS in vascular tissues, particularly in areas with specific pathologies such as tumors, due to the enhanced permeability and retention effect. This effect occurs because inflamed tissues or tumor environments have increased permeability, allowing small nanoparticles (typically under 150 nm) to pass through blood vessel walls and accumulate in the target tissues (136,137). In contrast, active targeting involves attaching specific molecules, such as peptides, antibodies, or nucleic acids, to the surface of nanoparticles, enabling them to selectively bind to cellular receptors on target tissues. This recognition can lead to greater uptake of the DDS by the desired cells or tissues. Lastly, unlike small molecule or biological drugs, DDS are mainly cleared from the body by the reticuloendothelial system (RES), found in organs like the liver, spleen, bone marrow and lungs (134,138,139). Phagocytic cells, such as macrophages, recognize and remove the DDS from circulation, often aided by opsonization, where serum proteins like antibodies or complement proteins are adsorbed in the nanoparticle (NP) surface, promoting its elimination (139). This important interaction between NPs and plasma proteins forms a structure called “protein corona”, which strongly influences the fate of the NPs (140).

A broad variety of delivery systems have been explored as potential drug carriers for biomedical applications. Particularly, nanocarriers can be categorized using various criteria, including size, surface functionality, shape, or the nature of the nanoparticle itself. Nevertheless, they are

commonly classified according to their composition. This classification include: inorganic-based nanoparticles, polymer-based nanocarriers, protein-based nanoparticles and lipid-based nanoparticles (Fig. 2.6) (141–143).

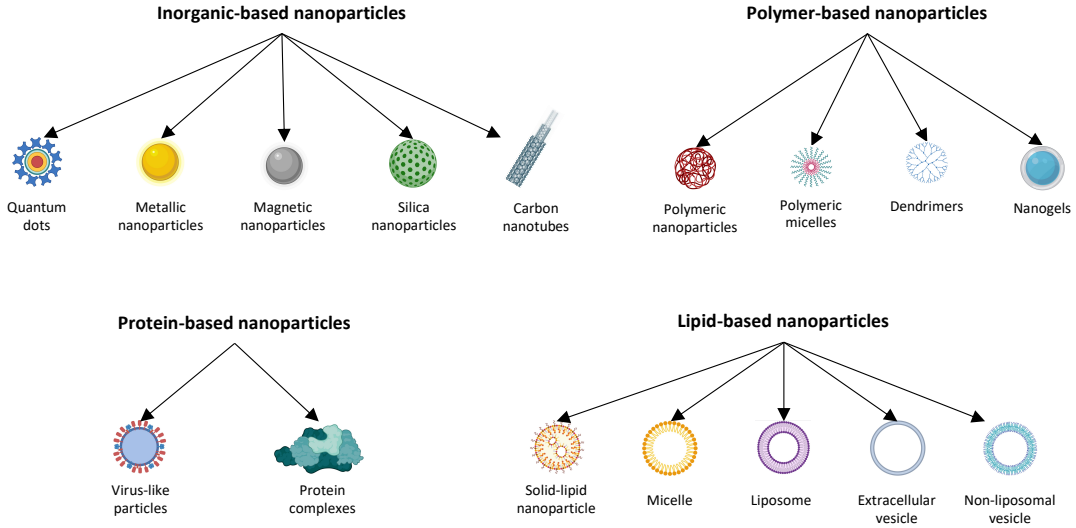

Fig. 2.6. Scheme of the classification of the different nanocarriers based on their composition. Adapted from Sercombe et al. (144).

In this thesis, two different nanostructures have been studied as DDS: nanoliposomes and extracellular vesicles (EVs), which will be explained in detail below.

2.4.1. Liposomes in drug delivery

Liposomes are considered one of the most promising delivery systems in nanomedicine. First described by Alec Bangham in the 1960s, liposomes are self-enclosed bilayer structures that spontaneously form in aqueous environments due to the self-assembly of amphiphilic molecules, primarily phospholipids (145). Their biocompatibility, biodegradability, and versatility have made them extensively studied as pharmaceutical carriers. Liposomes can be engineered with varying sizes, compositions, and surface properties, enabling the encapsulation of both hydrophilic compounds (within the aqueous core) and hydrophobic molecules (within the lipid bilayer) (138). These properties allow liposomes to overcome several limitations in conventional drug delivery, such as enhancing drug solubility, protecting drugs from degradation, reducing off-target effects, and improving targeted delivery to specific cells and tissues (138).

Structurally, liposomes are spherical nanostructures composed of one or more concentric lipid bilayers. The primary building blocks are phospholipids, which are amphiphilic molecules containing both a hydrophilic (polar) head and a hydrophobic (non-polar) tail. In an aqueous environment, these molecules spontaneously arrange into vesicles, with the hydrophilic heads facing outward towards the water phase, while the hydrophobic tails are shielded within the bilayer (146) (Fig. 2.7).

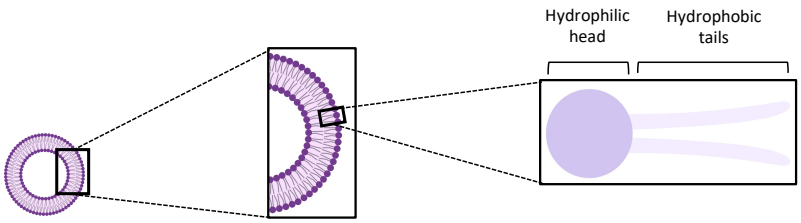

Fig. 2.7. Overview of the phospholipidic composition and self-organization of liposomes.

Liposomes can be categorized based on their size and number of bilayers (lamellarity) (147,148). In terms of size, liposomes are classified as small (< 200 nm), large (200 nm - 1 μm) or giant (> 1 μm). In this Thesis, small liposomes (< 200 nm) are referred to as nanoliposomes. In terms of lamellarity, they can either be composed by a single bilayer (unilamellar) or by several concentric bilayers (multilamellar). When multiple smaller liposomes are contained within a larger one, the structure is referred to as multivesicular vesicles. Small unilamellar vesicles (SUVs) are particularly valuable in medical applications, as liposomes in the small size range (100 – 200 nm) are suitable for intravenous injection. They are larger enough to avoid rapid renal clearance, yet small enough to minimize uptake by RES, allowing for prolonged circulation time (147,148). These nanoliposomes are the focus of investigation in this Thesis.

The earliest form, known as “first-generation” liposomes, consisted mainly of phospholipids and either water or lipid soluble drugs (138) (Fig. 2.8). However, these liposomes had notable drawbacks, including poor stability and rapid elimination from bloodstream. To address these issues, cholesterol (Chol) was introduced into the liposomal membrane. This improved the physical stability of liposomes, reduced membrane permeability, helped maintain colloidal stability and led to a more compact arrangement of phospholipids, which minimized drug leakage (134,148).

In addition, polyethylene glycol (PEG) is another molecule that can be attached to the components of membrane liposomes. Modifying the composition and ratio of phospholipids, adding Chol, or further decorating the liposome surface significantly impacts the physicochemical properties of the liposomes, as well as their behavior in both *in vitro* and *in vivo* environments, leading to the development of “second-generation” liposomes (146). The incorporation of PEG results in “stealth” liposomes that prolongs the circulating time in blood, as PEG is a hydrophilic and biocompatible polymer with low immunogenicity (149) (Fig. 2.8). PEGylation helps shield the liposomes from opsonins recognition, which are blood proteins that target particles for clearance, such as immunoglobins and complement factors, and reduces their removal by the RES (138,150). The first liposomal drug to gain approval was Doxil® in 1995. Doxil is a PEGylated liposome and encapsulates the chemotherapy drug doxorubicin in liposomes for the treatment of ovarian cancer and AIDS-related Kaposi’s sarcoma. PEGylated liposomes are now commonly used in clinical applications. However, while PEGylation protects the NP, it can also reduce cellular uptake and hinder endosomal scape, which may limit the overall therapeutic efficacy (149).

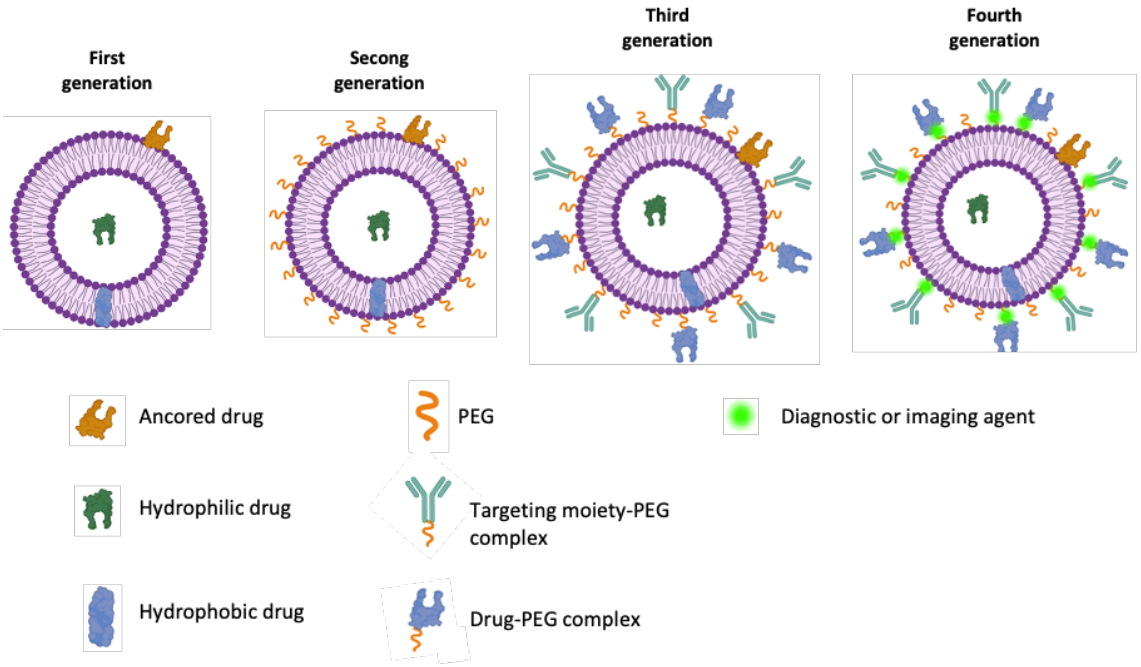

Fig. 2.8. Schematic representation of the different generations of liposomes as drug delivery systems. Figure adapted from Cruz et al. (151).

Furthermore, "third generation" liposomes or also called "ligand-targeted liposomes" offer enhanced therapeutic effects by incorporating multiple functionalities. These liposomes are engineered with specific ligands on their surface for a specific drug delivery (152) (Fig. 2.8). The targeting agents can include peptides, receptor ligands, monoclonal antibodies, etc. which are either directly attached to the liposome surface or linked via PEG molecule (138). Once these ligand-targeted liposomes reach their intended destination, they bind to their complementary receptors on target cells, facilitating the accumulation of the drug at the targeted location (152).

Theranostic liposomes are often referred to as the "fourth generation" of liposomes, as they aim to integrate both therapeutic and diagnostic functions into a single platform (Fig. 2.8). These liposomes combine multiple capabilities, such as drug delivering, targeting specific delivering by the addition of targeting ligands, and enabling bioimaging with the incorporation of imaging agents. As a result, significant progress in this field over the past few decades has led to the approval of several nanoparticles-based therapies (153).

Nowadays there are currently around 15 approved for clinical use and more than 100 others are undergoing clinical trials, most of which are second-generation liposomes (10,154–156).

2.4.2. Extracellular vesicles as therapeutic tools

Extracellular vesicles (EVs) are small, membrane-bound structures released by all types of cells into the surrounding extracellular environment. EVs carry a wide range of molecules, such as lipids, proteins, and nucleic acids, and act as vehicles for communication between cells. By interacting with recipient cells, they influence numerous biological processes in both nearby and distant tissues (157). They are classified based on their origin, function, and size.

According to their origin, EVs are classified as exosomes (50 – 150 nm), microvesicles (MVs) (100 – 1000 nm), and apoptotic bodies (1 – 5 μm) (158). Exosome biogenesis occurs via the endocytic pathway, where the cytoplasmic membrane folds inward to create early endosomes (159,160). These then mature into late endosomes and eventually form multivesivular bodies

(MVBs) (161,162). MVBs have two possible fates: they can either fuse with lysosomes for degradation or fuse with the plasma membrane to release exosomes into the extracellular space (157,163,164) (Fig. 2.9). MVs are produced by the direct outward budding of the plasma membrane (165,166) (Fig. 2.9). Apoptotic vesicles, which are formed during cell death (Fig. 2.9), arise through membrane bubbling and are marked by phosphatidylserine (PS), which induces phagocytosis (167).

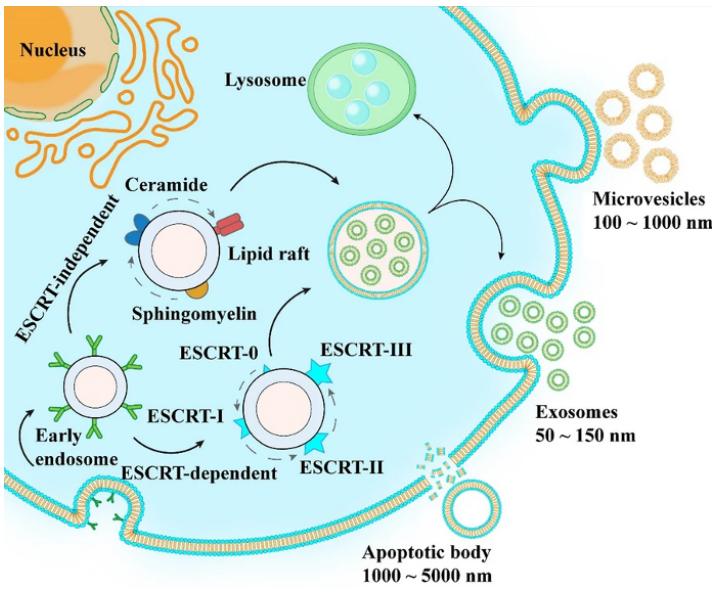

Fig. 2.9. Biogenesis and release of the different types of EVs. Figure extracted from Du et al. (168).

According to MISEV2023 guidelines (169), EVs are also divided into small EVs (sEVs), typically between 30 to 200 nm (mostly consisting of exosomes) and large extracellular vesicles (lEVs), which range from 150 to 1000 nm. Markers like SNAREs (soluble N-ethylmaleimide-sensitive-factor attachment protein receptor), ESCRT (endosomal sorting complex required for transport), tetraspanins (CD9, CD63 and CD81), ADAM (a disintegrin and metalloproteinase) proteins, and Rab are commonly associated with sEVs, while lEVs tend to express more proteins related to cytokinesis, ribosomal activity, mitochondria, and nucleus (170,171).

As for the "natural" EV cargo, it is largely determined by the cell type from which they originate and the mechanisms involved in their formation. As DDS, EVs can be classified as either natural or engineered. Natural EVs are unmodified and produced by cells with intrinsic therapeutic properties. For example, EVs derived from mesenchymal stem cells (MSCs) show promising potential for tissue repair, as they can reach sites of inflammation or damage and modulate immune responses (172,173). They hold significant potential for treating a wide range of diseases, such as inflammatory disorders (174), cardiovascular conditions (173), neurodegenerative diseases (175), and cancer (176). In fact, ongoing clinical trials are investigating their potential in therapies, including the use of MSC-derived EVs to treat severe COVID-19 (NCT04384445) and dry eye syndrome (177).

In contrast to natural EVs, engineered EVs are modified to carry specific bioactive molecules. This modification can be achieved through genetic modifications of the producer cells, enhancing their therapeutic potential by expressing the protein of interest (178). Additionally, EVs can be modified with specific ligands to target particular cells or tissues, optimizing their therapeutic impact while minimizing off-target effects (179–185). The lipid bilayer of EVs acts as a natural shield, preserving the stability and functionality of the cargo throughout its journey,

ensuring that it reaches the intended target site effectively (186). Furthermore, post-isolation loading techniques, such as chemical or mechanical methods, can be used to introduce various molecules, such as siRNA, enzymes, and chemotherapy agents (187).

Regarding biodistribution, EVs and liposomes exhibit similar patterns after i.v. administration (188,189). EVs are quickly cleared from circulation, mainly by phagocytes, showing an initial half-life of 20 min, followed by a secondary half-life of 180 min (181). Within 30 min after administration, most EVs accumulate in the liver, with smaller amounts found in the spleen, kidneys and lungs. Full tissue clearance generally occurs within 6 to 48 h, depending on the EV type, surface modifications, and the isolation or purification techniques used (183,184). Recent research has highlighted that, despite their similarities, EVs offer enhanced potential for safeguarding and delivering therapeutic payloads compared to lipid-based formulations (188,189,193). This has positioned EVs as an innovative and highly promising natural DDS, outperforming other alternatives.

EV-based therapies hold great promise, but several challenges must be addressed before they can reach their full potential. One major hurdle is the intrinsic variability of EVs, including differences in size, cargo, surface markers, and biogenesis pathways, which complicates standardization in production, characterization, and dosing. Ensuring large-scale production with consistent quality remains a significant barrier (194). Another critical challenge is achieving precise targeting, as EVs may be unintentionally taken up by non-target tissues, reducing their therapeutic efficacy (132,195). While surface modifications can enhance targeting, they may also trigger immune responses, further complicating their clinical application (196,197). Additionally, stability during storage and transport is a concern, as EVs can lose functionality over time, potentially affecting their therapeutic effectiveness (198,199). Regulatory challenges also pose a significant obstacle, as the framework for EV-based therapies is still evolving, which could delay approval and clinical translation (157).

To overcome these challenges, ongoing research is focusing on enhancing EV engineering, refining isolation techniques, and improving characterization methods. Addressing these issues will be key to unlocking the full potential of EV therapies in clinical applications.

This thesis explores the use of liposomes and EVs as DDS to improve ERT in FD, serving as a model for LSDs. Liposomes and their protein corona will be examined in detail in sections 5 and 7 and EVs in section 7.

3. Hypothesis and objectives

3.1. Hypothesis

Enzyme replacement therapy (ERT) remains the most widely used treatment for Fabry disease (FD) and other lysosomal storage disorders (LSDs), but its efficacy is limited by short half-life, poor biodistribution, low enzymatic stability, and immune responses against the therapeutic enzyme. This thesis explores the hypothesis that drug delivery systems (DDSs), such as nanoliposomes and extracellular vesicles (EVs), can enhance ERT by improving enzyme protection, stability, biodistribution, and uptake by target cells.

Specifically, we propose:

- DDSs can improve ERT in LSDs. The use of nanoliposomes and EVs as carriers for recombinant α-galactosidase A (GLA) will enhance enzyme stability and functional delivery.
- Functionalization of DDS with targeting moieties can improve biodistribution and cellular uptake. Functionalization with RGD peptides in nanoliposomes and F7 peptides in EVs will enhance enzyme uptake in target cells, leading to improved therapeutic efficacy.
- The protein corona (PC) influences DDS performance. Understanding the composition and effects of the PC on nanoliposomal formulations will help optimize their biodistribution and internalization.

3.2. Objectives

To test these hypotheses, this thesis focuses on two key research directions:

1. Targeted nanoliposome-based for enzyme delivery:
    a. Evaluate the effect of RGD-functionalized nanoliposomes on *in vitro* internalization and efficacy in target cells.
    b. Investigate the *in vivo* biodistribution (BD) of RGD-targeted nanoliposomes in a Fabry disease mouse model.
    c. Characterize the protein corona (PC) composition of nanoliposomes and assess its impact on cellular uptake and BD.
2. Feasibility of EV-based delivery of GLA:
    a. Assess the feasibility of loading GLA into EVs from different cell sources (CHO DG44 and HEK 293F) using stable and transient expression systems.
    b. Optimize EV isolation methods (precipitation, ultrafiltration with size exclusion chromatography or tangential flow filtration) to maximize yields of EVs carrying active GLA.
    c. Evaluate the impact of F7-functionalization on EV uptake and efficacy in target cells.

By addressing these objectives, this thesis aims to contribute to the development of next-generation targeted ERT strategies that enhance enzyme delivery, stability, and efficacy in Fabry disease, with broader implications for other LSDs.

4. Experimental section

4.1. Production and characterization of nanoliposomal formulations

All nanoliposomal formulations were designed, produced and physiochemically characterized by Prof. N. Ventosa' team at ICMAB-CSIC following their established and published methodologies, which will be briefly explained in the following sections.

4.1.1. Production of rh-GLA

The rh-GLA was produced at Leanbio SL facilities using mammalian CHO cell line, following protocols outlined in previous studies (200). Briefly, CHO cells were co-transfected with a recombinant plasmid that included the cDNA coding region for human alpha-galactosidase A (i.e. GenBank® Gene ID: 2717; UniProt number P06280). A stable subcloned CHO cell line expressing GLA was used to prepare a single large batch at 50 L scale. The culture medium was clarified through centrifugation and filtration, followed by a concentration step using TFF. This included two chromatography steps: anion exchange chromatography and hydrophobic interaction chromatography. A virus inactivation step was incorporated before chromatography purification process. The resulting eluate was concentrated and diafiltrated via TFF. Finally, the product was formulated using the same buffer as the commercial agalsidase beta formulation (Fabrazyme®) and passed through a 0.22 µm polyvinylidene difluoride (PVDF) filter.

4.1.2. Manufacturing of nanoliposomal formulations by DELOS-susp

All nanoliposomal formulations investigated in this thesis were produced by Prof. N. Ventosa' team at ICMAB-CSIC following DELOS-susp methodology (200–202) plus TFF purification and concentration step, as was detailed in section 4.1.3 and 4.1.4.

Briefly, a solution of EtOH:DMSO (4:1 volume ratio) was prepared containing DPPC (13.31 mg/mL), cholesterol (4.56 mg/mL), with or without chol-PEG400-RGD (1.56 mg/mL), MKC (0.64 mg/mL) and DiR (XenoLight™ DiR) (150 nM, i.e., 0.008 mol%). This mixture was sonicated for 10 min at 40°C and loaded into a high-pressure vessel. The solution was expanded volumetrically with liquid compressed CO_2, maintaining a CO_2 molar fraction between 0.45 to 0.55, at a temperature of 35 °C and a pressure of 8.5 MPa. The CO_2-expanded solution was left for 1 h to ensure thorough homogenization. A volume of rh-GLA stock solution (3.11 mg/mL, provided by Leanbio SK), was diluted in purified water to achieve a final rh-GLA concentration of 30 µg/mL. The CO_2-expanded solution was depressurized into this aqueous rh-GLA solution to form the nanoGLA. A nitrogen flow at 10 MPa was used to release the CO_2-expanded solution from the reactor. This process resulted in intermediate liposomal batches (1.2 ml/mL of lipid, 1.25% v/v DMSO and 5% v/v ethanol), which underwent a purification step via TFF (KrosFlo Research IIi Repligen). Hollow fiber columns -CO04-E300-05 or D04-E300-05- were hydrated with water (2 mL/cm^2). The intermediate nanoGLA and empty liposome (EL) preparations were concentrated 2-fold or 7.5-fold and diafiltrated over six cycles in water or glucose solution (5% w/v), maintaining a transmembrane pressure (TMP) of 5-10 bar throughout the process. The samples were stored at 2-8°C and handled preferably within the laminar flow cabinet.

4.1.3. Size distribution, ζ-potential and polydispersity index (PDI) by Dynamic Light Scattering (DLS)

Particle size distribution, ζ-potential and polydispersity index (PDI) of liposomal systems were assessed using a dynamic light scattering (DLS) following the procedure detailed in (200) and electrophoretic light scattering (ELS) analyser, integrated with non-invasive backscatter technology (NIBS) (Malvern Zetasizer Nano ZS, Malvern Instruments). The equipment was equipped with a 4 mW "red" He-Ne laser (λ = 632.8 nm) and a thermostatically controlled sample chamber. The detector was positioned at 173° for particle size distribution analysis and 13° for ζ-potential measurements. A 1 mL sample was placed in a disposable polystyrene cuvette for DLS measurements or a disposable folded capillary cell for ζ-potential analysis (with an applied voltage 40 mV). If necessary, samples were diluted in water to achieve a final concentration of 1.2 mg/mL of lipid concentration. Each reported values represents the average of three consecutive measurements at 20°C using the Zetasizer Software 7.13 (Malvern Panalytical). Particle size data, determined by intensity size-distribution, is expressed as the z-average (diameter) ± standard error of the mean (SEM) from the three measurements. The ζ-potential values were calculated using Smoluchowski model and are reported as the average ζ-potential ± SEM from the three measurements. Measurements were done by Prof. N. Ventosa' team at ICMAB-CSIC as established in J. Tomsen-Melero Doctoral Thesis (2021) (203) and (200).

4.1.4. Determination of GLA concentration in nanoGLA by RP-HPLC

The rh-GLA present in nanoGLA was quantified by Leanbio SL, manufacturers of rh-GLA, following the same methodology described in previous works (200,203). Briefly, samples were analyzed using a RP-HPLC system (Infinity 1260 II HPLC system). The analysis was performed on a Zorbax 300SB-C18 column (3.5 µm, 4.6 x 150 mm) equipped with a UV-detector (λ=215 nm) (Agilent Technologies) at 60 ºC. NanoGLA was diluted with water to approximately 20-30 µg/mL of rh-GLA before being dispersed in an organic mixture containing acetic acid (AcOH, 0.010 M, pH = 5.5) and methanol (MeOH) in 1:1:1 volume ratio (sample:AcOH:MeOH). Samples were prepared in replicates, filtered through 0.22 µm polytetrafluoroethylene (PTFE) filter and injected (100 µL) into the HPLC system, operating at a flow rate 1 mL/min. The mobile phase A was a mixture of 95% water, 5% acetonitrile and 0.1% trifluoroacetic acid, while mobile phase B consisted of 5% water, 95% acetonitrile and 0.09% trifluoroacetic acid. Separation was achieved through a linear gradient from 0 to 60 % of mobile phase B over 30 min, followed by a cleaning step with 100 % of phase B for 5 min.

4.1.5. Determination of membrane content of nanoliposomal formulations by RP-HPLC-ELSD

Quantitative chemical analysis of nanoliposomal membrane components (i.e., DPPC, chol, ChoPEG400-RGD, and MKC) was performed by Prof. N. Ventosa's team at ICMAB-CSIC using reversed-phase high performance liquid chromatography-evaporative light scattering detector (RP-HPLC-ELSD), as established in A. Carreño's Doctoral Thesis (2024). An HPLC equipment 1260 Infinity II from Agilent Technologies (Santa Clara, USA), composed of a quaternary pump, an automatic injector, an ELSD, and a column oven where the column was placed. The ELSD is coupled to the HPLC equipment to allow component quantification and determination of purity degree. All modules were controlled using the OpenLab CDS ChemStation software.

4.1.6. DiR fluorescence quantification of nanoliposomal formulations

Fluorescence emission spectra were collected by Prof. N. Ventosa' team at ICMAB-CSIC as established in J. Tomsen-Melero's Doctoral Thesis (2021) (203) with a Varian Cary Eclipse (Agilent Technologies) fluorescence spectrophotometer.

For fluorescence spectra recording of DiR-labelled liposomes (DiR ~ 300 nM), samples (50 µL) were placed in a quartz SUPRASIL® precision cell (Hellma Analytics, High Precision Cell, quartz glass, 3 x 3 mm), and were analyzed directly, without any modification or dilution, unless otherwise noted.

Emission spectra was recorded using the following parameters: λexc = 685 nm, scanning from 720 nm to 900 nm, excitation/emission slit 5/5 nm, scan rate 60 nm/min, averaging time 1 s, data interval 1 nm, PMT detector voltage High option, S/N mode with S/N 1000 and time out 1.000 s.

4.1.7. Stability of the enzymatic activity in nanoGLA and free rh-GLA

Nanoliposomes and free rh-GLA were stored at 2-8°C for 2 weeks. During this period, all experiments related to the use of nanoliposomes in this thesis were conducted to ensure optimal quality of the NPs. Enzymatic activity (EA) of nanoGLA and free rh-GLA was evaluated on days 0, 6 and 13 of storage at 2-8°C using the same protocol described in section 10.5. EA of each sample was normalized to that quantified on day 0 (% of EA) to observe the loss of activity over time. Alagsidase alfa (Agal. A) and empty nanoliposomes formulations were included in every assay as positive and negative controls, respectively.

4.2. Characterization of the protein corona in the nanoliposomal formulations after incubation with mouse plasma

4.2.1. Plasma source and obtention

Plasma was obtained via intracardiac puncture from male C57BL6 mice (4 to 5 months old). This procedure was previously approved by the ethics committee of the Vall d'Hebron Animal Experimentation Ethics Committee and the Catalan government (CEA-OH/9572). Mouse blood was collected in Microvette® K3 EDTA tubes (Sarstedt) following manufacturer's instructions and centrifuged (800 x g) for 10 min at 4°C. Then, different plasma samples were pooled and stored at -80°C.

4.2.2. Formation of the protein corona in nanoliposomes

For the protein corona (PC) formation, different liposomal formulations were diluted with PBS 1X to a final lipid concentration of 0.24 mg/mL and incubated with mouse plasma (v/v), which had been previously centrifuged at 1,000 x g for 15 min at 4°C. The mixture was incubated at 37°C under shaking conditions (300 rpm) for a selected period of time (0.5, 1, 2, 3, 6 or 24 h).

4.2.3. Isolation of PC-nanoliposomal complexes by size exclusion chromatography (SEC)

Different DiR-labelled liposomal formulations at a lipid concentration of 0.24 mg/mL were incubated with mouse plasma for 1h at 37°C in shaking conditions (300 rpm). Subsequently, 1 mL of protein corona-liposomes samples from each formulation were isolated by size exclusion chromatography (SEC) using an Automatic Fraction Collector (AFC) with a qEV1 35 nm column (Izon Science Limited), in accordance with the manufacturer's instructions. Filtrated PBS 1X was used as the elution buffer. Thirty fractions of 0.5 mL were collected, and the DiR fluorescence intensity was measured using a multimode microplate reader (Thermo Scientific™ Varioskan™ LUX multimode microplate reader). The fractions with the highest fluorescence intensity were pooled for further characterization of their protein corona composition. Samples were stored at -80°C.

4.2.4. Cryo-TEM

Morphometric analysis of purified nanoliposomes with or without previous incubation with mouse plasma was performed using CryoTEM at Servei de microscòpia i Difracció de Raigs X of UAB. A 3 µL sample drop was placed onto holey carbon on a 400-mesh copper grid, previously treated by glow discharge. The grid was then mounted on a plunger (Leica EM GP), excess water was removed by blotting with filter paper, and sample was rapidly vitrified through immersion in liquid ethane. The sample was transferred to a Gatan 626 cryo-transfer system and inserted into a Jeol JEM 2011 Cryo-electron microscope. It was operated at 200 kV, and varying degrees of defocus (500–900 nm) were used to achieve optimal phase contrast. Images were captured with a Gatan Ultrascan US1000 CCD camera and subsequently processed using ImageJ NIH software (204).

4.2.5. Proteomic analysis of the composition of the PC

Samples preparation and protein quantitative analysis were performed by Dr. Francesc Canals' team (Proteomics group) at VHIO following their established and published methodologies (205,206), which will be briefly explained in the following sections.

4.2.5.1 Sample preparation and trypsin in-gel-digestion

Fractions of the SEC chromatography containing purified liposomes were pooled and SDS was added to 0.1% (w/v). The pooled samples were then concentrated by ultrafiltration using 3 kDa cut-off Amicon Ultra devices (Merck Millipore). Total protein content was quantified using the RC DC™ (reducing agent and detergent compatible) protein assay kit (Bio-Rad). A total of 10 µg of each sample were then run on a 10% SDS-PAGE gel. The gels were stained with colloidal Coomassie blue to visualize the proteins and acrylamide sections containing the protein mixtures were isolated.

Gel fragments were cut into small pieces, washed with 200 µL of 50 mM ammonium bicarbonate/50% ethanol 200 µL for 20 min and dehydrated with 200 µL of ethanol for 20 min. Reduction and alkylation was performed by incubating samples with 200 µl of 10 mM DTT in 50 mM ammonium bicarbonate for 1 h at 56°C, followed by alkylation with 200 µL of 55 mM Iodoacetamide in 50 mM ammonium bicarbonate for 30 minutes, protected from light. The gel pieces where then washed with 200 µL of 25 mM ammonium bicarbonate for 20 min, and dehydrated with 100 µL of acetonitrile for 10 min. Enough volume of 2.7 ng/µL trypsin (Promega)

in 25 mM ammonium bicarbonate solution was added to rehydrate and fully cover the acrylamide pieces. Trypsin digestion was run overnight at 37°C. Peptide extraction was carried out by addition of half of the digestion volume of acetonitrile, followed by incubation for 15 min at 37°C, and then addition of 300 µL of 0.2% TFA, and further incubation for 30 min at RT. The eluted peptides were dried in a SpeedVac and stored at -20°C until further analysis.

4.2.5.2 Liquid chromatography-mass spectrometry (LC-MS) analysis

Samples were analyzed using a Orbitrap Eclipse mass spectrometer (Thermo Fisher Scientific) coupled to an EASY-nLC 1200 (Thermo Fisher Scientific). Peptides (2 µg) were loaded directly onto the analytical column and were separated by reversed-phase chromatography using a 50-cm column with an inner diameter of 75 µm, packed with 2 µm C18 particles.

Chromatographic gradients started at 95% buffer A and 5% buffer B with a flow rate of 300 nl/min for 5 min and gradually increased to 25% buffer B and 75% A in 78 min and then to 40% buffer B and 60% A in 12 min. After each analysis, the column was washed for 10 min with 10% buffer A and 90% buffer B. Buffer A: 0.1% formic acid in water. Buffer B: 0.1% formic acid in 80% acetonitrile.

The mass spectrometer was operated in positive ionization mode with nanospray voltage set at 2.4 kV and source temperature at 305°C. The acquisition was performed in data-dependent acquisition (DDA) mode and full MS scans, with 1 micro scans at resolution of 120,000, were acquired over a mass range of m/z 350-1400 with detection in the Orbitrap mass analyzer. Auto gain control (AGC) was set to 'standard' and injection time to 'auto'. In each cycle of data-dependent acquisition analysis, following each survey scan, the most intense ions above a threshold ion count of 10,000 were selected for fragmentation. The number of selected precursor ions for fragmentation was determined by the "Top Speed" acquisition algorithm and a dynamic exclusion of 60 s. Fragment ion spectra were produced via high-energy collision dissociation (HCD) at normalized collision energy of 28% and they were acquired in the ion trap mass analyzer. AGC and injection time were set to 'Standard' and 'Dynamic', respectively and isolation window of 1.4 m/z was used.

4.2.5.3 Protein identification and quantitative analysis

LC-MS data was analyzed using Proteome Discoverer software (v. 2.5, Thermo Fisher Scientific) (207), following a specific workflow outlined in Fig. 4.1. Three replicates of every sample (except for the plasma without nanoliposomes) were analyzed. The process begins with peptide sequence determination from fragmentation spectra data, followed by reconstruction of these sequences into original proteins by searching a target database derived from in silico digestion of protein sequences. A peptide spectrum match (PSM) score is then calculated for each spectrum, comparing it with theoretical fragmentation data. Mascot software (208) is used to generate a probability-based score for protein identification by combining mass measurements, peptide molecular weights, and tandem mass spectrometry data. Tolerances for precursor and fragment mass are crucial parameters that affect peptide candidate selection and matching accuracy. To minimize false discovery rates (FDRs), a second search against a decoy database is performed, removing low-confidence identifications and ensuring a higher percentage of true positive results.

In this thesis, proteins were identified using Mascot (v. 2.5. Matrix Science) (208) to search a database constructed with *Mus musculus* proteins from the Swissprot database plus AGAL

HUMAN protein, P06280. MS/MS spectra were searched with a precursor mass tolerance of 10 ppm, fragment tolerance of 0.5 Da. Trypsin was selected as the enzyme allowing up to two missed cleavages. Cysteine carbamidomethylation was set as fixed modification and methionine oxidation as variable modification. Identifications were filtered at less than 1% FDR as evaluated by searching a decoy database.

Quantification of protein abundances was performed by label-free method based on the sum of the peptide ion peak areas of the corresponding MS extracted ion chromatograms. Only unique peptide signals were used for quantification. In label-free quantification, spectra for various samples are obtained through individual LC-MS/MS experiments. Nevertheless, this approach can lead to unwanted variations, including discrepancies in chromatographic measurements across different experiments. To mitigate this problem, intensity normalization can be applied. In this case, measured abundances were normalized on the basis of total peptide signal for each sample, obtaining the relative abundance of each protein.

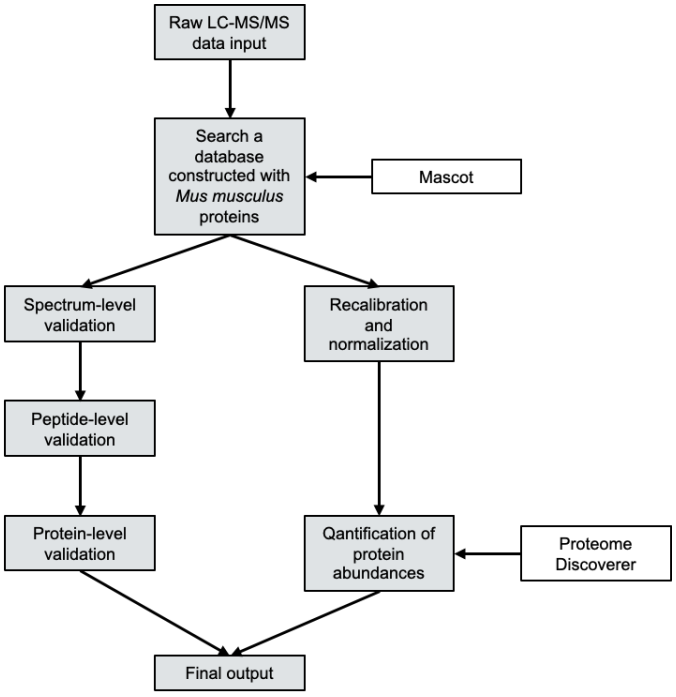

Fig. 4.1. **Schematic workflow of proteomic analysis used for the quantification of protein abundances**. Figure adapted from (209).

The relative abundances of the 25 most abundant proteins in the samples from the different nanoliposomal formulations were compared to those in plasma without nanoliposomes, with the goal of identifying the proteins enriched in the PC of the nanoliposomes. Proteins with a grater fold change than 1.1 compared to plasma were considered enriched in the PC of the different nanoliposomes.

To identify proteins whose relative abundance changed due to the presence of RGD, including apolipoproteins, complement factors and immunoglobulins, we selected those exhibiting a fold change > 1.1 in abundance in all of the following comparisons: EL-3%RGD vs. EL-0%RGD, EL-6%RGD vs. EL-0%RGD, EL-6%RGD vs. EL-3%RGD, nanoGLA-3%RGD vs. nanoGLA-0%RGD, nanoGLA-6%RGD vs. nanoGLA-0%RGD and nanoGLA-6%RGD vs. nanoGLA-3%RGD. Additionally, to identify proteins whose relative abundance changed due to the presence of rh-GLA on

nanoliposomal surface, we selected only those exhibiting a fold change greater than 1.1 in abundance in all of the following comparisons: nanoGLA-0%RGD vs. EL-0%RGD, nanoGLA-3%RGD vs. EL-3%RGD and nanoGLA-6%RGD vs. EL-6%RGD.

4.3. Isolation of EV-GLA from CHO DG44 and HEK 293F cell lines

4.3.1. Stable expression of GLAcmycH6

The GLA gene construct used to obtain the CHO cell stably expressing GLA was described previously by Prof. José Luis Corchero from IBB-UAB (210,211). It expresses the full-length human GLA gene (UniProt P06280; AGAL_HUMAN) with the c-myc and hexahistidine (6-His) tags fused to their C-terminus for detection and purification purposes (178). The transgene was cloned in a pOptiVEC™-TOPO® plasmid (Invitrogen, Themofisher) (Fig. 4.2). In the resultant expression vector pOptiVEC-GLAcmycH6, GLA production is under the control of cytomegalovirus (CMV) promoter. This vector also allows the expression of dihydrofolate reductase (DHFR) as auxotrophic selection marker in CHO DG44 (DHFR-) cells (a dihydrofolate reductase deficient cell line) (Table 4.1) and thus the selection of GLA expressing cells by using methotrexate hydrate (MTX, Sigma). A single clone (namely CHO-DG44-GLA clone #3) was isolated and used for further studies in this thesis and other published works (178).

4.3.2. Transient gene expression (TGE) of GLAH6

GLAH6 synthetic sequence (UniProt P06280; AGAL_HUMAN) was cloned by in-fusion methodology in a pTriEx-2 (Novagen) derivative expression vector called pOpinE by Prof. Corchero. The resultant expression vector pOpinE-GLA encodes the human GLA gene sequence containing a 6-His tag fused to its C-terminus (Fig. 4.2). In pOpine-GLA expression vector, GLA production is under the control of cytomegalovirus (CMV) immediate-early enhancer fused to chicken β-actin (CBA) promoter. For the obtention of SNs with GLAH6 and EV-GLAH6, HEK cells (Table 4.1) were transfected at 1 x 10^6 cells/mL with polyethyleneimine (PEI) (Polysciences) and a mixture of pOpinE-GLA and pADVantage™ (Promega) plasmids at 0.5 and 0.25 µg pDNA/million cells, respectively (210). The addition of pADVantage™ vector (GenBank® Accession Number U47294) was purposed to enhance protein expression by increasing translation initiation in cells transiently transfected (212). Nanoconjugates of pDNA and PEI were mixed following pDNA:PEI ratio of 1:3 (w/w) and added dropwise to cells. In addition, valproic acid (VPA, Merck) was added to cells at a final concentration of 4 mM after 4 h post-transfection, to enhance recombinant protein expression. Cells were maintained and grown in FreeStyle™ Expression medium (Thermo Fisher Scientific), at 37 ºC in an 8 % CO2 atmosphere with gentle shaking (120 rpm).

4.3.3. Co-transfection of HEK 293F for the obtention of rF7-EV-GLAH6

The F7 peptide (LKWWCRGAIWRDCKILVKTS), a cell-penetrating sequence developed by our research group (213), was incorporated into the surface of EVs by introducing its sequence into the N-terminal domain of the EV membrane protein lysosome-associated membrane glycoprotein 2 (Lamp2b) (UniProt P13473-2; LAMP2_HUMAN), immediately following the signal peptide sequence. This strategy, previously described by other researchers (183), facilitates the display of the sequence of interest on the outer surface of the EV membrane.

The F7-Lamp2b fusion construct was cloned into a pcDNA3 vector (Invitrogen) by GeneArt under the control of a CMV promoter to promote strong transcription and efficient protein expression. The resulting expression plasmid, consisting of 6647 base pairs, was designated pcDNA3-F7-Lamp2b (Fig. 4.2).

All transfection procedures and cell maintenance were conducted by Prof. Corchero at UAB, as previously described. In detail, HEK 293F cells (Table 4.1) were co-transfected with pOpinE-GLAH6, pcDNA3-F7-Lamp2b and pADVantage™ (Promega) plasmids at a 4:1 DNA ratio. Transfection was performed using PEI as the transfection reagent, with 0.4 µg and 0.1 µg of plasmid DNA per million cells, respectively, in FreeStyle™ Expression medium. Additionally, VPA was applied to enhance protein expression.

Isolation of F7-functionalized EV-GLAH6 (rF7-EV-GLA) was conducted at VHIR.

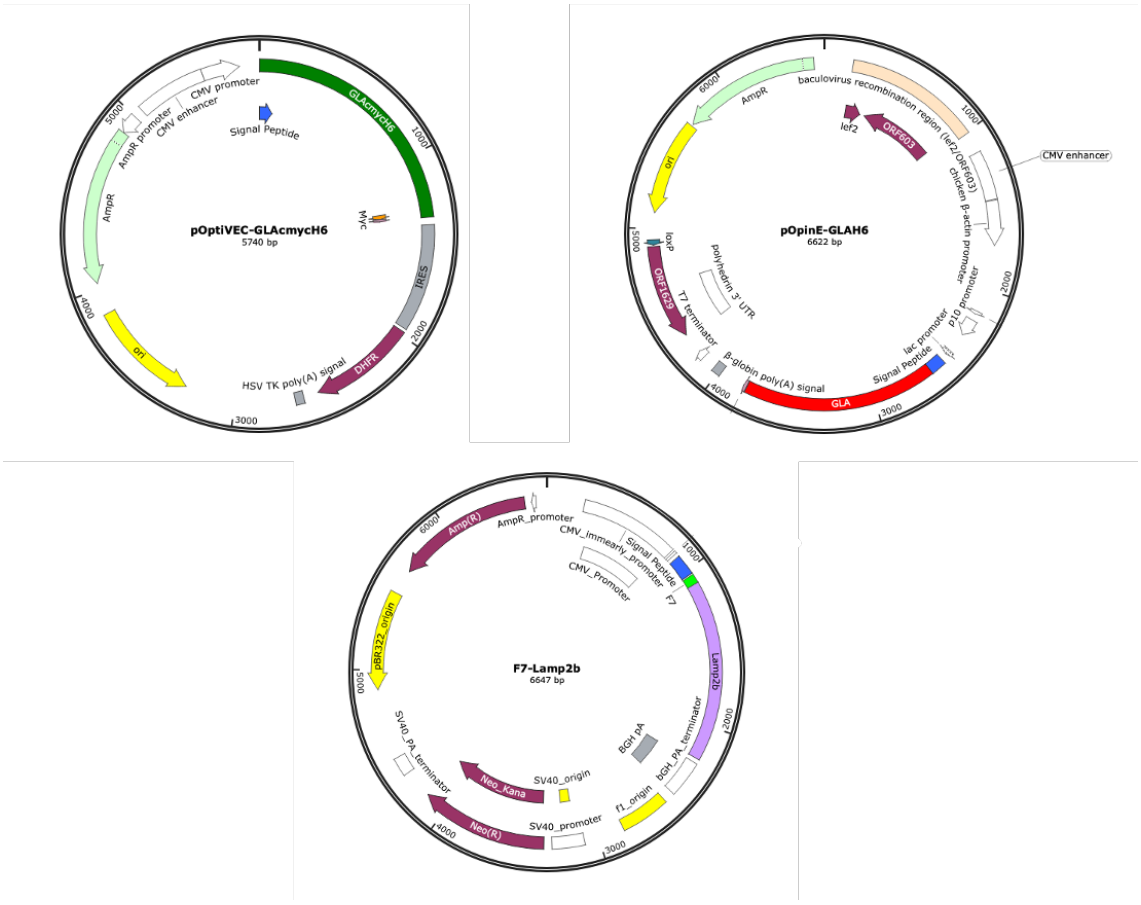

Fig. 4.2. **Schematic representation of pOpinE-GLAH6, pOptiVEC-GLAcmycH6 and F7-Lamp2b plasmids.**

4.3.4. Purification of GLAcmycH6 and GLAH6 by His-affinity chromatography

Purification of His-tagged GLA enzymes from cell SNs was performed in IBB-UAB facilities by Prof. Corchero, using an affinity chromatography with a HisTrap™ Excel column (GE Healthcare), such as ÄKTA start™ chromatography system (Cytiva), according to the manufacturer's instructions. Briefly, supernatant was directly injected to the column and later eluted by applying an imidazole gradient (20 to 500 mM). Protein was dialyzed against 0.01 M acetic acid

(pH 5.5), centrifuged (3900 rpm, 15 min) and filtered (0.2 µm) to discard putative aggregates. Purified enzyme was stored at -80◦C for further uses.

4.3.5. Isolation and purification of EV-GLAcmycH6 by precipitation

This procedure was adapted from previous publications of the group (178). Briefly, SNs coming from CHO-DG44-GLA clone #3 containing EVs and free GLAcmycH6 were harvested by centrifuging the cell culture at 3,900 rpm for 15 min. SN were centrifuged at 300 x g at 4°C for 10 min to remove dead cells. Additional centrifugation steps at increasing centrifugation speed 2,000 x g, 10 min 4°C and 10,000 x g 20 min 4°C were carried out to remove potential sub-cellular debris. Clarified SNs were concentrated 100X via VIVAspin 300 kDa (Sartorius) concentrators using mild centrifugation (300 x g) for 10 min at 4°C. EV-GLAs were precipitated from concentrated SNs through the addition 1:0.5 (v/v) of 'Total Exosome Isolation Reagent' (Invitrogen) and overnight incubation at 4°C. Samples were centrifuged at 16,000 g for 1 h at 4°C and pellets containing the EV-GLAs resuspended in filtered PBS 1X.

4.3.6. Isolation of EV-GLA by benchtop filtration

This procedure was performed following the steps detailed by Tan et al (214). Briefly, SNs from CHO and HEK cells containing EVs and free GLA were centrifuged at 300 x g at 4°C for 10 min to remove dead cells. Additional centrifugation steps at increasing speeds (2,000 x g for 10 min and 10,000 x g for 20 min at 4°C) were carried out to remove potential sub-cellular debris. SNs were concentrated using Centricon Plus-70 centrifugal filters (100 kDa) (Millipore) at 3,500 x g for 20 min at 4°C. The concentrated sample was then recovered by reverse centrifugation (1,000 x g) for 2 min at 4°C to obtain uncleaned EV-GLA. Then, cold PBS 1X was added and sample was concentrated (3,500 x g for 20 min at 4°C) to a final volume of ~1.2 mL, which was further purified by SEC (see section 4.3.8).

4.3.7. Isolation of EV-GLA by tangential flow filtration

SNs from CHO and HEK cells were centrifuged (300 x g) at 4°C for 10 min to remove dead cells. Additional centrifugation steps at increasing speeds (2,000 x g for 10 min and 10,000 x g for 20 min at 4°C) were performed to remove potential sub-cellular debris. Tangential flow filtration (TFF) procedure was carried out using KrosFlo KR2i TFF System (Repligen) equipped with a 500 kDa hollow fiber filter column. Depending on the initial SN volume, different hollow fiber columns were used: MicroKros column (ref. C02-E500-05-N, Spectrum Labs) with 20 cm^2 was used for SN volumes lower than 1 L, while MidiKros column (ref. D02-S500-05-N, Spectrum Labs) with 190 cm^2 was used for SN volumes exceeding 1 L. To maintain a shear rate of 2,000 s−1, the flow rate was kept constant at 50 mL/min. All samples were processed at a transmembrane pressure (TMP) of 15 psi. Samples were first concentrated 4 times, then diafiltrated 6 times in filtered PBS 1X to exchange the buffer. Sample was concentrated to a final volume of 5 mL. Further concentration was performed using an Amicon Ultra-15 (10 kDa) centrifugal concentrator (Millipore) to achieve a final volume of ~1.2 mL, resulting in partially cleaned EV-GLA, which was further purified by SEC (see section 4.3.8).

4.3.8. Purification of EV-GLA by SEC

From the 1.2 mL of EV-GLA obtained from benchtop filtration or TFF isolation, 1 mL was purified via SEC using an automated fraction collector (AFC) with a qEV1 35 nm column (Izon Science Limited), following the manufacturer's instructions. The columns were first flushed with filtered

PBS. Then, 1 mL of the EV-GLA sample was loaded onto the column, and 26 fractions of 0.7 mL each were collected, using filtered PBS as elution buffer.

The remaining 0.2 mL was diluted with 0.8 mL filtered PBS and stained with 75 µM 3,3'-Dioctadecyloxacarbocyanine Perchlorate (DiOC) (Invitrogen) and applied to the SEC column in the same conditions explained above. Collected fractions were measured in a fluorimeter (TECAN Spark®) to identify the presence of DiOC-stained EVs. The three fractions with the highest fluorescence were pooled here and also in equivalent non-stained samples. Pooled samples were concentrated to 0.5 mL using 3 kDa cut-off Amicon Ultra concentrators (Millipore).

4.4. Characterization of EV-GLA from CHO DG44 and HEK 293F cell lines

4.4.1. Nanoparticle Tracking Analysis (NTA)

Particle size distribution and concentration were analyzed by Nanoparticle Tracking Analysis (NTA) and was performed by U6 of ICTS Nanbiosis at ICMAB-CSIC using a Nanosight NS300 (Malvern Panalytical, Malvern, UK) and following the same procedure detailed in (178). The sample was appropriately diluted in PBS to adjust the particle concentration per frame to the working range of the system (10^6–10^9 particle/ml). A total of 3 videos were captured at a cell temperature of 21-24.5°C and a syringe speed of 30. A total of 1498 tracks were acquired per video. Data was further processed using NanoSight Software NTA 3.4 Build 3.4.4 with a detection threshold set at 5.

4.4.2. EV-GLAH6 and rF7-EV-GLAH6 processing for transmission electron microscopy (TEM) analysis

Transmission electron microscopy (TEM) visualization of EVs was performed at Servei de microscòpia i Difracció de Raigs X of the UAB, using a 80 kV – 120 kV JEM-1400 TEM model (Jeol Ltd.). For sample preparation, a 12 µL drop of 2% uranyl acetate (Sigma) was placed on a clean, stretched parafilm. Then, a 10 µL drop of the EV sample was added onto the same parafilm. A formvar carbon grid (Sigma) was placed on top of the sample drop and left to sit for 2 min. The grid was then dried by gently touching a filter paper and placed on top of the uranyl acetate drop for 1 min and then dried again.

4.4.3. Molecular characterization of EVs by western blot (WB)

EVs or cell lysates were prepared by diluting 1:5 in CelLytic reagent (Sigma), homogenized by 2 cycles of 15 s of sonication at 80% amplitude using Labsonic® M (Sartorius Biotech) device. Total protein amount was quantified by micro-BCA method (Pierce). Specific antibodies against GLA (ref. ab168341, Abcam), CD63 (ref. 10628D, Invitrogen), CD81 (ref. sc-7637, Santa Cruz Biotechnology), TSG101 (ref. ab30871, Abcam), Alix (ref. ab76608, Abcam) and Lamp2B (ref. ab18529, Abcam) and β-tubulin (ref. MA5-16308, Invitrogen) were used to characterize EVs. A total of 12 µg of protein was loaded per lane in a TGX Stain-Free™ FastCast™ Acryladmide gel (BioRender), except for the WB characterization of EV-GLAH6 and rF7-EV-GLAH6 (section 7.5) in which 2 µg of total protein were employed to detect GLA, Alix and Lamp2B, and 1.5 µg for CD81. Secondary HRP-conjugated antibody, diluted 1:10,000, was used for protein detection (ref. P0447, Dako for CD63, CD81 and β-tubulin and ref. P0448, Dako for GLA, TSG101, Alix and Lamp2b). Images were acquired with ImageQuant™ Las4000.

4.4.4. Determination of GLA concentration in EV-GLA by enzyme-linked immunosorbent assay (ELISA)

Quantification of GLA protein was performed by ELISA using specific anti-GLA antibodies with the sandwich method following previously standardized methodology (200). First, 96-well Nunc® MaxiSorp (Thermo Scientific™) plates were coated with 50 µL of mouse anti-GLA (1:1,000, ref. ab169315, Abcam) in Coating Solution (0.1 M sodium bicarbonate pH 9.0) overnight at 4°C and then blocked using 200 µL SuperBlock® (Thermo Fisher™) for 2 h at room temperature (RT) in agitation. Then, samples were added and incubated in agitation 1 h at RT. Then, sheep polyclonal antibody against GLA (1:200, AF6146, R&D Systems) was added and incubated for an additional 1 h to complete the sandwich. Finally, HRP-linked anti-sheep IgG (1:5000, A3415, Sigma) was used to visualize the GLA content with 3,3',5,5'-Tetramethylbenzidine (TMB) (Sigma). HPR reaction was stopped by adding 50 µL of 0.5 M sulfuric acid and results were quantified by measuring absorption at 450 nm using the microplate reader Epoch (BioTek). Samples were analyzed in triplicates. Dilutions of samples and standard (GLAcmycH6 or GLAH6, 0-500 ng/mL) were prepared in Low Cross Buffer (Thermo Fisher™) containing 2% (w/v) Triton X-100. (Sigma) Washing steps were conducted using 0,05% Tween-20/PBS. GLA concentration EV samples were determined in each assay by interpolating the absorbance values to a sigmoidal four-parameter logistic (4PL) curve using GraphPad Prism 9.2.0. The goodness of the fit and replicates was ensured also in each assay ($R2 > 0.98$ and $p > 0.05$ for regression and lack of fit, respectively).

4.4.5. Determination of GLA enzymatic activity in EV-GLA

EVs were lysed by diluting 1:5 in CelLytic reagent (Sigma) and homogenized by 2 cycles of 15 s of sonication at 80% amplitude using Labsonic® M (Sartorius Biotech) device. Then, EA was determined following the protocol detailed in section 4.5.

4.5. GLA specific enzymatic activity

GLA enzymatic activity was assayed using fluorometric methods initially described by Desnick e*t al.* (215) with the modifications of Mayes *et al.* (216), and applied in other publications of our research group (178,200). Briefly, the EA assay is based on the conversion of a non-fluorescent substrate (4-MUG) into a fluorescent product 4-methylumbelliferone (4-MU) by active GLA. The protocol included the use of 4-methylumbelliferyl α-D-galactopyranoside (4-MUG) (Sigma Aldrich) as substrate (10 mM) in assay buffer (0.01 M acetic acid, 0.01 M acetate, pH 4.5). A typical assay reaction mixture contains 100 µL of 4-MUG and 25 µL of the sample. Enzymatic reactions took place in agitation (GLS Aqua 12 Plus) at 25 rpm, 37°C for 1 h. The reaction was stopped by glycine buffer (1.25 mL, 0.2 M, pH 10.4) and the released 4-MU was determined by fluorescence measurement (λexc = 365 nm, λem = 450 nm) using a microplate fluorescence reader (FLx800™, Biotek™). Two dilutions of each sample were made, and each dilution was analyzed in duplicate to reduce the variability of the quantification. Commercial product 4-MU (Sigma Aldrich) ranging from 5 to 500 ng/mL in glycine buffer was used to obtain a calibration curve to transform fluorescence readings into product 4-MU concentration. Measurements were adjusted per time and protein quantity.

4.6. *In vitro* cell internalization in endothelial cells

4.6.1. Cell culture

HMEC-1 cells (CRL-3243, ATCC) (Table 4.1) were maintained in MCDB-131 medium (Corning®) supplemented with 10% of hiFBS (Gibco™), 2 mM L-glutamine (Gibco™), and 1X antimycotic-antibiotic solution (Gibco™) at 37°C and 5% CO_2.

Mouse endothelial aortic cells (MAEC) were isolated from descending aorta of C57BL6 GLA deficient mice (Gla^{tmKul1}) (Table 4.1) (217) following previously established procedures (218–220). This procedure was previously approved by the Ethic Committee for Animal Experimentation of VHIR institution (CEEA) with the procedure code of 22/15. Endothelial origin of isolated cells was confirmed by CD105 staining (12-1051, eBioscience) and flow cytometry (LSRFortessa™, BD Biosciences). These cells were maintained in RPMI 1640 medium (Gibco™) supplemented with 25% of heat-inactivated FBS (hiFBS) (Gibco™), MEM Non-essential aminoacids (1X) (Gibco™), 2 mM of L-Glutamine (Gibco™), Antibiotic-Antimycotic (1X) (Gibco™), heparin at 6 µg/mL (Sigma), hydrocortisone at 50 µg/mL (Sigma) and Endothelial Cell Growth Supplement (ECGS) at 500 µg/mL (Corning™).

Table 4.1. **Summarizing table containing relevant information about the cell lines used in this thesis**, including their origin and type, source species, key characteristics their specific applications.

Cell Line	Origin	Cell type	Species	Characteristics	Application/Scope in Study
CHO DG44	Chinese hamster ovary	Ovarian cell line	Hamster	Immortalized cells with the ability to grow in suspension culture under serum-free conditions and commonly used for stable recombinant protein production	Production of GLAcmycH6 and EV-GLAcmycH6 through stable expression of GLAcmycH6
HEK 293F	Human embryonic kidney	Kidney	Human	Immortalized cells with the ability to grow in suspension culture under serum-free conditions and widely used for transient transfections	Production of GLAH6, EV-GLAH6 and rF7-EV-GLAH6 through transient expression of GLAH6 and F7-Lamp2b
HMEC-1	Human microvascular endothelial cells	Microvascular endothelial cells	Human	Immortalized endothelial cells with GLA expression	Internalization studies using flow cytometry and confocal microscopy
MAEC	Murine aortic endothelial cells from GLA deficient mouse	Aortic endothelial cells	Mouse	Primary, non-immortalized endothelial cell line from GLA deficient mice	Internalization studies by blocking M6PR and *in vitro* efficacy due to their lack of functional GLA expression

4.6.2. Internalization in HMEC-1 by flow cytometry

For internalization assay using nanoliposomes, HMEC-1 were seeded in 24 well plates and incubated overnight at 37°C and 5% CO_2. Then, DiR labelled nanoliposomes at 0.05 mg/mL of lipid concentration were added to HMEC-1 cultures and incubated for 0.5, 1 and 6 h at 37 °C. In contrast, for DiOC labelled EVs, HMEC-1 cells were incubated with $1{\cdot}10^8$ EVs/mL for 3 h at 37 °C. After incubation, plates were treated with trypsin 0.05 % (w/v) (Gibco™) to detach cells and neutralized in complete MCDB-131 medium supplemented with 7-aminoactinomicina D (7AAD) (Life Thechnologies) (5 µg/mL final concentration), in order to remove dead cells from analysis.

Percentage of DiR or DiOC positive cells and cell median fluorescence intensity (MFI) were determined by flow cytometry using a LSRFortessa™ (BD Biosciences) instrument and FlowJo™ v10 analysis software.

4.6.3. Internalization in HMEC-1 by confocal microscopy

HMEC-1 cells were seeded in an 8-well m-slide (Ibidi GmbH) pre-coated with poly-L-lysine solution (Sigma) and incubated overnight at 37°C and 5% CO_2. Then, DiR labelled nanoGLA with 0%, 3% or 6% of RGD at 0.05 mg/mL of lipid concentration were added and incubated for 1 and 6 h. Cell medium was removed and cells were stained with 1 µM LysoTracker® Green DND-26 (Invitrogen) during 30 min at 37°C. Image acquisition was carried out by confocal microscopy "widefield" multidimensional Thunder Imager 3D Cell Culture (Leica) with a HC PL APO 40x/0.95 DR, using the following optical settings:

- DiR: 35% power 747 nm excitation LED, CYR71010 filter cube set, 100% high-speed emission wheel (excitation filter: 730-740; dichroic filter: 763; emission filter: 770-840).
- LysoTracker® Green DND-26: 15% power 475 nm excitation LED, DFT51010 filter cube set, 535/70 high-speed emission wheel (excitation filter: 446-512; dichroic filter: 500; emission filter: 494-544).

Z projections sections were acquired with a step size of 0.5 µm and further reconstructed using Fiji ImageJ (221).

4.6.4. Uptake of nanoGLA by blocking M6PR in MAEC cells

MAEC from GLA deficient mice (see section 4.6.1.) at passages 2 to 5 were seeded in 24 well plates and were incubated overnight at 37°C and 5% CO_2. Then, cells were treated with 1 µg/mL of equivalent GLA concentration of free rh-GLA, nanGLA-0%RGD and nanoGLA-3%RGD, in the presence or absence of 5 mM M6P, following adapted protocols described by other authors (222,223). After 6 h of incubation at 37°C and 5% CO_2, the plates were washed twice with PBS 1X and treated with trypsin 0.05 % (w/v) (Gibco™) to detach cells, which were then neutralized in complete MCDB-131 medium. The cells were then pelleted by centrifugation (180 x g) at 4°C, and the medium was replaced with sterile MQ water. Cells were lysed by 2 cycles of 15 s of sonication at 80% amplitude using Labsonic® M (Sartorius Biotech) device. Next, intracellular GLA enzymatic activity was quantified using the method described previously in section 10.5 (200). Samples were analyzed in triplicates. Ratio of internalization was calculated dividing the intracellular enzymatic activity in presence of M6P by that found in the absence of M6P for each treatment (rh-GLA, nanoGLA-0%RGD and nanoGLA-3%RGD).

4.6.5. Internalization in HMEC-1 using endocytosis inhibitors by flow cytometry

For nanoliposomes, HMEC-1 were seeded in 24 well plates and incubated overnight at 37°C and 5% CO_2. Next, HMEC-1 cell cultures were pre-treated for 30 min with or without the following endocytosis inhibitors at two different concentrations: Dyn (50 and 100 µM) (Sigma), EIPA (75 and 100 µM) (Sigma), Nys (25 and 50 µM) (Sigma), and CPZ (10 and 20 µM) (Sigma). Then, HMEC-1 cells were incubated for 6 h with DiR labelled EL-0%RGD, EL-3%RGD and nanoGLA-3%RGD at 0.05 mg/mL of lipid concentration. In contrast, for DiOC labelled EVs, HMEC-1 cells were pre-treated with only one concentration of endocytosis inhibitors (50 µM for Dyn, 100 µM for EIPA,

25 µM for Nys, and 10 µM for CPZ) and then were incubated with $1 \cdot 10^{10}$ EVs/mL for 6 h at 37 C. After incubation, cells were then detached with trypsin 0.05 % (w/v) (Gibco™) and neutralized in complete MCDB-131 medium supplemented with 4',6-diamidino-2-phenylindole, dihydrochloride (DAPI) (Thermo Scientific™) (0.2 µg/mL final concentration) to remove dead cells from analysis. Percentage of DiR and DiOC positive cells and cell median fluorescence intensity (MFI) were determined by flow cytometry (LSRFortessa™, BD Biosciences) and FlowJo™ v10 software. Samples were analyzed in triplicates.

4.7. *In vitro* efficacy in endothelial GLA KO cells

MAEC at passages 2 to 5 were seeded in 24 well plates. Twenty-four h after seeding, 0.6 µM of fluorescent N-Dodecanoyl-NBD-ceramide trihexoside (NBD-Gb3, Matreya LCC), previously conjugated to bovine serum albumin (BSA, Sigma Chemical), was added to the cultures along with specified concentrations of tested compounds. After 48 h incubation, cells were trypsinized and NBD-Gb3 fluorescent signal was analyzed by flow cytometry (LSRFortessa™, BD Biosciences) and FlowJo™ v10 software. Samples were analyzed in triplicates. To calculate the percentage of NBD-Gb3 signal, fluorescent signal in control cells (without treatment) was established as 100% and the values accordingly normalized. The efficacy of GLA in reducing the Gb3 deposits was obtained as the percentage of Gb3 loss (i.e., % Gb3 loss = 100 - % Gb3-NBD signal).

4.8. *In vivo* assays using Fabry KO mouse model

4.8.1. Fabry mouse model

Fabry mouse model was a GLA knock out (KO) mouse (Gla^{tmKul1} in C57BL6 background) that completely lacks the expression of the GLA protein (217). All animals used in this study were males, as FD is an X-linked genetic disease and males are primarily affected by this disease (224). These Fabry animals have no pathological phenotype and a normal laboratory life span (about 2 years) (217). Animals were kept at VHIR's animal facilities, under a procedure previously approved by the ethics committee of the Vall d'Hebron Animal Experimentation Ethics Committee and the Catalan government (CEA-OH/9572) and executed within the FVPR/U20 *In vivo* Experimentation Platform of ICTS Nanbiosis.

4.8.2. *In vivo* BD assay

The biodistribution assay of different versions of nanoGLA (0, 3 and 6 % RGD) was assayed in Fabry KO mice of 2.5 to 4 months. Animals were randomized by age into 4 groups of treatments: free rh-GLA (n = 6), nanoGLA-0%RGD (n = 8), nanoGLA-3%RGD (n = 8) and nanoGLA-6%RGD (n = 8). C57BL6 wild-type (WT) mice (n = 3) and non-treated Fabry KO mice (n = 3) were also included as controls (Fig. 4.3). The animals were administered with a single intravenous (i.v) dose at 1 mg/Kg of GLA or 5 mL/kg of PBS in controls by tail vein injection. Half of each group was euthanized 1 min post-administration and the other half 30 min after. Upon euthanasia, tissues such plasma, liver, spleen, kidneys, lungs, heart, brain, intestine, skin and muscle were collected for *ex vivo* BD analysis by FLI and EA.

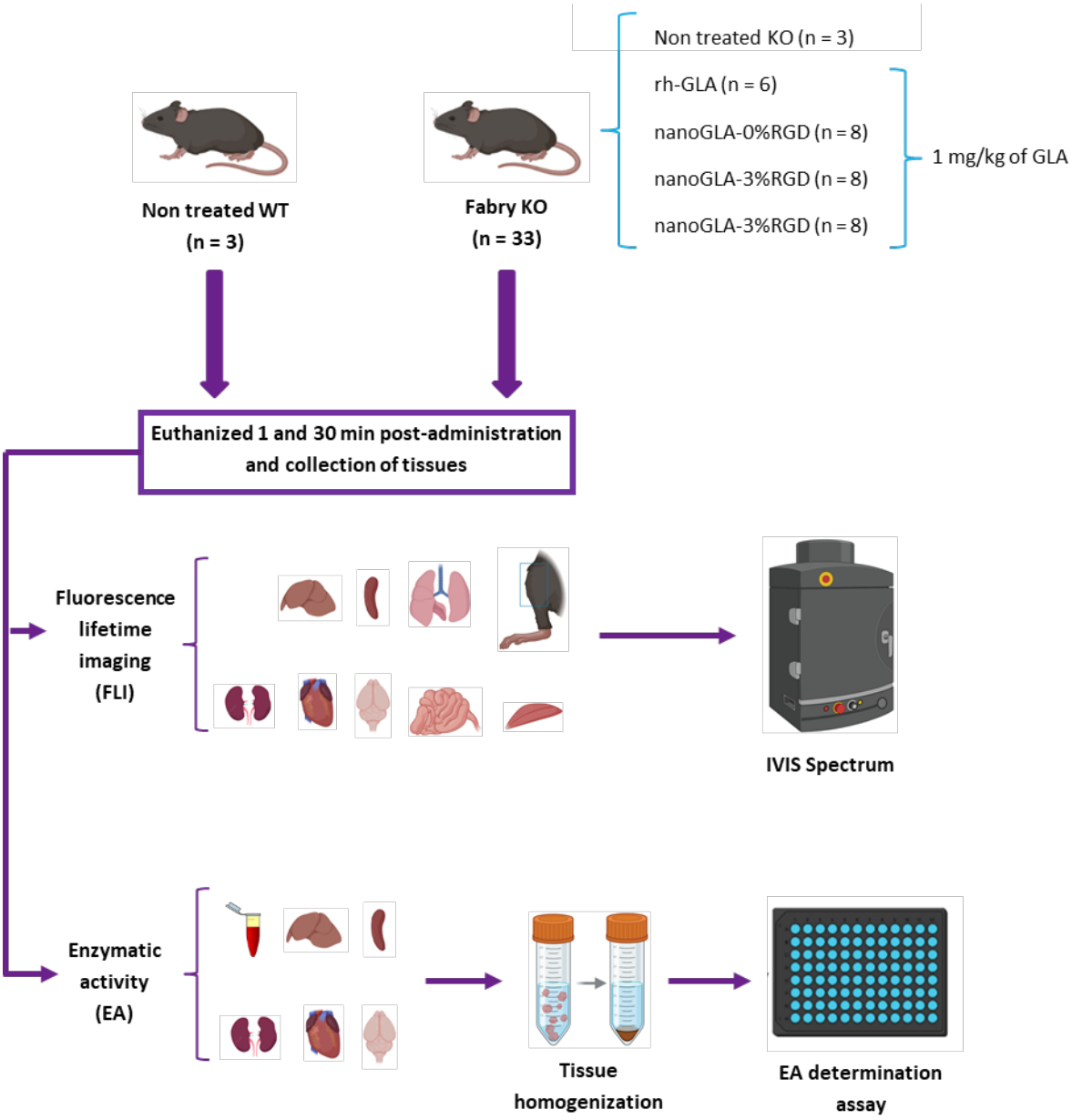

Fig. 4.3. Schematic representation of the biodistribution assay and processing of samples for the FLI and EA quantification. Randomized animals were divided into 6 groups. Knock Out (KO) for GLA were treated with 1 mg/kg of free protein (rh-GLA) or different nanoliposomes (nanoGLA). Non treated wild type (WT) and KO mice were used as a control. Animals were euthanized 1 or 30 min post-administration and plasma, liver, spleen, kidneys, lungs, heart, brain, intestine, skin and muscle were obtained.

For the *ex vivo* DiR FLI quantification, fluorescent images were acquired by IVIS® Spectrum imaging system and quantified using Living Image® 4.5.2 software (PerkinElmer). The fluorescence signal was qualitatively quantified in radiant efficiency units (a fluorescence emission radiance per incident excitation power). To calculate the % DiR FLI, radiant efficiency of each tissue was referred to the total fluorescence (sum of the FLI of all tissues).

For the quantification of the BD by EA, tissues were collected and homogenized in PBS with 1:200 of Protease Inhibitor Cocktail Set III, EDTA-Free (Millipore™) using Fast-Prep®-24 (MP™) sample disruption instrument. For that, 5 to 10 times the volume of PBS was added to each sample in 2 mL Fast-Prep tubes type (Lysing Matrix type A, MP™) and repeated homogenization cycles (5 m/s, 20 s) were applied until completed desegregation of the tissue. All the procedure

was carried out on ice. Homogenized tissues were centrifuged at 4 ºC (10 min, 16 x g) and supernatant was collected. Once tissues were homogenized, protein extraction was carried out. First, the homogenized sample and Lysis Buffer (30 µM monohydrate citric acid, 51 µM dibasic sodium phosphate and 0.17% Triton X-100 in MQ water, at pH 4.6) were mixed in 1:1 or 1:2 (v/v) (depending on the tissue). Second, after the mixture rested in ice for 30-60 min, centrifugation in maximum speed (16,1 x g) was done for 10 min at 4°C. Finally, supernatant was collected to determine the EA following the procedure previously described in section 10.5 (200). The percentage of injected dose (%ID) of enzymatic activity was calculated referring the EA (nmol/h·mg) of GLA in tissue to the activity detected in plasma samples obtained 1 min post-administration.

4.8.3. Anti-drug antibodies (ADAs) detection in KO mouse plasma

Single dose and repetated dose effiay experiments are already described by Tomsen-Melero et al (200). Briefly, for the single dose experiment, Fabry KO mice with ages ranging from 2 to 4 months were treated with Agal. A, free rh-GLA, or nanoGLA-3%RGD (n = 8 for all groups) by tail i.v. administration at 1 mg/kg of equivalent GLA. C57BL6 WT mice and non-treated Fabry KO mice were included as controls and were administered with 5 mL/kg of serum. After 1 week, animals were administered with a second dose and euthanized 1 min (n = 4/group) or 30 min (n = 4/group). Then, plasma was collected via intracardiac puncture. In contrast, for the repeated dose assay the same number of animals and group distribution were used. Fabry KO mice received eight doses of 1 mg/kg every other day and were euthanized 24 h after the last administration and plasma was also obtained via intracardiac puncture. Control animals received the corresponding volume of PBS 1X.

Detection of ADAs (IgG) in plasma from Fabry KO mice was performed adapting a protocol described by Tsukimura et al. for the detection of ADAs in serum from Fabry patients (225). A 96-well Nunc® MaxiSorp (Thermo Scientific™) was coated with 100 µL of 1 µg/mL Agal.A (Shire-Takeda) overnight at 4°C. Then the wells of the microtiter plate were washed three times with PBS 1X and blocked with 2% BSA in PBS for 1 h at room temperature (RT). Subsequently, the plate was washed three times with PBS containing 0.1% Tween-20. Then, a 100 µL aliquot of a diluted plasma sample (1:100) was applied, followed by incubation for 1 h at RT. After incubation, the plate was washed three times with PBS containing 0.1% Tween-20. Then, a 100 µL aliquot of 1:5,000-diluted peroxidase (HRP)-conjugated goat antimouse IgG antibody (Ref. 1030-05; Southern Biotech) was applied, and the plate was incubated for 1 h at RT. After incubation, the plate was washed three times with PBS containing 0.1% Tween-20, and then 100 µL of TMB ELISA Substrate Solution (Sigma) was applied and reacted for 15 min at RT. The reaction was stopped by adding 50 µL of 2M H_2SO_4, and results were quantified by measuring absorption at 450 nm using the microplate reader Epoch (BioTek). Plasma from non-treated KO mouse was used as antibody-negative control, and plasma from KO mouse treated with high doses of Agal. A (5 mg/kg) for 2 weeks, with 2 administrations per week, was included as antibody-positive control.

4.9. Statistical analysis

Whenever data followed a normal distribution (Saphiro-Wilk test) ordinary one-way ANOVA with Tukey's multiple comparisons test was used for multiple comparisons or unpaired Student's t-test was used for peer comparisons. Alternatively, when data did not follow a normal distribution, non-parametric Kruskal-Wallis test with Dunn's multiple comparisons test or non-

parametric Mann-Whitney test were applied for multiple comparisons or peer comparisons respectively. The significance threshold was established at ns ($p < 0.05$), and significance levels were schematically assigned ns($p > 0.05$), *($0.01 \leq p < 0.05$), **($0.001 \leq p < 0.01$), ***($0.0001 \leq p < 0.001$), ****($0.0001 \leq p$). All the analyses and graphs were performed using GraphPad Prism software version 9.5.0. All values were indicated as Mean ± Standard error of the mean (SEM).

In proteomic studies, statistical analysis was performed using Proteome Discoverer software (v. 2.5, Thermo Fisher Scientific). Proteins displaying greater than 1.1-fold change, and $p < 0.05$ (t-test background based) between groups were considered significantly differential.

5. RGD targeted nanoliposomes as a drug delivery systems

5.1. Introduction

It has been demonstrated that nanoliposomes loaded with GLA enzyme and decorated with cholesterol-PEG400-c(RGDfk) targeting moiety (hereafter referred to as RGD) enhance the efficacy and biodistribution of enzyme replacement therapy (ERT) in Fabry KO mice, and consequently, the delivery of the GLA enzyme to endothelial cells (226,227). However, no comparisons have been made between nanoliposomes with or without RGD or GLA to understand how their presence affects nanoliposomal cellular uptake and *in vivo* behaviour. In this section, we investigate how the functionalization with RGD targeting unit and recombinant human GLA enzyme (referred to as rh-GLA), influences nanoliposomal cell internalization, biodistribution (BD) and efficacy of these nanoliposomes.

These nanoliposomal systems are currently being investigated through various collaborative and interdisciplinary projects focused on creating a novel nanopharmaceutical to improve ERT for Fabry disease. All nanoliposomal formulations investigated in this section were designed and produced by Prof. Nora Ventosa's research group from the Institut de Ciència de Materials de Barcelona (ICMAB-CSIC).

The research presented in this section provides insights into the biological role of RGD and rh-GLA in the nanoliposome and how they may affect the nanoliposomal biological fate, contributing to the continuous optimization of this nanoparticulated system.

5.1.1. Liposomes as tools to improve enzyme delivery

Enzyme have been explored as therapeutic agents since the 19th century (151), with the first Food and Drug Administration (FDA) approved enzyme treatment, Alteplase, introduced in 1987 for treating acute ischemic stroke (228). Enzymes have significant therapeutic potential, addressing a wide range of conditions, including metabolic and inflammatory disorders, heart diseases, and even cancer (228). However, their clinical use has been hindered by challenges such as immunogenic responses, short half-life in the body, rapid degradation, and loss of activity during storage (151). To overcome these limitations and enhance the effectiveness of therapeutic enzymes, various strategies have been developed over the years, such as encapsulating enzymes in DDS (229,230).

Among all DDS, liposomes are the most widely used carriers for enzyme encapsulation (151). They offer numerous advantages over other nanocarriers, including structural versatility, biodegradability, biocompatibility, non-immunogenic and non-toxic nature. Furthermore, the encapsulation of hydrophilic molecules can be fine-tuned based on the vesicle's internal aqueous volume, which is determined by the chosen preparation method (231). Additionally, incorporating cholesterol into vesicles made from phospholipids decreases lipid bilayer permeability, a strategy commonly employed to enhance the encapsulation efficiency of hydrophilic drugs, ensuring that the loaded material remains inside the vesicles (232). Additionally, if liposomes are functionalized with PEG chains, enzymes can be also covalently

attached to this molecule to functionalize the outer surface of liposomes (233). However, this strategy can expose the enzyme to the immune system causing its recognition.

Table 5.1. Examples of pre-clinical studies using liposomes as enzymatic drug delivery systems. Adapted from Cruz et al. (151)

Enzyme	Target disease	Liposomal composition	Targeted liposome	*In vivo* outcome	Reference
Acylated L-Asparaginase	Lymphoma	EPC:Chol:PI EPC:Chol:SA	No	Enzyme loaded liposomes showed 8-fold increase in half-life (i.v.) improving antitumor effect compared to free enzyme	(234)
L-Asparaginase	Lymphoma	EPC:Chol:GM1 EPC:Chol:PI EPC:Chol:SA	No	Enzyme loaded liposomes exhibited 15-fold increase in half-life (i.v.), higher antitumor activity compared to free enzyme	(235)
	Lewis lung carcinoma	SPC:Chol:DSPE-PEG	No	L-Asparaginase liposomes improved the survival rate in mice compared to the free enzyme	(236)
Catalase	Melanoma	SPC:Chol:DSPEPEG:DSPE-PEG-NH2-aPDL1	Yes	Targeted liposomes accumulated at tumor locations, slowing tumor growth and improving the survival rate of the treated animals	(237)
Superoxide dismutase	Adjuvant rheumatoid arthritis	EPC:Chol:SA EPC:Chol:PI	No	Enzyme loaded liposomes exhibited higher therapeutic activity than the free enzyme	(238)
	Ear oedema	EPC:Chol:DSPE-PEG	No	Enzyme loaded liposomes showed higher edema inhibition compared to free enzyme	(239)
Streptokinase	Human clot inoculated rat model	DOPE:c(RGD)	Yes	Thrombolytic activity was improved when the enzyme was encapsulated into liposomes	(240)
	Thromboembolism	DSPC:Chol:DSPE-PEG	No	Encapsulation into the liposome increased blood circulation half-life of streptokinase (16-fold higher compared to free enzyme)	(241)
Urokinase	Thromboembolism	DPPC:DSPE-PEG:c(RGD)	Yes	Liposomes increased enzymatic half-life and improved thrombolytic efficacy (4-fold compared to free enzyme)	(242)
Uricase	Uric acid reduction	nanosomal microassemblies	No	Increased bioavailability and enhanced efficacy	(243)

EPC: egg phosphatidyl choline; Chol: cholesterol; PI: phosphatidyl inositol; SA: stearylamine; GM1: monosialo gangliosides; SPC: soya phosphatidyl choline; DSPE-PEG: distearoyl phosphatidyl ethanolamine covalently bunded to polyethylene glycol; DOPE: dioleoyl phosphatidyl ethanol amine; DSPC: distearoyl phosphatidyl choline; DPPC: dipalmitoyl phosphatidyl choline

Since the first encapsulation of insulin (244) and lysozyme (245) into liposomes, the entrapment of proteins and enzymes in these NPs has been continuously developed. Table 5.1 summarizes some examples of liposomes that have been pre-clinically tested as delivery systems for various enzymes, such as L-Asparaginase, superoxide dismutase, catalase, streptokinase, urokinase and uricase for the treatment of different pathologies (Table 5.1). All of them demonstrated higher enzymatic activity, greater efficacy and enhanced half-life in circulation compared to the free enzyme, showing that liposomes are effective nanocarriers for enzyme delivery (Table 5.1).

Due to their efficiency as enzyme delivery systems, liposomes have also been preclinically tested to improve ERT for treating various LSDs, including GD (246,247), Niemann-Pick disease type B (248), MPS type I (249), PD (250) and FD (200,226,251). Some of these studies are summarized in Table 5.2. Additionally, liposomes are being investigated as nanocarriers for genes encoding the deficient enzyme (non-viral gene therapy) for some LSDs, such as Sandhoff disease (252), MPS type VII (253), MPS type I (254,255) and Niemann-Pick disease type C1 (256), further demonstrating the versatility of liposomes as DDSs.

Table 5.2. Examples of pre-clinical studies using liposomes as ERT delivery systems to treat LSDs. Adapted from Tomsen-Melero et al. (10).

Target LSD	Encapsulated enzyme	Liposomal composition	Targeted liposome	*In vitro*/*in vivo* outcome	Reference
GD	Velaglucerase alfa (VPRIV™)	EPC:Chol:Rh	Yes	Improvement in cellular uptake and lysosomal localization of glucocerebrosidase-loaded targeted liposomes in Gaucher fibroblasts and macrophages, as assessed by flow cytometry and confocal microscopy.	(246)
	rh-GCase	SapC:DOPS	No	Improvement in cellular uptake of SapC-DOPS liposomes loaded with rh-GCase via an M6PR-independent pathway and *in vitro* efficacy in GCase KO mouse fibroblasts, compared to free GCase. Detection of the enzyme in brain tissue from GCase KO mice treated with the liposomal formulation through immunolabeling and enzymatic activity.	(247)
NPB	rh-ASM	DPPC:DOPS:BMP: Chol:DiD	Yes	Improvement in cellular uptake by NPB fibroblasts and macrophage-like cell lines, as well as *in vitro* efficacy through substrate clearance in NPB fibroblasts, compared to the free enzyme.	(248)
MPS I	rh-IDUA	DOPC:DOPE:Chol: GNeo:Cy5	Yes	Significant increase in cell uptake and lysosomal delivery of targeted liposomes loaded with IDUA in CHO cells and MPS I fibroblasts, compared to unmodified liposomes.	(249,257)
PD	rh-GAA	PI:DMPC:Chol	No	After administration in GAA KO mice, the immunogenicity of rh-GAA was slightly reduced due to encapsulation in liposomes, but the *in vivo* efficacy of GAA-liposomes was minimal.	(250)
FD	rh-GLA	DPPC:Chol:MKC:Chol-PEG400-RGD	Yes	The uptake of GLA-loaded liposomes targeted with RGD (nanoGLA) by endothelial cells was improved compared to non-targeted liposomes, enhancing GLA delivery to the lysosome. RGD-targeted liposomes also showed better clearance of the GLA substrate in endothelial cells derived from GLA-KO mice compared to the free enzyme. *In vivo* studies in Fabry KO mice demonstrated that nanoGLA had an extended half-life in plasma and greater efficacy in various organs, including the brain, heart, and kidneys, compared to free rh-GLA.	(200,226)
		DOPC:Chol:H16	Yes	H16-modified liposomes were internalized by HT1080 cells and localized in lysosomes. The efficacy of H16-modified GLA-loaded liposomes was tested in a GLA-KO cell line, which exhibited slower cell proliferation compared to normal cells. The results showed an increase in cell proliferation after treatment with H16-targeted liposomes loaded with GLA. These liposomes successfully delivered GLA to lysosomes, restoring enzymatic activity and enhancing cell proliferation.	(251)

EPC: egg phosphatidyl choline; Chol: cholesterol; Rh: octadecyl-rhodamine B; rh-GCase: recombinant human β-glucosidase; SapC: saposin C; DOPS: dioleoylphosphatidylserine; rh-ASM: recombinant human acid sphingomyelinase; NPB: Niemann-Pick disease type B; DPPC: dipalmitoyl phosphatidyl choline; DOPS: 1,2-dioleoyl-sn-glycero-3-phospho-L-serine; BMP: bis(monoacylgly cerol)phosphate; DiD: 1,1'-Dioctadecyl-3,3,3',3'-Tetramethylindodicarbocyanine, 4-Chlorobenzenesulfonate; rh-IDUA: recombinant human α-L-iduronidase; DOPC: 1,2-dioleoyl-sn-glycero-3-phosphocholine; DOPE: dioleoyl phosphatidyl ethanol amine; GNeo: guanidinylated neomycin; Cy5: Cyanine-5; rh-GAA: recombinant human acid α-glucosidase; PI: phosphatidyl inositol; DMPC: 1,2-dimyristoyl-sn-glycero-3-

phosphocholine; rh-GLA: recombinant human a-galactosidase A; DPPC: dipalmitoyl phosphatidyl choline; MKC: myristalkonium chloride; PEG: polyethylene glycol; RGD: Arginyl-glycyl-aspartic acid; H16: polyhistidine peptide.

5.1.2. Production of GLA loaded and RGD targeted nanoliposomes by DELOS-susp

Production methods utilizing compressed carbon dioxide (CO_2) offer a sustainable alternative to conventional techniques by eliminating the need for environmentally harmful organic solvents. This makes them safer, more energy-efficient, and resource-conserving. CO_2 stands out as an ideal solvent due to its abundance, eco-friendly nature, and low cost, making it particularly well-suited for pharmaceutical processing. Additionally, CO_2 is considered a safe solvent by the FDA, and their critical parameters (critical temp, 31.1 °C; critical pressure, 72.8 atm) make it easily accessible and user friendly when working with labile bioactive compounds, such as enzymes, proteins, and other biomolecules, helping to preserve the therapeutic integrity of biological molecules (10,201,211,258–260).

A novel CO_2-based technique, known as Depressurization of an Expanded Liquid Organic Solution-Suspension (DELOS-susp) (Fig. 5.1), was developed and patented by Prof. Nora Ventosa ICMAB-CSIC research group and currently it is exploited by Nanomol Technologies spin-off company (201). This method offers a promising one-step approach for creating homogeneous and multifunctional nanoliposomes, and enables the conjugation of active biomolecules, such as rh-GLA (201,211,227,261). Furthermore, DELOS-susp meets key criteria for clinical application of vesicle-based products, including high batch-to-batch consistency and scalability potential (211,227).

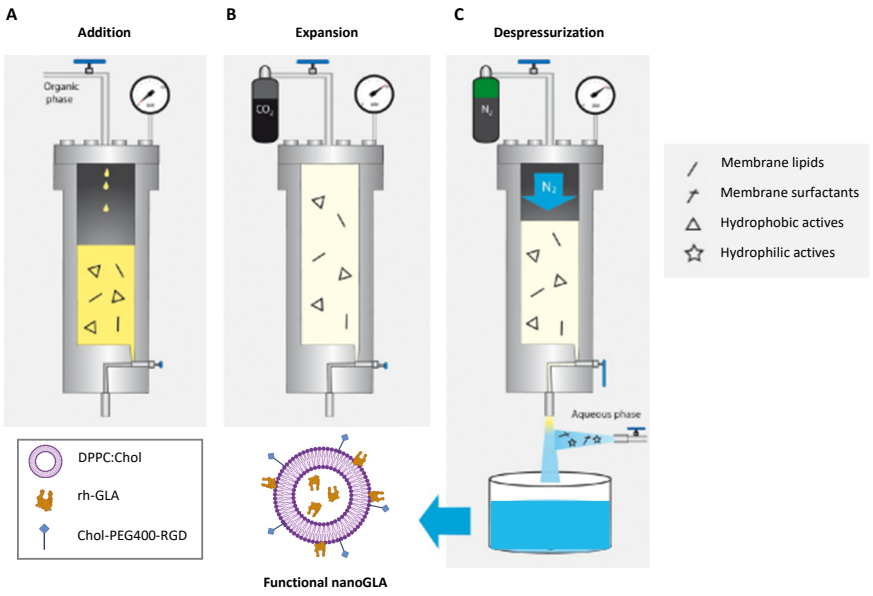

Fig. 5.1. Scheme of the nanoGLA production by DELOS-susp methodology edited from Cabrera et al. (201). **A)** Addition of organic solution containing the membrane components. **B)** Expansion of the membrane components solution by the addition of liquid compressed CO_2. **C)** Depressurization into an aqueous solution, which contain water-soluble components or hydrophilic biomolecules.

All nanoliposomes used in this thesis were produced by DELOS-susp methodology and provided by Prof. Nora Ventosa's research group (ICMAB-CSIC). Briefly, the DELOS-susp procedures includes:

1. An organic solution (typically ethanol) containing cholesterol, cholesterol derivatives, phospholipids and other hydrophobic membrane components is introduced into a high-pressure vessel, maintained at a working temperature of 35°C and atmospheric pressure (Fig. 5.1A).

2. Liquid compressed CO_2 is then added, resulting in a CO_2-expanded solution where all membrane components are dissolved. This occurs at 35°C and a working pressure of 10 MPa. The system is kept in this state to ensure complete homogenization and thermal equilibration (Fig. 5.1B).

3. The CO_2-expanded solution is depressurized into an aqueous solution (usually water), which may contain water-soluble components or hydrophilic biomolecules. Nitrogen (N_2) is flowed into the vessel at a pressure of 11 MPa to facilitate the transfer of the CO_2-expanded solution, maintaining a consistent pressure within the vessel during the depressurization process (Fig. 5.1C).

During depressurization, the rapid and uniform temperature drop results from the phase transition of CO_2 from liquid to gas. This sudden cooling effect may explain the improved vesicle-to-vesicle uniformity and supramolecular organization observed with this technique compared to traditional methods (201,262). In fact, DELOS-susp has proven to be an effective tool for producing a wide range of nanovesicles that can be conjugated with therapeutical molecules of interest. The process ensures high structural consistency and allows for controlled parameters, making it a promising approach for the development of new NPs for therapeutical purposes (201,262).

5.1.3. Purification of nanoliposomes by Tangential Flow Filtration

After nanoliposomes production, a step of purification is essential to eliminate unincorporated components, such as free rh-GLA, non-incorporated small molecules, and residual organic solvent that was added during the DELOS-susp process.

The most commonly used purification technique involves microfiltration membranes with pore sizes ranging from 0.1 to 10 µm, allowing for size-based separation of components.

Two primary membrane filtration techniques can be employed in the purification process: direct flow filtration (DFF), also known as dead-end filtration (Fig. 5.2A), or tangential flow filtration (TFF), also referred to as crossflow filtration (Fig. 5.2B). In DFF, the feed stream is applied perpendicular to the membrane and the goal is to pass the entire fluid through. In contrast, TFF directs the feed stream parallel to the membrane, where a portion of the fluid known as permeate, passes through, while the remaining retentate is recirculated back to the feed reservoir.

Compared to DFF, TFF is generally faster and more efficient for size-based separations, as the crossflow prevents molecule accumulation at the membrane surface, reducing the risk of fouling. Additionally, TFF avoids the rapid decline in flux rate typically observed in DFF, allowing for larger volumes to be processed per unit membrane area. Due to these advantages, TFF is widely used in biomolecule purification. Regardless of the filtration mode, transmembrane pressure (TMP), which represents the pressure difference between the feed and permeate sides, serves as the primary driving force for permeation.

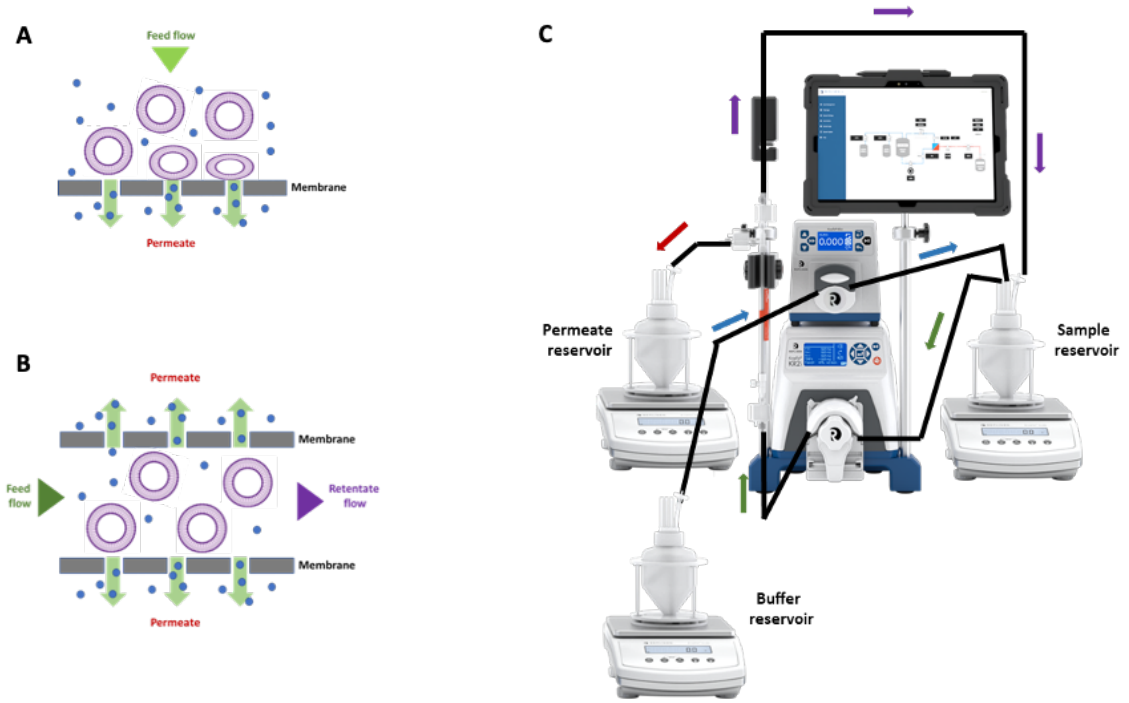

Fig. 5.2. Tangential flow filtration (TFF) for liposome purification. A) Scheme of direct flow filtration. B) Scheme of TFF. C) Scheme of the TFF procedure using KrosFlo KR2i Tangential Flow Filtration System (Repligen). Arrows represents the direction flow of the feed stream (green), permeate stream (red), buffer circulation (blue) and recirculation of the retentate flow (purple).

In this thesis, TFF was employed for nanoliposome purification following DELOS-susp (Fig. 5.2C). In detail, the purification process can be summarized into three key steps:

1. Diafiltration: This step selectively eliminates smaller components using a membrane with a specific pore size, while maintaining a constant volume sample. Any fluid lost through permeate is immediately replenished with an equivalent amount of buffer (usually water) from the buffer reservoir (Fig. 5.2C).

2. Buffer exchange: Similar to diafiltration, this step not only removes impurities but also replaces the original medium with a new one from the buffer reservoir. Throughout this process, the sample volume remains constant (Fig. 5.2C).

3. Concentration: Once desired nanoliposomes are retained by the membrane, the sample is recirculated through the membrane and returned to the sample reservoir. Unlike diafiltration and buffer exchange, this step does not involve the buffer reservoir, leading to sample concentration as excess liquid is removed (Fig. 5.2C). This allowed the sample to became more concentrated as volume was being removed. The degree of concentration (Concentration Factor, CF) corresponds to the initial volume (Vi) divided into the final volume (Vf), CF = Vi / Vf.

By implementing TFF, nanoliposomes produced via DELOS-susp achieve high purity, precise buffer composition, and controlled concentration, ensuring optimal physicochemical properties for further experimental applications.

5.1.4. Improving the formulation of GLA loaded and RGD targeted nanoliposomes

The main components of the nanoliposomal system consist in phospholipid DPPC (1,2-dipalmitoyl-sn-glycero-3-phosphocholine), cholesterol (Chol) and RGD targeting moiety (tripeptide Arginine-Glycine-Aspartic acid) (263). The RGD peptide was incorporated into the nanoliposomes to enhance their recognition by αvβ3-integrins (264), which are highly expressed in endothelial cells and in certain Fabry disease target cells, such as podocytes in the kidneys (265–267). Due to its strong affinity for αvβ3-integrins, the RGD peptide represents a promising targeting moiety that facilitates the internalization of GLA-loaded nanoliposomes into Fabry disease cells. This provides an alternative pathway to the mannose-6-phosphate receptor (M6PR)-mediated internalization, which is the main endocytic route used by the free GLA enzyme (268,269).

Among various types of RGD peptides, the c(RGDfk) (cyclo pentapeptide Arginine-Glycine-Aspartic acid-D-phenylalanine-Lysine) was specifically selected due to its cyclic structure, which enhances targeting specificity and stability to the nanoliposome (270,271).

The composition of GLA-loaded and RGD-targeted nanoliposomes, also known as nanoGLA, has undergone continuous optimization since its initial development (226). Iterative modifications in their composition led to the final version of these nanoliposomes, which was used in the experiments of this section and received the orphan drug designation by the European Medicines Agency (EMA) in 2021 (272). This final version is also being used in other research projects, such as Phoenix (H2020, ID 953110) and Nano4Rare (Horizon, ID 101136772), in preparation for upcoming clinical trials (Fig. 5.3).

The final version of nanoGLA resulted from a series of progressive modification aimed at optimizing its composition and functionality. These modifications included the addition of miristalkonium chloride (MKC), a positively charged surfactant and antimicrobial preservative, to enhance the cationic characteristics in order to increase the GLA loading in the nanoliposome due to the negative charge of the enzyme (273–275). Therefore, the final formulation consisted of DPPC:Chol:Chol-PEG400-RGD (10:6.5:0.5 molar ratio) with a 3% mol of MKC (Fig. 5.3). This nanoGLA contained a GLA enzyme derived from stable CHO clones without the His tag, a modification implemented to reduce the potential immunogenicity of this nanoliposome caused by the affinity tag (276,277). This new GLA enzyme, called rh-GLA, was developed in collaboration between the Genetic and Microbiology department of IBB-UAB and LeanBio SL, in the frame of Smart4Fabry EU project.

This final and improved version of nanoGLA was selected to perform all the experiments in section 5 as well as in section 6. It also received the orphan drug designation (ODD) due to its improved preclinical efficacy compared to classical ERT and its ability to cross the blood-brain barrier (BBB) (200).

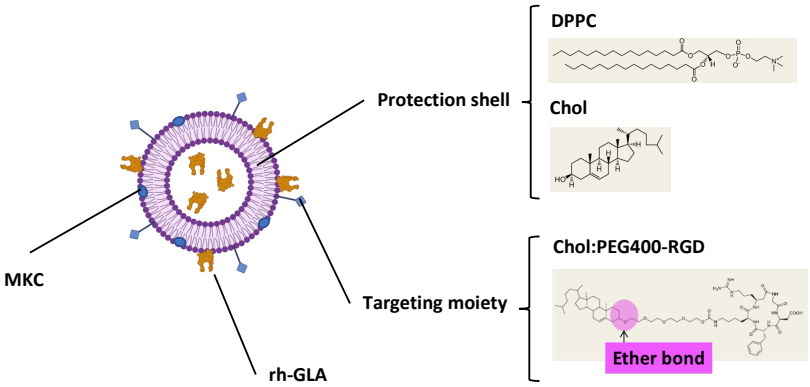

Fig. 5.3. Scheme of the structure and all the components of the final version of nanoGLA. Importantly, the Chol is attached to the PEG linker via an ether bond, rather than the typical carbamate bond.

Dr. Judit Tomsen-Melero (2021) and Dr. Aida Carreño (2024) from ICMAB-CSIC made a significant contributions to the development of nanoGLA through their respective doctoral theses (203). Without their perseverance and quality work, these findings presented in this section would not have been possible.

5.2. Characterization of GLA loaded and RGD targeted nanoliposomes

Nanoliposomes loaded with or without GLA enzyme were produced by DELOS-susp methodology followed a TFF step and provided by Prof. Nora Ventosa group at ICMAB-CSIC. To assess the effect of RGD functionalization on the BD and efficacy of these nanoparticles, six different nanoliposome formulations were produced, each varying in RGD content (0, 3, and 6 mol% in relation to the rest of membrane components) and loaded or unloaded with rh-GLA.

A deep chemical and physicochemical characterization of these systems was performed. First, the chemical composition of both empty nanoliposomes (EL, i.e., GLA enzyme unloaded) and GLA-loaded nanoliposomes (nanoGLA) was characterized using reversed-phase high-performance liquid chromatography (RP-HPLC) at ICMAB-CSIC. This analysis confirmed that lipid concentrations remained consistent across all tested formulations (Table 5.3; Fig. 5.4A, 5.4B and 5.4C). The DPPC and cholesterol content was found to be nearly identical among all nanoformulations (Fig. 5.4B and 5.4C). Similarly, the cationic surfactant miristalkonium chloride (MKC) was present in comparable concentrations across all samples, ranging between 2.4 mol% and 3.2 mol% relative to other membrane components (Table 5.3; Fig. 5.4B and 5.4C). These findings indicate that the addition of RGD peptides and the presence of rh-GLA did not significantly alter the overall nanoliposomal chemical composition, suggesting that the production manufacturing, consisting in DELOS-susp followed by TFF, ensures consistent formulation properties regardless of functionalization or enzyme loading. As for the targeting moiety and the loaded cargo, the RGD content in the nanoliposomes was lower than theoretically expected for both the 3%RGD and 6%RGD formulations. However, nanoliposomes with 6%RGD exhibited nearly double RGD content compared to those with 3%RGD. Specifically, the nanoliposomes with a theoretical 3%RGD content exhibited 2.3 mol % of RGD for EL-3%RGD and 1.9 mol % for nanoGLA-3%RGD, while those with a theoretical 6%RGD content displayed higher RGD levels, with 3.7 mol % of RGD in EL-6%RGD and 4 mol % in nanoGLA-6%RGD (Table 5.3; Fig. 5.4C). These results indicate that the incorporation of RGD on the nanoliposomal surface is effective, although it differs from the theoretical or expected percentage. This should be taken

into account when interpreting the subsequent results. On the other hand, enzymatic rh-GLA content was consistent across the different versions of nanoGLA, ranging from 0.04 to 0.05 mg/mL (Table 5.3).

Table 5.3. Summary table of composition and physicochemical properties of the liposomal formulations used in this Section. Hydrodynamic size, dispersity index (PDI), and ζ -potential were determined by dynamic and electrophoretic light scattering; lipid concentration and enzyme concentration were determined by RP-HPLC. All data is showed as Mean ± SEM. Characterization performed by Prof. N. Ventosa's team from ICMAB-CSIC.

	EL-0%RGD	EL-3%RGD	EL-6%RGD	nanoGLA-0%RGD	nanoGLA-3%RGD	nanoGLA-6%RGD
Membrane composition	DPPC:Chol 10:7 (0 mol % RGD) (2.4 mol % MKC)	DPPC:Chol:Chol-PEG400-c(RGDfk) 10:6.5:0.5 (2.3 mol % RGD) (3.2 mol % MKC)	DPPC:Chol:Chol-PEG400-c(RGDfk) 10:6:1 (3.7 mol % RGD) (2.9 mol % MKC)	DPPC:Chol 10:7 (0 mol % RGD) (3 mol % MKC)	DPPC:Cho:Chol-PEG400-c(RGDfk) 10:6.5:0.5 (1.9 mol % RGD) (3 mol % MKC)	DPPC:Chol:Chol-PEG400-c(RGDfk) 10:6:1 (4 mol % RGD) (2.7 mol % MKC)
Scheme						
Size (nm)	115 ± 2	127 ± 2	137 ± 2	127 ± 1	171 ± 1	205 ± 2
PDI	0.16 ± 0.01	0.17 ± 0.02	0.18 ± 0.01	0.17 ± 0.02	0.18 ± 0.02	0.19 ± 0.02
ζ – potential (mV)	44 ± 1	45 ± 2	42 ± 1	41 ± 1	36 ± 1	36 ± 1
[Lipid] (mg/mL)	1.9 ± 0.1	1.9 ± 0.1	1.7 ± 0.1	1.7 ± 0.1	1.7 ± 0.1	1.9 ± 0.1
[GLA] (mg/mL)	-	-	-	0.044 ± 0.003	0.046 ± 0.001	0.047 ± 0.002
[DiR] (nM)	300	300	300	300	300	300

Regarding physicochemical properties, dynamic light scattering (DLS) analysis revealed differences in the size distribution of these nanoparticles. Specifically, nanoGLA-3%RGD and nanoGLA-6%RGD exhibited a shifted distribution toward larger sizes (171 ± 1 nm and 205 ± 2 nm) compared to the EL (115 ± 2 nm), EL with RGD (127 ± 2 nm for EL-3%RGD and 137 ± 1 nm for EL-6%RGD) or nanoGLA without RGD (127 ± 1 nm) (Table 5.3; Fig. 5.4D). Despite the increased size of the nanoliposomes with the addition of rh-GLA and the RGD peptide, the polydispersity index (PDI) remained below 0.2 in all cases, indicating that the samples were monodisperse, homogeneous and acceptable for a drug delivery system (278). Additionally, the ζ-potential (measured by electrophoretic light scattering, i.e., ELS) decreased with the combined presence of RGD and rh-GLA (from +45 mV to +36 mV) (Table 5.3), likely due to a charge shielding effect on the surface of the liposome, which is normally positive because of the presence of MKC, and becomes less positive due to the probable electrostatic interaction with rh-GLA, as well as the presence of PEG400-RGD. This slight reduction in the ζ-potential of the nanoliposomes did not affect to their storage stability (more than 2 weeks) as demonstrated in previous studies (211), probably due to the negative net charge provided by the rh-GLA to the mixture (IEP = 5.2). In addition, values of ζ-potential of ± 30 mV are considered acceptable for the stability of liposomes (279) but ζ-potential values higher than + 30 mV were also reported in previous studies with other nanoGLA productions (211).

Overall, the results obtained for the production and characterization of the nanoliposomes are in agreement with those previously obtained in other studies (200,201,211), which indicates the robustness and reproducibility of the formulation method.

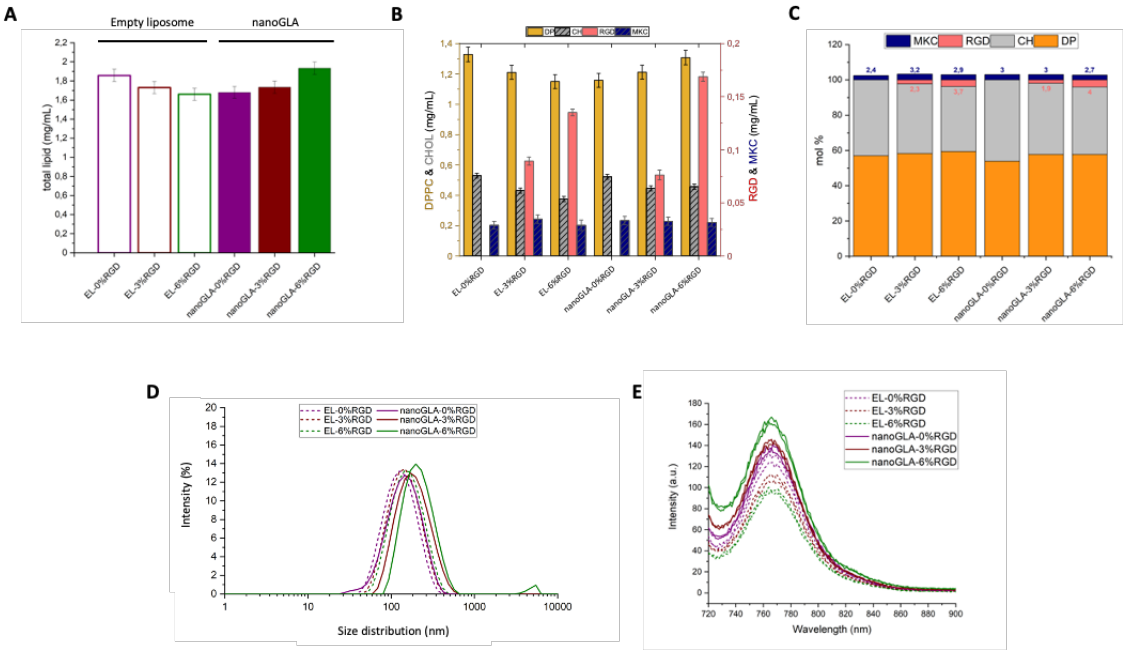

Fig. 5.4. Characterization of different liposomal formulations. A) Lipid content (mg/mL) quantified by HPLC. Results were represented as Mean ± SD. **B-C)** Concentration of the different liposomal components (mg/mL and %mol) in each nanoformulation. Results in C were represented as Mean ± SD. **D)** Size distribution measured by DLS. **E)** Fluorescence emission spectra of each DiR-labeled liposomal formulation. Different scattering contribution is also observed (see at 720 nm). Characterization performed by Prof. N. Ventosa's team from ICMAB-CSIC.

In order to track the internalization and biodistribution of nanooliposomes *in vitro* and *in vivo*, it was required the use of fluorescent molecules to monitor and track the testing substances. Therefore, the lipophilic DiR carbocyanine fluorophore (1,1'-dioctadecyl-3,3,3',3'-tetramethylindotricarbocyanine iodide) was incorporated to the rest of membrane components of the liposomes during the manufacturing process of all versions of EL and nanoGLA.

Fluorescence emission spectra analysis revealed that all nanoformulations exhibited a fluorescence signal (Fig 5.4E). Surprisingly, nanoliposomes with rh-GLA showed slightly higher fluorescence intensity than the EL versions, likely due to a greater incorporation of DiR in the nanoliposomes containing rh-GLA (Fig. 5.4E) or it could also be attributed to a higher scattering contribution (due to the larger size of nanoGLA compared to EL). Despite these variations in fluorescence intensity, all *in vitro* and *in vivo* studies were conducted using normalized fluorescence values, ensuring accurate and corrected comparisons across different formulations.

The functionality and stability of the rh-GLA protein loaded in nanoGLA formulations were assessed by measuring the GLA enzymatic activity. Up to 14-days after production, all nanoGLA formulations showed similar GLA enzymatic activity (1,468 ± 118 µmol/h·mg for nanoGLA-0%RGD, 1,287 ± 26 µmol/h·mg for nanoGLA-3%RGD and 1,467 ± 33 µmol/h·mg for nanoGLA-6%RGD), but these values were lower than the activity of both agalsidase alfa (1,890 ± 26 µmol/h·mg) and rh-GLA (2,146 ± 228 µmol/h·mg) (Fig. 5.5A). As expected, all versions of empty nanoliposomes (EL-0%RGD, EL-3%RGD, and EL-6%RGD, therefore without rh-GLA enzyme) showed no enzymatic activity (data not shown).

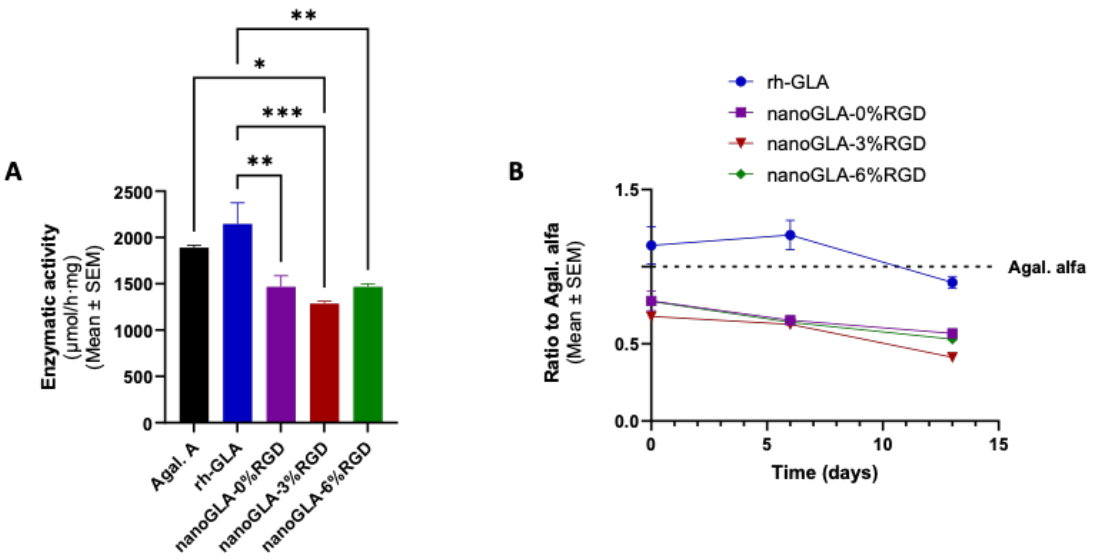

Fig. 5.5. Specific GLA enzymatic activity of different liposomal systems. **A)** Enzymatic activity of clinical free enzyme Agalsidase alfa (Agal. A), recombinant human free enzyme (rh-GLA) and different nanoGLA formulations. **B)** Stability of enzymatic activity after 2 weeks at 4°C of free GLA enzyme (rh-GLA) and different formulations of nanoGLA. Enzymatic activity observed after different days of storage were referred to enzymatic activity observed at day 1 (% of enzymatic activity). Agal. A was included as a control. Statistical significance levels were schematically assigned *($0.01 \leq p < 0.05$), **($0.001 \leq p < 0.01$), ***($0.0001 \leq p < 0.001$), ****($p < 0.0001$).

Upon storage at 4°C, both versions of rh-GLA, free enzyme or nanoGLA, exhibited gradual loss of enzymatic activity over time. After 6 days of storage at 4°C, the nanoGLA versions showed better preservation of enzymatic activity than both free rh-GLA and Agal. A. Specifically, nanoGLA-3%RGD exhibited the best preservation (Fig. 5.5B). However, after 13 days of storage at 4°C, nanoGLA-0%RGD and nanoGLA-3%RGD showed similar levels of enzymatic activity preservation, which were better than those of both free enzymes. In contrast, nanoGLA-6%RGD showed a decrease in enzymatic activity after 13 days of storage (Fig. 5.5B). This likely indicates that higher concentrations of RGD could negatively affect GLA stability. However, this may be specific to this batch of nanoliposomes, so other batches need to be tested to confirm this hypothesis. It is important to note that free rh-GLA exhibited a higher % of enzymatic activity than what was observed after 6 days of storage. Similar behaviour of rh-GLA was observed over time in other studies (202). This may indicate that free rh-GLA undergoes a progressive loss of stability over time, while its encapsulation within nanoliposomes enhances its stability.

Overall, these results indicated that all the different versions of nanoliposomes are stable with defined composition and good physicochemical properties, such as size, PDI and ζ-potential. In addition, nanoGLA formulations maintain charge stability for at least two weeks, allowing for experimental studies to be conducted within this timeframe. For long-term storage and clinical applications of the product, ICMAB-CSIC is currently developing a lyophilized final formulation of nanoGLA (200).

5.3. Internalization of targeted nanoliposomes in endothelial cells

5.3.1. Effect of RGD functionalization in nanoliposomal uptake in endothelial cells

To demonstrate that the presence of RGD as a targeting moiety in nanoliposomes enhances their uptake by endothelial cells, various internalization assays were conducted using a final theoretical lipid concentration of 0.05 mg/mL of each nanoformulation, previously labelled with DiR-dye. As discussed in previous sections, endothelial cells are one of the most affected cell types in FD. Therefore, Human Microvascular Endothelial Cells-1 (HMEC-1) were chosen as the cell model to investigate the nanoliposomal internalization.

First, flow cytometry analysis of EL-0%RGD and EL-3%RGD internalization in HMEC-1 revealed that the inclusion of the RGD peptide in empty nanoliposomes significantly improved their uptake by endothelial cells after 1 h (p = 0.03) and 6 h (p = 0.0001) of incubation, increasing the median fluorescence intensity (MFI) of DiR in HMEC-1 cells (Fig. 5.5A). This was also evidenced by an increase in the percentage of DiR-positive cells (Fig. 5.6C). Similarly, the presence of RGD enhanced endothelial cell internalization of nanoGLA formulations, as observed by flow cytometry after 0.5, 1, and 6 h of incubation in both MFI and percentage of DiR-positive HMEC-1 cells (Fig. 5.6B and 5.6C). This improvement in the internalization in HMEC-1 cells due to RGD was also reported in previous studies with similar nanoliposomes (202).

Importantly, after 1 and 6 h of incubation, HMEC-1 cells treated with nanoGLA-6%RGD showed higher cell mortality compared to those treated with EL and the other nanoGLA formulations. This increased cell death was visually confirmed using optical microscopy, suggesting that higher concentrations of RGD may have cytotoxic effects under certain conditions.

These findings were further corroborated by confocal microscopy, which showed that nanoGLA formulations with RGD targeting moiety were internalized more rapidly than nanoGLA-0%RGD (Fig. 5.6D). Among the RGD-containing nanoformulations, nanoGLA-3%RGD emerged as the optimal choice due to the high cell mortality observed in HMEC-1 cells treated with nanoGLA-6%RGD. This effect of the nanoGLA-6%RGD to the HMEC-1 cells was also observed by the internalization assay using flow cytometry.

Co-localization studies demonstrated an overlap between the DiR signal from nanoGLA formulations and LysoTracker™ stain, indicating that nanoGLA successfully reached the lysosomes (Fig. 5.6D and 5.6E). These findings are consistent with previous studies using DiD-loaded EL-RGD and nanoGLA-RGD (202), further demonstrating the robustness and reproducibility of these results.

The combined presence of RGD and rh-GLA on the nanoliposomal surface significantly increased the percentage of DiR-positive cells in HMEC-1 cells treated with nanoGLA-0%RGD and nanoGLA.3%RGD compared with EL-0%RGD and EL-3%RGD, after 6 h of incubation (p = 0.02 in both cases). This suggests a possible interaction between the rh-GLA on the nanoliposomal surface and mannose-6-phosphate receptors (M6PR), which are the main pathway through which lysosomal enzymes, such as the GLA, enter the cell (12,268,280). This interaction could contribute to an overall enhanced cellular uptake of these NPs.

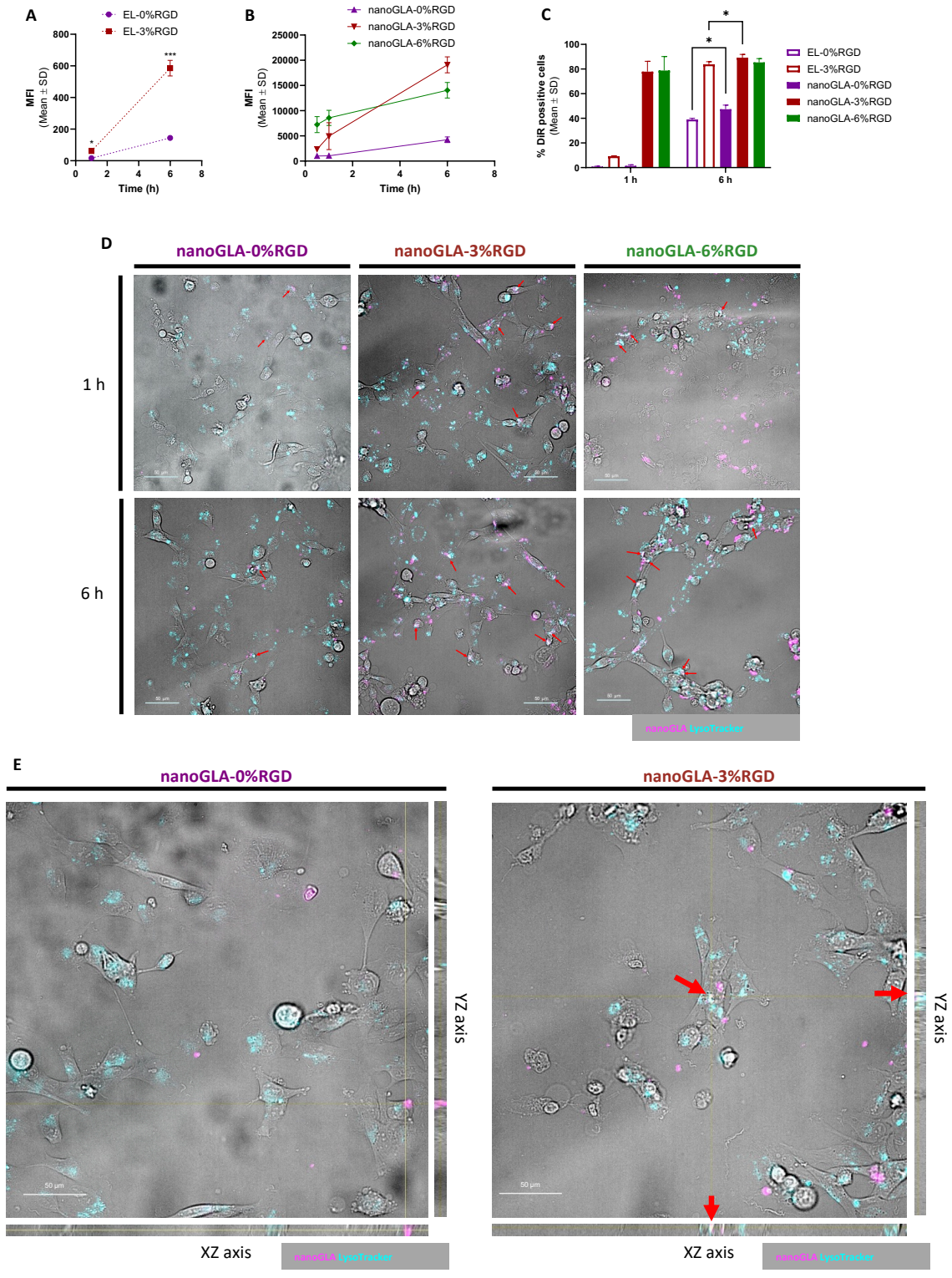

Fig. 5.6. Cellular internalization of different liposomal systems labeled with DiR dye at 0.05 mg/mL of theoretical lipid content in HMEC-1 cells. **A)** Median fluorescence intensity (MFI) of DiR in cells treated with EL-0%RGD and EL-3%RGD after 1 h and 6 h of incubation by flow cytometry. **B)** Median fluorescence intensity (MFI) of DiR in cells treated with nanoGLA-0%RGD, nanoGLA-3%RGD and nanoGLA-6%RGD after 0.5 h, 1 h and 6 h of incubation by flow cytometry. **C)** Percentage of DiR positive cells after incubation of 1 h and 6 h with different liposomal systems by flow cytometry. Statistical significance levels were schematically assigned *($0.01 \leq p < 0.05$), **($0.001 \leq p < 0.01$), ***($0.0001 \leq p < 0.001$), ****($p < 0.0001$). **D)** Internalization of different DiR-labeled nanoGLA systems in HMEC-1 cells after 1 and 6 hours of incubation by confocal microscopy (40X). Magenta: DiR-labeled nanoGLA liposomes, cyan: LysoTracker™ Green DND-26, scale bar: 50 µm. Red arrows showed co-location of two colors. **E)** Ortho view of Z-stack

images of HMEC-1 cells after incubation with DiR-loaded nanoGLA-0%RGD (left) and nanoGLA-3%RGD (right) at 1h (40X). Magenta: DiR-labeled nanoGLA dendrimers, cyan: LysoTracker™ Green DND-26, scale bar: 50 µm. Red arrows showed co-location of two colors.

Interestingly, the increased internalization of nanoliposomes in HMEC-1 cells due to the presence of rh-GLA was not observed in previous studies (202). This discrepancy is likely due to several factors, such as differences in GLA concentration and sequence. In the present study, the enzyme levels used were ten times higher, the GLA sequence did not contain His-tag, and liposomal formulation was optimized, in contrast to the conditions used in previous experiments.

5.3.2. MP6R-dependent internalization of nanoliposomes

The GLA enzyme is primarily internalized by cells through interaction with M6PR (268,281). This receptor is widely expressed in various cell types, including macrophages, fibroblasts and kidney cells (282–284). As discussed in section 5.3.1, the internalization of rh-GLA is enhanced in the presence of rh-GLA in the nanoliposome, suggesting a possible interaction between the enzyme and M6PR. However, nanoGLA does not necessarily follow this endocytic pathway, due to the presence of RGD in the nanoliposome or because some of the rh-GLA is located in the internal part of the nanoliposome and is not exposed to the M6PR on the cell surface.

To further investigate the cellular uptake mechanism of nanoliposomes, internalization assays were performed by blocking M6PR cell receptors with high concentrations of mannose-6-phosphate (5 mM) in primary cultures of mouse aortic endothelial cells (MAEC) from GLA KO Fabry mice (217). The natural absence of endogenous GLA in these cells allowed for the quantification of intracellular enzymatic activity resulting only from the internalization of rh-GLA and nanoGLA formulations. Results showed that, after 6 h of incubation, intracellular enzymatic activity was very low in MAEC treated with 1 µg/mL of free rh-GLA in the presence of M6P, indicating an effective blockade of GLA cellular uptake (Fig. 5.7A). However, when cells were treated with nanoGLA formulations (0% RGD and 3% RGD) at the equivalent concentration, enzymatic activity levels remained similar regardless of M6P incubation, suggesting that nanoGLA uptake occurs independently of M6PR (Fig. 5.7A).

Interestingly, cells treated with nanoGLA-3%RGD in the presence of M6P showed a significant increase in intracellular enzymatic activity compared to those treated with nanoGLA-3%RGD in the absence of M6P (p = 0.02). This might indicate the activation of alternative endocytic pathways because of the inactivation of the M6PR-dependent internalization route, suggesting a compensatory mechanism that bypasses the inhibition of M6PR function (285–287).

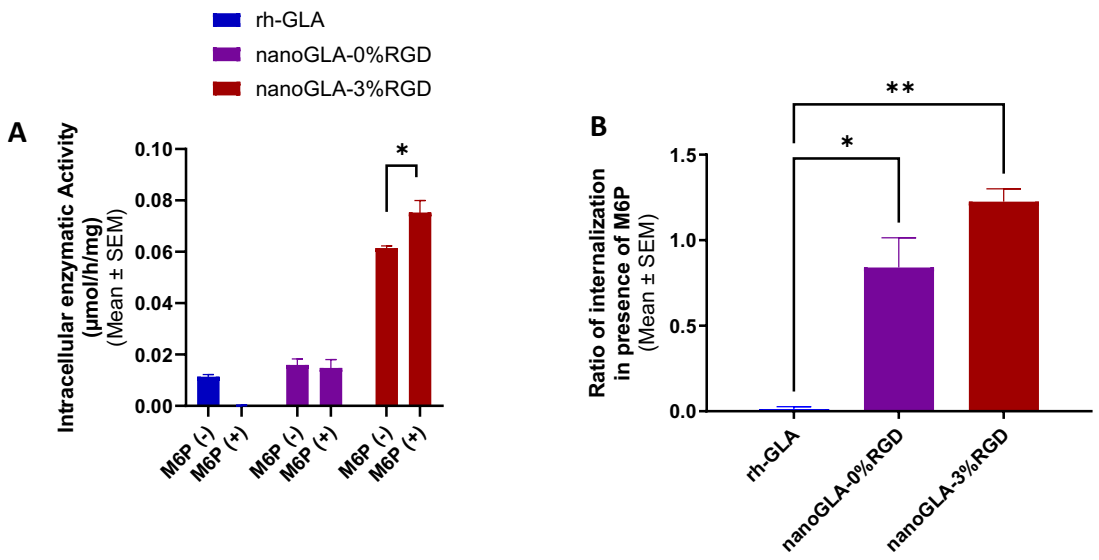

Fig. 5.7. Uptake of nanoGLA-0%RGD and nanoGLA-3%RGD in the absence (-) and presence (+) of mannose-6-phosphate (M6P) in KO GLA endothelial cells (MAEC) after 6 h. A) Intracellular enzymatic activity after treatment with free GLA (rh-GLA) or nanoGLA with or without RGD in the absence or presence of 5 mM of M6P (M6P (-) and M6P (+) respectively). **B)** Ratio of internalization was calculated dividing intracellular enzymatic activity in presence of M6P to those in absence of M6P for every treatment (rh-GLA, nanoGLA-0%RGD and nanoGLA-3%RGD). Statistical significance levels were schematically assigned *($0.01 \leq p < 0.05$), **($0.001 \leq p < 0.01$), ***($0.0001 \leq p < 0.001$), ****($p < 0.0001$).

To further assess the role of M6PR-independent pathways in nanoliposome internalization, the internalization ratio was calculated for each treatment (rh-GLA, nanoGLA-0%RGD, and nanoGLA-3%RGD) by dividing intracellular enzymatic activity in the presence of M6P by that in the absence of M6P (Fig. 5.7B). The results indicated that RGD functionalization enhances nanoliposome internalization, particularly in conditions where M6PR-mediated uptake is blocked.

5.3.3. Endocytic internalization of nanoliposomes

We also investigated the specific internalization route by using different endocytosis inhibitors. The assay included Dynasore (Dyn), 5-(N-ethyl-N-isopropyl) amiloride (EIPA), Nystatin (Nys) and Chlorpromazine (CPZ). Dyn is a GTPase inhibitor of dynamin activity that blocks endocytic vesicle scission from the cell membrane and thereby inhibits macropinocytosis (288). On the other hand, EIPA is a selective blocker of the Na+/H+ antiport that also inhibits macropinocytosis (289). Nys, is an inhibitor of caveolae-dependent endocytosis by binding sterols and disrupting caveolae formation (290) and CPZ is a clathrin-dependent endocytosis inhibitor that binds clathrin and the adaptor protein 2 (AP2) complex, blocking the formation of clathrin-coated pits on the inner surface of the plasma membrane (291). All these inhibitors were co-incubated with 0.05 mg/mL of lipid concentration of EL-0%RGD, EL-3%RGD, or nanoGLA-3%RGD labeled with DiR at 300 nM in HMEC-1 cells for 6 h.

Since endocytosis inhibitors can affect cell viability (292,293), two different concentrations of each inhibitor were tested (50 µM and 100 µM for Dyn, 75 µM and 100 µM for EIPA, 25 µM and 50 µM for Nys, and 10 µM and 20 µM for CPZ). Cell viability was around 80% in all cases (Fig. 5.8A), and no significant differences compared to control except for the case of nystatin at 50 µM that slightly reduced cell viability ($p = 0.02$). This phenomenon was not observed in the other nanoformulations, indicating that it was an isolated case.

Regarding internalization, none of the endocytosis inhibitors tested were able to completely abolish nanoliposomal internalization in HMEC-1 cells at any concentration tested. In agreement with previous experiments, a clear improvement in nanoliposomal cellular uptake in HMEC-1 cells due to the presence of RGD was also observed (Fig. 5.8B and 5.8C). Additionally, Dyn and Nys were the only inhibitors that significantly reduced nanoliposomes internalization, independent of the presence or absence of RGD (Fig. 5.8B and 5.8C). This decrease in HMEC-1 uptake was dose-dependent.

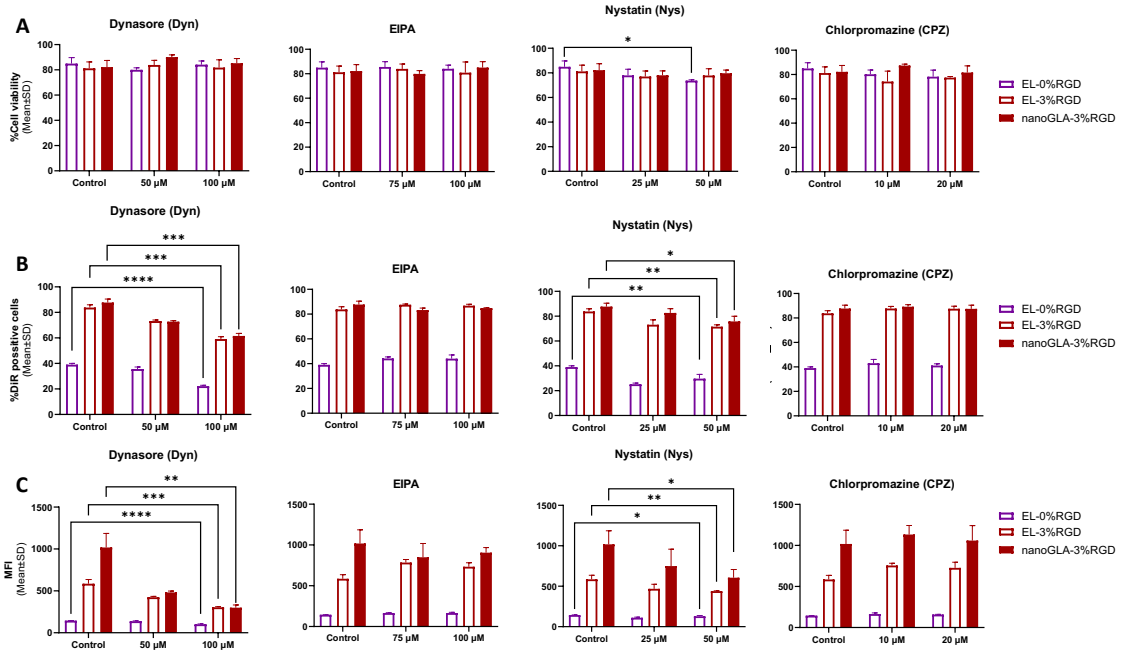

Fig. 5.8. Internalization of DiR-labeled EL-0%RGD, EL-3%RGD and nanoGLA-3%RGD in HMEC-1 cells after 6 h of incubation in the absence or presence of endocytosis inhibitors, by flow cytometry. A) Cell viability (%) of HMEC-1 cells after incubation with different concentrations of endocytosis inhibitors. Only in cells treated with EL-0%RGD and the highest dose of nystatin showed a significant decrease ($P<0.05$) in cell viability. **B)** Percentage of DiR positive HMEC-1 cells determined by flow cytometry. **C)** Median fluorescence intensity (MFI) of HMEC-1 cells. Results confirmed what was observed in %DiR positive cells. In all figures (A-B-C), two different concentrations of every inhibitor of endocytosis were tested and the control bar corresponded to the internalization of the nanoparticle with the absence of endocytosis inhibitor. Statistical significance levels were schematically assigned *($0.01 \leq p < 0.05$), **($0.001 \leq p < 0.01$), ***($0.0001 \leq p < 0.001$), ****($p < 0.0001$).

The inhibition of dynamin-dependent macropinocytosis with Dyn (100 µM) led to a significant reduction in DiR-positive cells across all nanoliposomal formulations. Specifically, internalization was reduced by 17% for EL-0% RGD, 25% for EL-3% RGD, and 26% for nanoGLA-3% RGD (Fig. 5.8B). In addition, in terms of MFI, Dyn treatment reduced 30% of EL-0%RGD internalization and 48% and 70% of EL-3%RGD and nanoGLA-3%RGD uptake, respectively, further supporting the role of dynamin-mediated macropinocytosis in nanoliposomal internalization. (Fig. 5.8C).

The inhibition of caveolae-mediated endocytosis using Nys (50 µM) also impacted nanoliposome uptake, though to a lesser extent than Dyn. DiR-positive cell percentages were reduced by 9% for EL-0% RGD and 12% for both EL-3%RGD and nanoGLA-3%RGD (Fig. 5.8B). Similarly, MFI analysis showed a 10% reduction for EL-0%RGD, 25% for EL-3%RGD, and 40% for nanoGLA-3%RGD upon treatment with Nys (Fig. 5.8C). These results indicate that caveolae-mediated uptake contributes significantly to nanoGLA-3%RGD internalization.

These results demonstrate that all tested nanoliposomes (with and without RGD) were mainly endocytosed via macropinocytosis, followed by caveolae-dependent endocytosis in HMEC-1

cells. However, these two endocytic routes were more important for the internalization of nanoliposomes with 3% of RGD compared to EL-0%RGD. Some studies with RGD-targeted liposomes have reported that one of the main endocytic pathways for the cellular uptake of RGD-targeted liposomes is clathrin-mediated endocytosis, driven by the interaction between RGD and cellular integrins (293–295). Other studies have also reported that caveolae-mediated endocytosis and macropinocytosis contribute to their uptake (296,297). Furthermore, it is well established that the endocytic pathway selected by the cell is sized dependent, with particles ranging from 100 nm to 5 µm in size being preferentially endocytosed via macropinocytosis (278).

Additionally, as shown by MFI analysis, nanoGLA-3%RGD showed a greater reduction in macropinocytosis and caveolae-dependent endocytosis upon treatment with Dyn and Nys, respectively, compared to EL-3%RGD. This suggests that rh-GLA may play a role in nanoliposomal internalization (Fig. 5.8B), independent of M6PR-mediated uptake (Fig. 5.7). To further investigate this, an internalization assay combining Dyn or Nys with M6P blockade could clarify the involvement of rh-GLA on the nanoliposomal surface in facilitating endocytosis.

Importantly, fibroblasts from Fabry patients exhibit impaired clathrin-dependent endocytosis and, consequently, altered M6PR-dependent endocytosis (298). The fact that chlorpromazine (CPZ), a clathrin-mediated endocytosis inhibitor, did not affect nanoGLA-3% RGD uptake in HMEC-1 cells suggests that nanoGLA-3% RGD may bypass the defective clathrin-dependent pathway observed in Fabry cells.

5.4. *In vitro* efficacy of RGD-targeted nanoliposomes

To evaluate whether enhanced internalization of RGD-decorated nanoliposmes translates into better efficacy for Gb3 clearance, *in vitro* efficacy experiments were conducted using MAEC cells derived from GLA KO mice. These experiments compared nanoGLA with different concentrations of RGD (0%, 3%, and 6% mol) against free GLA enzymes (Agal. A and rh-GLA). Various concentrations of equivalent GLA were tested: 0.03, 0.1, 0.3, 0.5, and 1 µg/mL, based on GLA experimental concentration values in nanoGLA previously quantified by HPLC. The results demonstrated that Agalsidase alfa and rh-GLA exhibited similar efficacy at different concentrations after 48 h of incubation. However, all nanoGLA formulations displayed greater Gb3 clearance compared to the free enzymes, starting at 0.1 µg/mL of equivalent GLA (Fig. 5.9A). These findings indicate that integration of GLA into nanoliposomes enhances its *in vitro* efficacy.

As expected, RGD-targeted nanoGLA (i.e., nanoGLA-3%RGD and nanoGLA-6%RGD) showed better Gb3 clearance in KO MAEC. However, nanoGLA-3%RGD outperformed nanoGLA-6%RGD in *in vitro* efficacy (Fig. 5.9A and 5.9B), indicating that higher RGD densities in liposome' surface does not necessarily correlate with greater *in vitro* effectiveness. This observation aligns with previous internalization experiments, where nanoGLA-6% RGD was associated with increased cell cytotoxicity, which may have compromised its efficacy.

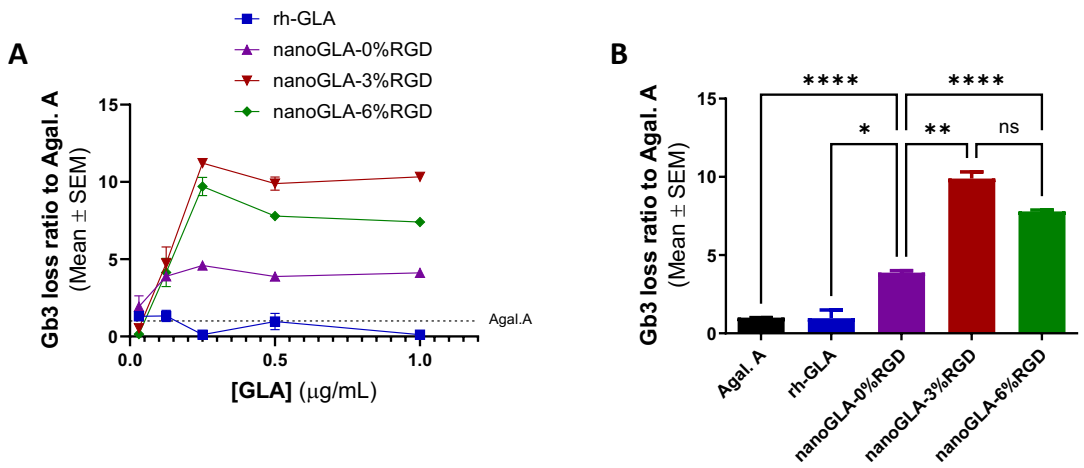

Fig. 5.9. *In vitro* efficacy in endothelial primary cultures derived from Fabry KO mice after 48 h. Gb3 clearance showed by different treatments was normalized by *in vitro* efficacy of free agalsidase alfa. A) Different versions of nanoGLA compared with free enzyme rh-GLA at different GLA equivalent concentrations (0.03, 0.1, 0.25, 0.5 and 1 μg/mL). B) *In vitro* efficacy of both free enzymes (Agal. A and rh-GLA) compared with the different formulations of nanoGLA at 0.5 μg/mL of equivalent GLA. Results corresponded to a three independent experiments with different batches of liposomes. Statistical significance levels were schematically assigned *($0.01 \leq p < 0.05$), **($0.001 \leq p < 0.01$), ***($0.0001 \leq p < 0.001$), ****($p < 0.0001$).

Overall, these results confirm that all nanoGLA formulations enhanced *in vitro* efficacy compared to the free enzymes (Fig. 5.9A and 5.9B). This finding is consistent with previous experiments using other batches of nanoGLA-3%RGD, which also showed higher *in vitro* efficacy compared to both free enzymes (200,202).

5.5. *In vivo* biodistribution of different versions of nanoGLA in Fabry KO mice

Following the observed enhancement in endothelial cell internalization and the greater Gb3 clearance of RGD-functionalized nanoGLA in primary cell cultures, an *in vivo* biodistribution study was conducted. This study aimed to evaluate the distribution of free rh-GLA, nanoGLA-0% RGD, nanoGLA-3%RGD, and nanoGLA-6%RGD in Fabry KO mice after i.v. administration. A single dose of these systems at 1 mg/kg of equivalent GLA was administered to 1- to 4-month-old KO Fabry mice (Gla^{tmKul1}) from the C57BL/6J lineage. The age of the mice was selected based on previous efficacy assays that determined Gb3 levels, conducted previously by the group. It was observed that in mice older than 5 months, the accumulation of Gb3 was too high to observe an effect from the administered treatments. Therefore, the age range of 1-4 months was selected for future efficacy experiments, as more precise results regarding the effectiveness of the treatments in reducing Gb3 levels in these Fabry KO mice could be obtained. Although the present study is for BD rather than efficacy, the same age range of 1-4 months was selected.

Biodistribution was assessed at 1 and 30 min post-administration, using DiR fluorescence from nanoGLA and enzymatic activity (EA). Five different treatment groups were defined: non-treated KO mice (n = 3), rh-GLA-treated mice (n = 3 per time point), nanoGLA-0%RGD-treated mice (n = 4 per timepoint), nanoGLA-3%RGD-treated mice (n = 4 per time point), and nanoGLA-6%RGD-treated mice (n = 4 per time point).

For this assay, new batches of different versions of nanoGLA, each loaded with a theoretical concentration of 1 μM of DiR, were produced using DELOS-susp followed by TFF, with some

differences compared to those used *in vitro* (Table 5.3). Specifically, these new nanoGLA versions were concentrated and diafiltrated in a 5% (w/v) glucose isosmolar solution by TFF system to obtain the final liposomal batches with the minimal rh-GLA concentration required for intravenous administration in Fabry mice at a dose of 1mg/kg, in accordance with other *in vivo* studies involving nanoGLA formulations (200).

All versions of nanoGLA were isosmolar (approximately 280 mOsm/kg) (Table 5.4), making them suitable for intravenous administration, ensuring liposomal stability and hemocompatibility (200). They also exhibited similar enzymatic activity (Fig. 5.10A) and fluorescence emission spectra (Fig. 5.10B), confirming the suitability of the formulations for *in vivo* evaluation.

Table 5.4. Summary table of composition and physicochemical properties of the liposomal formulations used for *in vivo* experiments. Hydrodynamic size and ζ -potential were determined by DLS and ELS, and GLA enzyme concentration by RP-HPLC. All data is showed as Mean ± SD. Characterization performed by Prof. N. Ventosa's team from ICMAB-CSIC.

	nanoGLA-0%RGD	**nanoGLA-3%RGD**	**nanoGLA-6%RGD**
Theoretical membrane composition	DPPC:Chol 10:7 (0 mol % RGD) (5 mol % MKC)	DPPC:Cho:Chol-PEG400-c(RGDfk) 10:6.5:0.5 (3 mol % RGD) (5 mol % MKC)	DPPC:Chol:Chol-PEG400-c(RGDfk) 10:6:1 (6 mol % RGD) (5 mol % MKC)
Scheme			
Size (nm)	113 ± 1	111 ± 1	116 ± 1
PDI	0.23 ± 0.01	0.17 ± 0.01	0.20 ± 0.01
ζ – potential (mV)	52 ± 1	46 ± 1	44 ± 1
Osmolarity (mOsm/kg)	293 ± 5	308 ± 5	305 ± 5
Theoretical [Lipid] (mg/mL)	9.0	9.0	9.0
[GLA] (mg/mL)	0.16 ± 0.004	0.20 ± 0.006	0.20 ± 0.002
[DiR] (nM)	1125	1125	1125

In detail, free rh-GLA exhibited higher enzymatic activity (2,889 ± 334 µmol/h·mg) than the different nanoGLA formulations (1,745 ± 55 µmol/h·mg for nanoGLA-0%RGD, 2,110 ± 47 µmol/h·mg for nanoGLA-3%RGD and 1,899 ± 89 µmol/h·mg for nanoGLA-6%RGD). These differences were statistically significant for nanoGLA-0%RGD and nanoGLA-6%RGD (p = 0.03 for both) but not for nanoGLA-3%RGD (p = 0.06) (Fig. 5.10A). Interestingly, among the nanoGLA formulations, nanoGLA-3%RGD exhibited the highest enzymatic activity, which was significantly higher than nanoGLA-0%RGD (p = 0.03) (Fig. 5.10A). These findings demonstrated that the increase in RGD density in the nanoliposome did not affect their EA.

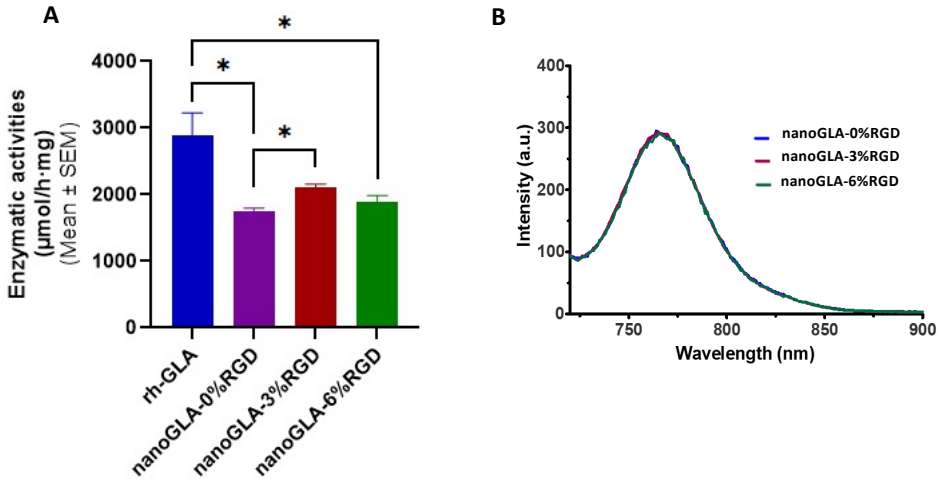

Fig. 5.10. Characterization of different nanoGLA formulations for *in vivo* testing. A) Enzymatic activity of rh-GLA and different nanoGLA. Statistical significance levels were schematically assigned *($0.01 \leq p < 0.05$), **($0.001 \leq p < 0.01$), ***($0.0001 \leq p < 0.001$), ****($p < 0.0001$). **B)** Fluorescence emission spectra DiR-labeled nanoGLA formulations, performed by Prof. N. Ventosa's team from ICMAB-CSIC.

Similar to the findings observed in *in vitro* experiments (Fig. 5.5A), all nanoGLA formulations exhibited lower enzymatic activity compared to free rh-GLA. However, the specific enzymatic activity of these new batches of nanoGLA formulations was higher than that of the nanoGLA used for *in vitro* studies.

All these results confirm that the different nanoGLA formulations adhered to the Critical Quality Attributes (CQAs) required for *in vivo* administration, as previously reported (200). The consistency in enzymatic activity across nanoformulations supports the reliability and reproducibility of the DELOS-susp manufacturing process, ensuring that the nanoGLA formulations maintain their functional integrity when prepared for *in vivo* applications.

5.5.1. *Ex vivo* FLI biodistribution of the different DiR-labelled nanoGLA versions

This experiment aimed to compare the biodistributions (BD) of the different nanoGLA formulations to determine whether the presence of RGD on the nanoliposomal surface had a beneficial role in the targeted delivery of nanoliposomes to Fabry disease-relevant organs such as the kidney, brain, and heart. The distribution of DiR-labeled nanoGLA-0%RGD, nanoGLA-3%RGD, and nanoGLA-6%RGD was assessed in GLA-deficient (KO) mice using IVIS™ Optical Imaging to quantify DiR signal. At 1 and 30 min post-administration, treated animals were euthanized and the percentage of DiR FLI was determined in liver, spleen, kidneys, lungs, heart, brain, intestine, skin and muscle. Non-treated KO mice was also euthanized and their tissues were used as a control (Fig. 5.11A).

Results showed that after 1 min post-administration, most of the DiR FLI signal was located in the liver, kidneys and lungs in all nanoformulations. However, after 30 min, the DiR signal decreased in all tissues, except for the liver and spleen, where DiR FLI was higher compared to what was observed at 1 min (Fig. 5.11B and 5.11C).

In the liver, DiR signal increased between 1 and 30 min for nanoGLA-0%RGD (from 70.7% to 82.26%) and nanoGLA-3%RGD (from 68.1% to 77.4%), while it remained stable for nanoGLA-

6%RGD (79% to 77.4%). Notably, at 30 min, nanoGLA-0%RGD showed the highest DiR signal in the liver, whereas nanoGLA-3%RGD and nanoGLA-6%RGD exhibited similar levels (Fig. 5.11C).

In spleen, the DiR signal also increased after 30 min compared to 1 min. Specifically, the signal increased from 3.4% to 6.6% for nanoGLA-0%RGD, 3.2 to 11.3% for nanoGLA-3%RGD and 4.2 to 13.8% for nanoGLA-6%RGD (Fig. 5.11B and 5.11C). These results suggest that higher RGD concentrations enhanced nanoliposome accumulation in the spleen, indicating a possible involvement of immune-related mechanisms in their sequestration.

In contrast, in the lungs, the DiR signal from all nanoGLA formulations decreased after 30 min compared to 1 min. In detail, nanoGLA-0%RGD reduced its DiR FLI from 8.1% to 2.6%, nanoGLA-3%RGD from 8.1% to 3% and nanoGLA-6%RGD from 7% to 3.3% (Fig. 5.11B and 5.11C). As observed, similar DiR FLI values were quantified across the different nanoGLA formulations at both 1 and 30 min post-administration. Similar DiR FLI values were observed across all formulations at both time points, indicating that RGD did not influence lung biodistribution.

As for target tissues in Fabry disease such as the kidneys, heart and brain, DiR FLI from all nanoGLA formulations also decreased after 30 min compared to 1 min. Specifically, in kidneys, the percentage of DiR signal decreased after 30 min in nanoGLA-0%RGD (from 9.3% to 4.3%), nanoGLA-3%RGD (from 9% to 5.3%) and nanoGLA-6%RGD (from 6.9% to 3.3%) (Fig. 5.11B and 5.11C). The similar biodistribution profiles among all nanoGLA formulations suggest that RGD functionalization did not enhance renal targeting.

In heart, a reduction in DiR FLI was observed after 30 min nanoGLA-0%RGD (from 1.5% to 0.6%), nanoGLA-3%RGD (from 4.3% to 0.3%) and nanoGLA-6%RGD (from 1.8% to 0.6%) (Fig. 5.11B and 5.11C). Again, these results indicate that RGD did not improve nanoliposome biodistribution to the heart.

Finally, in brain DiR signal in nanoGLA-0%RGD was reduced after 30 min compared to 1 min (from 3.4% to 2%) and nanoGLA-3%RGD, it decreased from 1% to 0.05% (Fig. 5.11B and 5.11C). However, no DiR FLI was detected in nanoGLA-6%RGD, either after 1 min or after 30 min (Fig. 5.11B and 5.11C).

Overall, these results showed that, after 30 min post-administration, nanoGLA was redistributed and sequestered in the liver and spleen. Retention of RGD-targeted nanoparticles, including liposomes and solid lipid nanoparticles, in the liver and spleen has also been reported by other authors (299–301). Moreover, a higher concentration of RGD peptide appears to correlate with increased nanoliposomal retention in the spleen (Fig. 5.11C). This could likely be due to the possible recognition of RGD (302–304) or PEG (305) by the immune system, as reported by some authors. Importantly, *ex vivo* images showed higher DiR FLI intensity in the liver and spleen of mice treated with nanoGLA-6%RGD compared to those treated with nanoGLA-3%RGD and nanoGLA0%RGD (Fig. 5.11A). However, these differences were not as evident in FLI quantification (Fig. 5.11C). This was probably due the normalization of FLI intensities during the *in vivo* experiment, where nanoGLA-6%RGD showed higher DiR fluorescence intensity than nanoGLA-0%RGD and nanoGLA-3%RGD. Crucially, no improvement in nanoGLA delivery was observed in Fabry target tissues such as kidneys, heart and brain due to the presence of RGD. In fact, nanoGLA-0%RGD showed significantly better brain BD than nanoGLA with RGD ($p = 0.03$). This effect may be explained by the higher retention of RGD-targeted nanoGLA in the liver and spleen, potentially reducing the number of circulating nanoparticles available for uptake in the brain.

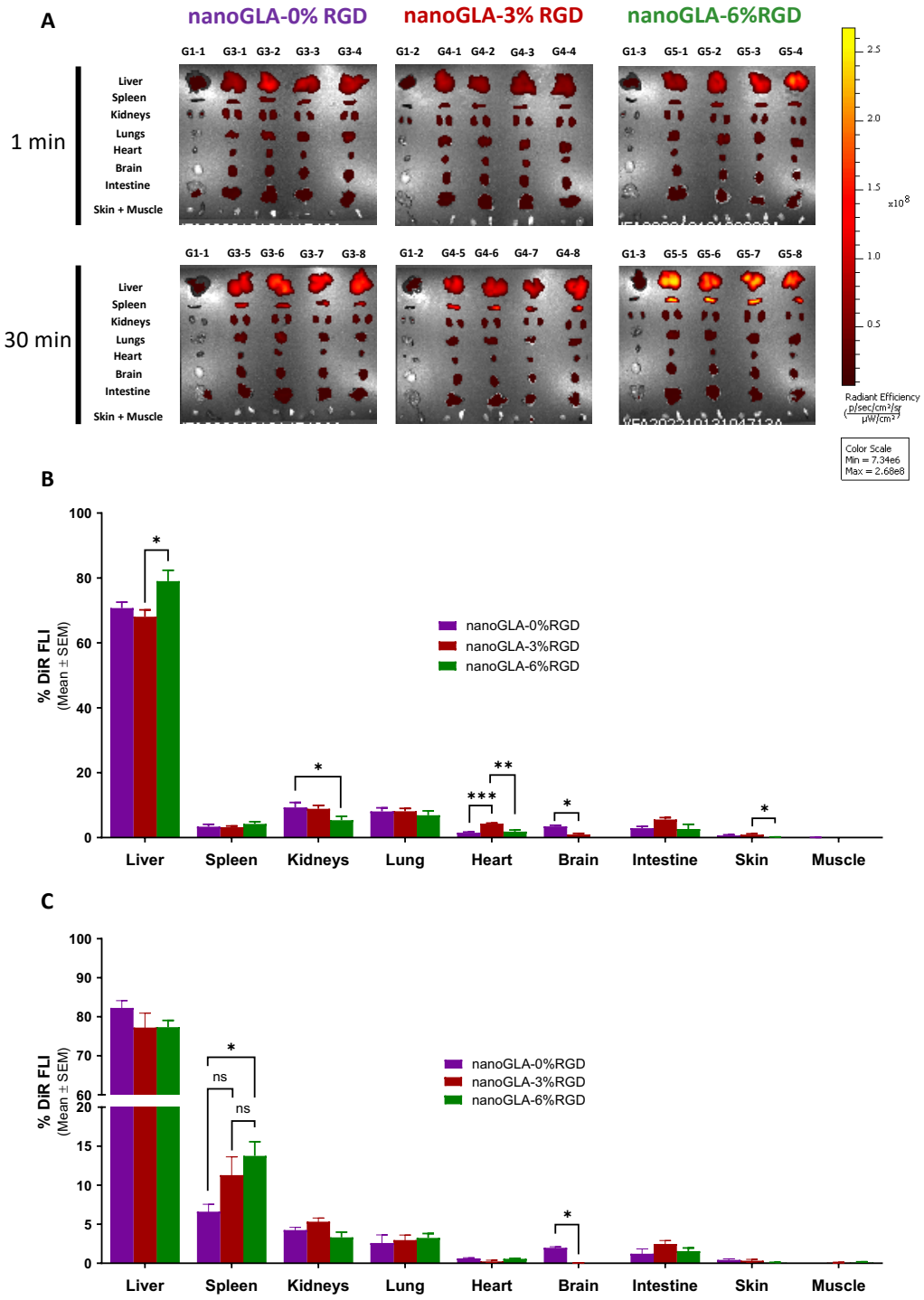

Fig. 5.11. ***Ex vivo*** **biodisitribution of the different DiR-labelled nanoGLA versions in Fabry KO mice after 1 min and 30 min post-administration**. **A)** *Ex vivo* images of different tissues from non-treated and treated KO Fabry mice. Four different groups of treatment were included in this assay: non-treated KO mice (G1; n=3), nanoGLA-0%RGD treated mice (G3; n=8), nanoGLA-3%RGD treated mice (G4; n=8) and nanoGLA-6%RGD treated mice (G5; n=8). Scale bar with Radiant Efficiency [p/s] is represented. **B)** *Ex vivo* quantification of DiR signal accumulated (%DiR FLI) after 1 min post-administration. **C)** *Ex vivo* quantification of DiR signal accumulated (%DiR FLI) after 30 min post-administration. Statistical significance levels were schematically assigned *(0.01 ≤ p < 0.05), **(0.001 ≤ p < 0.01), ***(0.0001 ≤ p < 0.001), ****(p < 0.0001).

It is important to mention that DiR labeling and the use of this fluorescent tracers to monitor nanoparticle biodositribution has its limitations. On the one hand, the interactions between DiR and the environment could lead to the loss of DiR from the nanoliposomes, resulting in

nonspecific detection or a lack of fluorescence in certain tissues. On the other hand, quantification of fluorescence in tissues is always limited by the absorption of the tissues and their intrinsic autofuorescence. Additionally, the dye concentration was not optimized for *in vivo* imaging; instead, the standard concentration used for *in vitro* assays was employed, which is typically lower in order to minimize potential alterations to the compound's physicochemical properties. Therefore, to overcome these limitations, BD was also analyzed through GLA enzymatic activity quantification in the treated GLA KO mice. These results are presented in the following section.

5.5.2. Biodistribution of enzymatic activity of the different nanoGLA versions

Once DiR FLI was quantified *ex vivo*, the next step was to confirm that nanoGLA variants were capable of delivering enzymatic activity (EA) to the target tissues. These were KO animals for the GLA enzyme, so all EA quantified in their tissues corresponded to the exogenously administered GLA. This experiment also allowed for a comparison of the biodistribution of free enzyme rh-GLA and different nanoGLA versions.

EA was determined in plasma, liver, spleen, kidneys, heart and brain 30 min after administration and percentage of injected dose (%ID) was calculated referring this EA to the activity determined in plasma 1 min after administration (Fig. 5.12). Other tissues included in the FLI analysis were excluded in this experiment, such as muscle, intestine, skin and lungs.

Overall, tissues from mice treated with nanoGLA showed higher EA than those treated with rh-GLA, except for the liver and heart (Fig. 5.12). Specifically, in plasma nanoGLA-0%RGD and nanoGLA-3%RGD exhibited significantly higher EA (28.2% and 17% of the injected dose, ID, respectively) than free rh-GLA in plasma ($p < 0.0001$ and $p = 0.003$, respectively). NanoGLA-6%RGD also showed greater enzymatic activity (12.7% of ID) than rh-GLA (8.2% of ID) in plasma, although the difference was not statistically significant.

Interestingly, in most tissues except brain, EA increased with the percentage of RGD in nanoGLA (Fig. 5.12). In the liver, nanoGLA-6%RGD showed significantly higher EA (19.2% of ID) than rh-GLA (15% of ID) ($p = 0.03$), nanoGLA-3%RGD (13.6% of ID) ($p = 0.0006$), and nanoGLA-0%RGD (11.4% of ID) ($p < 0.0001$). In the spleen, all nanoformulations showed significantly higher EA than rh-GLA (0.5% of ID) ($p \leq 0.005$), that increased with the RGD presence 5.6% of ID for 6%RGD, 3.5% for 3%RGD and 2.5% for 0%RGD ($p = 0.002$).

In tissues particularly affected by Fabry disease, such as the kidneys and heart, nanoGLA-6%RGD delivered higher quantities of EA compared to free rh-GLA and the other nanoformulations (Fig. 5.12). Specifically, the EA detected in the kidneys of mice treated with nanoGLA-6%RGD was 0.4% of ID, while in those treated with nanoGLA-3%RGD and nanoGLA-0%RGD, the values were 0.3% and 0.2%, respectively. In contrast, rh-GLA showed a similar %ID to nanoGLA-0%RGD in the kidneys (0.2%), with significant differences observed when compared to nanoGLA-6%RGD ($p = 0.01$). On the other hand, nanoGLA-6%RGD showed significantly better EA delivery (0.19% of ID) ($p < 0.0001$) than nanoGLA-0%RGD (0.07% of ID), nanoGLA-3%RGD (0.06% of ID), and rh-GLA (0.06% of ID) (Fig. 5.12). These results suggest a trend toward improved enzymatic delivery to the kidney and heart with increasing RGD concentrations, reinforcing the role of RGD-functionalization in enhancing enzyme biodistribution to these organs.

Finally, mice treated with different nanoGLA versions showed significantly higher EA in brain than those treated with rh-GLA (0.01% of ID) ($p < 0.05$). In this occasion, nanoGLA-0%RGD and nanoGLA-6%RGD showed the highest %ID (0.08% and 0.07%) compared to nanoGLA-3%RGD (0.05%). The difference between nanoGLA-0%RGD and nanoGLA-3%RGD was statistically significant ($p = 0.047$). These results indicate that while rh-GLA is unable to cross the BBB, nanoGLA formulations can successfully deliver enzyme activity to the brain. However, the presence of RGD did not correlate with increased BBB penetration, suggesting that RGD-mediated targeting does not enhance enzyme delivery to the brain.

Although GLA encapsulation increased the delivery of EA in plasma and brain, this was not correlated with a higher concentration of RGD on the nanoGLA (Fig. 5.12). In fact, some authors have reported the crossing of the BBB by liposomes co-functionalized with RGD and other targeting moieties, such as transferrin, a well-known protein that can facilitate the BBB crossing by various types of NPs, cell penetrating peptides and others (306–309). However, the role of RGD alone in BBB penetration remains unclear, suggesting that additional targeting mechanisms may be required to optimize nanoliposomal transport across the BBB.

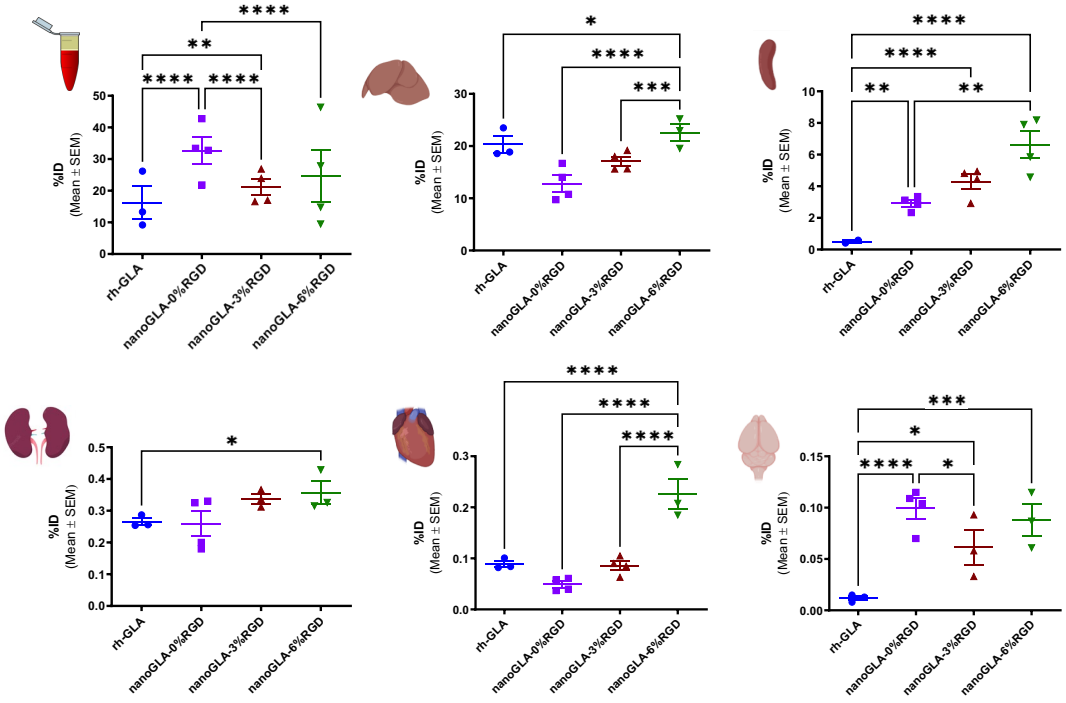

Fig. 5.12. *In vivo* biodisitribution of nanoGLA versions in Fabry KO mice by enzymatic activity determination. Enzymatic activity levels in plasma, liver and spleen (upper) and kidney, heart and brain (bottom) of Fabry KO mice intravenously administered with 1 mg/kg of equivalent GLA of free rh-GLA and different nanoGLA formulations. Activity was measured 30 min post-administration and referred to activity in plasma at 1 min (i.e., % injected dose, %ID). Statistical significance levels were schematically assigned *($0.01 \leq p < 0.05$), **($0.001 \leq p < 0.01$), ***($0.0001 \leq p < 0.001$), ****($p < 0.0001$).

Consistent with previous FLI studies (Fig. 5.11), nanoGLA-3%RGD and nanoGLA-6%RGD exhibited similar retention in the liver and spleen when EA was analyzed. Not only this , but this accumulation being dependent on the RGD concentration, reinforcing the impact of RGD on nanoliposomal sequestration in these organs.

In plasma, nanoGLA-3%RGD showed higher %ID than rh-GLA, in alignment with published studies (200). On top of this, our results show that encapsulation of rh-GLA in nanoliposomes increases the half life of the protein, while the functionalization of the nanoliposomal surface

might reduce this slightly (%ID for 3% and 6%RGD is significantly lower than that for 0%RGD) (Fig. 5.12).

In accordance with previous studies comparing Agal. A, free rh-GLA and nanoGLA-3%RGD (200), nanoGLA-3%RGD showed no significant differences in the %ID compared to free rh-GLA in key tissues such as kidneys and heart 30 min post-administration. In the present study, nanoGLA-6%RGD exhibited the highest EA in both kidneys and heart at 30 min post-administration, surpassing free rh-GLA and nanoGLA-3%RGD.

Overall, these results confirm that encapsulating the enzyme in nanoliposomes increases its lifetime in plasma. However, the presence of RGD in the nanoliposomes reduces this effect and increases their retention in the liver and spleen. Despite this sequestration, high densities of RGD also enhance enzymatic activity in Fabry target organs such as kidneys and heart (Fig. 5.12). These findings support the potential of certain RGD-functionalized nanoGLA formulations as an effective strategy for improving ERT in FD, particularly by optimizing enzyme delivery to key target tissues.

5.6. Detection of anti-drug antibodies (ADAs) in KO mouse plasma after single or repeated doses of free enzyme and nanoGLA-3%RGD

One of the limitations of the current ERT for Fabry disease is the generation of anti-drug antibodies (ADAs) against the therapeutic molecule (GLA) due to repeated intravenous infusions (every 15 days) (310). ADAs may neutralize the therapeutic effects of ERT, consequently impairing the clinical outcomes of Fabry disease patients (311,312). Therefore, encapsulating the GLA enzyme in nanoliposomes, making it less accessible to the immune system, could reduce ADAs generation.

To confirm this hypothesis, Fabry KO mice previously used in earlier studies (200) were used as controls and received a single intravenous administration of Agal.A (n = 3), rh-GLA (n = 3), or nanoGLA-3%RGD (n = 3) at a dose of 1 mg/kg of equivalent GLA. Seven days after the initial administration, the animals received a second dose and were euthanized 30 minutes later (Fig. 5.13A) to enable the detection of enzymatic activity in plasma and organs for additional experiments not included in this thesis. To promote the generation of ADAs, Fabry KO mice were repeatedly administered intravenous injections of Agal.A (n = 3), rh-GLA (n = 3), or nanoGLA-3%RGD (n = 3), with a total of eight doses (see Fig. 5.13B), each at a dose of 1 mg/kg of equivalent GLA. Following the eighth dose, animals were euthanized 24 h after the final administration, and plasma was collected via intracardiac puncture (n = 4 per group, Fig. 5.13B). Non-treated Fabry KO mice (n = 3) were included as controls.

The determination of ADAs in plasma after a single dose or repeated doses of Agal. A, rh-GLA, and nanoGLA-3%RGD in KO mice was assessed by ELISA. Compared to the absorbances in mice with a single dose, results showed that all treatments induced the presence of ADAs after repeated admnistrations (Fig. 5.13C), with nanoGLA-3%RGD showing the highest level of ADAs compared to both free enzymes. However, differences were only significant when compared to Agal. A (p = 0.005). On the other hand, no significant differences were found between rh-GLA and Agal. A, indicating that both enzymes showed similar titters of ADAs. The fact that nanoGLA-3%RGD showed the highest levels of ADAs could be explained by the presence of the rh-GLA enzyme on the nanoliposomal surface, which exposes the enzyme to the immune system.

Another possible explanation could be the composition of the nanoGLA-3%RGD protein corona, which may enhance the recognition of the nanoliposome by immune system, making it more immunogenic. This increased immune recognition might also explain the higher spleen BD observed in nanoGLA formulations compared to free enzymes (Fig. 5.12).

To fully understand the immunogenic potential of nanoGLA formulations, additional studies should be conducted. Specifically, it would be important to also quantify the total amount of antibodies, not just the ADAs, to confirm whether nanoGLA is more immunogenic than the free enzyme. Additionally, assessing the neutralizing capacity of these ADAs by evaluating their effect on GLA enzymatic activity is a critical next step. It would be important to include nanoGLA-0%RGD in order to investigate whether the presence of PEG400-RGD has an effect in the ADAs formation, as some authors have reported the presence of antibodies against PEG (305) and the possible recognition of RGD by the immune system (302–304).

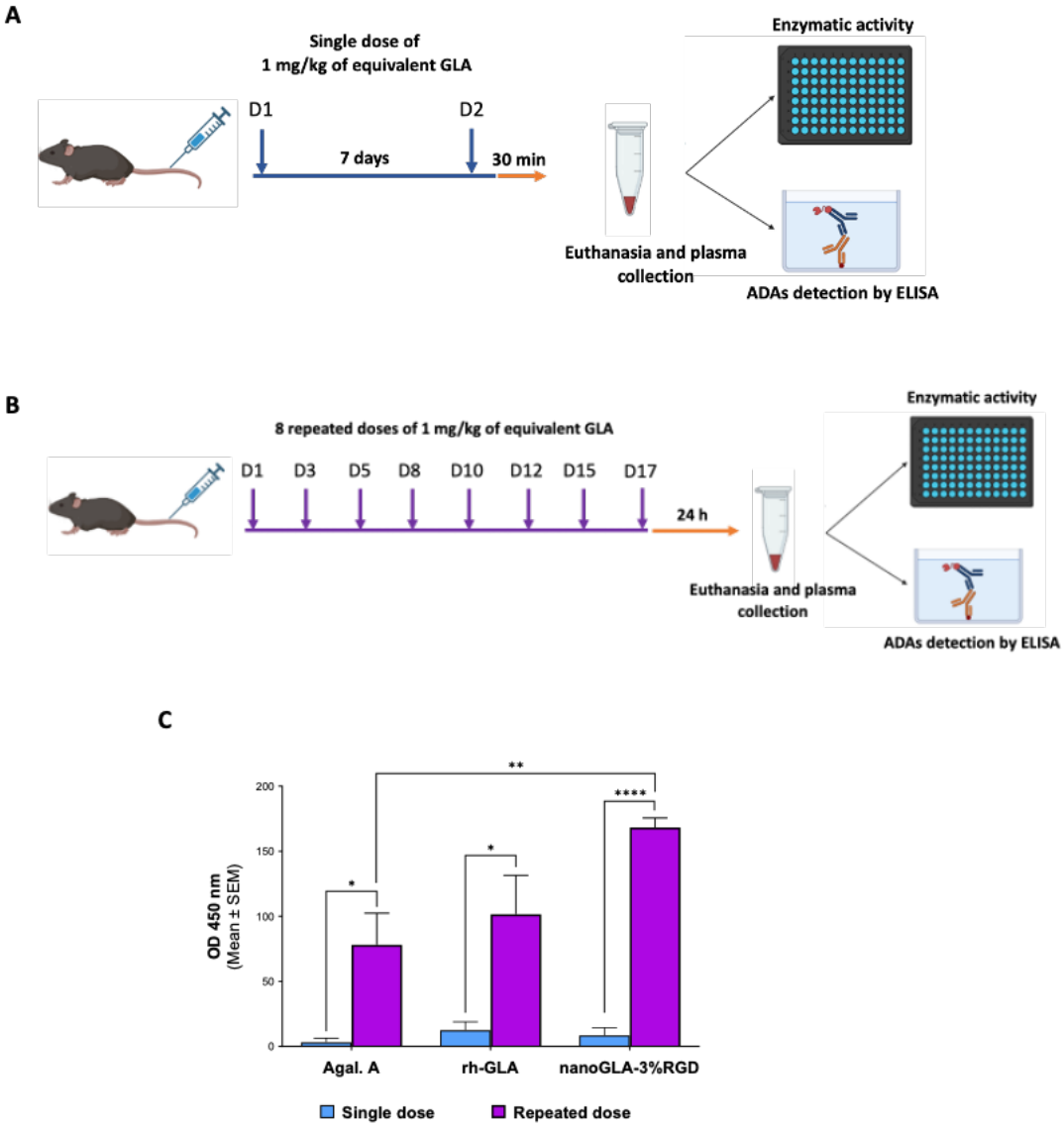

Fig. 5.13. Determination of anti-drug antibodies (ADAs) and enzymatic activity in KO mouse plasma after a single dose or repeated dose of free enzymes and nanoGLA-3%RGD. A) *In vivo* experimental design of single dose assay: Fabry KO mice were administered intravenously with a single dose of Agal. A or rh-GLA or nanoGLA-3%RGD (n=4 per group) and were euthanized 30 min after a second dose for other purposes. **B)** *In vivo* experimental design of repeated dose assay: Fabry KO mice were administered intravenously with repeated doses of Agal. A or rh-GLA or nanoGLA-

3%RGD (n=3 per group). **C)** Detection by ELISA of ADAs in plasma from Fabry KO mice treated with a single dose or repeated doses of Agal. A, rh-GLA and nanoGLA-3%RGD. Statistical significance levels were schematically assigned *($0.01 \leq p < 0.05$), **($0.001 \leq p < 0.01$), ***($0.0001 \leq p < 0.001$), ****($p < 0.0001$).

5.7. Summary and conclusions

This section explored the use of nanoliposomes with different densities of RGD (0%, 3% and 6 mol%) and with or without rh-GLA, to demonstrate that the presence of RGD improves the endothelial cellular uptake of the nanoliposomes and this can be reflected in a better clearance of Gb3 in MAEC KO cells as well as an improved *in vivo* BD.

Characterization of the different nanoliposomal formulations indicated good stability along with favorable physicochemical properties, such as size, PDI and ζ-potential across the various nanoformulations. Additionally, the nanoGLA formulation showed similar *in vitro* enzymatic activity, although lower than that of both free enzymes. All formulations were stable for 2 weeks when stored at 4°C and exhibited better preservation of EA than the free enzymes.

RGD clearly enhances the internalization of nanoliposomes in endothelial cells, such as the HMEC-1 cell line, allowing them to reach the lysosome. Similar results in cellular uptake have been reported by other authors using different targeted liposomal formulations as nanocarriers for other lysosomal enzymes and LSDs. Some of these studies are summarized in Table 5.2. Interestingly, in this thesis, presence of RGD combined with rh-GLA significantly increased their internalization in HMEC-1 cells, suggesting a potential interaction between the rh-GLA on the nanoliposomal surface and M6PR of endothelial cells. However, after blocking the M6PR with an excess of M6P, nanoGLA internalization was not reduced, indicating that the nanoliposomes enter the cells via an M6PR-independent mechanism. This suggests that nanoGLA utilizes alternative endocytic pathways distinct from those used by the free enzyme. This internalization mechanism was also described by other authors using other liposomal formulations with GCase enzyme (247).

Moreover, results from internalization assays using endocytic inhibitors showed that nanoliposomes, regardless of RGD presence, were primarily endocytosed via macropinocytosis and caveolae-dependent endocytosis in HMEC-1 cells after 6 h of incubation. This suggests that their uptake by endothelial cells is clathrin-independent. However, these results should be interpreted with caution, as several authors have reported that the endocytosis of RGD-targeted liposomes is mediated by clathrin due to their interaction with membrane integrins (αvβ3) (295,313). Interestingly, in our experiments, this clathrin-mediated uptake was not observed. One possible explanation is the longer incubation period used in our study (6 h), compared to the shorter incubation times (1 – 3 h) typically employed in other studies involving RGD-targeted liposomes (313–316). This suggests that the extended incubation time in our endocytosis assays may have masked RGD-dependent effects. Therefore, to confirm whether the RGD peptide facilitates clathrin-dependent endocytosis of nanoliposomes, future experiments should include shorter incubation times.

All nanoGLA formulations effectively reduced Gb3 accumulation *in vitro* in MAEC KO cells more efficiently than the free enzymes. The presence of RGD further enhanced this *in vitro* efficacy, likely due to the improved internalization of RGD-nanoliposomes. However, higher levels of RGD did not correlate with increased *in vitro* efficacy, possibly due to the cell mortality observed in cells treated with nanoGLA-6%RGD, or suggesting that high amounts of RGD might negatively affect the stability of nanoGLA. Improvement of *in vitro* efficacy due to the encapsulation of

lysosomal enzymes into liposomes (both targeted and non-targeted) has been reported by other authors using liposomes with different membrane compositions (Table 5.2).

In *in vivo* studies in Fabry KO mice, nanoliposomes were primarily retained in the liver and spleen 30 min after intravenous administration. A clear RGD-mediated effect was observed in the spleen, where higher levels of EA and FLI were detected. However, no significant improvement in FLI signal was observed in Fabry target tissues, such as kidneys, heart and brain due to the RGD presence. Nevertheless, RGD improved the EA BD in these organs compared to the free enzyme, demonstrating that nanoGLA with the highest density of RGD enhanced rh-GLA enzyme delivery to these target tissues. Interestingly, EA could be detected in brain of KO mice treated with all nanoGLA formulations. Results of the BD by EA were in accordance with previous studies (200). Discrepancies between EA and FLI can be explained by the limitation of the DiR labeling, resulting in nonspecific detection or a lack of fluorescence in certain tissues.

As for the production of ADAs, all treatments induced them after repeated dosing, but nanoGLA elicited the highest level of ADAs compared to both free enzymes. This could be due to the arrangement of GLA on the liposome surface, which may enhance its immunogenic potential by facilitating recognition by the immune system and subsequently triggering the antibody production cascade. This may also explain the improvement in spleen BD for nanoGLA compared to the free enzyme. Further studies are necessary to quantify total antibody levels and determine whether nanoGLA is more immunogenic than the free enzyme. Additionally, it would be valuable to include nanoGLA-0%RGD in future experiments to investigate whether the presence of RGD influences ADAs formation. Interestingly, despite the higher levels of ADAs observed in these mice, treatment with nanoGLA proved to be more effective than administration of the free enzyme in previous studies (200).

In summary, in our hands, nanoGLA funcionalized with RGD targeting moiety is a promising therapeutic option to enhance the ERT. It enhances endothelial cells internalization via M6PR-independent pathways, uses alternative endocytic pathways to enhance cellular uptake, delivers EA more efficiently than free enzyme to target tissues such as kidneys and heart and reaches the brain, despite the presence of ADAs against the GLA.

6. Characterization of the protein corona in nanoliposomes for GLA delivery

6.1. Introduction

Upon intravenous administration, NPs can interact with a large number of plasmatic proteins. The adsorption of these proteins onto NP surfaces forms a dynamic structure called protein corona (PC). It is well known that the formation of PC around NPs can alter their biological identity (317). The presence of a PC can have both detrimental and beneficial effects. On the one hand, undesired interactions with cells and opsonization, might lead to accelerated clearance, reducing circulation time (318–321). On the other hand, the presence of the PC can facilitate targeted delivery, aid in crossing biological barriers such as the BBB, and enhance therapeutic efficacy (322–325).

A key determinant of PC formation and composition is the surface modification of the NP. Polyethylene glycol (PEG), for example, is widely used to impart "stealth" properties, reducing protein adsorption and prolonging systemic circulation (320). However, PEGylation does not prevent PC formation entirely and may even alter the nature of the adsorbed proteins (326,327). Similarly, functionalizing nanoparticles with targeting peptides, such as RGD (arginine-glycine-aspartic acid), can influence PC composition and nanoparticle-cell interactions.

In this section, we investigate how the presence of RGD targeting moiety and rh-GLA loaded enzyme on the surface of nanoliposomes influences PC formation and composition. We also assess how these modifications impact the biological function of nanoliposomes.

6.1.1. Protein corona: the crown to rule them all

Since the introduction of the term *protein corona* in 2007 by Dawson, Linse and co-workers (328,329), numerous studies have sought to understand NP-protein interactions and their implications for nanomedicine. PC formation is a dynamic and fast process that occurs within a few minutes after the NP comes into contact with plasma or another biological fluid (330). This dynamism in PC formation is explained by the fact that the proteins with high abundance in plasma, but low affinity for the NP, are the first adsorbed to its surface. However, these are gradually replaced over time by other proteins that are less abundant in plasma but have a higher affinity for the NP surface. This phenom is known as the Vroman effect (Fig. 6.1) (331).

Several physicochemical characteristics of NPs influence the PC composition. The NP material plays a significant role in the PC composition, as different core materials (e.g. lipidic, gold or silica) interact uniquely with plasma proteins (332,333). Size and shape can be also critical in the PC composition, as different diameters and geometries of NPs exhibit distinct PC profiles (334–337). Lastly, surface charge and chemistry can also affect to the PC composition, as the net charge and functional groups on NP surfaces influence protein adsorption affinity (338–342). In fact, the addition of PEG to the surface of NPs is one of the most commonly used methods to "stealth" NPs from the immune system and extend their blood circulation time by reducing protein adsorption, but without impeding PC formation (326,327). Furthermore, certain environmental factors in biological fluid also affect the composition and formation of the PC,

such as temperature, pH, exposure time, composition and the specie of origin of biological fluid (320,343).

The PC is structured in two distinct parts, referred to as *hard corona* and *soft corona* (Fig. 6.1). The hard corona is composed by environmental proteins that exhibit a strong affinity for the NPs, interacting directly with their surface. In contrast, proteins that form the soft corona exhibit weak affinity for the NPs (328,335), interacting with the NP surface through weak protein-protein interactions with the hard corona (344,345). Consequently, the hard corona exhibits better stability over time (346) and is thought to primarily govern NP-cell interactions (347–351), whereas the soft corona is a less stable protein layer, composed by a greater number of proteins than the hard corona (352,353), which are in continuous exchange over time (354,355). Consequently, the most abundant proteins in the PC are crucial determinants of biodistribution and therapeutic efficacy (Fig. 6.1).

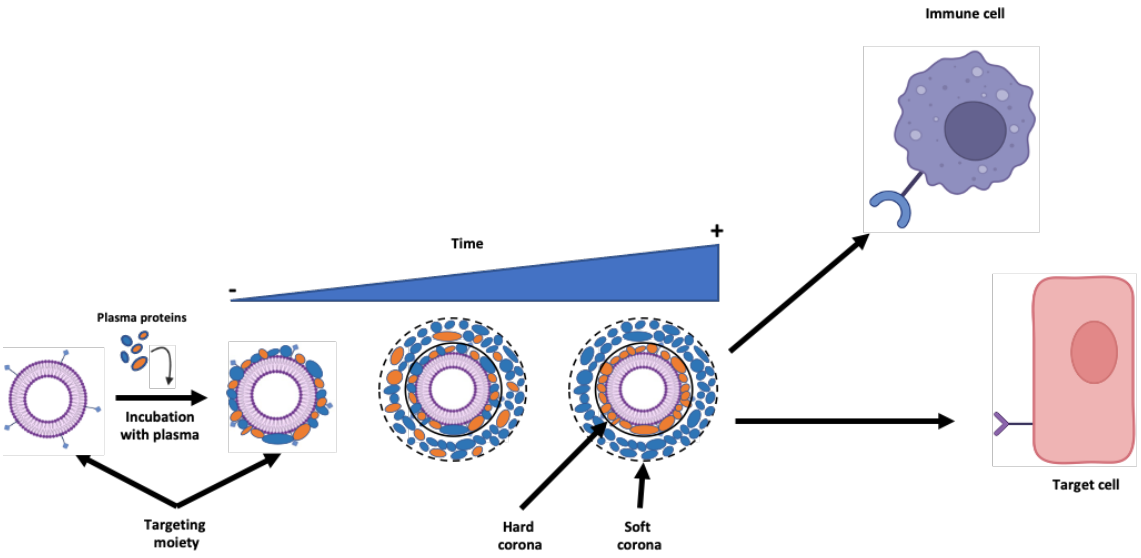

Fig. 6.1. Scheme of the dynamic process of the protein corona (PC) formation over time. This PC targeted liposomes might alter their biological identity and recognition by different type of cells.

6.1.2. Isolation of PC-nanoparticle complexes

One approach for analyzing the PC is to perform *in situ* measurements, which do not affect to PC composition, as no separation from the surrounding plasma is required. However, due to the presence of unbound proteins, the information obtained from *in situ* studies is limited (356). For *ex situ* studies, there are several methods for isolating PC-liposome complexes, such as centrifugation and size-based techniques such as gel permeation chromatography (GPC), asymmetric flow field flow fractionation (AF4) and size exclusion chromatography (SEC).

Centrifugation at 14,000-20,000 g is commonly used to isolate PC-liposome complexes, where proteins are tightly adsorbed to the liposomal surface (322,325,357–359). This method is often praised for its ability to quickly and reproducibly separate liposomes. However, the similar density of these NPs to water and plasma (360,361), along with the alteration of the liposomal curvature due to centrifugal forces and the risk of liposomal aggregation, are potential limitations associated with this methodology (362).

GPC and AF4 are alternative methods that help preserve loosely bound proteins (363). These techniques are more time-consuming than centrifugation but tend to be more reliable for

separating unbound proteins. AF4 offers even more precise control over the separation conditions, making it ideal for handling liposomes more carefully. However, AF4 typically requires low protein concentrations, which limits its application in studies involving liposome–plasma protein interactions.

SEC is a rapid and widely used method that separates PC-coated nanoparticles from unbound plasma proteins, minimizing alterations to corona composition while maintaining colloidal stability of NP. It has been widely used to isolate PC from liposomal systems (364–366). The drawback is that there is a risk of contamination due to the co-isolation of plasmatic compounds such as exosomes and lipoproteins, whose size and density are similar to those of liposomes (367). Protein components of both exosomes (368) and lipoproteins (369) could be mistakenly detected as liposomal PC components. Furthermore, protein aggregates present in plasma may co-precipitate with liposome–protein complexes. To address this, these proteins can be removed from plasma before incubation with liposomes by prior centrifugation (362,370).

6.1.3. Opsonins

Among the proteins adsorbed onto NPs in their PC after contact with plasma, certain proteins can determine the fate of the NPs by increasing their removal from the bloodstream through enhanced degradation or immune system activation (opsonins). Key opsonins include immunoglobulins (IgG, IgA, and IgM), complement proteins (C3, C4, C5, etc.) and fibrinogen (Fg).

One of the most abundant types of opsonins in the PC of NPs are proteins participating in the **complement system**. The activation of complement system has a direct effect on immune system activation, increasing the removal of the NPs from the bloodstream. This system can be activated through 3 different pathways (Fig. 6.2) (371,372):

- The **classical pathway**, triggered by C1 complex (C1q-C1r-C1s) binding to IgG or IgM on NP surfaces. This is followed by the recruitment and subsequent activation of C4 and C2, which form the C3 convertase complex that cleaves C3 into C3a and C3b (373,374).
- The **alternative pathway**, involves the spontaneous hydrolysis and subsequent conversion of C3 into C3(H2O) (375), promoting the recruitment of complement factor B (CFB). The resulting complex interacts with complement factor D (CFD), allowing the formation of an alternative version of the C3 convertase, recruiting and cleaving C3 proteins into C3a and C3b (376,377).
- The **lectin pathway**, initiated by mannose binding lectins (Mbl) that promotes the recruitment of mannan-binding lectin-associated serine proteases (MASPs). This group of proteases activates C4 and C2 which form the C3 convertase complex that cleaves C3 into C3a and C3b (378).

All three complement pathways converge on C3b protein, which can bind directly to complement receptors expressed on various immune cell types or continue the complement cascade by cleaving C5 into C5a and C5b, leading to the formation of the membrane attack complex (MAC) through the interaction of C5b with C6, C7, C8 and C9, ultimately causing the destruction of the nanoliposome (Fig. 6.2). In addition, C3a, C4a, and C5a contribute to a pro-inflammatory environment (378), promoting the recruitment of more immune cells, which could interact with NPs, leading to further removal of these from the bloodstream.

Synthetic NPs primarily activate the alternative pathway of the complement system (376,377). This is because 1) the alternative pathway is constantly active at a low level due to the spontaneous hydrolysis of C3 into C3(H2O), 2) many synthetic NPs, especially anionic or neutral

surfaces, can facilitate C3 activation, leading to complement opsonization, 3) unlike the classical pathway, which requires antibody (IgG/IgM) binding, the alternative pathway does not require specific immune recognition, making it the default activation route for many NPs.

However, other complement pathways may also be activated, depending on NP composition, charge, and functionalization (373,379–381): classical pathway is activated by NPs coated with antibodies, immune complexes, or proteins like fibrinogen. Similarly, NPs displaying mannose or glycosylated structure will activate lectin pathway triggered by mannose-binding lectins.

Thus, while the alternative pathway is the most commonly activated, specific NP surface properties can modulate activation mechanisms.

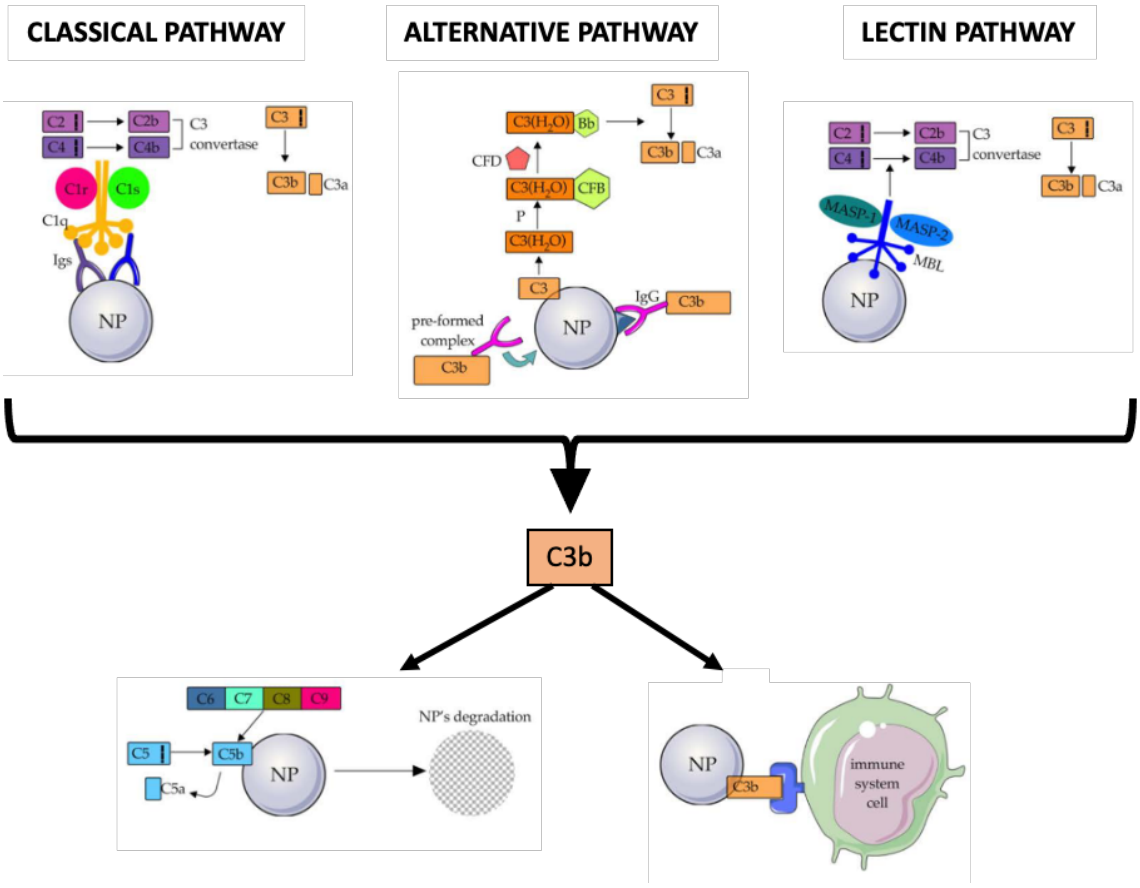

Fig. 6.2. Scheme of the different pathways of complement system activation due to NPs. This figure was adapted from Panico et al. (378).

Regarding PEGylation, it can activate the complement system (382). Specifically, PEGylated liposomes, such as liposomal doxorubicin (Doxil®), have been reported to mainly activate the alternative pathway of the complement system (378). Doxil® was the first liposomal-based cancer therapy approved by the FDA (383), and has demonstrated advantages over free doxorubicin, including reduced heart toxicity and improved efficacy. However, Doxil® also exhibits some adverse events after infusion, such as a high risk of acute hypersensitivity reactions (384,385), known as complement activation-related pseudoallergy (CARPA) syndrome (386,387). While most CARPA-related symptoms are mild, including rash, chest and back pain, and subjective distress, more serious reactions, such as cardiopulmonary distress, have been reported and may be life-threatening in certain individuals.

Other liposomal formulations, including Myocet, Abelcet, Ambiosome, DaunoXome, and Visudyne, have also shown hypersensitivity reactions after infusion (386), suggesting that CARPA reactions are not exclusive to PEGylated liposomes. Additionally, factors like negative ζ-potential and surface modifications (e.g., adding targeting ligands or therapeutic molecules) can trigger complement activation (388–390). These surface modifications can influence the liposomal particle composition and the presence of opsonins, which may affect *in vitro* internalization and *in vivo* biodistribution.

Another important type of opsonins frequently found in the PC of liposomes are the **immunoglobulins** (Igs). As previously mentioned, IgG and IgM are crucial for complement system activation. In fact, C3 opsonization of certain PEGylated liposomes is mainly initiated by the binding of IgG to their surface (376). However, Igs can also interact with receptors on immune cells, leading to the rapid clearance of liposomes (391).

Fibrinogen (Fg), a protein involved in blood coagulation, also plays a significant role in the interaction between coagulation and inflammation. It activates leucocytes through the interaction with fibrinogen-binding receptor Mac1 of activated leukocytes, promoting phagocytosis and activating complement system (392–394).

6.1.1. Dysopsonins

Other proteins adsorbed onto NP surface can extent its lifetime in systemic circulation by protecting it from phagocytosis, thereby enhancing its "stealth" capacity. These proteins are known as dysopsonins. Common dysopsonins found in the PC of NPs include albumin (Alb) and various apolipoproteins such as clusterin or apolipoprotein J (ApoJ), Apoa1, Apoa2, Apoa4, Apoc3 and Apoe (378,395). Interestingly, apolipoproteins (especially clusterin and Apoa1) are known to inhibit complement system proteins, such as C9 or C5, preventing the formation of MAC (396). Additionally, they can reduce opsonization of liposomes by Igs, thus decreasing phagocytosis and subsequent clearance from systemic circulation (397).

Alb is a classical component in the PC and can be found in different types of NPs. It has been shown to reduce phagocytosis even in the presence of opsonins like IgG (398) and can also limit hepatic uptake (399). However, Alb's role as a dysopsonin remains debated, as most studies use purified Alb, which does not reflect physiological plasma conditions (400).

In order to investigate how the presence of RGD targeting moiety and rh-GLA loaded enzyme on the surface of nanoliposomes influences PC formation and composition, we isolated the PC-nanoliposome complexes by SEC and performed *ex situ* characterization of the PC. We also included plasma without liposomes, to better control the contaminants that might come from there without being part of the liposomal PC.

6.2. Setting up conditions for PC formation by incubating nanoliposomes with plasma

Following systemic administration, PC provides nanoparticles with a new biological identity, consequently impacting in their cellular uptake and *in vivo* BD (343,401–403). Understanding the PC in the nanoliposomes described in section 5.2 (Table 5.3) is essential to for assessing their *in vitro* and *in vivo* behavior. Given that surface modification such as the addition of rh-GLA and PEG400-RGD, could affect the PC composition, we studied the PC composition in nanoliposomes

with varying PEG400-RGD surface density (0%, 3% and 6 mol%) and with or without the presence of rh-GLA.

6.2.1. The time-evolution of PC in EL-0%RGD and nanoGLA-3%RGD

PC formation is a dynamic process that depends on multiple factors, such as the physicochemical properties of the NPs and environmental conditions like temperature and incubation time with plasma (404–406). Therefore, selecting the appropriate conditions for the incubation of nanoliposomes with plasma is crucial. To determine when PC formation occurs, changes in the size, PDI and ζ-potential were monitored over time at 37°C.

The longitudinal analysis was conducted in two representative nanoliposomes: EL-0%RGD and nanoGLA-3%RGD, previously characterized in section 5.2 (Table 5.3). The first, was the unmodified nanoliposome which did not contain neither PEG400-RGD neither rh-GLA, while the second one contained both the cargo and the targeting moiety. To promote PC formation around these nanoliposomes, they were diluted with PBS 1X to a theoretical lipid concentration of 0.2 mg/mL and incubated with pooled C57BL6 mouse plasma (v/v) at 37°C under shacking conditions. PC formation was detected *in situ* in EL-0%RGD and nanoGLA-3%RGD using DLS at multiple time points post-incubation (0.5 h, 1 h, 2 h, 3 h, 6 h and 24 h). Mouse plasma without nanoliposomes was included as control for the DLS measurements.

Prior to plasma incubation, EL-0%RGD and nanoGLA-3%RGD exhibited different sizes (Fig. 6.3A, left). After 0.5 h of incubation, their sizes converged, with a slight increase in the nanoGLA-3%RGD size compared to EL-0%RGD. Interestingly, EL-0%RGD showed an increase in size (128 ± 5 nm) compared to the original size (120 ± 3 nm), probably due to protein adsorption (Fig. 6.3A, left). Conversely nanoGLA-3%RGD reduced its size (134 ± 3 nm) compared to its size in the absence of plasma (188 ± 3 nm) (Fig. 6.3A, left). This size reduction in nanoGLA-3%RGD could be explained by the osmotic pressure caused by plasma proteins adhering to the liposomal membrane, promoting water efflux from the nanoliposome interior. This effect was reported by Wolfram et al. (407) using liposomes composed of 1,2-dipalmitoyl-sn-glycero-3-phosphoethanolamine (DPPE) with or without PEG2000. In their study, the size reduction was more significant in PEGylated liposomes than in non-PEGylated ones. PEGylated liposomes exhibited greater size reduction due to enhanced PC formation, whereas non-PEGylated liposomes repelled plasma proteins, hindering corona formation.

Beyond 1 h of incubation with plasma, the size remained stable in both nanoliposomes until 24 h where a significant increase was observed (Fig 6.3A, left). However, this does not imply that the PC was not formed at earlier timepoints, it just evidences that DLS size determination might be insufficient to detect PC formation (408).

An increase in PDI, which is an indicative of loss of the liposome monodispersion and the emergence of other populations, probably indicating the formation of the PC (409), was also detected early in the in incubation period and remained stable over time (Fig. 6.3A, middle). This increase in polydispersity indicates that these samples became more heterogeneous upon incubation with mouse plasma. In fact, PDI values were similar to those observed in mouse plasma samples, indicating that the polydispersity observed in nanoliposomal samples was caused by the presence of plasma. No significant differences were observed in the comparison between EL-0%RGD and nanoGLA-3%RGD.

On the other hand, in ζ-potential measurements, both EL-0%RGD and nanoGLA3%RGD exhibited similar surface charge and became more negative over the time, probably due to the

adsorption of negatively charged plasmatic proteins. After 3 h of incubation, EL-0%RGD and nanoGLA-3%RGD showed similar ζ-potential values (-17.3 ± 0.7 mV and -16.6 ± 0.8 mV, respectively), which were lower than mouse plasma values (-13.3 ± 0.4 mV). These differences became more pronounced after 24 h of incubation (Fig. 6.3A, right). These results suggest that the PC formation in nanoliposomes can be detected *in situ* through surface charge measurements, as the PC-liposome complexes exhibited more negative ζ-potentials from those of mouse plasma.

Interestingly, initial ζ-potentials varied based on dilution medium. When prediluted in PBS 1X, surface charge of EL-0%RGD and nanoGLA-3%RGD were (-6 ± 2 mV for EL-0%RGD and -22 ± 2 mV for nanoGLA-3%RGD). In contrast, when pre-dilution was performed in Mili-Q water, the ζ-potentials of these nanoliposomes were positive (see section 5.2, Table 5.3).

Overall, these results showed that PC formation can be detected *in situ* by changes in their size, PDI and ζ-potential using DLS. After just 0.5 min of incubation with plasma, PC formation was detectable in both nanoliposomes. At 1 h of incubation, the size, PDI and surface charge of the nanoliposomes was stabilized and remained unchanged throughout the subsequent time points with no significant differences between EL-0%RGD and nanoGLA-3%RGD. Thus, supported by these results and others in the literature (345,356), 1 h was selected as the optimal incubation time for further PC characterization experiments.

6.2.2. Setting up SEC conditions with EL-0%RGD and nanoGLA-3%RGD

To further characterize the PC without the interference of unbound plasma proteins, we isolated the PC-nanoliposomes complexes using SEC. For this purpose, nanoliposomes were labelled with DiR and incubated with mouse plasma for 1 h (following optimized protocol from the previous section).

After SEC procedure, fractions with high DiR fluorescence signal indicated liposome presence and were collected and examined by DLS and cryoTEM. PC-nanoliposome complexes corresponding to EL-0%RGD and nanoGLA-3%RGD were identified in the same fractions (F6 to F8), which correlated with their expected size range. These fractions were pooled and used as post-SEC samples for DLS and cryoTEM analysis. DLS analysis revealed that, after SEC isolation, the PC-nanoliposome complexes exhibited a decrease in size, PDI and ζ-potential compared to the pre-SEC samples (Fig. 6.3B). Specifically, the sizes of EL-0%RGD and nanoGLA-3%RGD pre-SEC (121.9 ± 4.6 nm and 134.0 ± 4.6 nm, respectively) and post-SEC (114.1 ± 0.8 nm and 124.4 ± 1.1 nm, respectively) were still smaller than their initial sizes in the absence of plasma (Fig. 6.3B, left). This could be a consequence of the SEC procedure, during which only three fractions were selected; therefore, nanoliposomes that were either larger or smaller than those in the selected fractions were not collected. Another possible explanation is an osmotic effect caused by proteins adsorbed onto the nanoliposome surface.

Regarding the PDI, the observed decrease in PDI values of EL-0%RGD and nanoGLA-3%RGD post-SEC, suggests successful isolation of the PC-nanoliposome complexes corresponding to the subpopulation of nanoliposomes stained with DiR, with the removal of unbound proteins and aggregates (Fig. 6.3B, middle). The ζ-potential values also showed good quality measurements from DLS and further confirmed that SEC isolation allowed to obtain PC-nanoliposome complexes, as they exhibited lower ζ-potential values similar to those of mouse plasma samples (Fig. 6.3B, right). These findings indicate that EL-0%RGD and nanoGLA-3%RGD adsorbed plasma

protein, altering their surface charge, as previously described for other cationic liposomes (319,410,411).

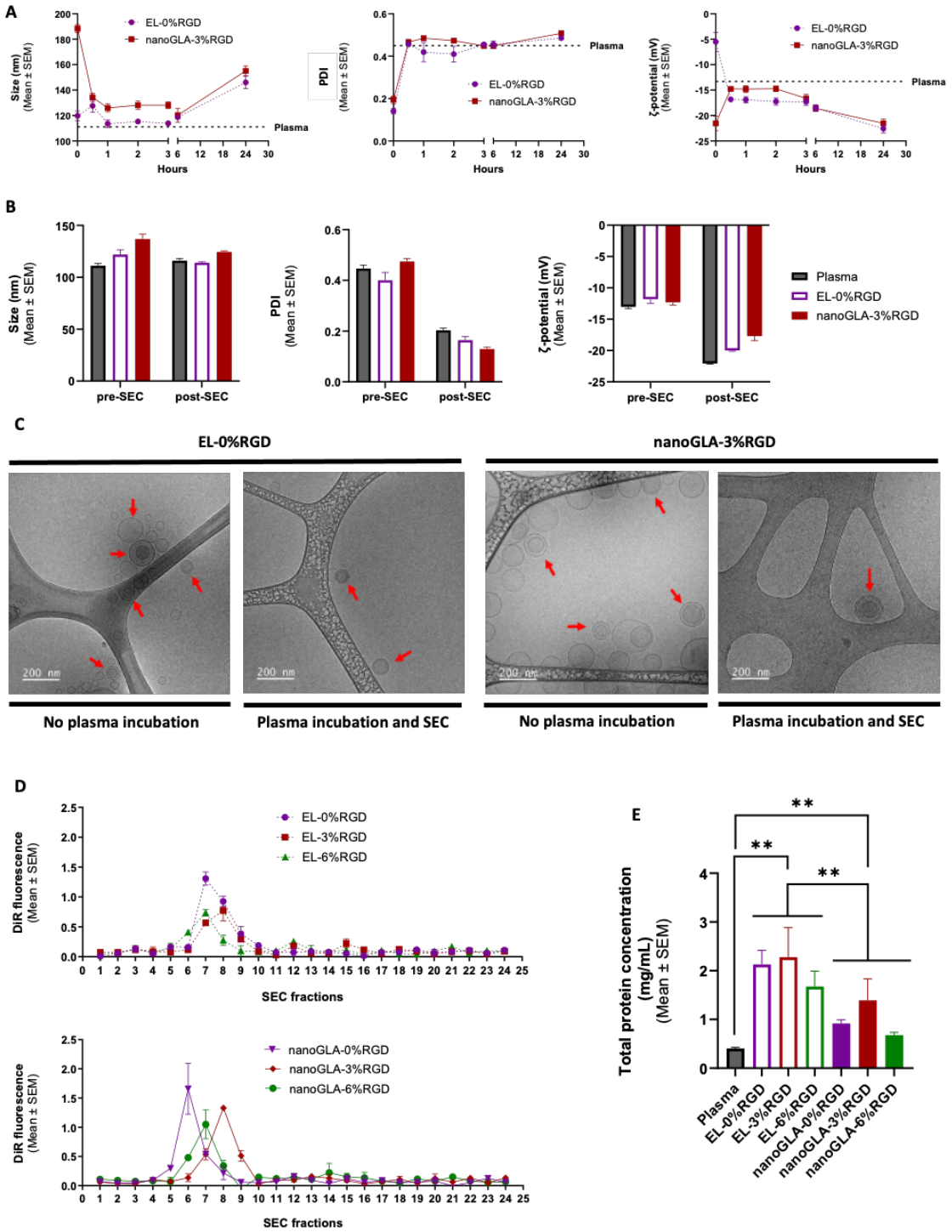

Fig. 6.3. Generation and isolation of PC-nanoliposome complexes. A) Changes in the hydrodynamic size, polydispersity index (PDI) and ζ-potential (mV) by DLS of EL-0%RGD and nanoGLA-3%RGD after different times of incubation (0.5 h, 1 h, 2 h, 3 h, 6 h and 24 h) with mouse plasma. **B)** Hydrodynamic size, PDI and ζ-potential of EL-0%RGD and nanoGLA-3%RGD incubated with mouse plasma (1 h) before and after isolation by SEC (pre-SEC and post-SEC, respectively). Mouse plasma was included as control**. C)** Cryo-TEM images of EL-0%RGD and nanoGLA-3%RGD with or without previous incubation with mouse plasma and posterior SEC purification. Red arrows indicated the presence of nanoliposomes. Magnification bar corresponds to 200 nm. **D)** Isolation of different DiR-labelled EL (upper) and nanoGLA (bottom) by SEC after 1 h of incubation with mouse plasma. **E)** Quantification of total PC protein

concentration of mouse plasma and different PC-nanoliposomes complexes. Statistical significance levels were schematically assigned ns ($p \geq 0.05$), *($0.01 \leq p < 0.05$), **($0.001 \leq p < 0.01$), ***($0.0001 \leq p < 0.001$), ****($p \leq 0.0001$).

The morphology of the nanoliposomes was assessed by cryo–transmission electron microscopy (cryo-TEM), to provided additional qualitative validation, demonstrating that both EL-0%RGD and nanoGLA-3%RGD preserved their structure and morphology after 1 h of incubation with mouse plasma and the subsequent SEC isolation process (Fig. 6.3C). This methodology allows direct investigation of colloidal systems, such as liposomes, in the hydrated state, so their structure is well preserved close to the native state. Furthermore, the formation of the PC in the nanoliposomes was also detectable in these images by a slight increase in the electron density of the nanoliposomes incubated with plasma. This phenomenon has also been observed in other types of liposomes by other authors (322). However, this result should be interpreted with caution, as the experimental conditions were not optimal. The samples were stored in a refrigerator overnight prior to cryo-TEM observation, which may have altered the structure of the PC. Of note, nanoliposomes incubated with plasma appeared more diluted than those not incubated with plasma. This is because, unlike the non-incubated nanoliposomes, the plasma-incubated ones underwent SEC processing, which involves the continuous addition of PBS to allow the sample to pass through the column, resulting in dilution of the collected fractions. Another factor that could contribute to this observation is the selection of specific subpopulation of nanoliposomes in the resulting fractions.

Overall, these results confirm that SEC isolation successfully yields PC-nanoliposome complexes suitable for further PC characterization. The resulting samples exhibited high monodispersity and minimal protein aggregation, minimizing potential interferences in PC analysis. However, it is important to note that some limitations exist in *ex situ* measurements following SEC, such as potential interactions between the nanoparticles and the stationary phase (or polymer matrix), as well as the co-isolation of plasma particles that share similar sizes with the isolated nanoliposomes, such as lipoproteins (356,366,412,413).

6.2.3. Isolation of different PC-nanoliposome complexes using SEC

After demonstrating that PC-nanoliposome complexes can be isolated by SEC for *ex situ* measurements and that the unbound protein can be removed to perform accurate analysis of the PC (Fig. 6.3B and 6.3C), the next step was to isolate the PC-nanoliposome complexes from different nanoliposomal formulations in order to study how surface components, such as PEG400-RGD and rh-GLA, can affect their PC composition.

To achieve this, DiR-labelled EL and nanoGLA with different percentages of PEG400-RGD (0%, 3% and 6%), which were characterized in Table 5.3 from section 5.2, were incubated with mouse plasma under the same conditions detailed in section 6.2.2. The presence of DiR dye allowed for the collection of SEC fractions that showed the highest intensity signal of DiR and ensuring that only PC-nanoliposome complexes were analyzed.

After 1 h of incubation with mouse plasma, fractions containing PC-nanoliposome complexes were identified based on DiR fluorescence intensity. In all samples, PC-nanoliposome complexes were consistently recovered between fractions F5 and F9, which correlates with their expected size range (Fig. 6.3D). SEC successfully separated PC-nanoliposome complexes from various EL and nanoGLA formulations, with some differences in elution patterns. Specifically, PC-nanoliposome complexes corresponding to different versions of EL were identified in the same fractions (F6 to F9), suggesting similar size distribution after plasma incubation (Fig. 6.3D, up).

However, in the case of nanoGLA, collected SEC fractions varied depending on PEG400-RGD content. NanoGLA-0%RGD eluted between fractions F5 and F7, nanoGLA-3%RGD between F7 and F9 and nanoGLA-6%RGD between F6 and F8 (Fig. 6.3D, down). These variations in elution patterns suggested size differences among the formulation after plasma incubation, possibly due to PC-induced nanoparticle aggregation (322,358). However, to confirm this theory, it is necessary to assess the isolation of nanoliposomes by SEC without prior incubation with plasma, in order to verify that these nanoformulations are not inherently isolated those fractions.

To ensure accurate PC characterization, control untreated mouse plasma was processed via SEC using the same conditions, and fractions F5 to F9 (the same used for isolation of liposomal PC) were collected as a baseline reference for protein abundances in plasma.

SEC fractions were concentrated, and total protein was determined by RC DC™ (reducing agent and detergent compatible) protein assay kit. All PC-nanoliposome complexes exhibited higher protein concentrations than mouse plasma, indicating the isolation of the PC of nanoliposomes. In detail, mouse plasma exhibited a significantly lower total protein concentration (0.4 ± 0.0 mg/mL) compared to EL (2.0 ± 0.2 mg/mL; $p = 0.003$) and nanoGLA (1.0 ± 0.2 mg/mL; $p = 0.009$) (Fig. 6.3E). Interestingly, the presence of rh-GLA in the nanoliposomes drastically reduced the amount of protein (Fig. 6.3E), indicating that the presence of the enzyme on the nanoliposomal surface could alter the adsorption of plasma proteins and modify their PC composition. In contrast, PEG400-RGD content had minimal impact on total protein concentration in the PC of nanoliposomal formulations. Only a slight decrease was observed in nanoliposomes with 6 mol% of RGD compared with those containing 3 mol% or no RGD. This is consistent with previous reports suggesting that PEGylation does not significantly influence total protein adsorption in certain liposomal formulation (324,338,414), highlighting the ongoing debate regarding PEG's role in PC formation.

6.3. Characterization of the PC in RGD-targeted nanoliposomes

Following the isolation of different PC-nanoliposome complexes in section 6.2.3, PC characterization and quantification of the relative abundances of proteins were performed using liquid chromatography-mass spectrometry (LC-MS) by the Dr. Francesc Canals's Proteomics group at VHIO. Three replicates of each PC-nanoliposome complexes sample (EL-0%RGD, EL-3%RGD, EL-6%RGD, nanoGLA-0%RGD, nanoGLA-3%RGD and nanoGLA-6%RGD) were analyzed, and untreated mouse plasma was included as a control.

6.3.1. Molecular weight (MW) and isoelectric point (IEP) of Top-25 proteins the PC

The top 25 most abundant proteins in different PC-nanoliposome complexes were classified according to their molecular weight (MW) and isoelectric point (IEP) to detect differences in the PC composition across different nanoliposomal formulations. Overall, the results showed that the majority of proteins in the PC of the different nanoliposomal formulation were small proteins (< 60 kDa) and with an IEP below the plasma pH (pH = 7.4), suggesting a predominantly negative charge (Fig. 6.4).

In mouse plasma, top 25 most abundant proteins consisted mainly small proteins (< 60 kDa, 56%), followed by large proteins (> 100 kDa, 32%) and proteins with a MW between 60 – 100

kDa (12%). A similar distribution was observed in PC of EL-0%RGD, with 56% of small proteins (< 60 kDa), 28% of large proteins (> 100 kDa), and 32% of proteins with MW between 60 - 100 kDa (Fig. 6.4, top). Interestingly, modifications such PEG400-RGD and rh-GLA incorporation led to shifts in the PC MW profile compared to non-modified EL-0%RGD. In detail, small proteins were more abundant in the modified nanoliposomes (64 – 68%) and large proteins showed similar percentages (24 – 28%), except in nanoGLA-6%RGD, where only 16% of proteins were > 100 kDa. Proteins between 60 – 100 kDa were less abundant (8%) than in EL-0%RGD and mouse plasma, though nanoGLA-6%RGD showed a slightly higher proportion (16%) (Fig. 6.4, top). These results indicate that the PC formation in modified nanoliposomes (i.e., with PEG-RGD targeting and loaded with GLA enzyme) favors the adsorption of smaller proteins. Similar findings were reported in other studies analyzing PEGylated liposomes incubated with plasma from mouse, human or FBS (322,410,415).

In terms of IEP, the top 25 most abundant proteins in plasma were mainly negatively or neutrally charged (IEP < 7.5, 80%) (Fig. 6.4, bottom), confirming that they are attracted by positively charged nanoliposomes. Indeed, most of the top 25 most abundant proteins in the PC of the different nanoliposomes showed a negative or neutral charge (IEP < 7.5). In detail, 72% of proteins in EL-0%RGD, 76% in EL-3%RGD, EL-6%RGD, nanoGLA-0%RGD and nanoGLA-3%RGD, and 80% in nanoGLA-6%RGD had an IEP < 7.5 (Fig. 6.4 bottom). These results showed no significant differences in the IEP of the PC among the different nanoliposomes.

Unexpectedly, negatively charged proteins preferentially adsorbed onto the nanoliposomes, which were negatively charged due to pre-dilution with PBS before incubation with plasma. This contradicts the expected electrostatic interactions. Similar observations have been reported by other authors (322,336,344), supporting the notion that interactions between the PC and nanoliposomes are not solely driven by electrostatic forces. In fact, other nanoliposomal characteristics, such as size, curvature, shape, surface structure, and hydrophobicity, have been described as critical factors in PC composition (343,378).

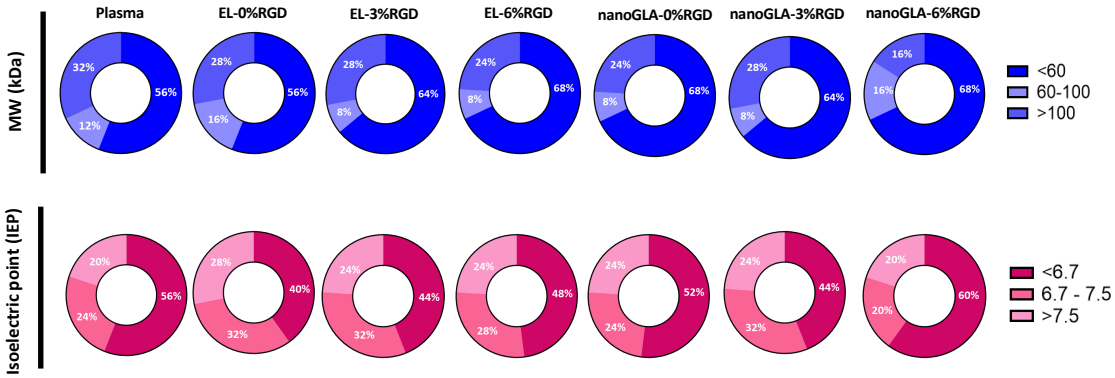

Fig. 6.4. C**lassification of the top 25 most abundant proteins in the PC of nanoliposomes according to the MW (kDa) and IEP**. **A)** Percentage of most abundant proteins smaller than 60 kDa, sized between 60 to 100 kDa and bigger than 100 kDa. **B)** Percentage of most abundant proteins with IEP < 6.7, IEP between 6.7 and 7.5 and IEP > 7.5. Mouse plasma was included as a control.

6.3.2. Top 25 proteins in the PC of RGD targeted nanoliposomes

Most studies on PC characterization in NPs typically analyze the top 20-25 most abundant proteins (319,322,403,410). These are the most abundant proteins in plasma and the first to

interact with NPs after systemic administration. They are also the first to be recognized by different types of cells, including those from the immune system (378,416).

In our study, the top 25 most abundant proteins in the PC of nanoliposomes closely resembled to the top 25 proteins detected in untreated mouse plasma (Fig. 6.5A - 6.5G). Many of these proteins have been previously described as prevalent components in the PC of other liposomes. They include Alb, serotransferrin, Fg, haemoglobin, complement factors and Apos, such as Apoe, Apoa1, Apoc3 and Apoa4 (322,410,417,418).

Although most of these proteins were common between whole plasma and nanoliposome protein coronas, some proteins were enriched in the PC of nanoliposomes compared to mouse plasma. These enriched proteins are indicated with a blue arrowhead in Fig. 6.5 and include: Fg chains (Fga, Fgb and Fgg), Alb, apolipoproteins such as Apoa1, Apoe, Apob, Apoc3, Apoc1 and Apoa4, complement factors and immunoglobins such as C3 and Ighg3 (F), murinoglobulin-1 (Mug1), thrombospondin 1 (Thbs1), hemoglobin beta adult s chain (Hbb-bs), chromodomain DNA binding protein 1 (Chd1), Clusterin (Clu), hemoglobin alpha, adult chain 1 (Hba-a1), serotransferrin (Tf), Serine protease inhibitor A3K (Serpina3k), Hemopexin (Hpx), Transthyretin (Ttr) and vitamin D binding protein (Gc) (Fig. 6.5H). Interestingly, Ttr, Ighg3 and Gc were only detected among the top 25 proteins in the PC of nanoGLA-6%RGD. Although these proteins were not present in the top 25 of the other nanoformulations, their abundance increased in the PC with the presence of RGD and rh-GLA (Fig. 6.5H).

These proteins, present in the top 25 and enriched in the PC of nanoliposomes (compared to mouse plasma) were selected for further analysis. The presence of rh-GLA on the nanoliposomal surface increased the abundance of Alb, Tf, several Apos (Apoe, Apoa1, Apoc3, Apoc1, Apoa4 and Apoc4), hemoglobin chains (Hbb-bs and Hbb-bs), and other proteins such as protease inhibitor Serpina3k, Hpx, Ttr, Gc, bradykinin (Kng1), Carboxylesterase 1C (Ces1c), alpha-1-antitrypsins Serpina1d and Serpina1b, antithrombin – III (Serpinc) and alpha-2-HS-glycoprotein (Ahsg) (Fig. 6.5A, left). On the other hand, the relative abundance of some proteins decreased in the nanoliposomal PC due to the presence of rh-GLA, such as complement factors (C4bpa, C4b and C1qc), Apos (Clu or Apoj), chromatin remodelers (Chd1) and coagulation factor XIII chains (F13b and F13a1) (Fig. 6.5A, right).

Several proteins that increased their relative abundances in the PC of nanoliposomes due to the presence of rh-GLA, such as Serpina3k, Hpx, Kng1 Ces1c, Serpina1d and Serpina1b are involved in inflammatory pathways and immune response. In detail, Serpina3k and Serpina1d are related to cytokine responses, while Serpina1b is involved in inflammatory processes (419–421). On the other hand, Kng1 and Ces1c are known to be involved in the immune response to bacterium (422,423). Finally, Hpx acts as a positive regulator of immune process, such as type II interferon-mediated signaling pathways (424).

These results suggest that the presence of rh-GLA plays a complex effect in the formation of the PC. On one hand, it could increase the nanoliposomal lifetime in systemic circulation by reducing the relative abundance of certain opsonins, such as complement factors, Fg and coagulation factors, while enhancing the presence of dysopsonins, such as Apos (especially Apoa1) and Alb in the PC (378). On the other hand, enrichment of proteins involved in immune response could promote nanoliposomal clearance from systemic circulation, thus reducing its circulation time. Evidences from BD assay in section 5.5.2 support this hypothesis, as all nanoGLA formulations exhibited higher EA in plasma compared to free rh-GLA enzyme at 30 min post-administration (Fig. 5.12), suggesting an increased circulation time for all nanoGLA formulations. However,

nanoGLA-0%RGD showed significantly higher plasma EA than nanoGLA-3%RGD and nanoGLA-6%RGD (Fig. 5.12). This could be explained by the increasing density of PEG-RGD on the nanoliposomal surface, which may play a significant role in their systemic circulation lifetime by modifying their PC composition.

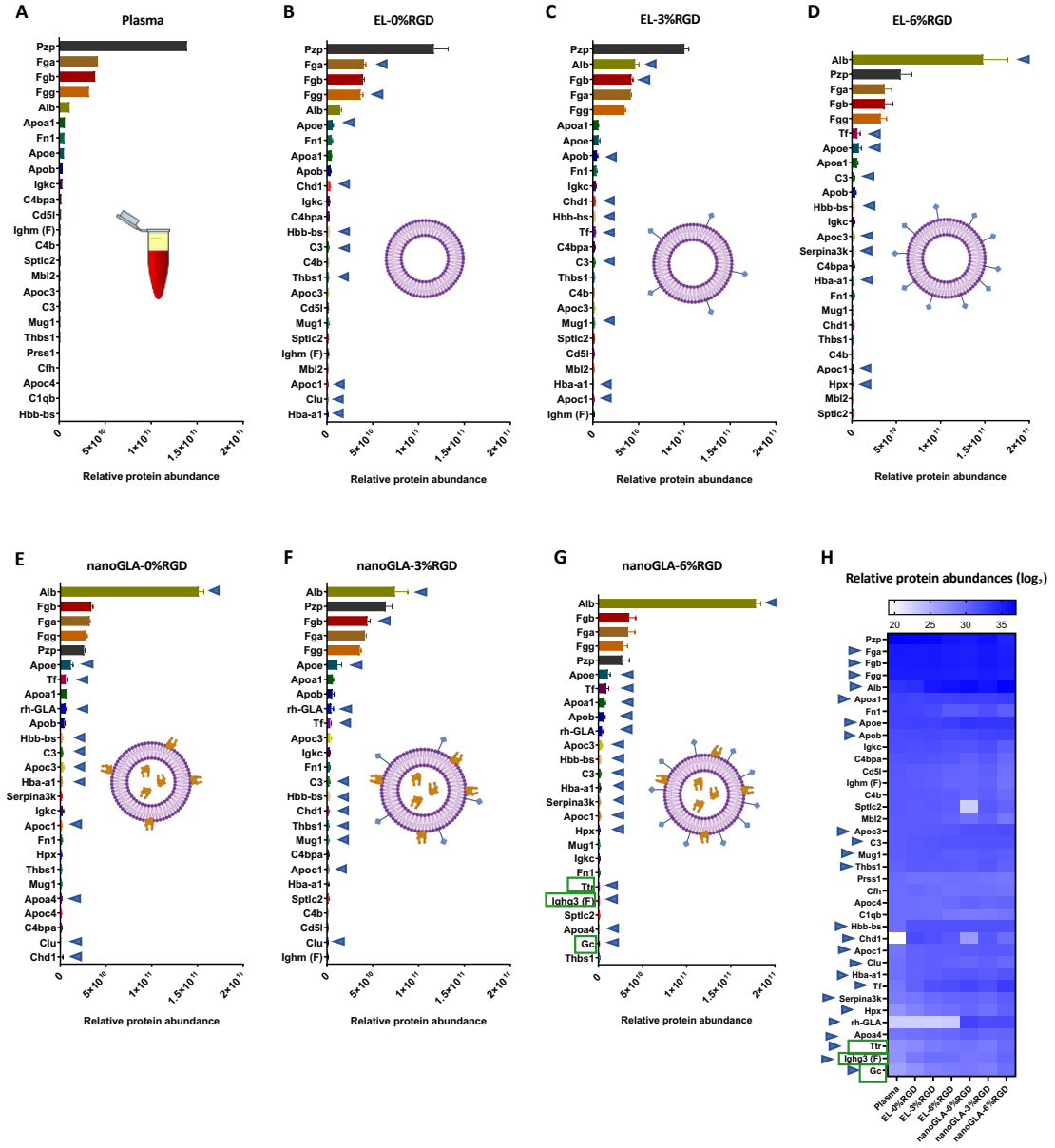

Fig. 6.5. Proteomic characterization by LC-MS of the PC in different nanoliposomal formulations after incubation with mouse plasma and purification by SEC. A-G) Top 25 most abundant proteins in mouse plasma and the protein corona (PC) of different nanoliposomal systems. Proteins are ordered according to their relative abundance. H) Heat map of the top 25 most abundant proteins in plasma and in the PC of different nanoliposomal formulations. Protein abundances were calculated as log2 of the relative protein abundances. Boxed proteins correspond to those that are unique for one nanoformulations, in this case, for nanoGLA-6%RGD. Blue arrows indicate proteins that are more abundant in the PC of the different nanoliposomes than in mouse plasma and include Fg chains (Fga, Fgb and Fgg), albumin (Alb), Apos such as Apoa1, Apoe, Apob, Apoc3, Apoc1 and Apoa4, complement factors and immunoglobins such as C3 and Ighg3 (F), murinoglobulin-1 (Mug1), thrombospondin 1 (Thbs1), hemoglobin beta adult s chain (Hbb-bs), chromodomain DNA binding protein 1 (Chd1), Clusterin (Clu), hemoglobin alpha, adult chain 1 (Hba-a1), serotransferrin (Tf), Serine protease inhibitor A3K (Serpina3k), Hemopexin (Hpx), Transthyretin (Ttr) and vitamin D binding protein (Gc).

In fact, the presence of RGD also affected the PC composition in nanoliposomes, either increasing or decreasing the relative abundance of certain proteins. However, the number of proteins influenced by rh-GLA (Fig. 6.6A) was higher than those affected by RGD (Fig. 6.6B). To identify proteins that changed their relative abundance due to the presence of RGD, we selected only those that exhibited changes in abundance either in the comparison between EL with and without RGD or in nanoGLA with and without RGD. Additionally, the change had to occur in the same direction in both groups and be dose dependent on RGD. Based on these criterions, the presence of PEG400-RGD, increased the abundance of Apoa1, opsonins such as complement factor C3 and immunoglobin Ighg3, and two proteins highly expressed in liver: the protease inhibitor murinoglobulin 1 (Mug1) (425) and the Kng1 in the nanoliposomal PC (Fig. 6.6B, right). Conversely, RGD functionalization reduced relative abundance of certain proteins, such as Fgg, complement factors C4bpa, C4b and Cfh, cell adhesion glycoprotein Thbs1, which is involved in platelet aggregation, angiogenesis, and tumorigenesis (426), Carboxypeptidase N catalytic chain (Cpn1), highly expressed in liver and predicted to be involved in several protein processing processes (427), glycosyl-phosphatidylinositol-specific phospholipase D (Gpld1), also highly expressed in liver and involved in the regulation of high-density lipoproteins clearance as a positive regulator (428), chromatin remodeler Chd1, and coagulation factor XIII chains (F13b and F13a1) (Fig. 6.6B, right). It is important to note that these proteins showed reduced abundances in the PC due to the presence of RGD in EL-3%RGD, EL-6%RGD and nanoGLA-6%RD compared to EL-0%RGD and nanoGLA-0%RGD, respectively. However, for some reason, this behavior was not observed in the comparison between nanoGLA-3%RGD and nanoGLA-0%RGD (Fig. 6.6B, right).

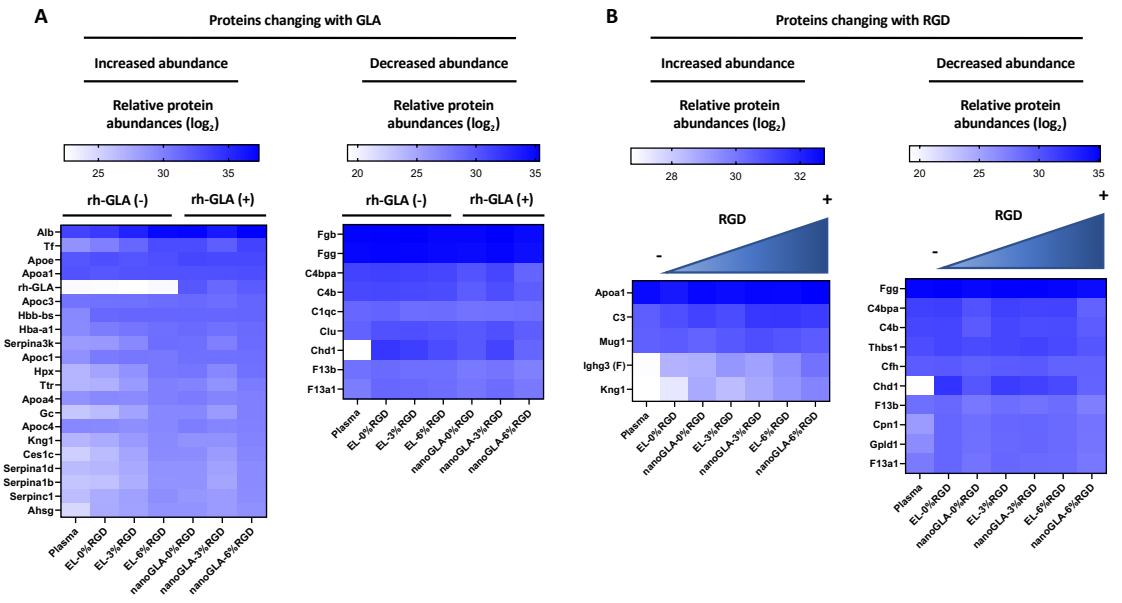

Fig. 6.6. Identification of proteins from the top 25 most abundant proteins that alter their relative presence in nanoliposomal PC, with RGD or GLA. **A)** Proteins that increase or decrease their relative abundance in the PC of nanoliposomes due to the presence of GLA. **B)** Proteins that increase or decrease their relative abundance in the PC of nanoliposomes due to the presence of RGD. Note that proteins Apoa1 and Kng1 increased their presence in PC with RGD and GLA, while Fgg, C4bpa, C4b, F13b and F13a1 did the opposite. Mouse plasma was included as control.

Despite this discrepancy, these results confirm that the presence of PEG-RGD influences the formation of the PC. Specifically, the addition of RGD appears to shorten the circulation lifetime of nanoGLA and promote their accumulation in organs rich in macrophages, such as the spleen (Fig. 5.11 and 5.12). This behavior can be explained by the composition of the PC, which contains C3 and IgG, two proteins known to enhance NP delivery to the spleen (321,429).

The incorporation of RGD on the surface of the nanoliposomes increased the relative abundance of immune-related proteins, such as Kng1, as well as opsonins like C3 complement factor and Ighg3, suggesting the presence of IgG in the PC. This outcome was expected, as other authors have reported the immunogenicity of RGD in other liposomal formulations (302,304,430) and microparticles (431). Furthermore, the presence of IgG may be further amplified by PEG, which can trigger the production of anti-PEG IgG, as observed with other PEGylated NPs by other authors (378,432).

Interestingly, not all opsonins showed the same pattern. Some, including additional complement proteins (C4bpa, C4b and Cfh), Fg and coagulation factors, exhibited a decrease in their relative abundance in the presence of RGD. On the other hand, RGD also increased the presence of Apoa1 in the PC, which could enhance the "stealth effect" of these PEGylated nanoliposomes, a phenomenon previously described for PEGylated NPs by other authors (400). However, the presence of this dysopsonin did not seem to influence the abundance of other opsonins like C3 and IgG.

In addition to these individual effects, some proteins in the PC were influenced by both rh-GLA and RGD, indicating a combined effect. In detail, Apoa1 and Kng1 showed increased abundance in nanoliposomal PC with RGD and GLA, while Fgg, C4bpa, C4b, F13b and F13a1 exhibited the opposite trend. The increased presence of the dysopsonin Apoa1 and the decreased presence of opsonins such as Fgg, C4bpa, C4b, F13b and F13a1 in the nanoliposomal PC could contribute to the stealth properties of the nanoGLA with PEG400-RGD, helping to evade phagocytic cells (400).

Overall, these results indicate that both RGD and rh-GLA influenced the PC composition. Individually, they can increase the presence of opsonins, such as immune response-related proteins, C3 and Ighg3, as well as dysopsonins, such as Apoa1 and Alb. At the same time, they also reduce the presence of other opsonins, including complement factors, Fg and coagulation factors. Ultimately, the balance of the relative abundance of these proteins in the PC might be critical for determining the fate and BD of the nanoliposomes.

6.4. Analysis of the proteins in the PC affecting nanoliposome bioavailability and function

The presence of specific proteins in the PC of NPs, such as complement factors, Igs and Apos, has been shown to be critical for the tolerance or activation of the immune system due to the recognition of NPs and their subsequent clearance from the systemic circulation, which limits their bioavailability and function. In this section, we list some of these proteins and evaluate how their relative abundances are affected by rh-GLA and RGD functionalization, based on proteomic results obtained in the previous section.

6.4.1. Complement factors

Complement factors are one of the most important type of opsonins, as they can reduce the lifetime of NPs in systemic circulation by activating the immune system or by directing them to clearing organs, such as from the liver, spleen and lungs (433). It is well-established that complement factors are among the common proteins found in the PC of liposomes (322,378,433). Interestingly, several studies show that NPs, even PEGylated ones, can activate the complement pathway (379,434,435), while others demonstrate the immunogenicity of RGD peptide in mice (302,304). For these reasons, we evaluated the complement factors that were

more abundant in the PC of the different nanoliposomal formulations compared to plasma, and how their abundances changed in the presence or absence of rh-GLA and RGD.

Our results revealed that the presence of complement proteins varied significantly across nanoliposomal formulations, depending on the presence of rh-GLA and/or RGD (Fig. 6.7). A total of 13 complement factors were found to be more abundant in nanoliposomal PC compared to plasma. These proteins were C3, C5, C1ra, C8b, C8a, Cfi, C8g, C9, Cfhr4, C6, C1sa, C1s2 and Cfhr1. The presence of rh-GLA increased the abundance of some of these complement proteins, such as C5, Cfi, C9 and Cfhr4 (Fig. 6.7A), while decreased the abundances of C1ra and C1s2 in the nanoliposomal PC composition (Fig. 6.7B). On the other hand, RGD increased the presence of C3 (the most abundant complement protein in plasma), C5, C8b, C8a, Cfi, C8g, C9, Cfhr4, C6, C1sa and Cfhr1 (Fig. 6.7C), while also decreased the abundance of C1s2 (Fig. 6.7D). In addition, the proteins C5, Cfhr4 and Cfhr1 increased their presence in the nanoliposomal PC with both RGD and rh-GLA, whereas C1s2 showed the opposite trend.

Interestingly, only C3 was found in the top 25 most abundant proteins in the PC of the nanoliposomes, while C5, C1ra and Cfi were found in the top 100. This suggests that these complement proteins may be more relevant than others for the nanoliposome BD, as they were the most abundant in the PC. In fact, C3 is frequently found as among the 25 most abundant proteins in the PC of liposomes (322,410,417). The conversion of C3 into C3a and C3b is a crucial step for initiating the downstream terminal classical pathway of complement. However, the mere deposition or cleavage of C3 on the surface of nanoliposomes does not automatically indicate the complement activation pathway. Nevertheless, an alternative pathway, which involves the spontaneous hydrolysis and subsequent activation of C3, could promote complement activation (378), leading to phagocytosis of the nanoliposome by immune cells and Kupffer cells from the liver (319).

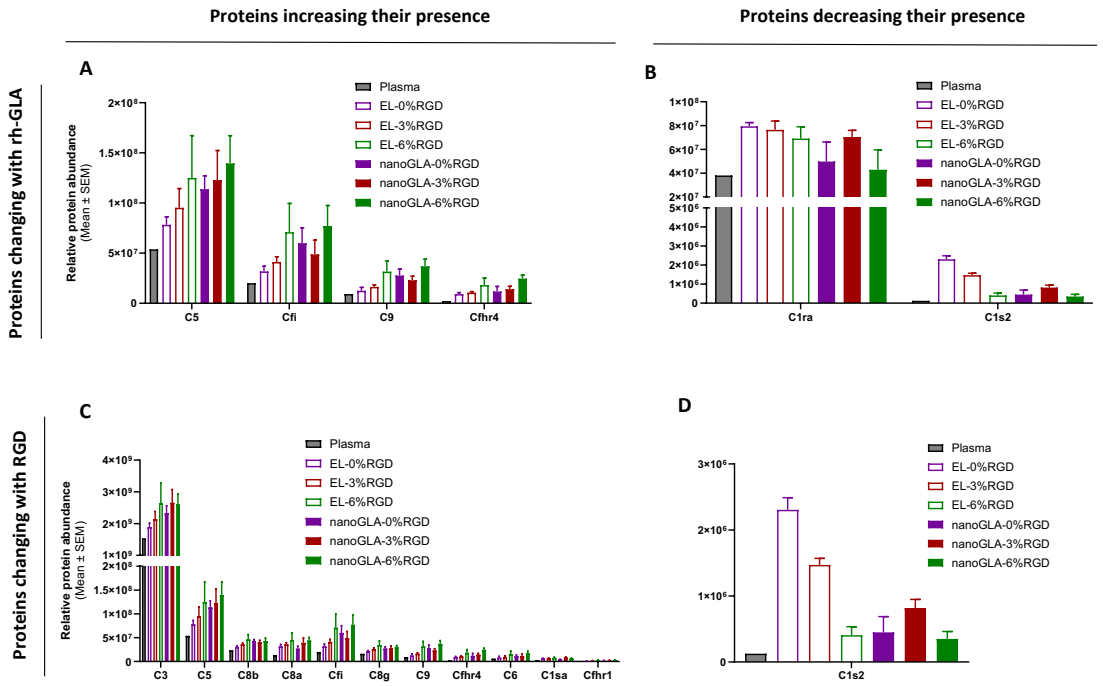

Fig. 6.7. Complement factors enriched in the PC of the nanoliposomal systems that altered their abundances with the presence of rh-GLA or RGD. A) Complement factors that increase their relative abundance in the PC depending on the presence of rh-GLA. B) Complement factors that decrease their relative abundance in the PC depending on the presence of rh-GLA. C) Complement factors that increase their relative abundance in the PC depending on the presence of RGD. D) Complement factors that decrease their relative abundance in the PC depending on the presence

of RGD. Note that proteins C5, Cfi and Cfhr4 increased their presence in PC with RGD and GLA, while C4b, C1qc, C1qa and C1s2 did the opposite. Mouse plasma was included as control.

On the other hand, C5 protein is involved in the final steps of complement activation. This protein contributes to the formation of the MAC, which promotes the degradation of nanoliposomes and their subsequent removal from systemic circulation (378,436). C1ra is one of the components of the C1 complex, which is the first complex that initiates the classical complement pathway by binding to IgG or IgM (378). A decrease in the abundance of this protein, along with a decrease in C1s2 (another component of C1 complex), due to the presence of both RGD and rh-GLA, could reduce the activation of the classical complement pathway. In contrast, the increased presence of Cfi in the PC of the nanoliposomes, due to RGD and rh-GLA, could improve the nanoliposomal circulation time, as Cfi plays a critical role in regulating all complement pathways by degrading activated critical proteins like C3b and C4b (437). However, the abundance of Cfi in the PC of the nanoliposomes is much lower than that of C3 and C5, suggesting that it is unlikely to fully inhibit the complement response.

C3 was found in high relative abundance in the PC of the nanoliposomes and may play a key role in their BD. Its presence could lead to increased opsonization of the nanoliposomes, enhanced recognition by immune cells such as macrophages, and subsequently greater clearance from blood circulation. This effect was observed in previous sections, where the presence of RGD on the nanoliposomes—associated with higher levels of C3 in their PC—correlated with a reduced plasma half-life. Furthermore, the presence of C3 in the PC may also explain the higher levels of antibodies in the PC and the increased presence of ADAs in the nanoGLA-3%RGD compared to free enzyme, as discussed previously.

Overall, these results showed that the presence of both rh-GLA and PEG400-RGD increased the abundance of complement factors such as C3 and C5 in the PC (Fig. 6.7A and 6.7C). It appears that RGD played a more important role than rh-GLA in increasing the abundance of key complement factors, such as C3. However, rh-GLA also contributed to enhancing the immunogenicity of nanoGLA by increasing the abundance of C5. Several studies by other authors have reported the immunogenicity of RGD (302,304) and have shown that complement activation can occur in PEGylated NPs (379,434,435). Additionally, the high abundance of complement factors associated with the presence of rh-GLA could be due to the different species origin of this enzyme, which might lead to the recognition of the protein as a foreign antigen, thereby activating the complement cascade. Again, the increased presence of complement factors observed in the PC of nanoliposomes, related to the presence of RGD, could contribute to higher nanoliposomal retention of these systems in liver and spleen (321), likely explaining the higher BD in liver and spleen observed with the RGD-targeted nanoGLA in the results from sections 5.5.1. and 5.5.2.

6.4.2. Immunoglobulins

Immunoglobulins (Igs) are another major type of opsonins, alongside complement factors. Thus, we evaluated the presence of Igs in the PC of the different nanoliposomal formulations, following the same methodology as before.

Results showed that the abundance of certain Igs varied in the PC of nanoliposomes due to the presence of rh-GLA and RGD (Fig. 6.8). Interestingly, the effect of RGD on Ig presence was smaller than that of rh-GLA, as RGD increased the abundance of fewer Igs while also reducing the levels of a large numbers of Igs compared to rh-GLA. Specifically, a total of 45 Igs were found to be

enriched in nanoliposomal PC compared to their abundance in plasma. However, only 5 of these Igs were among the top 100 most abundant proteins in the PC of the nanoliposomes, indicating a strong interaction with the nanoliposomal surface. Notably, the presence of rh-GLA increased the abundance of 7 Igs (15.5%), including Ighg2b (F) and Ighg1 (F), which are fragments from IgG (Fig. 6.6A, left). Additionally, rh-GLA decreased the abundance of 14 Igs (31.1%) in the nanoliposomal PC composition (Fig. 6.8A, right). In contrast, RGD increased the relative abundance of 4 Igs (8.9%), including Ighg3 (F), Ighg2b (F) and Ighg1 (F), which were also IgG fragments (Fig. 6.8B, left), while decreasing the abundance of 19 Igs (42.2%) (Fig. 6.6B, right), further suggesting that RGD presence alters Igs adsorption patterns in the PC, likely due to the presence of PEG. Furthermore, the proteins Ighg1 (F) and Ighg2b (F) increased their presence in the nanoliposomal PC with both RGD and rh-GLA, whereas other proteins such as Igkv6-15 (F), Igkv6-17 (F), Igkv2-109 (F), Igkv4-62 (F), Igkv-1-117 (F), Igkv3-7, Igkv8-34 (F), Igkv6-14 (F) and Igkv7-33 showed the opposite trend. Moreover, some opposing effects on the abundance of certain Igs were observed between rh-GLA and RGD. In detail, Ighv1-69 (F) reduced its abundance with rh-GLA but increased it with RGD, while Ighv11-2 (F) and Igkv14-126 (F) reduced their abundance with RGD but increased it with rh-GLA (Fig. 6.8).

Interestingly, only Ighg3 (F), Ighg2b (F), Ighg1 (F), which are fragments derived from IgG, as well as Ighv11-2 (F) and Igkv12-89 (F), were found among the top 100 most abundant proteins in the PC of the nanoliposomes (Fig. 6.8D). This suggests that these immunoglobulin fragments are particularly relevant within the PC of nanoliposomes compared to other immunoglobulins. In fact, IgG fragments showed high relative abundance in the PC of the nanoliposomes when both RGD and rh-GLA are present (Fig. 6.8D). However, Ighv11-2 (F) and Igkv12-89 (F), only increased in abundance in the PC of the nanoliposomes when rh-GLA was present, indicating a possible specificity for rh-GLA.

The presence of Igs is commonly observed among the 25 most abundant proteins in the PC of other liposomes (319,322,417). Moreover, IgG is one of the most abundant Igs in plasma, and its function include promoting phagocytosis and activating the complement system (319,378). Consequently, IgG can facilitate the clearance of NPs from the systemic circulation, reinforcing its role in immune recognition and elimination of nanocarriers.

Overall, these results showed that the presence of rh-GLA and RGD has an impact in the Ig composition of the PC. In fact, rh-GLA increased the abundance of more Ig fragments (15.5%) than the presence of RGD (8.9%). This was expected, as the presence of ADAs against GLA in Fabry patients has been well documented by other researchers (52,438). Nonetheless, an increased presence of IgG fragments in the PC of the nanoliposomes due to the presence of rh-GLA and RGD was also observed. In fact, other authors have reported the presence of IgG as anti-PEG antibodies in solid lipid nanoparticles, silica nanocapsules and liposomes (432,439,440). The increased presence of IgG fragments observed in the PC of nanoliposomes, associated with the presence of RGD, could contribute to the retention of nanoliposomes in the liver and spleen (321). This may explain the higher BD in the liver and spleen observed with the RGD-targeted nanoGLA, as shown in the results from sections 5.5.1. and 5.5.2.

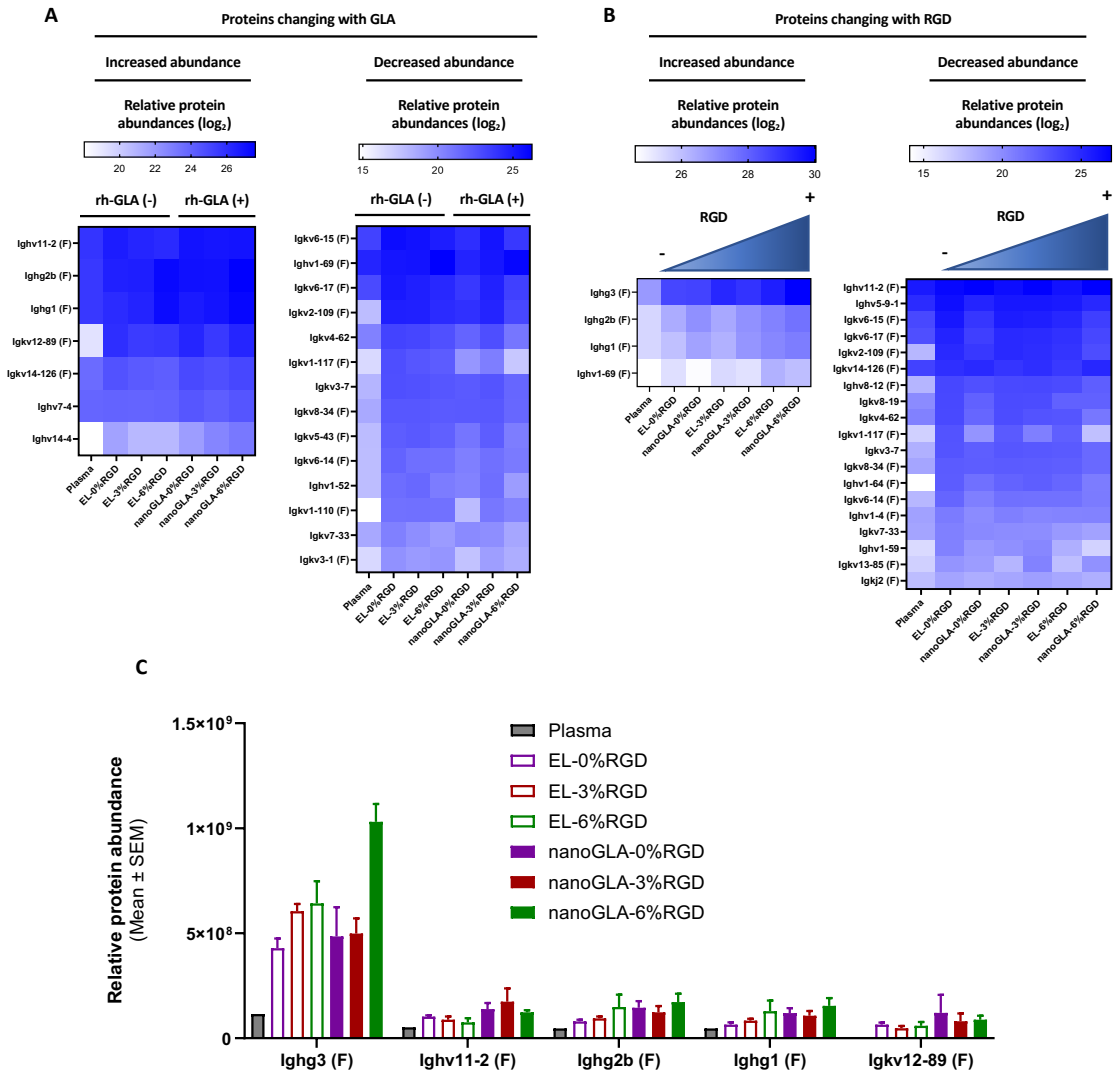

Fig. 6.8. Identification of immunoglobulins (Igs) enriched in the PC of the nanoliposomal systems that altered their relative abundances with the presence of rh-GLA or RGD. A) Igs that increase or decrease their presence in the PC of nanoliposomes with rh-GLA. **B)** Igs that modified their abundances in the PC of nanoliposomes with RGD. **C)** Igs from the top 100 of most abundant proteins the PC of the nanoliposomes that change their relative abundance due to RGD or rh-GLA. Mouse plasma was included as control.

6.4.3. Apolipoproteins

Apolipoproteins are a group of proteins involved in lipid transport and metabolism, generally classified as dysopsonins because they can downregulate complement factors (378), which increases the lifetime of NPs in plasma and can help them to cross biological barriers such as the blood-brain barrier (BBB) (441,442).

When studying the relative presence of apolipoproteins in the nanoliposomal PC, 8 apolipoproteins were found to be more abundant in the PC of the nanoliposomes than in plasma. These were Apoe, Apoc3, Apoa4, Apoc1, Clu (or Apoj), Apod, Apoa5 and Apof. However, only 5 of these apolipoproteins appeared among the top 100 most abundant proteins in the PC of the nanoliposomes (Fig. 6.9), demonstrating their relevant presence in the PC compared to other lipoproteins. Specifically, these were Apoe, Apoc3, Apoa4, Apoc1 and Clu. Furthermore, these lipoproteins were also found in the top 25 most abundant proteins in the PC of the liposomes in the present study and have been reported by some authors as being commonly

found in high abundances in the PC of other liposomes, particularly Apoe, Apoc3, Apoa4 and Clu (322,417,443–445).

In addition, the results showed changes in the abundance of certain apolipoproteins due to the presence of both rh-GLA and RGD. In detail, the presence of rh-GLA on the nanoliposomal surface increased the abundance of Apoe, Apoc3, Apoa4 and Apoc1, while slightly decreased the abundance of Clu in the nanoliposomal PC (Fig. 6.9). A similar trend was observed for RGD which also increased the relative abundance of the same apolipoproteins in the nanoliposomal PC (Fig. 6.9). However, unlike rh-GLA, no decrease in the abundance of the selected apolipoproteins was observed due to the presence of RGD.

Overall, these findings indicate that both rh-GLA and RGD enhance the abundance of the same apolipoproteins in the PC of the nanoliposomes. The most abundant apolipoprotein in the PC was Apoe, which, as reported by other authors, can bind to certain complement proteins, such as C1q and Cfh, activating the complement pathway (446). Additionally, it can enhance the uptake of NPs by the liver and spleen (321,447,448), increasing the clearance of nanoliposomes from systemic circulation. This may explain the higher levels of EA delivered by the different nanoGLA formulations to the liver and spleen observed in the BD assay from sections 5.5.1. and 5.5.2. On the other hand, Apoc3, Apoa4, Apoc1 and Clu were found to be abundant in the PC of the nanoliposomes, but at lower levels compared to Apoe. These apolipoproteins have been described as dysopsonins, enhancing the lifetime of some inorganic NPs, such as superparamagnetic iron oxide nanoparticles and silica nanoparticles, in systemic circulation (400,449–451).

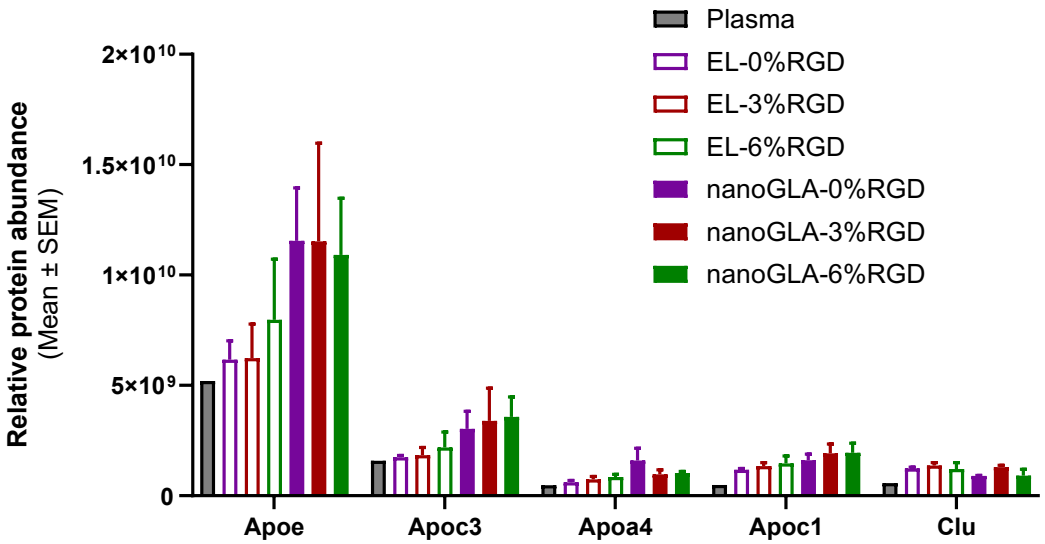

Fig. 6.9. Identification of lipoproteins enriched in the PC of the nanoliposomal systems with the presence of RGD or rh-GLA.

Importantly, other authors have found that presence of Apoe in the PC of NPs improved their ability to reach the brain by facilitating the crossing of the BBB (321,359,441). Therefore, the presence of this apolipoprotein in the PC of the different nanoGLA formulations may explain why these nanoliposomes were able to cross the BBB in the *in vivo* BD assay of sections 5.4.1. and 5.4.2.

6.4.4. Other selected proteins

6.4.4.1. Albumin

Albumin (Alb) is one of the most abundant proteins in the PC of various types of NPs. It has the capacity to modulate the BD of NPs and, due to its non-toxicity and non-immunogenicity, this protein is considered an excellent dysopsonin. In fact, several studies used a pre-coating of Alb in their NPs to reduce their phagocytosis, even in the presence of IgG (398,452). However, it is important to note that there is no clear consensus on the stealth capacity of Alb, as most of the studies using the Alb pre-coating strategy have utilized the purified protein, which differs significantly from the real presence of this protein in plasma (453).

Our proteomic analysis showed that Alb is one of the most abundant proteins in the PC of the different nanoliposomes, with its relative abundance being higher than in mouse plasma and increasing with the presence of rh-GLA. In the case of EL, Alb abundance increased with the presence of RGD (Fig. 6.5A and 6.10A). These findings indicated that Alb may play an important role in the *in vivo* fate of nanoliposomes due to its high abundance in the PC. This could explain why the presence of rh-GLA and RGD in the nanoliposomes, which is associated with a higher abundance of Alb in their PC, showed a decrease in the abundance of some Igs, as discussed in section 6.4.2.

6.4.4.2. Fibrinogen

Fibrinogen (Fg) is the second most abundant protein in plasma and is commonly detected in the PC of liposomes with different compositions (323,445,454–457). Fg is a 340 kDa glycoprotein composed by two groups of three polypeptide chains known as alpha, beta, and gamma, which are connected through disulfide bonds (458). This protein complex is involved in blood coagulation, inflammation, phagocytosis, complement activation, leukocyte activation and it also interacts with endothelial cells (378,414). Due to its involvement in multiple processes that could directly affect the bioavailability of NPs in systemic circulation, we evaluated the presence of the three Fg chains (Fga, Fgb and Fgg) in the PC composition of the different nanoliposomal formulations.

Results showed that Fg is present in the top 5 most abundant proteins in the PC of all nanoliposomal formulations (Fig. 6.5). The relative abundance of Fgb and Fgg decreased in the presence of rh-GLA in both nanoGLA-0%RGD and nanoGLA-6%RGD, and a trend can be observed in the reduction of Fgg abundance in the PC of the EL due to the presence of RGD (Fig. 6.10B). All EL formulations showed similar relative abundances of the three Fg chains in their PC compared to mouse plasma (Fig. 6.10B).

Overall, these results showed similar levels of Fg abundance between mouse plasma and the PC of the different nanoliposome versions, suggesting that this protein may not play a critical role in the *in vivo* fate of nanoliposomes due to its low enrichment in the PC. Additionally, the presence of Chol-PEG400-RGD seems to have no effect in reducing the levels of Fg in the PC of the different nanoliposomes. This observation contradicts previous studies in the literature where low amounts of fibrinogen was detected on negative PEGylated liposomes after in incubation with murine plasma (354,414,459,460). However, other liposomal formulations with DOTAP–DOPC–DC-Chol–DOPE–DOPE-PEG2000 adsorbed more fibrinogen after 90 min of dynamic incubation with FBS compared with static incubation (357).

6.4.4.3. Transferrin

Functionalization of NPs with transferrin (Tf) is one of the most commonly used strategies to cross the BBB and deliver therapies to the brain, due to the high presence of Tf receptors (Tf R) in this biological barrier (321,461). Interestingly, Tf is one of the top 25 most abundant proteins in the PC of RGD targeted EL and all nanoGLA versions (Fig. 6.5H).

Proteomic analysis showed that Tf is an important component of the PC of all nanoliposomal systems, as it showed higher relative abundance compared to mouse plasma. Tf levels increased with the presence of rh-GLA and, in some cases, with the presence of RGD (Fig. 6.10C). In fact, a significant increase in Tf relative abundance was found in EL-3%RGD compared to EL-0%RGD ($p < 0.02$), demonstrating that the presence of RGD also influenced the presence of Tf in the nanoliposomal PC. However, this correlation between the presence of RGD and the increasing abundance of Tf in the PC is not evident in nanoGLA-3%RGD compared to nanoGLA-0%RGD (Fig. 6.10C). A similar pattern was observed in nanoGLA-3%RGD for other proteins, such as Alb, fibronectin (Fn1), transthyretin (Ttr) and mannose-binding proteins (Mbl) (Fig. 6.10). The lack of correlation in nanoGLA-3%RGD suggests an unknown factor affecting its PC formation, which requires further investigation.

Importantly, several studies reported that both IgA and IgM reduced the capacity of Tf-Tf R recognition and, subsequently, reduce the ability of Tf-functionalized NPs to cross the BBB (462–464). This highlights the potential impact of immunoglobulins in the PC on the efficiency of Tf-mediated brain targeting, which should be considered when designing BBB-penetrating nanomedicines.

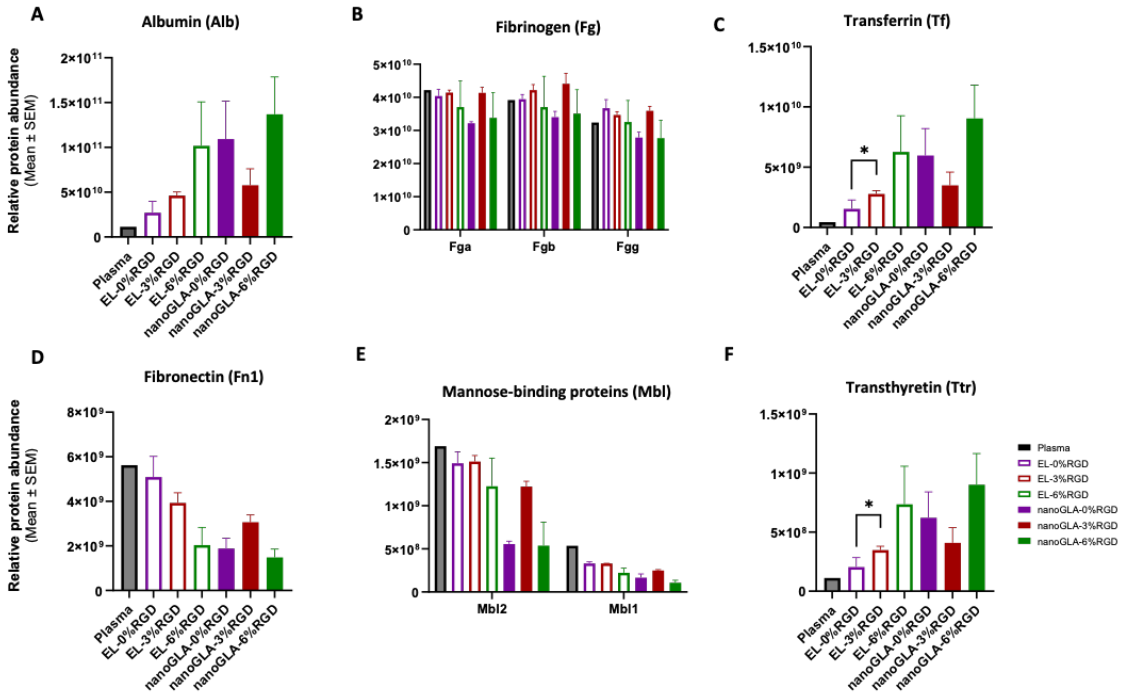

Fig. 6.10. Relative abundances in the PC of selected proteins. A) Relative abundance of Alb in the PC of the different nanoliposomal formulations. **B)** Relative abundance of the different Fg chains in the PC of the different nanoliposomal formulations. **C)** Relative abundance of Tf in the PC of the different nanoliposomal formulations. **D)** Relative abundance of Fn1 in the PC of the different nanoliposomal formulations. **E)** Relative abundance of different Mbl in the PC of the different nanoliposomal formulations. **F)** Relative abundance of Ttr in the PC of the different nanoliposomal formulations. Mouse plasma was included as control. Statistical significance levels were schematically assigned ns ($p \geq 0.05$), *($0.01 \leq p < 0.05$), **($0.001 \leq p < 0.01$), ***($0.0001 \leq p < 0.001$), ****($p \leq 0.0001$).

In this regard, the PC of all nanoliposomal formulations showed lower abundance of both Igha and Ighm, components of IgA and IgM, respectively, compared to plasma. In addition, the presence of rh-GLA further reduced the abundance of both Igha and Ighm. Therefore, the reduction in the abundance of these Igs, along with the increased abundance of Tf in the PC of the nanoliposomes, could facilitate the translocation across BBB of the nanoGLA. However, another important aspect is the expression of ubiquitous Tf R in other organs, such as liver and spleen (321), which could lead to undesired uptake of the nanoliposomes by these organs. This is probably what was observed in the *in vivo* BD assay in sections 5.5.1. and 5.5.2, where higher BD in liver and spleen was shown.

6.4.4.4. Fibronectin

Fibronectin (Fn1) is a large extracellular protein that promotes phagocytosis by mononuclear phagocytic system and has a high affinity for liposomes due to its ability to undergo conformational changes (465), their lipid composition and positive charge (466), and interaction with specific peptide sequences, such as RGD (467,468). Therefore, its presence in the PC could reduce the lifetime of nanoliposomes in the systemic circulation. In addition, Fn1 was detected among the top 25 most abundant proteins in PC of nanoliposomes. However, contrary to what we observed for Alb and Tf, Fn1 levels in the PC of nanoliposomes were lower than those in plasma (Fig. 6.5 and 6.10D).

The presence of RGD and, consequently, PEG400 reduced the relative abundance of Fn1 in the PC of EL (Fig. 6.10D). Additionally, the presence of rh-GLA in the nanoliposome also decreased the presence of Fn1. However, as was observed in previous sections, the increase in the Fn1 presence was not that evident in nanoGLA-3%RGD compared to nanoGLA-0%RGD and nanoGLA-6%RGD.

Overall, these results demonstrated that Fn1 is not enriched in the PC of the nanoliposomes, as its relative abundance is lower than in mouse plasma. The presence of RGD and rh-GLA in the liposomes reduce the abundance of Fn1, that might favor an increase in the circulation time of RGD functionalized and GLA loaded nanoliposomes.

6.4.4.5. Mannose-binding proteins (Mbl)

Mannose-binding proteins or lectins (Mbl) are molecules associated with the innate immune system that plays a role in promoting phagocytosis and activating the lectin pathway of complement cascade via C4 and C2 (Fig. 6.2) (469). Due to its ability to activate the immune system, Mbl could act as an opsonin for the NPs potentially reducing its lifetime in plasma and enhancing their delivery to organs such as liver and spleen.

Our results showed that Mbl2 is more abundant than Mbl1. In fact, Mbl2 is among the top 25 most abundant proteins in the PC of EL (Fig. 6.5B to 6.5D). However, its abundance is lower than in mouse plasma, indicating that is not enriched in the PC of the different nanoliposomes. A similar trend was observed for Mbl1 protein (Fig. 6.10E). In addition, the presence of rh-GLA led to a decrease in the relative abundance of both Mbl2 and Mbl1. As observed previously, nanoGLA-3%RGD did not follow the same trend as the other nanoliposomal formulations. Moreover, the presence of RGD did not result in a clear reduction of these proteins in the PC of the nanoliposomes (Fig. 6.10E).

Taken together, these results indicate that the presence of Mbl proteins in the PC of the nanoliposomes is reduced when compared to the plasma suggesting that their role in immune-mediated clearance of these formulations may be limited.

6.4.4.6. Transthyretin

Transthyretin (Ttr) is a protein involved in the transport of thyroid hormones and retinol. It also prevents beta-amyloid aggregation in humans, showing a neuroprotective role in Alzheimer's disease. Additionally, it has been explored as a targeting moiety in inorganic NPs due to its ability to cross the BBB (470).

The results showed that Ttr is enriched in the PC of all nanoliposomal systems and is among the top 25 most abundant proteins in the PC of nanoGLA-6%RGD (Fig. 6.5G). The relative abundance of this protein increased with the presence of rh-GLA and RGD (Fig. 6.10F). In fact, a significant increase in Ttr relative abundance was found in EL-3%RGD compared to EL-0%RGD ($p < 0.03$), demonstrating that the presence of RGD also influenced the abundance of Ttr in the nanoliposomal PC. However, as observed in previous sections, this correlation between the presence of RGD and the increasing abundance of Ttr in the PC is not evident in nanoGLA-3%RGD compared to nanoGLA-0%RGD (Fig. 6.10F).

Altogether, these results show that the presence of Ttr in the PC of the nanoliposomes is higher compared to the relative abundances of this protein in mouse plasma, suggesting its important role in the fate of the nanoliposomes. The occurrence of Ttr in the PC of nanoliposomes is favored by the presence of rh-GLA and RGD, which could promote the crossing of the BBB by nanoGLA. This is consistent with the findings from biodistribution (BD) assays in sections 5.5.1 and 5.5.2, where nanoGLA formulations demonstrated successful BBB penetration.

6.5. Impact of PC in the internalization of nanoGLA in endothelial cells

As observed in section 5.3, the presence of RGD in the nanoliposomes enhanced their internalization in HMEC-1 endothelial cells. However, several studies have reported that the formation of the PC can interfere with nanoparticle-cell interactions, potentially reducing targeting efficiency (357,471–473). To investigate whether the formation of the PC in the different versions of nanoGLA could mask the RGD-targeted moiety, a cell internalization assay in HMEC-1 cells was conducted using flow cytometry, similarly as conducted in section 5.3.1.

DiR-labeled nanoGLA systems were pre-incubated with FBS for 1 h at 37°C under shaking conditions to allow the PC formation and their internalization was compared to nanoGLA without pre-incubation with FBS. The final concentration of each nanoGLA version was 0.05 mg/mL of theoretical lipid content.

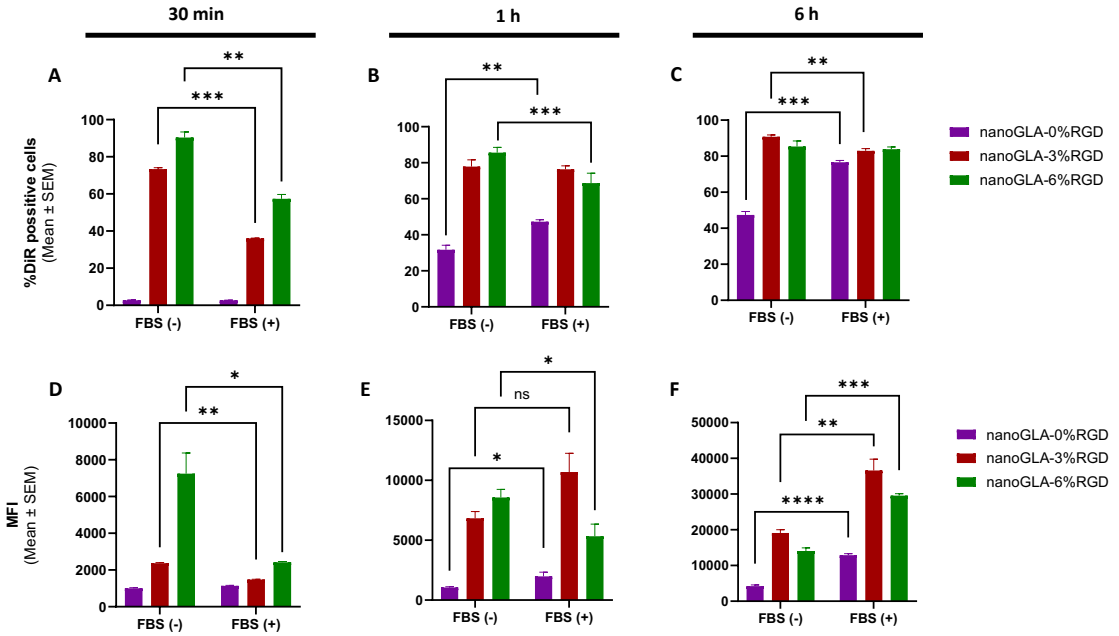

Fig. 6.11. Impact of the PC formation in HMEC-1 internalization of RGD functionalized nanoGLA. A-C) Percentage of DiR positive cells after 30 min, 1 h and 6 h of incubation. **D-F)** Median fluorescence intensity (MFI) after 30 min, 1 h and 6 h of incubation. Different nanoGLA formulations labelled with DiR were pre-incubated with fetal bovine serum (FBS (+)), and their internalization was compared to those that were not pre-incubated (FBS (-)). Statistical significance levels were schematically assigned ns ($p \geq 0.05$), *($0.01 \leq p < 0.05$), **($0.001 \leq p < 0.01$), ***($0.0001 \leq p < 0.001$), ****($p \leq 0.0001$).

The results demonstrated a beneficial role of RGD in enhancing internalization at short incubation times and in the absence of the PC (FBS (-)) (Fig. 6.11). Specifically, at 30 min, cellular uptake of nanoGLA was faster when RGD was present without pre-incubation with FBS, as evidenced by both %DiR positive cells and MFI (Fig. 6.11A and 6.11D). Additionally, nanoGLA-6%RGD exhibited better internalization than nanoGLA-3%RGD under both conditions, with and without the presence of the PC. However, these differences between nanoGLA-3%RGD and nanoGLA-6%RGD were no longer apparent after 1 h and 6 h of incubation in the presence of the PC.

The enhancement in internalization due to RGD is most evident at shorter incubation periods (30 min), whereas longer incubation times (1 and 6 h) diminish this effect. Therefore, the effect of the PC reducing the internalization of the nanoGLA is more evident after short incubation periods compared to longer ones. These findings suggest that the PC likely masks part of the RGD, thus slowing the internalization of RGD-targeted nanoGLA.

In contrast, nanoGLA-0%RGD exhibited slower internalization compared to RGD-targeted nanoGLA formulations, but its cellular uptake increased after 1 h and 6 h of incubation, as indicated by both %DiR positive cells (Fig. 6.11B and 6.11C) and MFI (Fig. 6.11E and 6.11F). Interestingly, after 1 h and 6 h of incubation, nanoGLA-0%RGD pre-incubated with FBS showed enhanced internalization due to the presence of the PC (Fig. 6.11B, 6.11C, 6.11E and 6.11F).

Importantly, after 6 h of incubation, discrepancies were found between %DiR positive cells and MFI results for nanoGLA-3%RGD and nanoGLA-6%RGD. In detail, nanoGLA-3%RGD showed a significant decrease in %DiR positive cells ($p = 0.008$), suggesting that the PC could interfere with its cellular uptake (Fig. 6.11C). In contrast, MFI results showed the opposite, with a significant increase in nanoGLA-3%RGD internalization in the presence of FBS ($p = 0.0001$) (Fig. 6.11D). A similar scenario was observed for nanoGLA-6%RGD, where %DiR positive cells showed no

significant difference in cellular uptake with or without the PC, but MFI results showed significantly better internalization with nanpoaticles pre-incubated with FBS (p = 0.0001). These discrepancies may be explained by the fact that %DiR positive cells saturated after 1 h and 6 h of incubation, making it difficult to compare the different treatment groups. On the other hand, MFI did not saturate after longer incubation times.

Overall, these results demonstrate that the formation of the PC through pre-incubation with FBS can partially mask RGD, delaying the internalization of targeted nanoliposomes in endothelial cells (Fig. 6.11). However, despite the presence of the PC, RGD-targeting still enhances and accelerates nanoGLA internalization in HMEC-1 cells compared to nanoGLA without RGD at all time points (Fig. 6.11B, 6.11C, 6.11E and 6.11F), demonstrating the importance of RGD presence for the nanoliposomal endothelial uptake. Interestingly, nanoGLA without RGD exhibited slower internalization in HMEC-1 cells, but the presence of PC in these nanoliposomes improved its internalization after 1 and 6 h of incubation. This improvement is likely due to the presence of receptors in HMEC-1 for certain components of the PC, such as Alb and apolipoproteins, two of the main proteins adsorbed by nanoliposomes when incubated with FBS (318,357), which could enhance its internalization. This improvement in cellular uptake due to PC has been reported by other authors using other cells and other NPs (318,472).

6.6. Summary and conclusions

In this section, we evaluate the impact of surface modifications and nature on nanoliposomes, such as the addition of RGD at different densities (0%, 3% and 6 mol%) and the presence or absence of rh-GLA, on the formation and composition of the PC, as well as the effect of the PC on the internalization of these RGD-targeted nanoliposomes in endothelial cells. For this purpose, we used the same nanoliposomal systems as in section 5.2 (Table 5.3).

First, the optimal incubation time of nanoliposomes with mouse plasma for studying the composition of the PC was determined. Two different nanoliposomal formulations, EL-0%RGD and nanoGLA-3%RGD were incubated with mouse plasma at various time points at 37°C and in shacking conditions to determine when the PC was formed and stabilized. PC formation was detected by DLS in both nanosystems. Results showed that the formation of the PC in different nanoliposomal formulations can be monitored *in situ* by DLS. However, quality of the DLS measurements improved after *ex situ* isolation of PC-nanoliposome complexes through size exclusion chromatography (SEC), which avoided the interference of plasma components in DLS readings and allowed for more accurate characterizations. After incubation with plasma, nanoliposomes acquired a negative ζ-potential and increased their PDI due to the adsorption of plasmatic proteins. PC formation occurred rapidly (30 min), but after 1 h of incubation, the size, PDI and ζ-potential remained stable and without sedimentation throughout the subsequent time points in both nanoliposomes, indicating that, after 1 h of incubation, the PC remained stable over time.

Following PC formation, the PC-nanoliposome complexes were isolated using SEC, based on liposome fluorescence, after 1 h of incubation with mouse plasma. Results from DLS and cryo-TEM confirmed the successful isolation of the PC-nanoliposome complexes, allowing for further characterization of PC composition.

Proteomic analysis by LS-MS revealed that PC composition was largely consistent across different nanoliposomal formulations, with Alb and apolipoproteins being the most abundant proteins in all cases. The majority of proteins forming the PC in the different nanoliposomal

formulations were small proteins (< 60 kDa) and negatively charged in plasma (IEP < 7.5). The presence of rh-GLA and RGD in the nanoliposomes affected the composition of the PC, either reducing or increasing the presence of opsonins, such as Igs and complement factors, and dysopsonins, such as apolipoproteins and Alb. These changes suggest that PC composition plays a major role in determining the *in vivo* fate of nanoliposomes, as it can either promote or hinder immune clearance and circulation time. Interestingly, presence of rh-GLA and RGD increased the abundance of proteins such as Apoe and Tf in their PC, thereby endowing the nanoliposomes with the ability to cross the BBB. This finding is supported by the biodistribution (BD) assays in sections 5.5.1 and 5.5.2, which demonstrated successful BBB penetration by nanoGLA formulations.

For the internalization studies, nanoGLA formulations were pre-incubated with FBS for 1 h at 37°C under shacking conditions to allow the formation of the PC. Results demonstrated that the presence of the PC in RGD-targeted nanoGLA slowed their internalization in endothelial cells, indicating that the PC can reduce the availability of the targeting moiety. In contrast, nanoGLA without RGD exhibited slower internalization in endothelial cells compared to nanoGLA with RGD. However, the presence of the PC enhanced its internalization after 1 and 6 h of incubation, likely due to the presence of receptors in endothelial cells for certain components of the PC, such as Alb and apolipoproteins, which could facilitate cellular uptake via alternative endocytic pathways.

This study underscores the dual role of the PC in modulating nanoliposomal interactions with the biological environment. While PC formation can limit targeted uptake by masking functional ligands such as RGD, it can also facilitate alternative pathways of internalization, particularly in cases where PC components interact with cell surface receptors. The presence of rh-GLA and RGD altered the balance between opsonins and dysopsonins, influencing immune recognition, circulation time, and biodistribution patterns at a systemic level as later observed *in vivo*.

These results emphasize the importance in drug delivery research of not only thoroughly characterizing the nanosystem itself, but also understanding its interactions with plasma and relevant physiological media, a topic which was explored in greater depth for the first time in this thesis. This is crucial as the presence of the protein corona can significantly affect many physicochemical properties, which may help explain results obtained both *in vitro* and *in vivo*.

7. Production and isolation of extracellular vesicles for GLA enzyme delivery

7.1. Introduction

Extracellular vesicles (EVs) are involved in multiple intercellular signaling pathways, acting as vehicles for communication between cells under physiological conditions. This makes them ideal carriers for therapeutic agents due to their ability to transport and deliver proteins, nucleic acids, lipids, and other bioactive molecules in a target-specific manner through plasma membrane interactions (474,475).

Therapeutic agents can be loaded into EVs through both endogenous and exogenous methods. In the case of the endogenous method, it has been demonstrated that EVs can be engineered by genetically modifying the secreting cells, enhancing their ability to deliver therapies effectively, including targeting hard-to-reach tissues like central nervous system (CNS) (476). In addition, various post-isolation techniques, such as saponification, sonication or simple incubation, can be used as exogenous methods to load EVs with a wide range of therapeutic molecules, including siRNA, enzymes and chemotherapy drugs (474).

Additionally, the targeting capacity of EVs can be enhanced by deriving them from specific cell lines, such as EVs from cardiac cell lines to target drug delivery to the heart (477), or by adding targeting moieties to their surface to direct them to specific tissues or cells (179–182,184,185,196).

However, there are several key challenges that must be overcome before EV-based therapies can reach their full potential. One major issue is the inherent variability in EVs, including differences in size, cargo, surface markers, and biogenesis pathways. This heterogeneity complicates efforts to standardize EVs, making it difficult to establish consistent production, characterization, and dosing protocols. Achieving large-scale production of EVs with consistent quality and yield remains a significant barrier (194). While there are ongoing efforts to enhance scalability, such as the use of bioreactors for cell culture, these solutions are still in development (478,479).

Another challenge is ensuring precise targeting of EVs to avoid unwanted uptake by non-target tissues, which can reduce their therapeutic efficacy. Without effective targeting strategies, EVs may be distributed systemically, leading to a broader distribution that diminishes their effectiveness (132,195). On the other hand, modifying EV surfaces with exogenous peptides, antibodies, or synthetic molecules to improve targeting can also trigger immune responses, which must be carefully managed (196,197).

EV-based therapies also face concerns related to their stability during storage and transport. EVs may lose their functionality over time, which could limit their clinical utility (198,199). Additionally, the regulatory landscape for EV therapies is still evolving. Currently, it relies heavily on existing frameworks for biologics and cell therapies, which may slow down the approval process for clinical applications (157). To address these issues, ongoing research into improving

EV engineering, isolation, and characterization methods is crucial. Innovations in these areas will help to expand the clinical potential of EV-based therapies while tracking concerns such as immunotoxicity, bioavailability, and regulatory approval.

In this section, we explore the production of EVs loaded with GLA (EV-GLA) obtained from different cell factories, the use of various isolation methodologies to enhance the EV-GLA yield, and the use of these EVs to enhance ERT in endothelial cell cultures. In addition, we investigate the benefits of targeting EV-GLA with F7 cell-penetrating peptide to improve EV-GLA internalization and *in vitro* efficacy.

7.1.1. EVs for protein delivery: loading and surface modifications

EVs can be loaded with proteins using either exogenous or endogenous approaches. **Exogenous loading** involves directly incorporating therapeutic proteins into EVs through techniques such as fusion, electroporation, osmotic shock, sonication, saponification, or freeze–thaw cycles. These methods allow precise control over the amount of protein introduced (173,480–482), ensuring a defined therapeutic dose. However, they may also compromise EV membrane integrity (483), potentially affecting the stability and efficacy of the delivery system (194). Despite this limitation, exogenous loading remains particularly valuable for proteins that require high concentrations or lack a natural association with EVs. The efficiency of this method varies depending on the specific loading technique, and standardization remains a challenge (484). Additionally, exogenous loading can involve covalent attachment of therapeutic proteins to the EV surface, as demonstrated by the conjugation of anti-EGFR peptides to enhance EV accumulation in EGFR-positive cancer cells (485).

In contrast, **endogenous loading** takes advantage of the natural vesicle biogenesis machinery within producer cells, enabling the incorporation of therapeutic proteins during EV formation. This approach is well-suited for unmodified therapeutic proteins, such as lysosomal enzymes, and can be further enhanced by genetic engineering strategies. For instance, proteins can be fused with EV-associated molecules like Alix and TSG101 (luminal loading) (486) or fused with membrane proteins such as CD9, CD63 (487,488), or plasma membrane proteins (membrane loading) to facilitate their inclusion in EVs (489). Endogenous loading is particularly effective for larger molecules that are naturally secreted via vesicular pathways, including signaling proteins, inflammatory mediators, and surface receptors (486).

An advantage of endogenous loading is that it preserves the biological properties of EVs by eliminating the need for post-isolation modifications. However, its efficiency depends on factors such as the specific therapeutic protein and the ability of the producer cell to package and secrete it efficiently. Various strategies have been developed to enhance endogenous loading, including overexpressing therapeutic proteins fused to surface-associated markers like Lamp2 or CD63, or soluble proteins such as Alix or syntenin (486). The choice of anchoring protein plays a critical role in determining the amount of therapeutic protein incorporated into each EV (490).

Optimizing EV biodistribution is essential for maximizing their therapeutic effects. When administered intravenously, EVs are often sequestered by organs such as the liver, kidneys, spleen, and lungs. While this natural tropism can be beneficial for targeting diseases affecting these organs, additional modifications are often required to improve delivery to specific tissues. Surface engineering strategies, such as ligand attachment, can enhance EV targeting to desired sites. Notable examples include the use of the RVG peptide to facilitate CNS targeting (179,196),

anti-EGFR antibodies for selective cancer cell uptake (184), and cell-penetrating peptides (CPPs), which enhance intracellular delivery of nanoparticles and proteins (491–495).

Further modifications can improve EV stability and circulation time. The addition of polyethylene glycol (PEG) to the EV surface has been shown to prolong systemic circulation by reducing opsonization and clearance (180,496,497). Additionally, immune evasion strategies, such as overexpressing CD47 (181) to prevent phagocytosis or downregulating major histocompatibility complex (MHC) molecules (197), can further enhance EV longevity and therapeutic efficacy.

7.1.2. EVs for protein delivery in LSDs

EVs offer distinct advantages as carriers for therapeutic proteins, making them a promising strategy for delivering lysosomal enzymes (20). Their natural involvement in endosomal trafficking pathways and intrinsic enrichment in lysosomal proteins position them as effective tools for treating lysosomal storage disorders (LSDs). In fact, many lysosomal proteins, such as enzymes and transmembrane proteins, are naturally found within EVs (132,498,499). Several studies have explored the therapeutic potential of EVs in preclinical models, demonstrating their ability to transport functional enzymes to target cells and correct enzymatic deficiencies (Table 7.1).

In MPS IVA (Morquio A syndrome) and MPS VII, EVs derived from umbilical mesenchymal stem cells (MSC) have been employed as carriers for the GALNS enzyme, without the need to load the enzyme into the EVs. These vesicles have successfully delivered the enzyme to deficient fibroblasts, demonstrating that some lysosomal enzymes are naturally present and functional inside the EVs. Additionally, EVs from the same cell source have shown the ability to reduce glycosaminoglycan (GAG) accumulation in the corneas of MPS VII mice, demonstrating their potential for treating lysosomal deficiencies affecting connective tissues (498,500).

For Batten disease, EVs derived from macrophages and loaded with the TPP1 enzyme, either exogenously through sonication and saponification (195,501) or endogenously via transfection of the source cell (501,502), have been evaluated in both, *in vitro* and *in vivo* models, where they effectively restored enzyme activity and improved disease outcomes (195,501). Interestingly, EVs exogenously loaded with TPP1, showed the most efficient enzymatic delivery into target cells.

In Sandhoff syndrome, which is characterized by a deficiency in β-hexosaminidase, Calzoni and colleagues discovered that the enzyme is naturally found in EVs. By overexpressing a specific subunit of this enzyme in HEK 293 cells, they demonstrated that the derived EVs showed the ability to partially correct *in vitro* the enzyme deficiency in Sandhoff patient fibroblasts (503). In addition, an increase in enzymatic activity was observed in EVs endogenously loaded with N-sulphoglucosamine sulphohydrolase enzyme (SGSH) from HEK 293 (132). In Gaucher disease, EVs derived from HEK 293 cells endogenously expressing the glucocerebrosidase (GBA) enzyme fused with VSV-G have shown that functional enzymes can be delivered to the endocytic compartments of targeted cells (504). VSV-G served as a targeting moiety, due to its strong affinity for VLDL-receptor, which is commonly present on the surface of human cells, thereby enhancing the internalization of EVs into the endocytic compartment (504).

Beyond enzyme replacement therapies, EVs have also been explored for cystinosis, a metabolic disorder caused by defective cystine transport. Microvesicles (MVs) naturally or endogenously loaded with cystinosin (CTNS) transmembrane protein derived from MSC (499), and MVs derived from Baculovirus infected Spodoptera cells, endogenously loaded with human CTNS (505), have

shown an effective reduction of cystine storage in cell culture. Similarly, in infantile sialic acid storage disease, MVs endogenously loaded with mRNA and the sialin transporter protein, derived from Baculovirus-infected Spodoptera cells, have been effective in rescuing sialin-deficient fibroblasts (505).

Table 7.1. Summary of LSDs in which EVs were used as therapeutics in preclinical models. Edited from (20).

Disease	Therapeutic molecule	Cell source	Loading and modifications	Therapeutic outcomes	References
Fabry disease	GLA	HEK 293F and CHO DG44	Endogenous loading	EV-GLA is more active than free enzyme reducing kidney Gb3 deposits, and it is active also in brain	(132)
Gaucher disease	GBA	HEK 293	Endogenous loading and protein fused with VSV-G scaffold and GFP	EV-GBA exhibited higher enzymatic activity	(504)
Niemann-Pick C1	NPC1	MSC	Endogenous loading Transporter fused to CD63 or syntenin	Treatment of Npc−/− mice with NPC1-loaded EVs reduced cholesterol levels in the liver and brain	(506,507)
Sandhoff disease	α subunit of β-hexosaminidase enzyme (HexA)	HEK 293	Endogenous loading	HexA containing EVs induce-2-fold increment of the enzyme product in patient fibroblasts	(503)
CNL2 (Batten disease)	TPP1	Bone marrow-derived macrophages (BMM) and IC21 macrophages	Exogenous and endogenous loading	*In vivo* EV-TPP1 treatments increased lifespan of Batten mice	(195,501,502)
MPS IVA (Morquio syndrome)	GALNS	MSC	Empty EVs	Fibroblasts from patients treated with EVs increase GALNS activity	(498)
MPS VII	β-glucuronidase	MSC	Natural EVs (not confirmed directly)	Reduction in GAG content in corneas of mice receiving MSC transplantation. Effect is attributed to EVs but not confirmed directly	(500)
MPS III (Sanfilippo syndrome)	SGSH	HEK 293F and CHO DG44	Endogenous loading	Increase in enzyme activity of SGSH loaded EVs	(132)
Cystinosis	CTNS transporter protein and mRNA	MSC and Baculovirus-infected Spodoptera cells	Empty EVs and CTNS loaded EVs (fused to CD63) from MSC and CTNS loaded microvesicles from Spodoptera cells	Cystine accumulation is reduced in patient fibroblasts treated with EV-CTNS. Natural EVs, produced in mammal or insect cells have also a clear effect reducing cystine accumulation	(499,505,507)
Infantile Sialic Acid Storage Disease (ISSD)	Sialin transporter protein and mRNA	Baculovirus-infected Spodoptera cells	Endogenous loading	Around 75% of sialin depletion in ISSD fibroblasts after 96 h incubation	(505)

EV-based therapeutics are also under active development for Niemann-Pick type C1 disease (NPC1). Evox Therapeutics, a biotechnology company specializing in EV therapeutics, is currently developing engineered EVs derived from MSC and endogenously loaded with NPC1 transporter. This is achieved through fusion with syntenin/CD63 to facilitate its integration into the EV membrane and deliver the therapeutic transporter to neurons affected in NPC1 patients (507).

In FD, EVs endogenously loaded with GLA (EV-GLA) from CHO cells have demonstrated therapeutic efficacy in both, *in vitro* and *in vivo* disease models (132). Specifically, EV-GLA were endocytosed by cultured endothelial cells derived from KO Fabry mice and delivered to lysosomes. Enzyme activity measurements of recipient cells revealed an increase in GLA activity compared to cells treated with the free GLA enzyme. In *in vivo* studies using KO Fabry mice, it was demonstrated that EV-GLA was distributed among targeted tissues, including kidneys and brain. Additionally, after a single intravenous administration of EV-GLA, Gb3 levels were reduced more efficiently than with the free enzyme in both the kidneys and brain of KO Fabry mice.

7.1.3. CHO DG44 and HEK 293F as recombinant GLA cell factories

CHO cells and HEK cells are widely used as "cell factories" for producing recombinant proteins. This is because, compared to production in prokaryotic cells, CHO and HEK cells can perform post-translational modifications (PTMs), such as glycosylation, which is crucial for regulating protein activity, cell adhesion, and immune evasion (508). Additionally, both cell types are easy to culture and can be scaled up, enabling high yields of protein production (509). However, PTMs can vary depending on the choice of cell factory, potentially affecting protein stability and function (508,510,511). For example, agalsidase beta (Agal B) and agalsidase alfa (Agal A), the two recombinant GLA enzymes approved for ERT in Europe, are expressed using different mammalian cell systems (116). Agal A is produced in a human cell line of unspecified origin, while Agal B is obtained from CHO cell line. This later cells allow for higher levels of sialylation and phosphorylation, enhancing cellular uptake through M6PR interactions (116). Agal A and Agal B also differ in their pharmaceutical forms and dosing regimens as previously explained in general introduction. This suggests that the varying PTMs linked to the choice of "cell factory" may influence the enzyme stability.

To induce the expression of the therapeutic protein in producer cells, such as CHO and HEK, the gene encoding the specific protein is introduced into these mammalian cells, in a process that is called transfection. There are different transfection methods, including electroporation, recombinant viruses or the use of chemical approaches such as cationic polymers, lipid-based components or phosphate compounds (512). Furthermore, therapeutic protein expression can be performed either transiently or stably.

Transient gene expression (TGE) methods typically enable the production of substantial amounts of protein in a relatively short time (a few weeks) (513). These methods involve the introduction of foreign genetic material into cells via delivery vehicles such as polyethylenimine (PEI), which leads to a mixed population of transfected and non-transfected cells. The foreign plasmid DNA (pDNA) is not integrated into the cell genome, meaning that the expression of the recombinant protein decreases over time due to environmental factors and dilution during cell division (512,514). HEK cells are widely used for TGE due to their rapid growth rate and their ability to grow in suspension culture under serum-free conditions. This allows for higher protein yields compared to adherent cells. Additionally, they can be easily transfected and manipulated (515). Despite the scalability of TGE, it is an expensive method due to the high quantity of pDNA required, often 1 mg or more per liter of culture. In addition, the yield of recombinant protein may be decreased by different factors such as the cytotoxicity associated with PEI (516–520).

Stable gene expression (SGE) implies the integration of the foreign pDNA into the cell genome. This allows for the continuous expression of the recombinant protein over multiple cell divisions. After transfection, a mixed population of transfected and non-transfected cells is obtained. However, after several months, a selection process is carried out to identify the best clones

based on their productivity and protein quality, which involves eliminating non-transfected cells and low-efficiency clones (521–523). The most popular cell line for SGE is CHO cells, which, similarly to HEK cells, are able to grow in suspension culture under serum-free conditions. The main disadvantage of this method is the significant amount of time required to generate the optimal stable clone. Nevertheless, stable gene expression has been shown to result in higher productivity compared to TGE on several occasions (513,521,524).

In this thesis, CHO DG44 and HEK 293F cells were used as cell factories to obtain free GLA enzyme and EVs loaded with GLA (EV-GLA) through SGE and TGE, respectively. CHO cells are typically preferred for stable transfections, as they offer long-term stable gene expression with high expression levels. However, CHO cells are more challenging to transfect for transient expression and their expression levels tend to be lower than those of transiently transfected HEK cells (525). On the other hand, HEK 293 cells are commonly used for TGE due to their ability to grow in serum-free conditions and to be transfected in suspension cultures (526). High yields of secreted recombinant proteins are typically produced using HEK 293 cells (524), especially in serum-free, suspension-adapted cultures like HEK 293F, which are commonly used in industrial applications. Additionally, serum-free media not only improve efficiency but also eliminate the presence of EVs found in serum that could interfere in EV-GLAH6 isolation and simplify downstream processing by reducing impurities from the media.

7.1.3.1 Stable expression of GLAcmycH6 in CHO DG44

Stable clone of CHO DG44 for the expression of GLAcmycH6 was previously developed at IBB-UAB by Dr. José Luis Corchero before this thesis (210,211). The detailed protocol for transfection with pOptiVec-GLA plasmid, resulting from pOptiVEC™-TOPO® plasmid, as well as the process for selecting positive clones, was outlined in Merlo-Mas et al. (210,211) (Fig. 7.1). The GLA construct includes the full-length human GLA gene (UniProt P06280; AGAL_HUMAN) and both c-myc and 6-His tags at its C-terminus. This His tag enabled the purification of the soluble protein from the cell media through a HisTrap™ column using an ÄKTA start™ chromatography system.

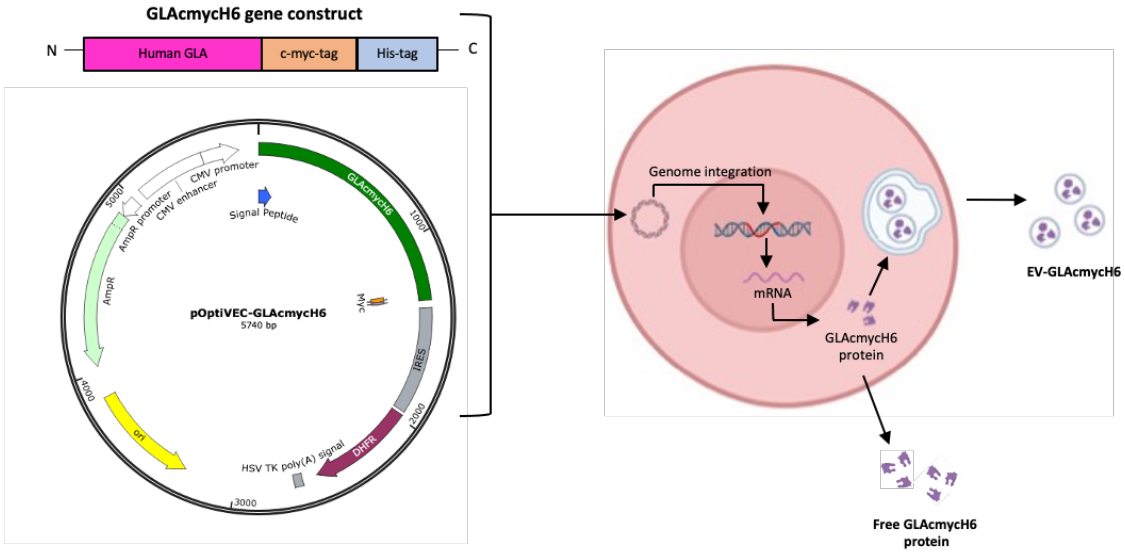

Fig. 7.1. Scheme of the stable expression of GLAcmycH6 and EV-GLAmycH6. The pOptiVEC-GLAcmycH6 plasmid was used for stable expression of GLA in CHO DG44 cells by integration into genomic DNA and obtention of free enzyme and EV-GLAcmycH6 in the extracellular space.

7.1.3.2 Transient expression of GLAH6 in HEK 293F

TGE of GLA in HEK 293F cells was performed via PEI-mediated transfection using the GLAH6 expression vector (Fig. 7.2). As outlined in Corchero et al. (210), the pOpinE-GLA expression vector encodes the same human GLA gene sequence used for CHO cells (UniProt P06280; AGAL_HUMAN), with 6-His tag at the C-terminus to enabled the isolation of free GLAH6 enzyme through ÄKTA start™ chromatography system.

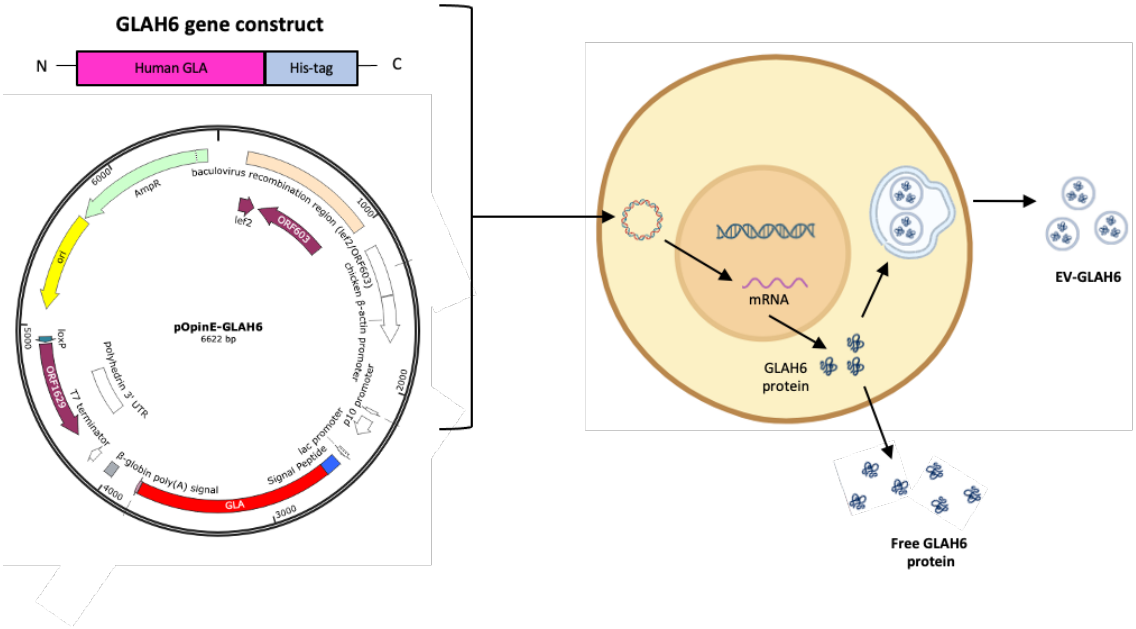

Fig. 7.2. Transient expression of GLAH6 and EV-GLAH6. The pOpinE-GLAH6 plasmid was incorporated into HEK 293F cells and free enzyme and EV-GLAH6 was obtained in the cell media. Unlike in the stable expression, the pOpinE-GLAH6 plasmid is not integrated into the cell genome, resulting in transient expression of GLAH6.

7.1.4. Methodologies for EVs isolation and purification

Research on the use of EVs as drug delivery systems has increased in recent years due to the advantages they offer as therapeutic vehicles. These advantages include their low immunogenicity, safety, high stability in circulation, and ability to target specific cells. However, one of the major limitations in the translation of EVs is finding an efficient isolation method that minimizes time consumption and optimizes both purity and yield of EVs (527). To this end, several isolation techniques have been explored over years (Fig. 7.3 and Table 7.2).

Ultracentrifugation (UC) is considered the gold standard for EVs isolation (Fig. 7.3A) (528). It involves several differential centrifugation steps in order to separate exosomes from dead cells, cell debris and other types of vesicles such as apoptotic vesicles and MVs (163,529,530). Despite its effectiveness, UC has several limitations, including low recovery rates, potential vesicle damage due to high shear forces, and co-isolation of protein aggregates and contaminants (168).

Density gradient ultracentrifugation (DGU) isolates EVs based on their size, shape and density (Fig. 7.3A). In a density gradient solution, typically sucrose or iodixanol (531), particles accumulate at different levels within the gradient depending on their specific densities (532,533). After isolation, washing steps are required to remove the gradient solution, as it can interfere with EV functional analysis (534). This methodology is particularly useful in research focused on the basic biology and heterogeneity of EVs, as it can distinguish exosomes from other

types of EVs (535–538). Despite its effectiveness in distinguishing exosomes from other EV subtypes, the clinical application of this method is limited due to its low yield, high cost, and labor-intensive nature (539).

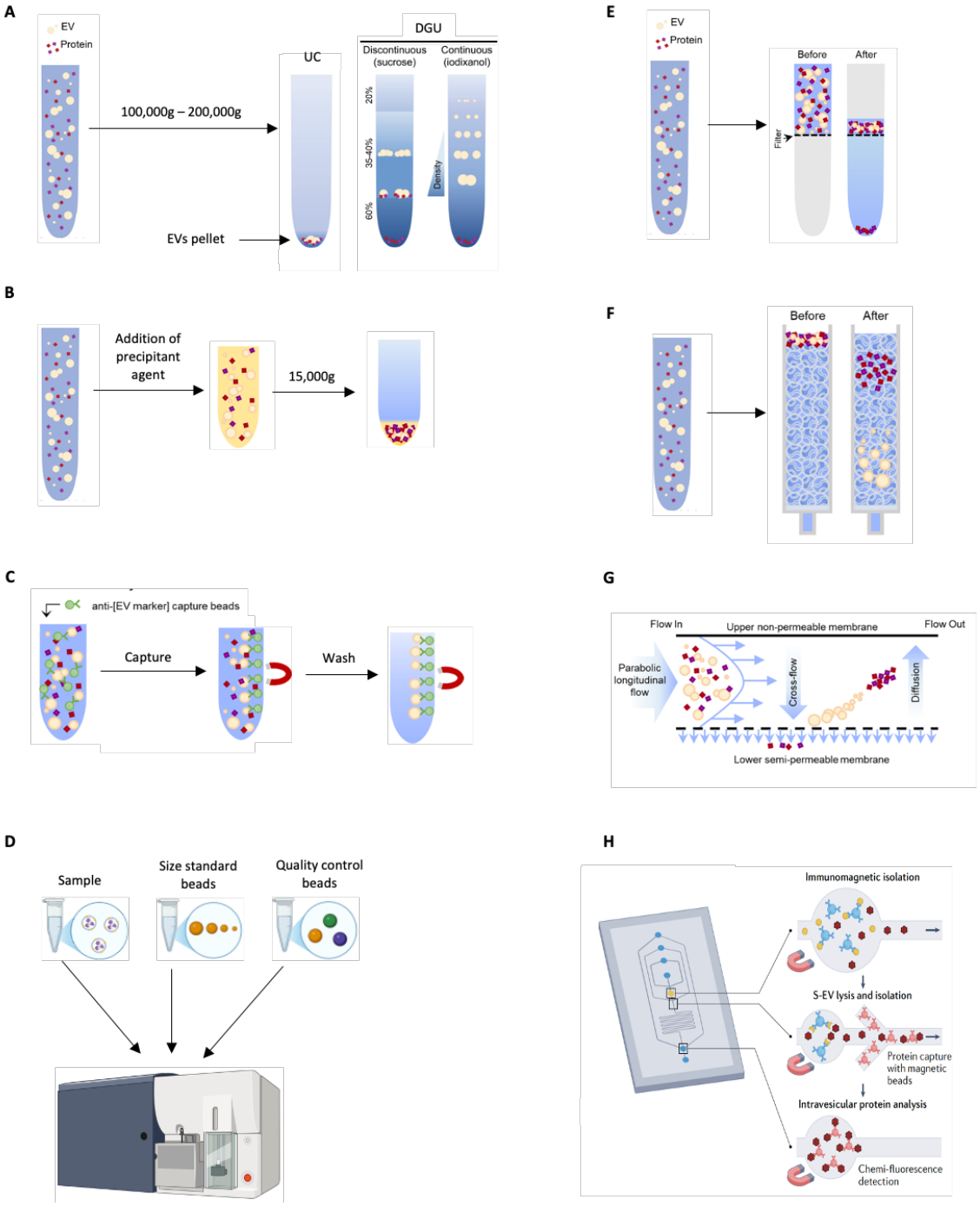

Fig. 7.3. Scheme of the different EV isolation procedures. A) Isolation by ultracentrifugation (UC) and density gradient ultracentrifugation (DGU). **B)** Isolation by precipitation (Pp). **C)** Immunoaffinity isolation (IA). **D)** Flow cytometry isolation method (FC). **E)** Ultrafiltration isolation method (UF). **F)** Size exclusion chromatography isolation (SEC). **G)** Asymmetric flow-field flow fractionation (AF4). **H)** Microfluidic isolation method (Mf). Adapted from Monguió-Tortajada et al., Goss et al. and Lattmann et al.(534,540,541).

Precipitation (Pp) methods (Fig. 7.3B) often use polyethylene glycol (PEG)-based volume exclusion to precipitate EVs. This approach allows high recovery but often results in low purity, as co-precipitation of protein aggregates and residual precipitating agent is common (542,543).

Therefore, Pp methods are generally not recommended for EV characterization and functional studies of EVs (544). Precipitation methods are easy, cost-effective and simple to perform, and are being explored as alternatives to UC due to their ease of standardization and scalability. However, UC typically provides a lower recovery but higher purity of EVs compared to precipitation commercial kits (545,546).

Immunoaffinity isolation (IA) separates specific EVs based on their surface protein expression. These methods can also be combined with magnetic isolation to improve the purity of EV samples, making them suitable for content or functional analysis (547) (Fig. 7.3C). With this method, isolated EVs obtained represent only a subset of the entire EV population, specifically those expressing the selected markers. This methodology is not suitable for large-scale productions, due to its low yield and high cost (168).

Flow cytometry (FC) isolation methods (Fig. 7.3D) require that EVs be labelled with fluorescent markers, as particles with the size of EVs are not detectable by cytometer light detectors. In addition, appropriate size standardization beads are needed to correlate scatter data with EV diameter accurately (548), and there is a need to serially dilute the EV sample to ensure the concentration is low enough for accurate EV quantification (549). This isolation methodology is still being optimized for EV isolation.

Table 7.2. Summary of the characteristics of EV isolation methodologies. Adapted from Monguió-Tortajada et al. (534).

	UC	DGU	Pp	IA	FC	Mf	FFF	UF	SEC
Purity	Low	High	Low	High	Medium	High	High	Medium	High
EV yield	Medium	Low	High	Medium	Low	Low	High	Medium	High
Suitable for functional studies	Yes	No	Yes	No	No	No	Yes	Yes	Yes
Ease of use	Medium	Low	High	Medium	Low	Medium	Low	High	High
Automatable	No	No	Yes	Yes	Yes	Yes	Yes	Yes	Yes
Time requirement	Medium	High	Low	High	Medium	Medium	Medium	Low	Low
Scalability	Yes	No	Yes	Yes	No	No	Yes	Yes	Yes
Use of specialized equipment	Yes	Yes	No	No	Yes	Yes	Yes	No	No
Cost	Low	High	Low	High	Medium	Medium	High	Medium	Low

Size exclusion chromatography (SEC) isolates EVs based on size differences using a column filled with a stationary phase of porous beads of Sepharose, Sephadex (550) or Sephacryl (551,552). The porous structure allows the separation of large particles from small ones, as larger particles cannot penetrate the pores as easily as smaller particles (Fig. 7.3F). This results in larger particles eluting faster than smaller particles. SEC provide higher recovery and purity of EVs, as well as better preservation of EV structure, compared to other methods such as UC and precipitation methods (544,553–555) (Table 7.2). However, SEC can also co-isolate some lipoproteins, such as chylomicrons, VLDL or LDL, due to their similar size to EVs (556,557).

Field-flow fractionation (FFF) isolates EVs by applying a force field perpendicular to the sample flow, causing particles to distribute at varying distances from the channel based on their size (558,559) (Fig. 7.3G). One example of this methodology is **asymmetric flow-field flow**

fractionation (AF4). This technique uses a small volume during separation, offers high resolution and reproducibility but it is not adequate for large-scale separations.

Microfluidic (Mf) methods for EV isolation (Fig. 7.3H) offers several advantages, including automation, minimal sample requirements and the ability to handle high-throughput tasks. Microfluidics can separate EVs based on size, surface markers, or innovative sorting mechanisms such as acustic, electrophoretic or electromagnetic fields. These methods are still under active research and hold significant potential for the future of EV isolation (560–562), but they are not yet optimal for large-scale productions.

Overall, UF methodology seems to be the best option to isolate EVs for drug delivery purposes, as it allows large-scale isolations of EVs with good purity (543). Additionally, SEC can be used after pre-concentration and diafiltration, such as TFF (563–565) and UF (566–569), to improve EV purification.

In this section, two different UF methodologies, BF and TFF, were combined with SEC to isolate EV-GLA from SN of two different cell factories (CHO DG44 and HEK 293F). EV-GLA samples obtained by TFF and BF were then compared with EV-GLAcmycH6 samples obtained by Pp, as previously described (132) (Fig.7.4).

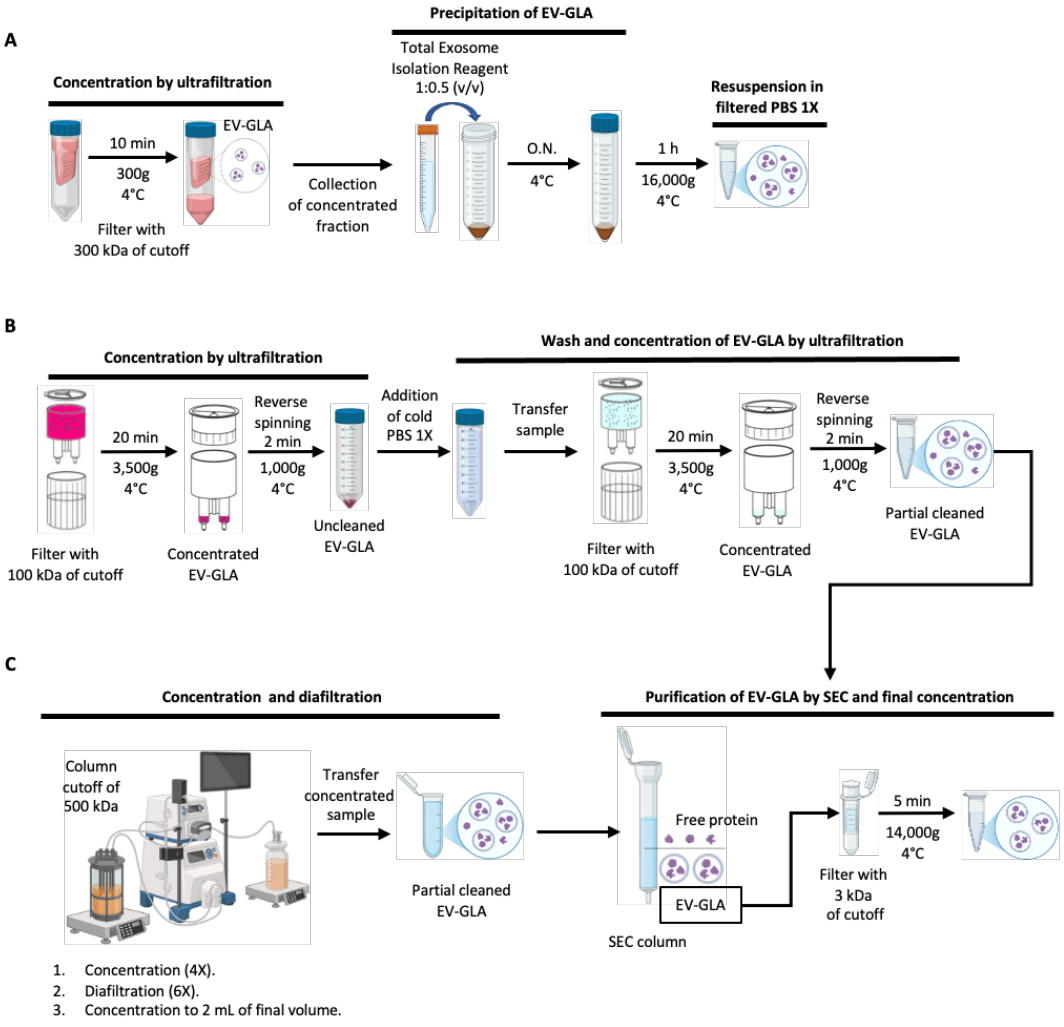

Fig. 7.4. Scheme of EV-GLA isolation and purification methodologies. A) Isolation by precipitation. **B)** Isolation by benchtop filtration (BF) and purification by size exclusion chromatography (SEC). Figure adapted from Kian Leong Tan et al. (214). **C)** Isolation by tangential flow filtration (TFF) and purification by size exclusion chromatography (SEC).

7.2. Characterization of EV-GLAcmycH6 obtained from CHO DG44

EV-GLAcmycH6 from CHO DG44 supernatants were isolated and purified by 3 different methods: Pp using Total Exosome Isolation Reagent (Invitrogen) (Fig. 7.4A), BF plus SEC (Fig. 7.4B), and TFF plus SEC (Fig. 7.4C).

For SEC purification, EVs were stained with 75 µM 3,3'-Dioctadecyloxacarbocyanine Perchlorate (DiOC) for 30 min at 37°C under shacking conditions, and then applied to the SEC column. Analyzing the fluorescence signal of different fractions, we observed a clear peak of fluorescence between fractions 7 and 11, containing the EVs (Fig. 7.5A). A second peak between fractions 15 and 22 was only observed in BF samples and probably corresponded to non-vesiculated DiOC aggregates (Fig.7.5A). However, these impurities did not affect to the final isolated sample, as these fractions were not collected.

Nanoparticle tracking analysis (NTA) was used to quantify and characterize the size of EVs (Fig. 7.5B). Mean sizes ranging from 154.5 to 182.0 nm were identified across the samples. The concentration of EVs was also determined by NTA, showing higher concentrations and a greater number of particles detected per analyzed frame in samples isolated and purified by TFF + SEC ($5.1{\cdot}10^{11} \pm 2.9{\cdot}10^{9}$ particles/mL) and BF + SEC ($3.9{\cdot}10^{11} \pm 2.3{\cdot}10^{9}$ particles/mL), compared with those obtained by Pp ($1.2{\cdot}10^{10} \pm 6.3{\cdot}10^{8}$ particles/mL) (Fig. 7.5B). To determine the EV yield (particles/L) obtained from each isolation method, both the initial volume of supernatant processed and the final volume of the EV-containing sample were considered. For the Pp sample, 200 mL of supernatant was processed, resulting in a final EV suspension volume of 0.5 mL. In contrast, for the samples isolated using TFF + SEC and BF + SEC, 140 mL of supernatant were used in each case, yielding a final volume of 0.5 mL. Results showed that TFF + SEC ($1.8{\cdot}10^{12} \pm 1.0{\cdot}10^{10}$ particles/L) and BF + SEC ($1.4{\cdot}10^{12} \pm 8.2{\cdot}10^{9}$ particles/L) yielded a higher number of EVs compared to those obtained by Pp ($3.1{\cdot}10^{10} \pm 1.6{\cdot}10^{9}$ particles/L) (Table 7.3). These results showed differences compared to other studies that tested different isolation methodologies for EVs from cell culture media and reported higher EV production yields with Pp methodologies (570–572). Other authors reported that SEC exhibited higher recovery of EVs compared to precipitation methods (544,553–555), which aligns with the lower EV yield observed with Pp methodologies in our hands. It is important to note that none of the studies reported in the literature followed the same methodology outlined in Fig. 7.4. Specifically, we performed previous steps of concentration such as UF (300 kDa) on samples from Pp, and BF (100 kDa) and TFF (500 kDa) followed by a SEC on samples from BF and TFF (Fig. 7.4). In contrast, the comparative studies reported in the literature used Pp or SEC without prior UF concentration steps.

Molecular characterization of EV-GLAcmyH6 by Western blot (WB) showed the presence of EV markers such as Alix, TSG101 and CD81 (Fig. 7.5C and 7.5D). All three EV-GLAcmycH6 samples obtained by the different isolation methods, exhibited high presence of the GLA enzyme (132,573). Additionally, β-tubulin was no detected in the purified EV-GLAcmycH6 samples, confirming that there was no contamination of cytosolic content.

NTA and WB findings demonstrate that all three isolation and purification methods successfully produced samples enriched with small EVs (sEVs) or exosomes (<200 nm) (Fig. 7.5B) (574,575). Importantly, NTA analysis with a lower limit of detection between 70–90 nm (575), may underestimate the presence of EV subpopulations smaller than 70 nm—still within the exosome

size range— (576–578). NTA analysis further revealed that EV-GLAcmycH6 obtained via the Pp method exhibited a more heterogeneous size distribution compared to those obtained by TFF + SEC and BF + SEC (Fig. 7.5B). However, these results could be influenced by the low number of particles detected per analyzed frame in the Pp samples, due to the low concentration of EVs (Fig. 7.5B). Therefore, the results suggesting that TFF and BF allow for more precise EV isolation compared to precipitation-based methods should be interpreted with caution. Nevertheless, other authors have reported high EV yields when using UF methods, including TFF (579–581).

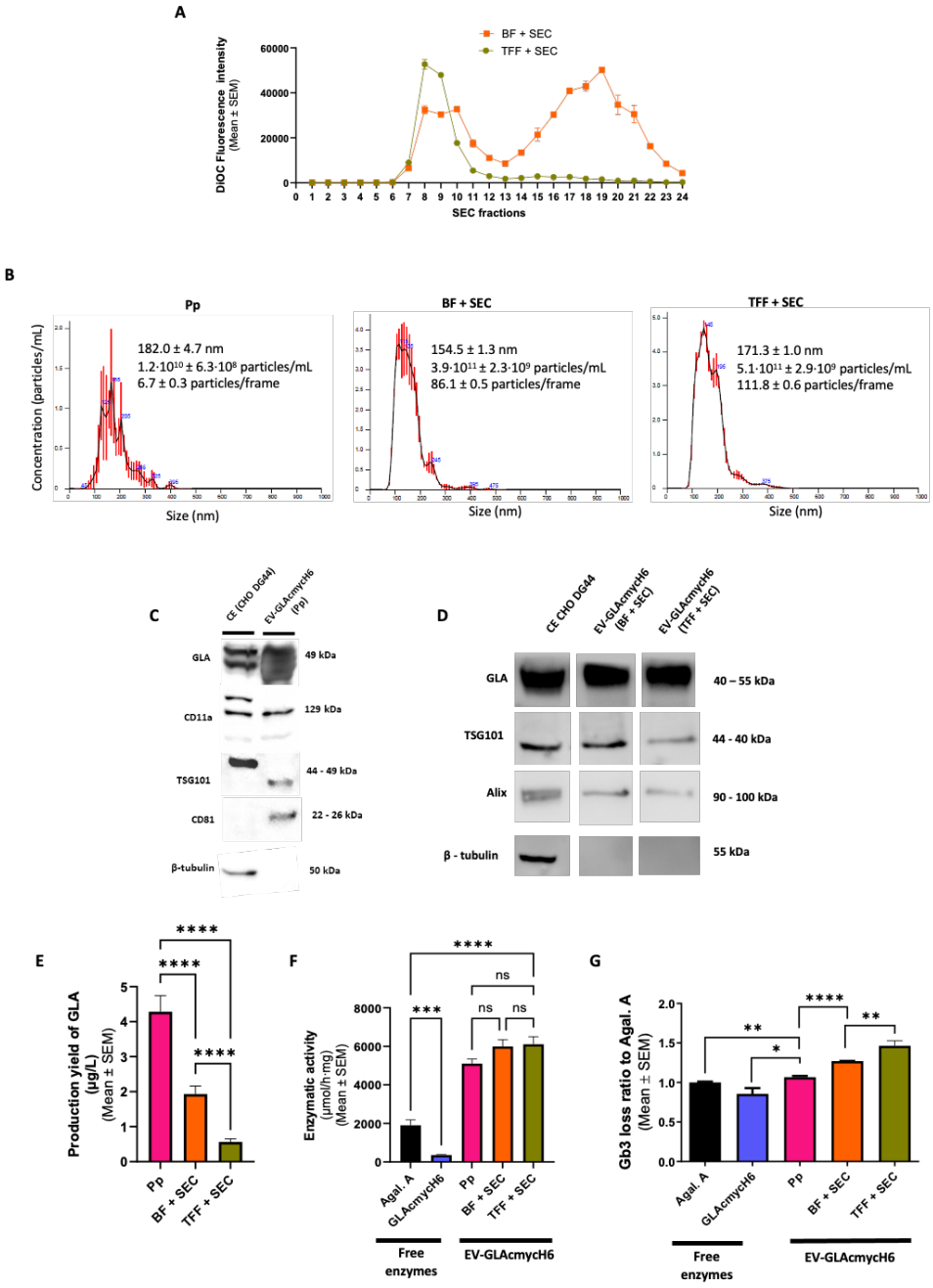

Fig. 7.5. Characterization of EV-GLAcmycH6 obtained by different procedures of isolation and purification from stable clone CHO DG44. A) SEC profile of EV-GLAcmycH6 isolated by BF + SEC and TFF + SEC. **B)** Size distribution and concentration of EV-GLAcmycH6 (particles/mL) quantified by nanoparticle tracking analysis (NTA). Blue values correspond to the size of the main peaks in the histogram. Results are expressed as Mean ± SEM. **C)** Characterization by Western blot (WB) of precipitated EV-GLAcmycH6 as shown in (12). Cell extract of stable clone CHO DG44 was included as a control. Fifteen µg of total protein were loaded per lane**. D)** Molecular characterization by WB of EV-GLAcmycH6 isolated by BF + SEC and TFF + SEC. Cell extract of stable clone CHO DG44 was included as a control.

Twelve µg of total protein were loaded per lane. **E)** Production yield of GLA expressed as µg of GLA/L of supernatant in different EV-GLAcmycH6 as determined by ELISA. **F)** Enzymatic activity of EV-GLAcmycH6 isolated by Pp, BF or TFF vs. free GLAcmycH6 and the clinically approved agalsidase alfa (Agal A). **G)** Comparison of *in vitro* efficacy of EV-GLAcmycH6 obtained by different methods at 0.1 µg/mL of GLA in MAEC cells. Gb3 loss was normalized by *in vitro* efficacy of free Agal A. Statistical significance levels were schematically assigned ns ($0.05 \leq p$), *($0.01 \leq p < 0.05$), **($0.001 \leq p < 0.01$), ***($0.0001 \leq p < 0.001$), ****($0.0001 \leq p$).

Conversely, the production yield of GLA (µg/L), quantified by ELISA, showed significantly higher enzyme yields in EVs obtained by Pp (4.3 ± 0.5 µg/L) ($p < 0.0001$) than in those isolated by BF + SEC (1.9 ± 0.2 µg/L) and TFF + SEC (0.7 ± 0.1 µg/L) (Fig. 7.5E and Table 7.3). These results can be explained by presence of soluble GLA enzyme, co-precipitated with the EVs (570). In the case of BF and TFF, EV-GLAcmycH6 resulting from BF + SEC exhibited higher amount of GLA than those obtained by TFF + SEC ($p < 0.0001$), likely due to the different cut-offs in both techniques, (100 kDa for BF and 500 kDa for TFF). To confirm this hypothesis, additional experiments employing a 100 kDa cut-off in the TFF process could be performed to compare the GLA yield with that achieved using both the 500 kDa TFF and BF methods.

Then, the enzymatic activity (EA) of different EV-GLAcmycH6 productions were compared to that of free enzymes (Agal A and GLAcmycH6). To improve the exposure of the encapsulated enzyme to the EA substrate, EV-GLAcmycH6 isolates were diluted 1:5 with CelLytic™ MT Cell Lysis Reagent and sonicated following previously stablished procedures (132). Importantly, free enzymes were processed under the same conditions to ensure valid comparison. The results showed similar EA among the different EV-GLAcmycH6 isolation methods (5,105 to 6,110 µmol/h·mg). Activity in EV-GLAmycH6 was significantly higher than the soluble GLAcmycH6, and the recombinant Agal A approved for clinical use ($p < 0.0001$) (Fig. 7.5F and Table 7.3). These results are aligned with previous ones in our lab (132,202), and indicate that the encapsulation/lipid association of the GLA protein enhances its stability and EA. Interestingly, EV-GLAcmycH6 from BF + SEC and TFF + SEC showed similar EA, which was slightly higher than that exhibited by the Pp method (Fig. 7.5F). However, these differences were not statistically significant.

Table 7.3. Summary of different productions of EV-GLAcmycH6. EV were isolated and purified by precipitation (Pp), tangential flow filtration (TFF) and bench-top filtration (BF) followed by size exclusion chromatography (SEC). All results were represented as Mean ± SEM.

		Production yield			Enzymatic activity		*In vitro* efficacy	
Isolation method	**Size (nm)**	**EVs concentration (EVs/L)**	**GLA concentration (µg GLA/L)**	**Enzymatic activity (EA/L)**	**Ratio to Agal. A**	**Ratio to free GLA**	**Ratio to Agal. A**	**Ratio to free GLA**
Pp	**182.4** ± 4.7	**$3.1 \cdot 10^{10}$** ± $1.6 \cdot 10^{9}$	**4.3** ± 0.5	**$2.0 \cdot 10^{9}$** ± $9.7 \cdot 10^{7}$	**2.8** ± 0.3	**14** ± 1	**1.1** ± 0.001	**1.1** ± 0.02
BF + SEC	**154.5** ± 1.3	**$1.4 \cdot 10^{12}$** ± $8.2 \cdot 10^{9}$	**1.9** ± 0.2	**$1.7 \cdot 10^{9}$** ± $1.5 \cdot 10^{8}$	**4.0** ± 0.3	**17** ± 1.5	**1.3** ± 0.001	**1.5** ± 0.01
TFF + SEC	**171.3** ± 1.0	**$1.8 \cdot 10^{12}$** ± $1.0 \cdot 10^{10}$	**0.7** ± 0.1	**$1.7 \cdot 10^{9}$** ± $9.7 \cdot 10^{7}$	**4.0** ± 0.2	**17** ± 1	**1.5** ± 0.044	**1.7** ± 0.03

7.2.1. Capacity of EV-GLAcmycH6 to reduce Gb3 accumulation in endothelial cells derived from KO Fabry mice

After characterizing the different isolated EV-GLAcmycH6 variants, *in vitro* efficacy experiments were conducted using MAEC cells derived from GLA KO mice (see section 5.4). These experiments aimed to confirm that EV-GLAcmycH6 also had the capacity to clear intracellular Gb3 deposits. MAEC cells were incubated with different samples of EV-GLAcmycH6 and free

enzymes (GLAcmycH6 and Agal.A) at 0.1 µg/mL of equivalent GLA, along with fluorescently labelled NBD-Gb3. The results, expressed as the ratio to Agal. A, showed a better Gb3 reduction in cells treated with different versions of EV-GLAcmycH6 compared to the free enzymes. Among the different isolates, EV-GLAcmycH6 obtained by TFF + SEC showed the highest Gb3 clearance capacity, followed by BF + SEC, and lastly, Pp. Specifically, Gb3 clearance ratios relative to Agal A were 1.5 ± 0.1, 1.3 ± 0.0, and 1.1 ± 0.0, respectively (Fig. 7.5G). These differences correlated with the crude EA of each EV formulation (Fig. 7.5F). This increased *in vitro* efficacy was also observed in EV-GLAcmycH6 isolated by Pp (132), and could be due to the protection of the intraluminal enzymes from degradation by external proteases (501) or to the increase in the intrinsic stability of the enzyme when immobilized in lipid environments (202).

Moreover, EV-GLAcmycH6 isolated by BF + SEC and TFF + SEC showed significantly better *in vitro* efficacy (Fig. 7.5G) compared to those obtained by Pp ($p < 0.0001$) (Fig. 7.5E). This is probably due to the fact that precipitation-based methods have been shown to alter EV characteristics, whereas SEC purification is more effective at preserving EV integrity and function. In other words, the presence of co-precipitated agents or protein aggregates in Pp samples could interfere with *in vitro* efficacy or even compromise EV integrity (544). On the other hand, EV-GLAcmycH6 obtained by TFF + SEC showed better Gb3 clearance than those isolated by BF + SEC ($p = 0.01$), likely due to the higher EVs concentration in the TFF + SEC samples.

7.3. Characterization of EV-GLAH6 obtained from HEK 293F

Compared to CHO cells that stably express the exogenous GLA, HEK 293F cells were transiently transfected with pOpinE-GLA and pAdVAntage every time EV-GLA had to be isolated. Cells were transfected when their concentration reached $1 \cdot 10^6$ cells/mL and SN containing soluble GLAH6 enzyme and EV-GLAH6 were collected 5 days later. The isolation of EV-GLAH6 and its separation from the free GLAH6 enzyme were assessed using BF + SEC and TFF + SEC. The Pp method was not used in this case, due to its lower EV purity and production yield observed with EV-GLAcmycH6 from CHO DG4.

Both methodologies, BF + SEC and TFF + SEC, enabled the isolation of pure and functional EV-GLAH6 from the SN of transfected HEK 293F cells (Fig. 7.6). NTA analysis results showed a monodisperse population of EV-GLAH6 obtained by TFF + SEC, with a mean size of 144.4 ± 0.3 nm and a high concentration of EVs ($1.7 \cdot 10^{12} \pm 2.7 \cdot 10^{10}$ particles/L) (Table 7.4). EV-GLAH6 isolated by BF + SEC exhibited a similar mean size of 151.9 ± 53.6 nm but a more polydisperse population and a lower number of EVs ($5.7 \cdot 10^{10} \pm 2.4 \cdot 10^{10}$ particles/L) (Fig. 7.6A and Table 7.4). Of note, these results could be conditionate by the low particles/frame exhibited by BF + SEC (Fig. 7.6A).

Table 7.4. Summary of different productions of EV-GLAH6. EVs were isolated and purified by tangential flow filtration (TFF) and bench-top filtration (BF) followed by size exclusion chromatography (SEC). All results were represented as Mean ± SEM.

		Production yield			**Enzymatic activity**		***In vitro* efficacy**	
Isolation method	**Size (nm)**	**EVs concentration (EVs/L)**	**GLA concentration (µg GLA/L)**	**Enzymatic activity (EA/L)**	**Ratio to Agal. A**	**Ratio to free GLA**	**Ratio to Agal. A**	**Ratio to free GLA**
BF + SEC	**151.9** ± 53.6	**$5.7 \cdot 10^{10}$** ± $2.4 \cdot 10^{10}$	**1.9** ± 0.1	**$1.3 \cdot 10^{8}$** ± $6.2 \cdot 10^{6}$	**0.4** ± 0.0	**0.8** ± 0.0	**1.4** ± 0.0	**2.3** ± 0.6
TFF + SEC	**144.4** ± 0.3	**$1.7 \cdot 10^{12}$** ± $2.7 \cdot 10^{10}$	**75.2** ± 27.2	**$6.3 \cdot 10^{8}$** ± $7.4 \cdot 10^{7}$	**0.2** ± 0.0	**0.2** ± 0.0	**0.7** ± 0.2	**1.9** ± 0.4

Molecular characterization by WB of both EV-GLAH6 samples confirmed the presence of GLA and EV markers, such as Alix and CD63, with no detection of β-tubulin, indicating that the obtained samples were enriched in EV-GLAH6 and free of cytosolic contaminants (Fig. 7.6B). However, the intensity of the bands observed in WB indicated that EV-GLAH6 from BF + SEC contained lower levels of GLAH6 and EV markers compared to those obtained by TFF + SEC, demonstrating a lower presence of EVs in the BF + SEC samples.

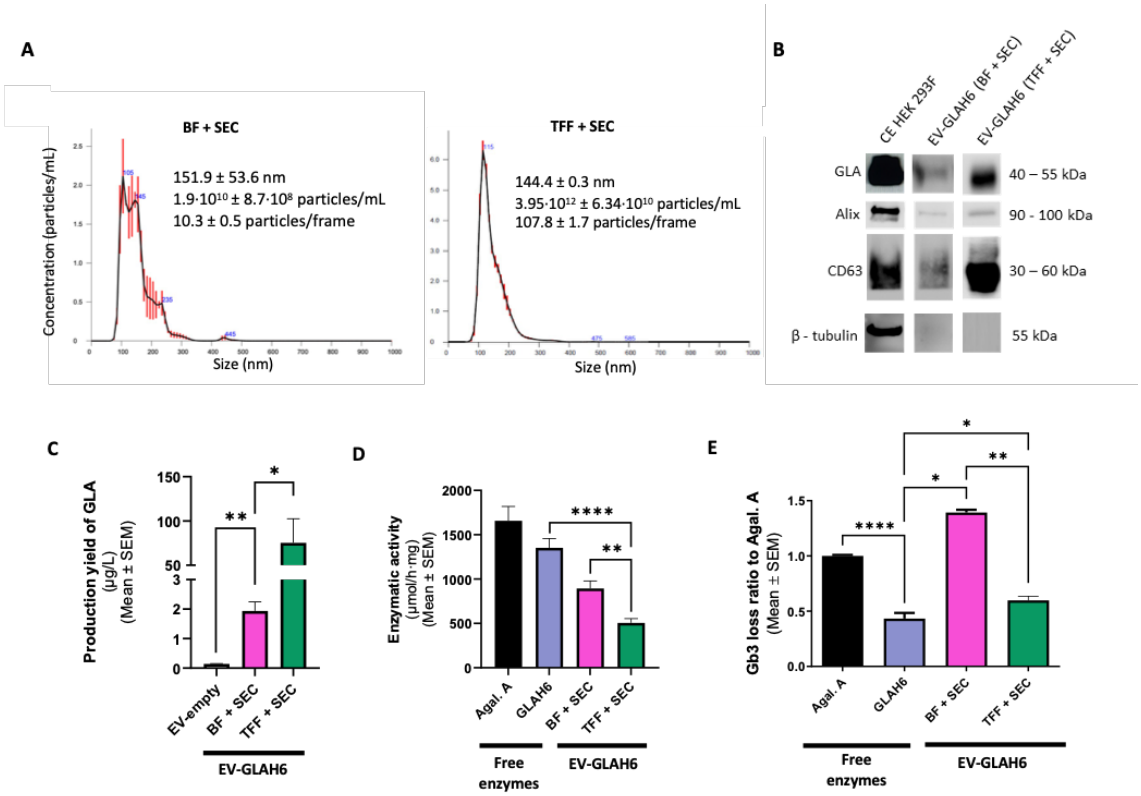

Fig. 7.6. Characterization of EV-GLAH6 from HEK 293F with transient expression of GLA isolated and purified by different procedures. **A)** Size distribution and concentration of EV-GLAH6 (particles/mL) after different isolation and purification procedures quantified by nanoparticle tracking analysis (NTA). Blue values correspond to the size of the main peaks in the histogram. Results are expressed as Mean ± SEM. **B)** Characterization by western blot (WB) of different EV-GLAH6. Cell extract of HEK 293F with transient expression of GLA was included as a control. twelve µg of total protein, previously determined by BCA assay, was loaded per lane. **C)** Production yield of GLA expressed as µg of GLA/L of supernatant in different EV-GLAH6 determined by ELISA. **D)** GLA enzymatic activity of EV-GLAH6 obtained from BF + SEC and TFF + SEC. **E)** Comparison of *in vitro* efficacy between different EV-GLAH6 and free enzymes at 0.1 µg/mL of equivalent GLA in endothelial primary cultures derived from Fabry KO mice after 48 h. Gb3 loss was normalized by *in vitro* efficacy of free Agal A. Statistical significance levels were schematically assigned ns ($0.05 \leq p$), *($0.01 \leq p < 0.05$), **($0.001 \leq p < 0.01$), ***($0.0001 \leq p < 0.001$), ****($0.0001 \leq p$).

ELISA quantification of GLA (µg/L) showed a significantly higher enzyme presence in EV-GLAH6 from TFF + SEC (75.2 ± 27.2 µg/L) compared to BF + SEC (1.9 ± 0.1 µg/L, $p = 0.01$). Both samples, contained significantly higher GLA levels than EV-empty isolated by TFF + SEC (0.1 ± 0.0 µg/L, $p = 0.003$ and $p = 0.01$, respectively) (Fig. 7.6C, Table 7.4).

Despite the successful encapsulation of GLAH6, both EV-GLAH6 samples showed lower EA than the soluble GLAH6 enzyme (Fig. 7.6D). Specifically, EV-GLAH6 from TFF + SEC showed significantly lower EA than BF + SEC-derived EVs ($p = 0.003$) and free GLAH6 ($p < 0.0001$) (Table 7.4). Free GLAH6 exhibited slightly higher EA than EV-GLAH6 obtained by BF + SEC, but this difference was not statistically significant ($p = 0.1$). No EA was detectable in EV-empty samples.

The low recovery of EV-GLAH6 using BF + SEC is consistent with previous studies that reported a 40% loss in EV recovery when using 100 kDa filters for EV isolation (582). This loss may be due to filter saturation, likely caused by the presence of cell debris or protein aggregates. Since transfection-induced cytotoxicity increases cell debris, it is plausible that this affected BF-based EV isolation efficiency (518,520,583,584). Interestingly, this issue was not observed in EV-GLAcmycH6 isolated from CHO DG44 stable clones, suggesting that transient transfection in HEK 293F cells may introduce additional challenges in EV recovery. Another possible cause to consider is the variability associated with these isolation procedures across different production batches, which will be explained in further sections.

Both EV-GLAH6 versions showed lower EA than free enzyme (Fig. 7.6D), contrary to what was observed in EV-GLAcmycH6 versions where the activity of the enzyme increased with the encapsulation (Fig. 7.5F). The differences observed between GLAH6 and GLAcmycH6, as well as between EV-GLAH6 and EV-GLAcmycH6, were likely due to post-translational modifications (PTMs) resulting from the different expression cell factories (HEK 293F or CHO DG44) (511,585). However, additional experiments comparing EV-GLAH6 or EV-GLAcmycH6 obtained from TGE and stable transfection are needed to confirm this hypothesis.

7.3.1. *In vitro* efficacy of EV-GLAH6 in endothelial cells derived from KO Fabry mice

To evaluate the ability of EV-GLAH6 to clear Gb3 accumulation, MAEC cells were treated with BF + SEC or TFF + SEC or free enzymes at 0.1 µg/mL of equivalent GLA. Agal A showed higher *in vitro* efficacy than free GLAH6 ($p < 0.0001$). However, both BF + SEC and TFF + SEC-derived EV-GLAH6 significantly improved Gb3 clearance compared to free GLAH6. The Gb3 clearance ratios relative to Agal A were 1.4 ± 0.0 for BF + SEC-derived EV-GLAH6, 0.7 ± 0.2 for TFF + SEC-derived EV-GLAH6, and 0.4 ± 0.1 for free GLAH6 (Fig. 7.6E).

Similar to what was observed in EV-GLAcmycH6 samples, encapsulation of GLAH6 enzyme inside an EV improved its *in vitro* efficacy, likely due to improved enzyme stability and protection from degradation (586). In addition, *in vitro* capacity to clear Gb3 accumulation in different EV-GLAH6 preparations was consistent with their EA (Fig. 7.6D).

7.4. Comparison between EV-GLAcmycH6 and EV-GLAH6.

In this thesis, various productions of EVs were performed using two different cell factories: CHO DG44 cells with stable expression of GLA and HEK 293F with transient GLA expression. Two different GLA-coding plasmids were used: pOptiVEC-GLA for CHO cells and pOpinE-GLA for HEK cells, with one enhancer plasmid (pAdVAntage) only used in HEK cells. pAdVAntage has been shown to enhance transient protein expression in mammalian cells by increasing translational initiation (587). Three different isolation procedures were tested (Pp, BF + SEC and TFF + SEC), some of which were performed using SN from the same production. All results are summarized in Table 7.7.

Table 7.5. Characteristics of free GLAcmycH6 and GLAH6. Values correspond to the Mean ± SEM.

Name	Cell source	Coding plasmid	GLA expression	GLA concentration (µg/mL)	Enzymatic activity (µmol/h·mg)
GLAcmycH6	CHO DG44	pOptiVEC-GLA	Stable	**1460** ± 104	**456** ± 57
GLAH6	HEK 293F	pOpinE-GLA	Transient	**2250** ± 108	**1540** ± 83

Differences in EV-GLA production yields were observed depending on the cell factory. In detail, EV-GLAH6 from HEK 293F showed better incorporation of GLAH6 inside the EVs compared to EV-GLAcmycH6 from CHO DG44. In contrast, EV-GLAcmycH6 appeared to be more active than EV-GLAH6, despite the higher EA observed in free GLAH6 compared to GLAcmycH6 (Table 7.5). This was further supported by *in vitro* efficacy experiments, where EV-GLAcmycH6 isolated by TFF + SEC showed higher efficacy than Agal. A, whereas EV-GLAH6 obtained by TFF + SEC did not.

Table 7.6. Summary of different productions of EV-GLAcmycH6 and EV-GLAH6. EVs isolated and purified by precipitation (Pp), tangential flow filtration (TFF) and bench-top filtration (BF) followed by size exclusion chromatography (SEC). Values in each cell corresponded to different productions. All results were represented as Mean ± SEM. (*) Concentration of GLA was quantified by WB in a single experiment.

		EV-GLAcmycH6			EV-GLAH6	
	Isolation method	**Pp**	**BF + SEC**	**TFF + SEC**	**BF + SEC**	**TFF + SEC**
	Size (nm)	**182.4** ± 4.7	**171.3** ± 1.0	**176.1** ± 8.4 **154.5** ± 1.3	**156.9** ± 4.9	**162.6** ± 2.9 **165.8** ± 4.3 **144.4** ± 3.5
Production yield	**EVs concentration (EVs/L)**	**$3.1\cdot10^{10}$** ± $1.6\cdot10^{9}$	**$1.4\cdot10^{12}$** ± $8.2\cdot10^{9}$	**$7.6\cdot10^{10}$** ± $6.9\cdot10^{9}$ **$1.8\cdot10^{12}$** ± $1.0\cdot10^{10}$	**$5.7\cdot10^{10}$** ± $2.4\cdot10^{10}$	**$9.2\cdot10^{11}$** ± $3.0\cdot10^{10}$ **$1.1\cdot10^{12}$** ± $4.3\cdot10^{10}$ **$1.7\cdot10^{12}$** ± $2.7\cdot10^{10}$
	GLA concentration (µg GLA/L)	**4.3** ± 0.5	**1.9** ± 0.2	**0.2** ± 0.0 **0.7** ± 0.1	**1.9** ± 0.1	**34.6*** **2.4** ± 0.3 **75.2** ± 27.2
	Enzymatic activity (EA/L)	**$2.0\cdot10^{9}$** ± $9.7\cdot10^{7}$	**$1.7\cdot10^{9}$** ± $9.7\cdot10^{7}$	**$4.1\cdot10^{9}$** ± $4.2\cdot10^{8}$ **$1.7\cdot10^{9}$** ± $1.5\cdot10^{8}$	**$1.3\cdot10^{8}$** ± $6.2\cdot10^{6}$	**$1.7\cdot10^{8}$** ± $2.7\cdot10^{7}$ **$4.5\cdot10^{8}$** ± $2.3\cdot10^{7}$ **$6.3\cdot10^{8}$** ± $7.4\cdot10^{7}$
Enzymatic activity	**Ratio to Agal. A**	**2.8** ± 0.3	**4.0** ± 0.2	**2.9** ± 0.4 **4.0** ± 0.3	**0.4** ± 0.0	**0.3** ± 0.1 **0.4** ± 0.0 **0.2** ± 0.0
	Ratio to free GLA	**14** ± 1	**17** ± 1	**7.4** ± 0.9 **17.0** ± 1.5	**0.8** ± 0.0	**0.7** ± 0.2 **0.4** ± 0.0 **0.2** ± 0.0
***In vitro* efficacy**	**Ratio to Agal. A**	**1.1** ± 0.0	**1.3** ± 0.0	**1.5** ± 0.0	**1.4** ± 0.0	**0.5** ± 0.0 **0.4** ± 0.0 **0.7** ± 0.2
	Ratio to free GLA	**1.1** ± 0.0	**1.9** ± 0.0	**1.3** ± 0.0	**2.3** ± 0.6	**0.9** ± 0.0 **0.8** ± 0.2 **1.9** ± 0.4

These findings suggest that stable clone of CHO DG44 cells likely produced more stable and active EV-GLA than TGE in HEK 293F. This could be explained by differences in the glycosylation of the two enzymes, due to the different cell sources (38), or because stable expression of GLA might offer advantages in terms of enzymatic activity and stability compared to TGE. However, additional experiments are needed to confirm this hypothesis, such as comparing EV-GLA obtained through TGE with EV-GLA obtained via stable expression, both produced by the same cell line.

All methodologies used to obtain functional EV-GLA from different cell sources produced EVs with similar mean size ranging from 155 to 182 nm. Additionally, all methodologies yielded comparable production rates, with a few exceptions, such as EV-GLAcmycH6 obtained from Pp and EV-GLAH6 obtained by BF + SEC, which showed lower EV recovery compared to the other methodologies.

It is important to note that there is variability among different productions of the same type of EV following TFF + SEC isolation, in terms of EV concentration, GLA concentration, EA and *in vitro* efficacy (Table 7.6).

7.5. Targeted EV-GLAH6 with cell penetrating peptide F7

7.5.1. rF7-EV-GLA obtained from HEK 293F cells

In an attempt to enhance cell internalization and overall biodistribution of the EVs, a cell penetrating peptide (CPP) was incorporated into the EV surface by fusing its sequence to the EV membrane protein Lamp2b. CPPs are short peptides (5-30 aa) with a positive charge that are used to improve the cell internalization of different nanoparticles and proteins (491–495). The strategy of incorporating targeting moieties to EV surface through the fusion with Lamp2b protein, was reported by other authors (196,588). The chosen CPP was F7, a peptide isolated from the CD300 immunoglobulin family (589), already protected in the group for its use in different drug delivery systems (213).

F7-functionalized EV-GLAH6 (rF7-EV-GLA) were obtained after transient co-transfection with pOpinE-GLAH6 and pcDNA3-F7-Lamb2b (4:1 ratio of total DNA). After 5 days post-transfection, EVs were isolated and purified by TFF + SEC. The rF7-EV-GLA were compared to non-targeted EV-GLAH6 and EV-empty obtained from non-transfected cells. The number of cells was lower in the transfected cultures compared to non-transfected cells. Specifically, in cells co-transfected with GLAH6 and Lamp2b-F7 plasmid ($3.4 \cdot 10^5$ cells/mL) compared to those transfected with only GLAH6 plasmid ($1.3 \cdot 10^6$ cells/mL) and non-transfected cells ($2.4 \cdot 10^6$ cells/mL). These results showed a clear reduction in cell viability associated with the transfection process, probably due to the cytotoxicity of PEI and the inherent toxicity of the F7 peptide (517,590).

NTA revealed a monodisperse population for EV-empty, EV-GLAH6 and rF7-EV-GLA with mean sizes of 157.3 ± 1.3 nm, 144.4 ± 0.3 nm and 141.9 ± 2.3 nm, respectively. As for the EV quantities high concentrations of EVs were obtained (Fig. 7.7A and Table 7.5) with similar yields among samples: $1.9 \cdot 10^{12} \pm 1.0 \cdot 10^{10}$, $1.7 \cdot 10^{12} \pm 2.7 \cdot 10^{10}$ and $1.7 \cdot 10^{12} \pm 9.4 \cdot 10^{10}$ particles/L, for EV-empty, EV-GLAH6 and rF7-EV-GLA, respectively (Table 7.7).

Table 7.7 Characteristics of EV-empty, EV-GLAH6 and rF7 targeted EV-GLAH6. EVs were isolated and purified by tangential flow filtration (TFF) followed by size exclusion chromatography (SEC). All results were represented as Mean ± SEM.

		EV-empty	EV-GLAH6	rF7-EV-GLAH6
	Size (nm)	157.3 ± 1.3	144.4 ± 0.3	141.9 ± 2.3
Production yield	**EVs concentration (EVs/L)**	$1.9 \cdot 10^{12} \pm 1.0 \cdot 10^{10}$	$1.7 \cdot 10^{12} \pm 2.7 \cdot 10^{10}$	$1.7 \cdot 10^{12} \pm 9.4 \cdot 10^{10}$
	GLA concentration (µg GLA/L)	0.4 ± 0.0	75.2 ± 27.2	8.63 ± 1.6
	Enzymatic activity (EA/L)	Not detectable	$6.3 \cdot 10^8 \pm 7.4 \cdot 10^7$	$1.5 \cdot 10^9 \pm 2.1 \cdot 10^8$
Enzymatic activity	**Ratio to Agal. A**	Not detectable	0.2 ± 0.0	0.4 ± 0.1
	Ratio to free GLA	Not detectable	0.2 ± 0.0	0.6 ± 0.1
***In vitro* efficacy**	**Ratio to Agal. A**	0.01 ± 0.0	0.7 ± 0.2	0.9 ± 0.0
	Ratio to free GLA	0.11 ± 0.06	1.9 ± 0.4	3.4 ± 0.1

As mentioned before, it is important to note that the size and concentration of EVs are not entirely accurate (575). In fact, TEM images confirmed the presence of EVs smaller than 100 nm, which likely correspond to exosomes (Fig. 7.7B).

During the isolation process, a portion of each EV sample was stained with DiOC (75 μM) to identify fractions with the highest fluorescence signal, corresponding to the highest EV content (Fig. 7.7C). The SEC fractions enriched in EVs were F8-9 for EV-empty and F7-11 for EV-GLAH6 and rF7-EV-GLA, aligning with previous studies where CD63, CD81, and CD9-enriched fractions were found in similar SEC fractions (544,591). All together, these results confirmed similar size distribution and morphology between the different EVs obtained.

Molecular characterization of EV-GLAH6 and rF7-EV-GLAH6 by WB revealed the presence of EV markers such as Alix and CD81 indicating that the samples were EV-enriched (Fig. 7.7D). In addition, both samples showed the presence of GLAH6, but stronger signal was detected in EV-GLAH6 compared to rF7-EV-GLA (Fig. 7.6D). This lower presence of GLAH6 in rF7-EV-GLAH6 was also observed in other productions and in lysates from transfected cells, as well as in the SN, probably due to the reduced amount of pOpinE-GLA (80%) added in the co-transfection with pcDNA3-F7-Lamb2b, compared to the full transfection with pOpinE-GLA (100%). Furthermore, the high level of cell mortality associated with the co-transfection of GLAH6 and the Lamp2b-F7 plasmid may have contributed to a reduced cell population, thereby affecting overall protein expression levels. These results were further confirmed by production yield of GLA quantified by ELISA and WB (Table 7.7).

Bands corresponding to Lamp2b were detected only in rF7-EV-GLAH6, confirming successful expression of the Lamp2b-F7 fusion protein (Fig. 7.7D). The band sizes (~100–110 kDa) were consistent with those reported for Lamp2b in other EV studies (588,592,593). The absence of Lamp2b in EV-GLAH6 is probably due to the low amount of total protein loaded in each sample (2 μg). For a better detection of the endogenous Lamp2b the lysosomal fraction of proteins should have been isolated.

ELISA confirmed that both EV-GLAH6 and rF7-EV-GLAH6 contained significantly higher GLAH6 concentrations than EV-empty, demonstrating that GLAH6 overexpression enhanced its encapsulation in EVs (Table 7.5). Additionally, both EV-GLAH6 and rF7-EV-GLAH6 exhibited detectable EA. However, rF7-EV-GLAH6 showed significantly higher EA than EV-GLAH6 ($p = 0.004$). Both EVs demonstrated significantly lower EA compared to free GLAH6 enzyme ($p = 0.003$ and $p < 0.0001$, respectively) (Fig. 7.7E). These results are consistent with those observed in Fig. 7.6D, where EV-GLAH6 from TFF + SEC exhibited significant lower EA values compared to free GLAH6 enzyme.

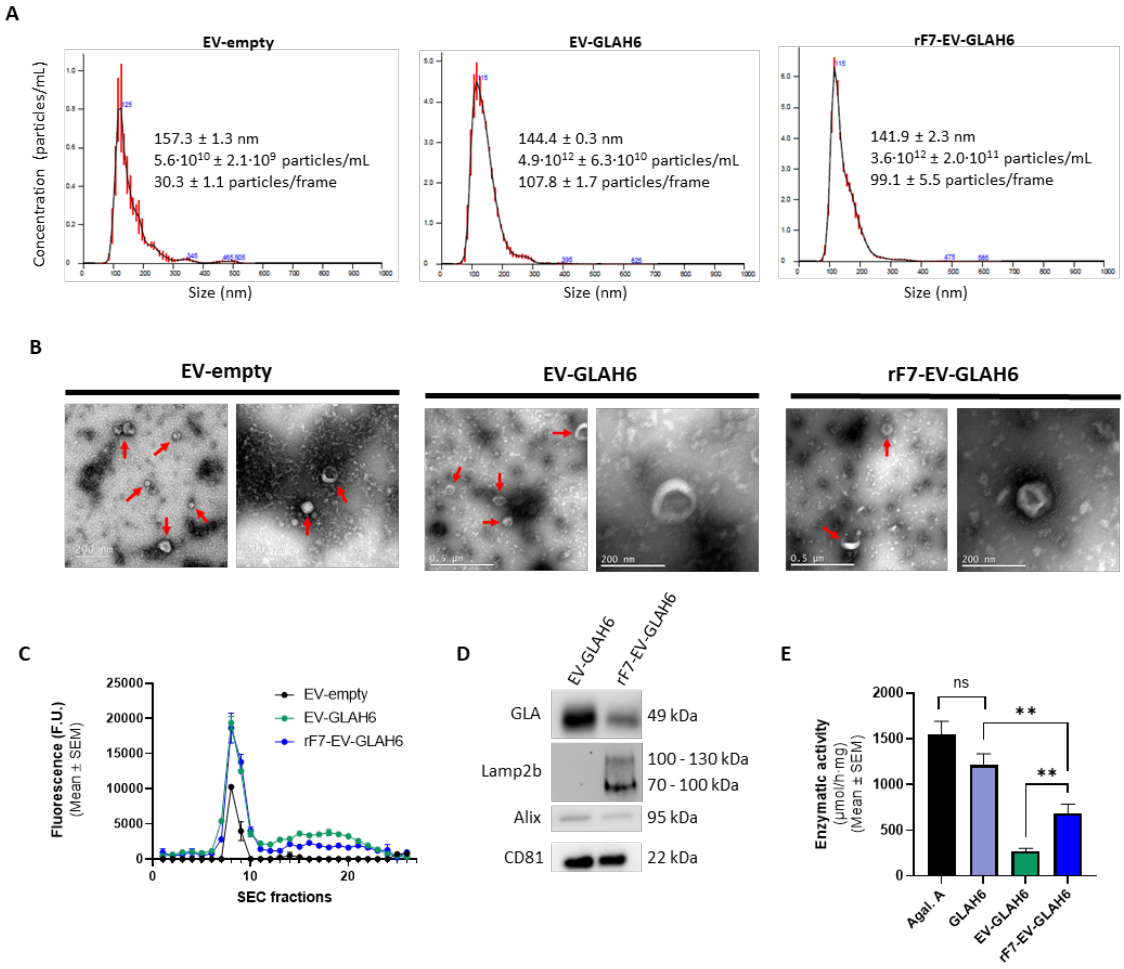

Fig. 7.7. Characterization of EV-GLAH6 and rF7-EV-GLAH6 used for *in vitro* assays. **A)** Size distribution and concentration of EV-GLAH6 (particles/mL) after different isolation and purification procedures quantified by nanoparticle tracking analysis (NTA). Blue values correspond to the size of the main peaks in the histogram. Results are expressed as Mean ± SEM. **B)** TEM images of EV-empty, EV-GLAH6 and rF7-EV-GLAH6 corresponding to the concentrated fractions of the SEC. Scale bars were represented in every image. **C)** SEC purification of EV-empty, EV-GLAH6 and rF7-EV-GLAH6 stained with DiOC at 75 µM after TFF. Total of 26 fractions of 0.7 mL were collected and fractions of higher DiOC fluorescence signal were concentrated (fractions 8-9 for EV-empty and 7-11 for EV-GLAH6 and rF7-EV-GLAH6). **D)** Molecular characterization of EV-GLAH6 and rF7-EV-GLAH6 by WB. Two micrograms of total protein were loaded to determine the presence of GLA, Alix and Lamp2B in every sample and 1.5 µg for CD81. **E)** GLA specific enzymatic activities of EV-GLAH6 and rF7-EV-GLAH6 compared with both free enzymes. Statistical significance levels were schematically assigned ns ($0.05 \leq p$), *($0.01 \leq p < 0.05$), **($0.001 \leq p < 0.01$), ***($0.0001 \leq p < 0.001$), ****($0.0001 \leq p$).

7.5.2. Internalization of rF7-EV-GLAH6 and EV-GLAH6 in endothelial cells

Internalization assays were conducted using flow cytometry in HMEC-1 cells to determine if the presence of rF7 enhances the internalization of EV-GLAH6. EVs were stained with DiOC at 75 µM and passed through a SEC column to remove unincorporated dye.

After 3 h of incubation with $1 \cdot 10^6$ EV/well, cells treated with rF7-EV-GLA showed the highest fluorescent signal (Fig. 7.8A). In detail, the results showed a significantly higher percentage of positive DiOC cells (%DiOC cells) in samples treated with rF7-EV-GLA (41.0 ± 3.0%) compared to EV-GLAH6 (23.7 ± 3.7%) ($p = 0.01$) and EV-empty (6.5 ± 1.3%) ($p < 0.0001$). Interestingly, EV-GLAH6 also showed higher %DiOC cells than EV-empty ($p = 0.004$).

These results indicate that rF7 significantly enhances EV-GLAH6 internalization. Similar improvements in cell internalization were observed in our group using polymeric micelles (PM) and solid lipid nanoparticles (SLN), decorated with F7 through chemical conjugation (594). These assays were performed with other cell types, such as RAW 264.7 and MDA-MB-231, which enhanced the robustness of the results.

As for the effect of GLA in cell internalization, the enhancement of internalization of GLA containing systems vs. controls was also observed with RGD-targeted liposomes (section 5.3). GLA located on the external surface could interact with M6PR, promoting EV internalization via this pathway. However, to further confirm this hypothesis additional assays should be conducted, such as blocking the M6PR internalization with an excess of M6P or comparing cellular uptake of EV-empty and EV-GLAH6 in the presence of endocytosis inhibitors.

To explore the specific route of internalization of both EV-GLAH6 and rF7-EV-GLA, EVs were stained with DiOC (75 μM) and internalization was assessed in HMEC-1 cells after 6 h of incubation in the presence of endocytic inhibitors, as detailed in section 5.3.2. No significant cytotoxicity was observed for the chosen inhibitor concentrations (cell viability ≥ 90%), further ensuring the validity of the results. To ease the interpretation, fluorescence values (positive cells or MIF) in the presence of endocytic inhibitors were referred to those obtained without inhibitors (ratio to control).

Results show that no endocytosis inhibitor was able to completely block EV uptake (Fig. 7.8B and 7.8C). However, Dyn and EIPA significantly reduced the internalization of both EV-GLAH6 and rF7-EV-GLAH6 in HMEC-1 cells (Fig. 7.8B and 7.8C). Interestingly, rF7-EV-GLAH6 internalization is more sensitive to the presence of endocytic inhibitors. In detail, Dyn (50 μM) and EIPA (100 μM) reduced EV-GLAH6 internalization by 28.2% (p = 0.0006) and 27.2%, respectively, as measured by the percentage of DiOC-positive cells, while Nys (25 μM) reduced internalization by only 6.2%. No changes in EV-GLAH6 uptake were detected in cells treated with CPZ (10 μM). On the other hand, both Dyn and EIPA reduced rF7-EV-GLAH6 internalization by 37% (p = 0.02 and p = 0.03, respectively), CPZ reduced internalization by 10.7%, and Nys a 7% (Fig. 7.8B). Furthermore, results analyzed by MFI showed a similar reduction in EV-GLAH6 internalization caused by Dyn and EIPA (43%) (p = 0.001 and p = 0.04, respectively), with only an 8% reduction observed for Nys (Fig. 7.8C). In contrast, Dyn and EIPA individually caused a 50% loss of rF7-EV-GLAH6 internalization (p = 0.002 and p = 0.001, respectively), but no reduction was observed in cells treated with Nys or CPZ (Fig. 7.8C).

These results demonstrate that the predominant route of endocytosis of both EV-GLAH6 and rF7-EV-GLA in HMEC-1 is macropinocytosis. This is probably due to the mean size of the EV-GLAH6 and rF7-EV-GLAH6 (144.4 ± 0.3 nm and 141.9 ± 2.3 nm, respectively), as macropinocytosis is the main endocytic route for nanoparticles in this size range (278). This primary endocytic pathway was also observed in the internalization of EVs from different cell sources and in various target cells, further supporting macropinocytosis as one of the main routes for EV endocytosis (595,596). On the other hand, caveolae dependent endocytosis involves only 6 - 8% of internalization of both EV-GLAH6 and rF7-EV-GLAH6.

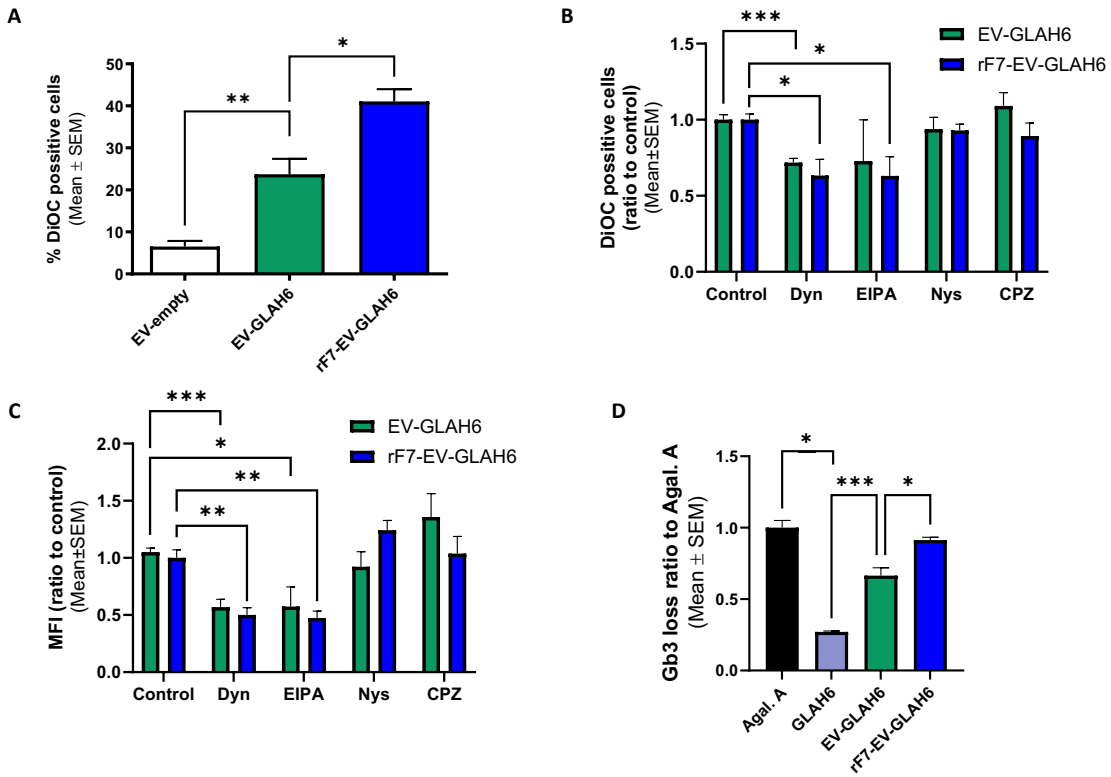

Fig. 7.8. Internalization of EV-GLAH6 and rF7-EV-GLAH6 and *in vitro* clearance of Gb3 in endothelial cells. **A)** Percentage of DiOC positive HMEC-1 cells after 3 h of incubation with EV-GLAH6 and rF7-EV-GLAH6 by flow cytometry. EV-empty was included as a control. **B)** Ratio of DiOC positive HMEC-1 cells in presence of different endocytosis inhibitors referred to control (absence of inhibitors) after 6 h of incubation. **C)** Ratio of MFI in presence of different endocytosis inhibitors referred to control (absence of inhibitors) after 6 h of incubation. **D**) *In vitro* efficacy of EV-GLAH6, rF7-EV-GLAH6 compared with free enzymes at 0.1 µg/mL of equivalent GLA in endothelial GLA KO cells after 48 h of incubation. Statistical significance levels were schematically assigned ns ($p \geq 0.05$) *($0.01 \leq p < 0.05$), **($0.001 \leq p < 0.01$), ***($0.0001 \leq p < 0.001$), ****($0.0001 \leq p$).

Slight differences were observed in the internalization of rF7-EV-GLAH6 and EV-GLAH6 in the presence of CPZ (Fig. 7.8B, 7.8C). The %DiOC cells showed that clathrin-dependent endocytosis, which is inhibited by CPZ, is involved in 10.7% of rF7-EV-GLAH6 internalization, while in the case of EV-GLAH6, endocytosis appears to be clathrin-independent, as CPZ does not seem to affect EV-GLAH6 internalization (Fig. 7.8B). However, the differences in %DiOC-positive cells between rF7-EV-GLAH6 with CPZ and without CPZ were not significant. Moreover, clathrin involvement in rF7-EV-GLAH6 internalization was not evident based on MFI analysis (Fig. 7.8C), indicating that the clathrin-dependent endocytic pathway has minimal impact on the internalization of rF7-EV-GLAH6.

It is worth mentioning that fibroblasts from Fabry patients exhibit impaired clathrin-dependent endocytosis (597) and, consequently, altered M6PR-dependent endocytosis, which is the main pathway for free GLA cellular uptake (268,269). Based in our results, EV-GLAH6 and rF7-EV-GLAH6 use clathrin-independent endocytosis pathways, presenting themselves as promising candidates for improving GLA delivery to cells affected by Fabry disease.

7.5.3. In vitro efficacy of rF7-EV-GLAH6

To determine whether the enhanced internalization of F7 decorated EVs translates into improved Gb3 clearance, *in vitro* efficacy experiments were conducted using MAEC cells. Cells

were treated with 0.1 µg/mL of equivalent GLA of Agal A, free GLAH6, EV-GLAH6 and rF7-EV-GLA and the efficacy of different treatments was referred to that shown by Agal. A.

The results showed that after 48 h, both EV-GLAH6 and rF7-EV-GLAH6 were able to clear Gb3 accumulation in MAEC KO cells more efficiently than free GLAH6 (Fig. 7.8D). rF7-EV-GLAH6 showed significantly higher *in vitro* efficacy (0.9 ± 0.0 ratio to Agal. A) than GLAH6 (0.3 ± 0.0 ratio to Agal. A) ($p < 0.0001$) and non-targeted EV-GLAH6 (0.7 ± 0.1 ratio to Agal. A) ($p = 0.03$). Additionally, EV-GLAH6 was significantly more efficient in reducing Gb3 levels than GLAH6 ($p = 0.0008$) (Fig. 7.8D).

Altogether, these results confirmed that the encapsulation of GLAH6 inside the EVs improved its *in vitro* efficacy (Fig. 7.8D). Furthermore, targeting the EV-GLAH6 with CPP rF7 significantly enhances its *in vitro* efficacy, probably due to a better internalization (Fig. 7.8A).

7.6. Summary and conclusions

This section explores the use of EVs as drug delivery systems for the GLA enzyme. EV-GLA was obtained from two different cell sources with distinct GLA expression strategies: CHO DG44 cells with stable GLA expression and HEK 293F cells with transient expression of the enzyme. Three different isolation procedures were tested (Pp, BF + SEC and TFF + SEC) to identify the optimal methodology for isolating functional EV-GLA from the SN of both cell types. In addition, EV-GLA from HEK cells (EV-GLAH6) was targeted with rF7 to enhance its cellular uptake.

All isolation methodologies (Pp, BF + SEC and TFF + SEC) successfully yielded functional EV-GLA from SN of both cell types. BF + SEC and TFF + SEC outperformed Pp in terms of EV concentration and *in vitro* efficacy, although in terms of GLA quantity, Pp method exhibited production yield compared to BF + SEC and TFF + SEC. The EA of the obtained EV-GLA was similar across all methodologies (Table 7.3).

In the case of EV-GLAcmycH6 from stable clone CHO DG44, all methodologies allowed the obtention of EV-GLA with higher EA and *in vitro* efficacy compared to the free enzyme (Table 7.3). However, Pp showed lower EV concentration compared to the other isolation methodologies, but it also exhibited the highest amount of GLA, probably due to the co-precipitation of free GLAcmycH6 enzyme. The EA/L of the obtained EV-GLA was similar across all methodologies, except for one batch from TFF + SEC, which exhibited better EA/L than Pp (Table 7.3). Importantly, EV-GLAcmycH6 obtained by BF + SEC and TFF + SEC exhibited the best purity qualities and *in vitro* efficacy compared to those obtained by Pp (Fig. 7.5G and Table 7.3).

For EV-GLAH6 resulting from TGE of GLA in HEK 293F, both BF + SEC and TFF + SEC allowed the obtention of functional EV-GLA. Although their EA was not higher than the free enzyme, there was an improvement in *in vitro* efficacy due to the encapsulation of the enzyme in the EVs. For the isolation of EV-GLAH6, TFF + SEC showed more advantages than BF + SEC in terms of EV concentration, amount of GLA protein and EA/L (Table 7.4). However, EV-GLAH6 from BF + SEC showed better *in vitro* efficacy than those obtained by TFF + SEC (Fig. 7.6E and Table 7.4).

An increase in enzymatic activity and improvement of *in vitro* efficacy due to the encapsulation in EVs has been reported by other researchers using EVs derived from HEK cells endogenously loaded with other lysosomal enzymes, such as SGSH (132), GBA (504) and HexA (503). This demonstrates that the strategy of encapsulating lysosomal enzymes in EVs could be valuable for enhancing ERT in several LSDs.

Additionally, other authors have demonstrated that the strategy of loading proteins into EVs through genetic engineering of the source cells can be applied to non-lysosomal proteins, such as cytokines (598–600) or growth factors (601,602). Therefore, this therapeutic strategy is not limited to LSDs and can also be applied to improve the treatment of other diseases, including cancer, cerebral ischemia, acute lung injury and more.

When comparing EV-GLAcmycH6 with EV-GLAH6, the BF + SEC method appears to work better for isolating EV-GLAcmycH6 than EV-GLAH6 (Table 7.7). This is likely due to the high mortality associated with the transfection process in HEK 293F cells, which led to the presence of cell debris that could reduce the efficiency of EV-GLAH6 isolation by clogging the filter during BF + SEC. On the other hand, EV-GLAH6 from HEK 293F contained a higher amount of GLA loaded into the EVs compared to EV-GLAcmycH6. However, the latter appeared to be more active than EV-GLAH6 in terms of EA and, in some cases, *in vitro* efficacy (Table 7.6). In addition, EV-GLAcmycH6 demonstrated an improved EA compared to the free enzyme, a result not observed with EV-GLAH6 (Table 7.7). This suggests that stable clone of CHO DG44 produced more stable and active EV-GLA than transiently transfected HEK 293F cells. However, additional experiments are needed to confirm this hypothesis.

Additionally, there is some variability associated with the EV-GLA production process, as differences can be observed between different productions of the same type of EV, even using the same isolation methodology. These differences are evident in terms of EV concentration, GLA concentration, EA and *in vitro* efficacy (Table 7.6).

Targeting EV-GLAH6 with rF7 enhanced its cellular uptake and *in vitro* efficacy in endothelial cells (Fig. 7.8A and 7.8D), despite its low EA (Fig. 7.7E). This demonstrated that targeted EVs can enhance *in vitro* efficacy and may represent a promising strategy to improve *in vivo* outcomes. In fact, several targeting strategies reported in the literature, using Lamp2b as the protein to incorporate targeting molecules, such as RVG (196), RGD (603) and other peptides onto the EV surface, have shown promising *in vivo* results, improving therapeutic delivery to target tissues (604–607). However, no significant differences were observed in the endocytosis of EV-GLAH6 compared to the “targeted” EVs (rF7-EV-GLAH6) in HMEC-1 cells, which occurred primarily through macropinocytosis (Fig. 7.8B and 7.8C). This lack of difference could be attributed to the long incubation time (6 h), which may have been too prolonged to detect endocytosis differences attributable to the targeting moiety.

In summary, EV-GLA has emerged as a promising tool to enhance ERT in Fabry disease, as the encapsulation of the enzyme within the EV preserves its EA and improves its *in vitro* efficacy. Furthermore, targeting EV-GLA with rF7 enhances its internalization and *in vitro* Gb3 clearance in endothelial cells. However, factors such as the cell source, the transfection process used to overexpress GLA and the isolation methodology, are important considerations that could impact the function and efficacy of EV-GLA as a drug delivery system. In fact, stable clone from CHO DG44 appears to be the best strategy for obtaining functional EV-GLA, with BF + SEC being the optimal method for isolation. On the other hand, TFF + SEC is the preferred approach for obtaining EV-GLA from transiently transfected HEK 293F.

8. General discussion

As stated in previous sections, nanotechnology has emerged as a powerful tool to protect recombinant enzymes and target them to the affected cells and organs (53,608). This thesis has explored the use of nanoliposomes and EVs as two different nanocarriers for the same therapeutic enzyme, the GLA. NanoGLA and EV-GLA were designed to improve ERT in FD, allowing a head-to-head comparison of both therapeutic strategies in FD models.

There are four specific aspects that are crucial for any drug delivery systems (DDS) being used in ERT: preservation of the enzymatic activity, proper cell/organ targeting, *in vivo* biodistribution and manufacturing/scale-up. Through this discussion, these four aspects will be covered, directly comparing the nanoliposomes and EVs and putting them in context with other DDS with application in LSDs.

8.1. Crude enzymatic activity in nanoGLA and EV-GLA

Results from this thesis and previous publications by our group have demonstrated that encapsulating the GLA enzyme in nanoliposomes or EVs preserved both its stability and functionality (53,132,200,226). This effect may be due to the association of GLA enzyme with lipid-membranes, which helps stabilize the enzyme and protect it from degradation (202). Besides, the sequence of the GLA as well as its glycosylation might have a direct impact of the final EA of the drug delivery system.

In this thesis, nanoliposomes containing MKC in their membrane composition were loaded with a GLA variant lacking a His tag (rh-GLA) and exhibited lower EA levels compared to the free enzyme. In contrast, liposomes without MKC, loaded with a different His-tagged GLA variant from previous studies, showed higher EA levels than the free GLA enzyme (202). This suggests that the GLA sequence may play a significant role in the enzyme's functionality. **Sequence-related differences in GLA** were also observed in EVs. As crude enzyme, GLAH6 exhibited higher EA than GLAcmycH6. These findings align with the observations reported by Dr. Aida Carreño in her PhD thesis (2024), in which GLA enzymes produced by HEK 293F cells through TGE exhibited higher EA and protein solubility. In contrast, GLAcmycH6 produced in CHO cells via SGE showed reduced structural stability at pH 5.5 and a greater tendency to aggregate. These differences in crude EA may be due to variations in glycosylation patterns resulting from the different cell sources (38). However, once encapsulated in EVs, results shifted. Although EV-GLAH6 contained a higher amount of GLA compared to EV-GLAcmycH6, it showed lower EA than the free enzyme. Conversely, EV-GLAcmycH6 exhibited higher EA than both the free GLAcmycH6 and EV-GLAH6. This suggests that the **method of GLA expression** may influence enzyme activity and stability once encapsulated in EVs, with SGE potentially producing a more active and/or stable enzyme under these conditions than TGE. These differences could be attributed to several factors, including the amount of GLA encapsulated in the EVs, the enzyme's stability within the vesicles, or differences in PTMs between the two enzyme variants. Regarding the cellular systems used, EV-GLAcmycH6 obtained from the stable CHO DG44 clone exhibited higher EA and improved *in vitro* efficacy compared to EV-GLAH6 derived from transiently transfected HEK 293F cells. This is likely due to the more consistent expression of GLA into EVs in the stable system.

In a boarder context, several studies have demonstrated that encapsulating lysosomal enzymes into NPs other than nanoliposomes and EVs, such as ICAM-1-targeted polystyrene nanoparticles (609–612) and PLGA nanoparticles (613,614) can improve EA delivery to cells and *in vitro* efficacy. However, none of these studies reported an increase in crude EA as a result of enzyme encapsulation compared to the free enzyme. For instance, Thekkedath et al. (246), Sun et al. (247) and Aldosari et al. (248) demonstrated that encapsulation of enzymes in liposomes increased the intracellular EA in cellular models more efficiently than free enzyme. However, they did not compare the crude liposomal EA to the free enzyme, making it difficult to discern whether the increase in intracellular EA by the use of the nanocarriers was due to the stabilization of the enzyme, to the protection from degradation in extracellular space, due to an increased cell internalization/delivery or to the combination of all this factors. Similar results were observed for EVs encapsulating lysosomal enzymes for Sandhoff disease (503), Batten disease (195,502,615), with lower EAs in the encapsulated versions. Two exceptions to these observations are EVs endogenously loaded with SGSH or GBA fused to VSV-G to for the treatment of MPS type III and GD, respectively. EV-SGSH showed a clear increase in EA compared to the free enzyme (132) and EVs with GBA showed significantly higher GBA activity than unmodified EVs (504). Interestingly enough, in both examples enzymes were endogenously incorporated into EVs and vesicles were isolated by precipitation, meaning that free soluble enzyme might accompanying the EVs and contribute to the enhanced EA.

Overall, these findings highlight the critical impact of both enzyme sequence and encapsulation strategy on GLA EA. The composition of nanoliposomes significantly influences EA. Furthermore, the expression system and cellular source used for GLA production play a key role in determining its functionality. Notably, while encapsulation in EVs can modulate these effects, the observed variability in EA suggests a complex interplay between expression method, enzyme sequence, and vesicle environment. These findings underscore the importance of optimizing both the enzyme production process and nanoparticle design to maximize therapeutic efficacy. Future studies involving controlled comparisons of expression systems and encapsulation conditions will be essential to further elucidate the factors that govern enzyme stability and functionality within nanoliposomes and EVs, ultimately contributing to the development of more effective treatments for LSDs.

8.2. Enhancing endothelial cell uptake and Gb3 clearance by encapsulating the GLA enzyme

Our results demonstrated that the encapsulation of GLA in RGD-targeted nanoliposomes **favors enzyme's internalization** into endothelial cells through M6PR- but also clathrin-independent endocytic pathways. Regarding EVs, the results of this thesis demonstrate that the predominant endocytic pathway for EV-GLAH6 in HMEC-1 cells is macropinocytosis. Just this already represented a major advantage. Like other lysosomal enzymes used in ERT, soluble non-encapsulated GLA primarily internalizes via MP6PR located on the cell membrane (10–12). In contrast, our results show that the enzyme, when encapsulated in nanoliposomes or EVs, GLA could enter in endothelial cells via alternative pathways, such as macropynocitosis and caveolae-mediated endocytosis. This demonstrates that enzymatic encapsulation into nanoliposomes or EVs could be a promising strategy for delivering ERT to cells from patients with LSDs with low expression levels of M6PR, such as in Pompe disease (616,617), or diseases with impaired clathrin-dependent endocytosis (268,269,597,618).

Other liposomal formulations have already showed an improvement in the internalization of lysosomal enzymes compared to the free enzyme. Thekkedath et al. (246) and Sun et al. (247)

developed two different liposomal formulations loaded with GBA and acid β-glucosidase (GCase), respectively, to improve ERT in GD. The first demonstrated that phosphatidylcholine-based liposomes loaded with glucocerebrosidase improved enzyme's internalization in target cells, such as Gaucher fibroblasts and macrophages, as observed by flow cytometer and confocal microscopy (246). Additionally, Sun et al. reported an improvement in cellular uptake via M6PR-independent pathways of their GCase loaded saposin C (SapC) and dioleoylphosphatidylserine (DOPS) liposomes, in mouse fibroblasts derived from GCase KO mice (247). Furthermore, Hamill et al. (249) entrapped recombinant human IDUA enzyme in guanidinylated neomycin (GNeo)-targeted liposomes and showed that cellular uptake and lysosomal delivery of IDUA in MPS I fibroblasts were significantly increased. Of note, in our hands, RGD-targeted liposomes are internalizing mainly through clathrin-independent pathways. On the contrary, other authors have reported that RGD-targeted liposomes are typically endocytosed via clathrin-mediated endocytosis after an incubation period of approximately 1 h (313,314). The longer incubation time used in our endocytosis experiments (6 h) could have hampered the observation the RGD-dependent effects. Therefore, to confirm that the RGD peptide promotes clathrin-dependent endocytosis of the nanoliposomes, shorter incubation times (30 min – 1 h) should be tested.

In the case of EVs, macropinocytosis seems to be the major cell entry pathway. This is likely due to the average size of the EV-GLAH6 particles (144.4 ± 0.3 nm), as macropinocytosis is the primary endocytic route for nanoparticles within this size range (278). This observation is consistent with the endocytic behavior of nanoliposomes, which have a similar size range (115 ± 1 to 171 ± 2 nm) compared to EV-GLAH6. In fact, these findings align with previous studies using EV-GLAcmycH6 derived from CHO cells isolated by precipitation (132), as well as other reports involving various EVs and target cell types (595,596).

Regardless the initial EA, both, nanoliposomes and EVs encapsulating GLA are more effective at **reducing Gb3 accumulation** in primary cultures from Fabry KO mice than the free enzyme. These findings suggest that encapsulating GLA can enhance its cellular uptake, protect the enzyme from degradation, improve its delivery to lysosomes, and ultimately lead to a more effective reduction of Gb3 accumulation than the free enzyme.

Similar to our results, encapsulation of recombinant human acid sphingomyelinase (rh-ASM) into bis(monoacylgly cerol)phosphate (BMP)-based liposomes was performed by Aldosari et al. (248) to improve Niemann-Pick disease type B (NPB) therapy. Their *in vitro* studies using NPB fibroblasts demonstrated a better clearance of accumulated sphingomyelin when rh-ASM was encapsulated in a liposome compared to the free enzyme. Additionally, Sun et al. reported an improvement in *in vitro* efficacy of their GCase-SapC-DOPS liposomes, in mouse fibroblasts derived from GCase KO mice (247). As for the EVs, Calzoni et al. (503) overexpressed the α-subunit of lysosomal β-hexosaminidase in HEK cells and demonstrated that derived EVs, isolated by UC, were able to partially correct the enzyme deficiency in Sandhoff patient fibroblasts. In Batten disease, macrophage-derived EVs carrying the enzyme TPP1 by exogenous (615) or endogenous loading (195,502), and isolated by UC, have been shown to be effective in both *in vitro* and *in vivo* models. Interestingly, natural EVs are also being investigated as ERTs for other LSDs, such as MPS type IVA (Morquio A syndrome) (498).

Overall, these findings highlight the potential of encapsulating lysosomal enzymes, as an effective strategy for improving substrate clearance in primary cell cultures and may enhance ERT across various LSDs. AS for FD, our data show that encapsulated GLA can enter endothelial

cells via clathrin-independent pathways, fact that could be particularly advantageous for ERT in LSDs characterized by low M6PR expression or impaired clathrin-mediated endocytosis.

8.3. In vivo biodistribution of nanoliposomes and EVs

Glycosylation of lysosomal enzymes can promote accumulation in M6PR-rich tissues such as the liver, thymus, heart and kidneys (619,620), resulting in rapid clearance from circulation. In this thesis, encapsulation of the GLA was proposed as a potential strategy to address these limitations. This approach enhanced cellular uptake through M6PR-independent pathways and improved the enzyme's *in vivo* BD by increasing its circulation time and bioavailability, likely by reducing recognition by M6PR-expressing tissues and cells. Additionally, several factors are key in determining the biodistribution (BD) of nanoliposomes and EVs.

In the case of nanoliposomes, factors such as nanoparticle size, lipid composition, surface charge and modifications, the composition of the protein corona (PC), and the route of administration are all critical in governing their BD (621).

Small nanoliposomes (50–100 nm) tend to have longer circulation times and can more easily penetrate tissues, whereas larger liposomes (>200 nm) are more likely to be taken up by the liver and spleen (621). The lipid composition and surface charge of nanoliposomes also affects their interaction with biological membranes and proteins. Specifically, cationic nanoliposomes, like those used in this thesis, can interact more readily with negatively charged cell membranes, enhancing cellular uptake (621). Furthermore, surface modifications—such as PEGylation or the incorporation of targeting molecules—can help nanoliposomes evade the immune system, prolong circulation time, and improve biodistribution (621). The PC also plays a key role in the BD of nanoliposomes, which will be discussed in a subsequent section.

Similar factors influence the biodistribution of EVs, such as vesicle size, membrane composition and modifications, and the route of administration. As in the case of liposomes, smaller EVs, like exosomes (30–150 nm), tend to circulate longer and penetrate tissues more effectively than larger microvesicle (622) and intravenous administration often results in EV accumulation in highly vascularized organs such as the liver, lungs, spleen, and kidneys (622). The lipid and protein composition on the EV surface also influences their interactions with cells and tissues. Importantly, surface proteins such as CD9, CD63, and CD81 can affect EV uptake and targeting by different cell types (623). Moreover, modifying the EV surface with molecules like PEG can help them evade immune detection, thereby prolonging circulation time and improving biodistribution (623). Notably, the cellular source of EVs (e.g., mesenchymal stem cells, cancer cells) can influence both their biodistribution and therapeutic potential. EVs derived from different cell types may exhibit unique surface markers and cargo, affecting their interactions with target cells (622).

8.3.1. PC composition as a key factor affecting BD of nanoparticles

The composition of the PC can significantly alter the BD of otherwise similar nanoparticles (321,404,414). In the specific case of liposomes, proteins enriched in the PC include fibrinogen chains (Fga, Fgb and Fgg), albumin, apolipoproteins (Apoa1, Apoe, Apob, Apoc3, Apoc1, Apoa4 and Clu), complement factors (C3), immunoglobins (Ighg3) and others (Mug1, Thbs1, Hbb-bs, Chd1, Hba-a1, Tf, Serpina3k, Hpx, Ttr). As previously detailed in section 6, this PC composition is similar to other liposomes reported by other authors (322,410,417,418). Some of these proteins found in the nanoliposomal PC are well-known opsonins, such as Fg, C3 and Ighg3 (F) (624), or

dysopsonins, like Alb and Apos (395). In this thesis, we found that some of these proteins vary in their relative abundance in the PC due to the presence of rh-GLA or RGD on the liposomal surface, which could explain some of the results observed in the BD assay.

Presence of rh-GLA increased dysopsonins such as Alb, Apoe, Apoa1, Apoc3, Apoc1 and Apoa4 in the nanoliposomal PC. In contrast, it also decreased the abundance of Clu, a well-known dysopsonin, associated with the "stealth" ability of the NP (395). The presence of RGD increased the abundance of Alb and Apoa1, but also enhanced the presence of C3 and Ighg3. This increased presence of C3, Apoa1 and Ighg3 due to RGD could explain the higher retention of targeted nanoliposomes in the spleen and liver, as reported by other authors using other nanodrugs (321). This higher tissue-retention may explain the lower plasma and brain EA of targeted nanoGLA compared to nanoGLA without RGD, as observed in the BD assay from section 5 in this Thesis.

The presence of RGD seems to have more impact on increasing the abundance of complement factor proteins in the PC compared to the presence of rh-GLA. These results may be explained by the increased presence of certain dysopsonins in the PC due to rh-GLA, which may prevent the binding of Igs and complement factors to the nanoliposome, such as Apos and Alb (398,624,625). This suggests a reduced presence of anti-liposome antibodies in nanoGLA compared to empty liposomes. However, further experiments, such as determining total IgG and IgM levels by ELISA, are necessary to confirm this hypothesis.

Furthermore, the increased presence of IgG observed in the PC of nanoliposomes, associated with both RGD and rh-GLA, along with complement factors such as C3 and C5, could contribute to the nanoliposomal retention in liver and spleen (321). All these results may also explain the higher presence of ADAs observed in plasma from KO mice treated with nanoGLA-3%RGD, compared to free enzyme.

Unfortunately, parallel characterization of the PC composition in EV-GLA could not be performed, and no information is currently available in the literature regarding PC in EVs derived from CHO or HEK cells that would allow comparison with the PC composition we characterized in nanoliposomes. Moreover, compared to synthetic NPs, PC characterization in EVs is a challenging process due to protein contamination during EV isolation, EV heterogeneity in size and component (626), and chemical composition variations in EVs depending on their cell sources (627,628). In experiments carried out by other research groups, EVs derived from cancer cells exhibited unexpected tissue distribution after being incubated with plasma, showing low accumulation in the target sites, which indicates an effect of PC formation (629–631). Tóth and colleagues reported that certain proteins from human plasma, including C3, C4B, ApoA1, ApoB, ApoC3, ApoE, Fga, Ig heavy chains of γ2 and γ4 are common proteins found in the PC of EVs from THP1 cells (631). Despite the presence of several opsonins in PC of EVs, the authors did not observe any phagocytic activity from monocytes and neutrophils against EVs with PC. One possible explanation for this is the presence of immune-evading mechanisms on the EV surface, which promote their tolerability and prolonged circulation time (632). Interestingly, some of these proteins, but of mouse, including C3, C4b, Apoa1, Apob, Apoc3, Apoe and Fga are found in the PC of our nanoliposomes, suggesting that the PC of EVs and nanoliposomes could have similar compositions. However, this needs to be studied in detail. EVs exhibits higher intrinsic heterogeneity in size and composition compared to nanoliposomes and this heterogeneity can complicate the characterization of their PC. A single sample of EVs may contain subpopulations with distinct protein corona compositions, making it challenging to draw clear conclusions. Overall, this thesis paves the way for future experiments with EV-GLA, which could provide

valuable insights into the composition of PC in EVs from CHO and HEK cells. It also explores how factors such as the cell source, EV isolation methodology (Pp, BF + SEC and TFF + SEC), and the presence or absence of a targeting moiety (rF7) may influence PC composition, following a similar approach to that reported by Tóth and colleagues using EVs derived from THP1 cells (631).

In summary, the presence of rh-GLA on the nanoliposomal surface increases the adsorption of dysopsonins, such as albumin and apolipoproteins, in the protein corona (PC) of nanoliposomes. In contrast, RGD enhances the presence of opsonins, such as C3 and Ighg3. This differential PC composition may explain the increased retention of RGD-targeted nanoliposomes in the liver and spleen of KO Fabry mice after 30 min post-administration. These findings underscore the importance of understanding PC composition for optimizing the design and functionality of targeted nanoliposomes in biomedical applications.

8.4. Targeting strategies in nanoliposomes and EVs

In this thesis, we investigated two different targeted nanocarriers with two distinct targeting strategies: RGD-targeted nanoliposomes and F7-targeted EVs. Both targeted systems exhibited improved and faster cellular uptake in endothelial cells, as well as better *in vitro* efficacy, compared to their non-targeted counterparts and the respective free enzymes. This highlights the importance of incorporating targeting modifications into the surfaces of nanoparticles. Targeting strategies are critical for improving the therapeutic outcomes of nanoparticles by reducing side effects of therapeutical molecules, avoiding unspecific BD and improving drug delivery to target cells and tissues (633–638).

8.4.1. Targeted liposomes to improve therapies in different diseases

In liposomal formulations, different targeting approaches have been explored, including the use of antibodies, folate, aptamers or short peptide sequences.

The incorporation of specific antibody regions, such as fragment-antigen-binding (Fab), to the liposomal surface has shown advantages, such as high specificity of the therapy and improved pharmacokinetics (639–642). There are several examples of antibody-targeted liposomes that are currently in preclinical stages (643) and phase II clinical trials (NCT02833766) to treat breast cancer, as well as some examples of patented liposomes (644,645) However, the presence of these antibody regions can increase the immunogenicity of the liposome (634), effects that could hamper the clinical implementation of antibody-functionalized liposomes.

Many liposomes have been functionalized with folate, also called vitamin B9. This strategy has been applied in preclinical studies to different cancers (646,647). Folate is critical for the methylation of DNA and RNA (648), and due to the increased DNA synthesis in tumor cells necessary for their proliferation, they overexpress folate receptors (649). Several authors have observed a significantly increased cellular uptake and specificity of these targeted liposomes *in vitro* (650–652). However, other studies reported *in vivo* limitations of folate-targeted liposomes, such as reduced circulation time after i.v. administration and inefficient drug delivery to the tumor compared to non-targeted liposomes (651,653–655). These limitations may be due to variability in folate receptor expression or competition with circulating free folate for receptor binding, which can reduce the efficiency of the targeted liposomes.

Aptamers have been also used for liposome functionalization. They are single-stranded sequences of structured RNA or DNA that can interact with binding sites on a wide range of molecules, similar to antibodies (656). They have shown high versatility, low cost, scalable production, and low immunogenicity (657). Conjugating liposomes with aptamers has been explored in a wide range of therapeutic targets, including cancer cells (658–661), corneal cells (662), muscle tissue (663), and intestinal epithelium (664). However, aptamer-targeted liposomes are still far from FDA approval, as designing and optimizing aptamers for specific targets is a complex, time-consuming and expensive process, and there are concerns about potential side effects and immune responses to aptamers, which need to be thoroughly investigated (665,666).

Finally, peptides as targeting moiety exhibit higher specificity, bioactivity, and are less costly to develop (667). Several peptide-targeted liposomes have been already patented as drug delivery systems (668,669), while others still in preclinical stages (670). The RGD-targeted nanoliposomes explored in this thesis are an example of liposomal nanocarriers that utilize peptide-targeting strategies.

The RGD peptide (Arg-Gly-Asp) is one of the most commonly used peptides for targeting liposomes due to its high affinity for integrin receptors, particularly αvβ3 integrins, which are overexpressed in tumor cells and in endothelial cells of angiogenic blood vessels. Its relatively easy synthesis also makes it a popular choice for targeted drug delivery (671,672).

Selecting the optimal type of RGD (e.g., cyclic or linear, and the number of amino acids) is crucial for effective nanoparticle targeting. Cyclic RGD peptides generally exhibit higher binding affinity and stability than linear RGD peptides due to their constrained structure. In contrast, linear RGD peptides are easier to synthesize but may be less stable and have lower binding affinity (673). Additionally, modifications in amino acid number (674,675) and structural changes such as PEGylation or substitution of aspartate with other residues (e.g., lysine) (676,677) can enhance the peptide's stability, binding affinity, and overall efficacy. For these reasons, in this thesis, we selected a cyclic RGD peptide with a substitution of aspartate (D) by lysine (K)—specifically the c(RGDyK) cyclic targeting peptide—to improve GLA delivery to endothelial cells, which are among the primary affected cells in Fabry disease (FD) (678,679).

RGD-targeted liposomes have been used for other researchers to improve cancer therapies (670) and have shown higher internalization and efficacy *in vitro* in tumor cells, as well as better efficacy and bioavailability *in vivo* compared to untargeted liposomes and free drug (680,681). This demonstrates the high versatility of the RGD liposomal targeting strategy, as it can be used for the treatment of diseases such as cancer, in addition to LSDs. However, there are considerations for peptide-targeting strategy, such as optimizing procedures to quantify the density of peptides on the liposomal surface to avoid batch-to-batch variation (682). Moreover, a high density of peptides conjugated to the liposomes could lead to aggregation and subsequent clearance from circulation (683).

In our hands, RGD-targeted nanoGLA demonstrated better internalization in endothelial cells compared to non-targeted nanoGLA after short incubation periods, and this cellular uptake was faster with higher percentages of RGD. However, in terms of *in vitro* efficacy with longer times of incubation, a high density of RGD did not correlate with increased clearance of Gb3. This suggests that there is an optimal concentration of the targeting molecule required to achieve the best *in vitro* results. Beyond this optimal point, further increases in the density of the targeting moiety, such as the RGD peptide, may not significantly enhance targeting and could

potentially lead to issues such as receptor saturation, increased clearance by the immune system, or compromised stability and functionality of the nanoparticles or their cargo (684). The *in vivo* effect of RGD targeting in nanoliposomal BD will be discussed in a subsequent section.

Some authors have described the use of peptide-targeted liposomes to improve ERT in LSDs. For example, Thekkedath et al. (246) developed lysosomotropic octadecylrhodamine B (RhB)-targeted liposomes loaded with GBA to improve ERT in GD by enhancing the delivery of glucocerebrosidase-loaded liposomes to the lysosome of Gaucher fibroblasts and macrophages (246). Hayashi et al. (251) also developed peptide-targeted liposomes loaded with GLA to treat FD. These liposomes were functionalized with a lineal chain of 16 histidines (H16), which is known to act as a cell-penetrating peptide (685). *In vitro* studies showed that H16-targeted liposomes loaded with GLA were internalized by an in-house GLA-KO cell line (251). These authors used the proliferation capacity of these KO cells as a readout of liposomal efficacy and gave no insight on the Gb3 levels or the EA of the liposomes, making difficult to direct comparison of H16-targeted liposomes with the RGD-targeted nanoliposomes used in this thesis. Previous studies by our group demonstrated that MAEC KO cells also exhibited a lower proliferation rate compared to MAEC WT cells. Therefore, additional *in vitro* efficacy studies focusing on their proliferative capacity could be conducted in the future.

Taking all this information into account, targeting liposomes represented a versatile and powerful strategy to increase the specificity and improve drug delivery to target cells in various diseases, such as cancer and LSDs. It is crucial to identify the optimal targeting strategy for each disease or condition, as well as the ideal density and concentration of the targeting moiety to load onto the liposomal surface. This ensures both stability and efficacy, since a higher density of the targeting moiety may not necessarily correlate with enhanced treatment efficacy, as we have observed with RGD-nanoliposomes.

8.4.2. Targeted EVs to improve therapies in different diseases

EVs are involved in several processes like tissue repair, immune response and inflammatory resolution, as they are crucial for inter-cellular communication. They showed therapeutic potential for diseases from different origin, such as cardiovascular, neurodegenerative, metabolic, autoimmune and renal pathologies (686,687). Although EVs can be naturally targeted to specific cells and tissues depending on their cellular source (477,688,689), they can also be engineered modified to incorporate targeting moieties in their surface. Some of these targeting strategies include chemical modification, lipid insertion, metabolic labeling, enzymatic ligation, affinity binding and genetic engineering of the donor cells (633,687). A few of these methods will now be discussed in detail due to their relevance to the targeting approaches used in this thesis.

Chemical modification of EVs involves targeting reactive groups on the lipid or protein membranes, such as amino, thiol, and carboxyl groups, which undergo biorthogonal reactions with peptides tagged with reactive fragments. The most common method combines EDC/NHS coupling and azide-alkyne cycloaddition (click chemistry) to modify EVs, as demonstrated by Tian et al. (690) with curcumin-loaded MSC-EVs modified with the c(RGDyK) peptide for targeting ischemic brain lesions in a mouse model (691). This opens up the possibility for future experiments targeting our EV-GLA using the same targeting moiety as nanoGLA, enabling a more precise comparison between the two nanocarriers. Chemical modification for inserting targeting moieties is more robust than lipid insertion or affinity binding; however, it offers lower specificity and may alter EV properties.

Lipid insertion targeting strategy consists in the addition of targeting molecules (i.e. peptides or aptamers) tagged with a lipid fragment, which is inserted into the EV membrane. This method stands out from other modification techniques due to its simplicity, low cost, high efficiency, and ability to be applied to nearly all EV types without compromising their structure (633). Wang et al. (692) targeted EVs with RGD through 1,2-Distearoyl-sn-glycero-3-phosphoethanolamine-Polyethyleneglycol (DSPE-PEG), showing increased EVs arrival to the blood vessels. Other researchers reported the successful use of lipid insertion for targeted drug delivery in EVs, including treatments for lung cancer (693), glioblastoma (694), and Alzheimer's disease (695). Lipids like DSPE-PEG (692), DOPE-PEG (695), and cholesterol (696,697) are commonly used for surface modification, enhancing the targeted delivery of therapeutic agents, and improving outcomes while minimizing side effects in various cancer models and other diseases (633). Interestingly, Wan et al. (698) found that cholesterol-PEG exhibited the highest labeling efficiency in EVs derived from mouse dendritic cells, compared to other lipids such as DSPE-PEG and FITC-tagged stearoyl-PEG (C18-PEG), when targeting these EVs with the AS1411 aptamer. Therefore, this loading strategy could be applied in future experiments to load Chol-PEG400-RGD onto EV-GLA, allowing for a direct comparison with RGD-targeted nanoGLA—both of which are used in this thesis—through *in vitro* and *in vivo* studies.

Genetically engineered donor cells can modify the surface of EVs with targeting moieties by fusing peptides or proteins to membrane or lipid-binding proteins. These targeting moieties are then displayed on the surface of EVs, enabling targeted delivery. Key membrane proteins commonly used for this purpose include Lamp2b, tetraspanins (CD63, CD81, CD9), PDGFR, syntenin-1, PTGFRN, and CXCR4 (486). Lamp2b is the most frequently used protein for decorating EVs with targeting moieties. It was first applied in the creation of Lamp2b-RVG-exosomes, which were equipped with the neurotargeting peptide rabies virus glycoprotein (RVG) to deliver BACE 1 siRNA for Alzheimer's treatment (183). Since then, Lamp2b has been widely used for the targeted delivery of various molecules such as siRNA, miRNA, mRNA, circRNA, and aptamers to the brain for the treatment of neurological diseases (604,605,699–704). For instance, Lamp2b-RVG exosomes were used to deliver circDYM to treat Major Depressive Disorder (MDD) in mice, showing improved delivery to the brain. Additionally, Lamp2b has been employed to display other targeting peptides, such as T7, E7, and RGD on exosomes for cancer therapy (603,607,705–709).

Gečys et al. (709) reported the production of engineered RGD-targeted EVs from HEK 293FT through the stable expression of Lamp2b-iRGD-HA fusion protein. The targeted EVs were then isolated by precipitation and exogenously loaded with doxorubicin hydrochloride (DOX) and siRNA against glyceraldehyde 3-phosphate dehydrogenase (GAPDH) gene via electroporation, for the treatment of glioblastoma. *In vitro* results showed that RGD-EVs exhibited higher internalization and efficacy compared to empty EVs in glioblastoma cell models. Notably, this approach enabled the stable production of Lamp2b-RGD-targeted EVs in HEK cells, which could be directly applicable to our EV-GLA produced in both CHO and HEK cells. This strategy could be valuable for future experiments, where we aim to compare the efficiency of stable versus transient expression of both targeting moieties (RGD and F7) in terms of cellular internalization and efficacy.

Affibodies (small proteins with high affinity for specific targets) can also be displayed on exosomes by fusing them with Lamp2b, such as in the case of Her2-affibody-exosomes, which deliver chemotherapeutic agents and reverse drug resistance in cancer cells (710,711). Besides Lamp2b, tetraspanins like CD63, CD81, and CD9 are used to modify EVs, with these proteins

facilitating the incorporation of targeting peptides. These proteins can be fused with other molecules, such as Apo-A1 or ApoB, to direct EVs to specific cells or promote brain penetration (712). Other proteins, like PDGFR, PTGFRN, and CXCR4, also enable targeted delivery, particularly for cancer therapies (713–715) or immune modulation (716). For example, CXCR4-rich EVs can deliver therapeutic agents to treat brain metastases in breast cancer (717).

Overall, Lamp2b has emerged as a key player in modifying exosomes for targeted delivery, providing a versatile and effective platform for the development of engineered EVs for precision therapies. In this thesis, the F7 cell penetrating peptide was fused to Lamp2b membrane protein, enabling the incorporation of this targeting moiety to the EV-GLAH6 surface via genetic modification of HEK 293F and improved their cellular uptake. However, it is crucial to control the expression level of F7 and to quantify which EV subpopulations incorporate higher amounts of F7, due to the high intrinsic heterogeneity among EV subpopulations. Each vesicle may contain vastly different concentrations of membrane proteins (171), including Lamp2b, which can significantly affect the interpretation of *in vitro* results. To address these issues, the overexpression of Lamp2b-F7 fusion protein can be detected by WB through the detection of Lamp2b and compared to EVs without overexpression, as previously described by other authors (183,709). However, characterizing the EVs subpopulations with higher or lower levels of Lamp2b-F7 can be more challenging. One strategy is to modify the fusion protein by adding a purification tag, such as His-tag, to enable immunoaffinity purification of EVs with the highest expression of Lamp2b-F7. Another strategy is to use single-particle immunofluorescence-based characterization techniques, such as nanoscale flow cytometry (FCM) (718) and ExoView (719), to characterize the expression of Lamp2b in the EV samples.

The F7 targeting strategy improved the cellular uptake of EV-GLAH6 and enhanced their in vitro efficacy in MAEC KO cells. These findings are consistent with ongoing studies by our group, which have shown increased internalization of other types of nanoparticles (NPs) functionalized with the F7 peptide—such as polymeric micelles and solid lipid nanoparticles (SLNs)—even enhancing their ability to cross the blood–brain barrier (BBB) in *in vitro* models (594).

As observed with nanoliposomes, targeting EVs represented a versatile and promising strategy to increase specificity and improve drug delivery in various diseases. However, unlike nanoliposomes, the targeting process in EVs is more complex, as it involves methodologies that could compromise the integrity of the EV. Genetic modification of donor cells appears to be the best approach for obtaining modified and targeted EVs while preserving their biological properties and structural integrity.

8.4.3. Targeted nanoliposomes for improved GLA biodistribution

An enhanced *in vitro* internalization and efficacy does not necessarily correlate with better results *in vivo*. In fact, this is the case with some folate- or antibody fragment-targeted liposomes (634). Therefore, it is crucial to validate the advantages of targeted nanoparticles both *in vitro* and *in vivo*, using the non-targeted system as a counterpart. In this thesis, we have analyzed the BD of RGD-targeted nanoliposomes loaded with GLA in Fabry KO mice to validate whether the presence of RGD improves GLA delivery to target tissues in FD, such as kidneys, heart and brain.

The results in this thesis show that, after 30 min post-administration, nanoliposomes in blood preserve better the EA of the GLA compared to the free enzyme, in accordance with previous findings (200). Other authors using different liposomes and enzymes have also reported similar

results, showing that liposome increase the circulation time and bioavailability of enzymes (151,720,721), .

Furthermore, high densities of RGD on the liposomal surface had an impact in nanoGLA BD, enhancing its delivery to tissues such as the kidneys and heart, but also in liver and spleen. This higher retention of liposomes in the liver and spleen is a common observation when NPs are administered intravenously (722). However, our results suggested a relevant role of the RGD in the nanoliposomal retention in the spleen, suggesting a recognition of RGD-targeted nanoliposomes by the immune system. This was also observed by other authors using other RGD-targeted liposomes (299,723). In fact, several studies by other authors have reported the immunogenicity of the RGD in other NPs (302,303,431). This was supported by the results of this thesis in the characterization of the PC in the different nanoliposomal formulations, in which an increased relative abundance of complement factors such as C3 and immunoglobulins such as IgG was observed in the PC due to the presence of RGD. Taken together, these results suggest that a high RGD density in nanoliposomes may act as a double-edged sword: while potentially beneficial in BD, its *in vivo* efficacy could be limited due to increased immune system recognition, promoting nanoliposome retention in the spleen and accelerating nanoparticle clearance from circulation. This could be particularly critical following repeated administrations, where potential side effects—such as complement activation-related pseudoallergy (CARPA) syndrome—might occur, possibly requiring immunomodulators after nanoliposomal infusions. Consequently, the most suitable nanoliposomal system for future *in vivo* experiments appears to be nanoGLA-3%RGD, as supported by previous studies (200) and its granted Orphan Drug Designation (ODD) (272). This nanoformulation retains the targeting benefits of RGD with only 3% of density of the targeting moiety.

Surprisingly, no effect of RGD was observed on brain delivery, despite some authors reported high RGD-targeted nanoparticles delivery in the brain, including micelles (724,725) and other liposomes with different membrane composition (726). These discrepancies in BD may be due variations in their PC composition, which varies depending on the surface properties of the nanoparticles (332). This aspect will be discussed further below.

Compared to EVs, the other DDS explored in this thesis, other authors have reported that both liposomes and EVs show similar BD after being administered intravenously (188,189). After 30 min post-administration, most of the EVs are retained mainly in the liver, followed by the spleen, kidneys, and lungs (191,192). In fact, in previous *in vivo* experiments conducted by our group using EV-GLAcmycH6 isolated by precipitation, high retention of EVs was observed in liver and spleen 1 h after i.v. administration (132), demonstrating similarities with nanoliposomal BD. However, EV-GLAcmycH6 was able to deliver EA into Fabry target organs, such as kidney, more efficiently than free GLA enzyme, without the need of a targeting moiety (132). This is a significant advantage compared to nanoliposomes, which require a targeting moiety, such as RGD, to deliver higher levels of EA than the free enzyme. However, this superiority of EVs over nanoliposomes needs to be confirmed through additional *in vivo* experiments using EV-GLA from other cell sources (e.g. HEK 293F) and other isolation methodologies (BF + SEC and TFF + SEC) that reduce the potential contamination of EV-GLA samples with soluble GLA associated with precipitation procedures (727). These experiments are currently ongoing.

Overall, the results of this thesis showed that targeting nanoliposomes and EVs with RGD and F7, respectively, improved their *in vitro* performance—such as internalization into endothelial cells and Gb3 clearance in MAEC KO cells—compared to their non-targeted counterparts. However, the role of the targeting peptide *in vivo* has only been evaluated for nanoliposomes.

In this case, nanoliposomes increased EA levels in the plasma of Fabry KO mice 30 minutes post-administration, regardless of the presence of RGD. The presence of RGD on the surface of nanoGLA enhanced EA in Fabry target tissues, including the kidney and heart, but also led to retention of the nanoliposomes in the liver and spleen. No effect of RGD was observed in the brain. This may be due to the influence of RGD on the composition of the PC.

8.5. Scaled production and clinical translation of nanoliposomes and EVs

EVs and liposomes are both being explored for therapeutic purposes, but they face distinct challenges in their clinical translation. EVs, naturally occurring nanoparticles produced by cells, have garnered attention for their ability to mediate intercellular communication and carry RNA species, such as microRNAs, which can regulate target genes (728). However, despite their promising potential, EVs have not yet been approved by the FDA or EMA for therapeutic use, although over 100 EV-based products are in clinical trials (729). In contrast, liposomes have been in clinical use since 1993, with multiple liposomal-based drugs already approved by the US FDA and EMA (730–733). Liposomes are well-established in drug delivery, especially in encapsulating molecules like doxorubicin (e.g., in Doxil®) (731). The clinical success of liposomes reflects the ability of pharmaceutical manufacturers to address challenges in manufacturing, drug loading, and delivery.

In terms of **manufacturing**, production of therapeutic EVs is far more complex than producing therapeutic liposomes. EVs must be isolated, characterized, and purified, and these processes are less standardized compared to liposome production, which benefits from established techniques (732). Large-scale production of EVs faces challenges in achieving high yields, as multiple purification steps can lead to significant loss of material. As discussed in previous sections, to address these issues, this thesis explored the production of EV-GLA obtained from different cell factories and using 3 different isolation methodologies (Pp, BF + SEC and TFF + SEC) to enhance the EV-GLA yield with high concentration of GLA and optimal EA and *in vitro* efficacy. Results of this thesis demonstrated that BF + SEC and TFF + SEC offered significant advantages over Pp in terms of EV concentration, *in vitro* efficacy, and purity. Although Pp yielded higher quantities of GLA protein, this likely reflects co-precipitation of free, non-encapsulated enzyme, a phenomenon previously reported to confound EV analysis and therapeutic assessment (169,534,734). Therefore, more specific and selective purification methods, such as SEC-based protocols, are essential to ensure accurate characterization and consistent biological effects. When comparing the two EV variants, EV-GLAcmycH6 showed greater EA and better in vitro efficacy but lower producton yield. These results highlight the critical importance of both the cellular source and isolation methodology in determining the functional quality of therapeutic EVs. Furthermore, in the case of EVs, despite their favorable properties, often face challenges with drug loading efficiency (168).

Encapsulation efficiency is also a key consideration for both nanoliposomes and EVs for clinical translation. In terms of loading capacity, nanoliposomes generally exhibit higher encapsulation efficiency compared to EVs (735,736). For liposomes, factors influencing drug loading include the nature of the drug (e.g., hydrophilic or hydrophobic), the drug-to-lipid ratio, the preparation method, and the liposomal composition and size (737). In our case, we modified the nanoliposomal surface with the cationic surfactant MKC to enhance GLA loading, due to the enzyme's negative net charge in the aqueous phase during the DELOS-susp procedure. This improvement in GLA encapsulation efficiency with MKC was previously reported by Tomsen-

Melero et al. (227). Notably, MKC is also present in several approved therapeutic products, including Celestone®, Soluspan®, and Lorazepam® (738). Given the high doses of therapeutic molecules—such as recombinant lysosomal enzymes—required for clinical applications, strategies to enhance their encapsulation efficiency in nanoliposomes are essential for future clinical implementation. Regarding protein loading, EVs typically suffer from lower loading efficiency and capacity compared to liposomes, making it harder to deliver sufficient therapeutic doses (732). Thus, strategies to improve enzymatic loading to reach clinical dosages, such as co-expression of the lysosomal enzyme with EV proteins (e.g. Alix, TSG101, Lamp2, CD9 or CD63) (183,486–488) or by exogenous loading methods (e.g. saponification, electroporation, etc.) (173,480–482), are necessary to advance their clinical translation. Although engineered EVs and new drug loading techniques are being explored, liposomes offer a more straightforward solution to drug encapsulation.

Unfortunately, the nanoliposomes used in this thesis were not quantified by NTA, which prevented a direct comparison between nanoGLA and EV-GLA in terms of GLA loading to assess their enzyme encapsulation efficiency. However, this comparison can be approached by referencing other studies in the literature that utilized different nanoGLA formulations (227). For example, the study by Tomsen-Melero et al. reported a theoretical ratio of 11.4 molecules of GLA per vesicle.

In contrast, using the same calculation method as in reference (227), the EV-GLAH6 samples isolated in this thesis demonstrated higher theoretical ratios of GLA molecules per vesicle. Specifically, EV-GLAH6 isolated via BF + SEC and TFF + SEC showed ratios of 265 and 200 GLA molecules per vesicle, respectively. Conversely, EV-GLAcmycH6 displayed a wide range depending on the isolation method: 846.5 GLA molecules/vesicle for Pp, 8.3 for BF + SEC, and 2.38 for TFF + SEC.

These findings suggest that both the cellular source and the isolation methodology significantly influence GLA loading, likely due to differences in the cells' capacity to encapsulate the GLA enzyme and the presence of soluble GLA in certain EV samples, particularly those isolated by Pp. This supports the notion that EVs may outperform nanoliposomes in terms of GLA loading capacity. Nonetheless, further comparative studies involving the specific nanoliposomes used in this thesis are needed to validate this hypothesis.

From a **pharmacological perspective**, EVs show slower clearance from circulation compared to liposomes, primarily due to their natural biocompatibility and ability to evade the immune system (739). Strategies such as PEGylation have been effective for liposomes to increase blood circulation, and similar approaches are currently being investigated for EVs (740). Additionally, liposomes can be easily modified to incorporate targeting moieties in their surface (741,742), but EVs required of more complex procedures such as genetic modifications of the cell source or other procedures that could compromise the EV integrity.

In summary, while both EVs and liposomes show promise in drug delivery, liposomes are further along in clinical translation, particularly due to established production methods and better drug loading capabilities. EVs, on the other hand, face more complex manufacturing and regulatory challenges due to their heterogeneity in size and composition, but offer other advantages compared to liposomes such biocompatibility and an enhanced ability to evade the immune system (188,189,193) and intrinsic tissue-specific targeting capabilities based on their producer cell origin (633,687).

9. General conclusions

From the work carried out in this PhD thesis, the following conclusions can be withdrawn:

1. Encapsulation of the α-galactosidase A (GLA) in DPPC:Chol:MKC nanoliposomes (named nanoGLA), slightly reduces its enzymatic activity (EA). The incorporation of Chol-PEG400-c(RGDfk) (RGD) does not affect the EA and the final formulation is stable up to 2 weeks post-production.
2. RGD-functionalized nanoliposomes exhibit enhanced endothelial cell uptake, with higher RGD densities (6% vs. 3%) accelerating internalization. However, these differences diminish over longer incubation periods. The RGD-mediated internalization advantage persists even in the presence of the protein corona (PC). Both nanoGLA-0%RGD and nanoGLA-3%RGD are able to enter cells through M6PR-independent pathways.
3. *In vitro*, RGD-functionalized nanoGLA is more effective at reducing Gb3 accumulation in endothelial cells compared to non-targeted nanoliposomes.
4. *In vivo*, RGD-targeted nanoGLA enhances EA in Fabry target tissues including kidney and heart, 30 min post-intravenous administration. All nanoGLA formulations are able to increase the EA in plasma and deliver EA to the brain, independently of RGD presence.
5. Repeated administrations of nanoGLA-3%RD induces the expression of anti-drug antibodies (ADAs) in Fabry KO mice, to a higher extent than agalsidase alfa (Agal. A).
6. PC formation in nanoliposomes, as monitored by DLS, occurs rapidly (within 30 min), and is maintained stable over time, irrespective of RGD or GLA presence. The majority of proteins forming the PC in the different nanoGLA formulations are small proteins (< 60 kDa) and negatively charged in plasma (IEP < 7.5). The incorporation of rh-GLA increase the presence of dysopsonins, such as albumin and apolipoproteins, in the PC of nanoliposomes. The incorporation of RGD increases the presence of opsonins such as C3 and Ighg3. This differential PC composition might explain the higher retention of RGD-targeted nanoliposomes in liver and spleen of KO Fabry mice.
7. The quantity and activity of GLA encapsulated in extracellular vesicles (EVs) varies with the GLA construct (GLAcmycH6 or GLAH6) and the cell source (CHO DG44 or HEK 293F) used. EVs loaded with GLA (EV-GLA) produced in HEK 293 cells (EV-GLAH6) exhibits higher quantity of GLA per EV compared to EV-GLA produced in CHO DG44 cells (EV-GLAcmycH6), but with lower crude EA.
8. EV-GLA show higher *in vitro* efficacy compared to free enzyme, regardless of the isolation method and the cell source. Bench-top filtration (BF) with size exclusion chromatography (SEC) and tangential flow filtration (TFF) with SEC outperformed precipitation (Pp) in terms of EV yield and *in vitro* efficacy of GLA. Variability in EV isolation was observed between batches, influencing EV concentration, GLA concentration, EA, and *in vitro* efficacy. Therefore, further investigation is required to optimize the isolation method, cell source, and GLA construct to isolate EV-GLA with the highest quality in terms of GLA content and functionality.
9. Targeting EV-GLAH6 with recombinant F7 (rF7) enhanced its uptake by endothelial cells and improved its *in vitro* efficacy, although incorporation of rF7 through co-transfection of HEK 293F cells, reduces the loading of GLAH6 into the EVs.

Based on these global conclusions, this PhD. thesis has contributed to the optimization of drug delivery systems to improve ERT strategies that enhance enzyme delivery, stability, and efficacy in Fabry disease, with broader implications for other LSDs.

10. References

1. Nair V, Belanger EC, Veinot JP. Lysosomal storage disorders affecting the heart: a review. Cardiovasc Pathol. 2019;39:12–24.

2. Ratko TA, Marbella A, Godfrey S, Aronson N. Enzyme-Replacement Therapies for Lysosomal Storage Diseases [Internet]. Rockville (MD): Agency for Healthcare Research and Quality (US); 2013 [cited 2025 Feb 8]. (AHRQ Comparative Effectiveness Technical Briefs). Available from: http://www.ncbi.nlm.nih.gov/books/NBK117219/

3. Gros F, Muller S. The role of lysosomes in metabolic and autoimmune diseases. Nat Rev Nephrol. 2023 Jun;19(6):366–83.

4. Ballabio A, Bonifacino JS. Lysosomes as dynamic regulators of cell and organismal homeostasis. Nat Rev Mol Cell Biol. 2020 Feb;21(2):101–18.

5. Zhang Z, Yue P, Lu T, Wang Y, Wei Y, Wei X. Role of lysosomes in physiological activities, diseases, and therapy. Journal of Hematology & Oncology. 2021 May 14;14(1):79.

6. Scerra G, De Pasquale V, Scarcella M, Caporaso MG, Pavone LM, D'Agostino M. Lysosomal positioning diseases: beyond substrate storage. Open Biol. 12(10):220155.

7. Ioannou YA, Zeidner KM, Grace ME, Desnick RJ. Human alpha-galactosidase A: glycosylation site 3 is essential for enzyme solubility. Biochem J. 1998 Jun 15;332 (Pt 3)(Pt 3):789–97.

8. Böhm E, Seyfried BK, Dockal M, Graninger M, Hasslacher M, Neurath M, et al. Differences in N-glycosylation of recombinant human coagulation factor VII derived from BHK, CHO, and HEK293 cells. BMC Biotechnol. 2015 Sep 18;15:87.

9. Zaborowski MP, Balaj L, Breakefield XO, Lai CP. Extracellular Vesicles: Composition, Biological Relevance, and Methods of Study. Bioscience. 2015 Aug 1;65(8):783–97.

10. Tomsen-Melero J, Merlo-Mas J, Carreño A, Sala S, Córdoba A, Veciana J, et al. Liposomal formulations for treating lysosomal storage disorders. Advanced Drug Delivery Reviews. 2022 Nov;190:114531.

11. Ferreira CR, Gahl WA. Lysosomal storage diseases. Transl Sci Rare Dis. 2017 May 25;2(1–2):1–71.

12. Coutinho MF, Prata MJ, Alves S. Mannose-6-phosphate pathway: a review on its role in lysosomal function and dysfunction. Mol Genet Metab. 2012 Apr;105(4):542–50.

13. Tomanin R, Zanetti A, Zaccariotto E, D'Avanzo F, Bellettato CM, Scarpa M. Gene therapy approaches for lysosomal storage disorders, a good model for the treatment of mendelian diseases. Acta Paediatr. 2012 Jul;101(7):692–701.

14. Platt FM. Emptying the stores: lysosomal diseases and therapeutic strategies. Nat Rev Drug Discov. 2018 Feb;17(2):133–50.

15. Parenti G, Andria G, Ballabio A. Lysosomal Storage Diseases: From Pathophysiology to Therapy. Annu Rev Med. 2015 Jan 14;66(Volume 66, 2015):471–86.

16. Marques ARA, Saftig P. Lysosomal storage disorders – challenges, concepts and avenues for therapy: beyond rare diseases. J Cell Sci. 2019 Jan 16;132(2):jcs221739.

17. Parenti G, Medina DL, Ballabio A. The rapidly evolving view of lysosomal storage diseases. EMBO Mol Med. 2021 Feb 5;13(2):e12836.

18. Wasserstein MP, Caggana M, Bailey SM, Desnick RJ, Edelmann L, Estrella L, et al. The New York Pilot Newborn Screening Program for Lysosomal Storage Diseases: Report of the First 65,000 Infants. Genet Med. 2019 Mar;21(3):631–40.

19. Chin SJ, Fuller M. Prevalence of lysosomal storage disorders in Australia from 2009 to 2020. Lancet Reg Health West Pac. 2022 Feb;19:100344.

20. Lerussi G, Villagrasa-Araya V, Moltó-Abad M, Del Toro M, Pintos-Morell G, Seras-Franzoso J, et al. Extracellular Vesicles as Tools for Crossing the Blood-Brain Barrier to Treat Lysosomal Storage Diseases. Life (Basel). 2025 Jan 9;15(1):70.

21. Ramaswami U, Whybra C, Parini R, Pintos-Morell G, Mehta A, Sunder-Plassmann G, et al. Clinical manifestations of Fabry disease in children: data from the Fabry Outcome Survey. Acta Paediatr. 2006 Jan;95(1):86–92.

22. Schiffmann R, Warnock DG, Banikazemi M, Bultas J, Linthorst L, Packman S, et al. Fabry disease: progression of nephropathy, and prevalence of cardiac and cerebrovascular events before enzyme replacement therapy. Nephrol Dial Transplant [Internet]. 2009 Jul [cited 2024 Oct 16];24(7). Available from: https://pubmed.ncbi.nlm.nih.gov/19218538/

23. Coutinho MF, Santos JI, Alves S. Less Is More: Substrate Reduction Therapy for Lysosomal Storage Disorders. Int J Mol Sci. 2016 Jul 4;17(7):1065.

24. Tan EY, Boelens JJ, Jones SA, Wynn RF. Hematopoietic Stem Cell Transplantation in Inborn Errors of Metabolism. Front Pediatr. 2019 Oct 25;7:433.

25. Whittington R, Goa KL. Alglucerase. A review of its therapeutic use in Gaucher's disease. Drugs. 1992 Jul;44(1):72–93.

26. Lachmann RH. Enzyme replacement therapy for lysosomal storage diseases. Curr Opin Pediatr. 2011 Dec;23(6):588–93.

27. Del Grosso A, Parlanti G, Mezzena R, Cecchini M. Current treatment options and novel nanotechnology-driven enzyme replacement strategies for lysosomal storage disorders. Adv Drug Deliv Rev. 2022 Sep;188:114464.

28. Pohl S, Marschner K, Storch S, Braulke T. Glycosylation- and phosphorylation-dependent intracellular transport of lysosomal hydrolases. 2009 Jul 1;390(7):521–7.

29. Abasolo I, Seras-Franzoso J, Moltó-Abad M, Díaz-Riascos V, Corchero JL, Pintos-Morell G, et al. Nanotechnology-based approaches for treating lysosomal storage disorders, a focus on Fabry disease. WIREs Nanomed Nanobiotechnol. 2021 May;13(3):e1684.

30. LeBowitz JH, Grubb JH, Maga JA, Schmiel DH, Vogler C, Sly WS. Glycosylation-independent targeting enhances enzyme delivery to lysosomes and decreases storage in mucopolysaccharidosis type VII mice. Proceedings of the National Academy of Sciences. 2004 Mar 2;101(9):3083–8.

31. Tekoah Y, Tzaban S, Kizhner T, Hainrichson M, Gantman A, Golembo M, et al. Glycosylation and functionality of recombinant β-glucocerebrosidase from various production systems. Biosci Rep. 2013 Sep 25;33(5):e00071.

32. Ługowska A, Musielak M, Jamroz E, Pyrkosz A, Kmieć T, Tylki-Szymańska A, et al. Apolipoprotein E genotype and LRP1 polymorphisms in patients with different clinical types of metachromatic leukodystrophy. Gene. 2013 Sep 10;526(2):176–81.

33. Barton NW, Brady RO, Dambrosia JM, Di Bisceglie AM, Doppelt SH, Hill SC, et al. Replacement therapy for inherited enzyme deficiency--macrophage-targeted glucocerebrosidase for Gaucher's disease. N Engl J Med. 1991 May 23;324(21):1464–70.

34. Fernández-Pereira C, San Millán-Tejado B, Gallardo-Gómez M, Pérez-Márquez T, Alves-Villar M, Melcón-Crespo C, et al. Therapeutic Approaches in Lysosomal Storage Diseases. Biomolecules. 2021 Nov 26;11(12):1775.

35. Zhu MM, Mollet M, Hubert RS, Kyung YS, Zhang GG. Industrial Production of Therapeutic Proteins: Cell Lines, Cell Culture, and Purification. Handbook of Industrial Chemistry and Biotechnology. 2017 May 3;1639–69.

36. Dumont J, Euwart D, Mei B, Estes S, Kshirsagar R. Human cell lines for biopharmaceutical manufacturing: history, status, and future perspectives. Crit Rev Biotechnol. 2016 Nov 1;36(6):1110–22.

37. Tian W, Ye Z, Wang S, Schulz MA, Van Coillie J, Sun L, et al. The glycosylation design space for recombinant lysosomal replacement enzymes produced in CHO cells. Nat Commun. 2019 Apr 30;10(1):1785.

38. Croset A, Delafosse L, Gaudry JP, Arod C, Glez L, Losberger C, et al. Differences in the glycosylation of recombinant proteins expressed in HEK and CHO cells. Journal of Biotechnology. 2012 Oct;161(3):336–48.

39. He X, Galpin JD, Tropak MB, Mahuran D, Haselhorst T, von Itzstein M, et al. Production of active human glucocerebrosidase in seeds of Arabidopsis thaliana complex-glycan-deficient (cgl) plants. Glycobiology. 2012 Apr;22(4):492–503.

40. Hood EE, Requesens DVV. Recombinant protein production in plants: challenges and solutions. Methods Mol Biol. 2012;824:469–81.

41. Naphatsamon U, Ohashi T, Misaki R, Fujiyama K. The Production of Human β-Glucocerebrosidase in Nicotiana benthamiana Root Culture. Int J Mol Sci. 2018 Jul 6;19(7):1972.

42. Germain DP, Linhart A. Pegunigalsidase alfa: a novel, pegylated recombinant alpha-galactosidase enzyme for the treatment of Fabry disease. Front Genet. 2024;15:1395287.

43. Oder D, Nordbeck P, Wanner C. Long Term Treatment with Enzyme Replacement Therapy in Patients with Fabry Disease. Nephron. 2016;134(1):30–6.

44. Dinur T, Grittner U, Revel-Vilk S, Becker-Cohen M, Istaiti M, Cozma C, et al. Impact of Long-Term Enzyme Replacement Therapy on Glucosylsphingosine (Lyso-Gb1) Values in Patients with Type 1 Gaucher Disease: Statistical Models for Comparing Three Enzymatic Formulations. Int J Mol Sci. 2021 Jul 19;22(14):7699.

45. Concolino D, Deodato F, Parini R. Enzyme replacement therapy: efficacy and limitations. Ital J Pediatr. 2018 Nov 16;44(Suppl 2):120.

46. Sly WS, Vogler C, Grubb JH, Levy B, Galvin N, Tan Y, et al. Enzyme therapy in mannose receptor-null mucopolysaccharidosis VII mice defines roles for the mannose 6-phosphate and mannose receptors. Proc Natl Acad Sci U S A. 2006 Oct 10;103(41):15172–7.

47. Safary A, Akbarzadeh Khiavi M, Mousavi R, Barar J, Rafi MA. Enzyme replacement therapies: what is the best option? Bioimpacts. 2018;8(3):153–7.

48. Silva AKA, Sagné C, Gazeau F, Abasolo I. Enzyme replacement therapy: current challenges and drug delivery prospects via extracellular vesicles. Rare Dis Orphan Drugs J. 2022;1(3):13.

49. Solomon M, Muro S. Lysosomal enzyme replacement therapies: Historical development, clinical outcomes, and future perspectives. Adv Drug Deliv Rev. 2017 Sep 1;118:109–34.

50. Rombach SM, Aerts JMFG, Poorthuis BJHM, Groener JEM, Donker-Koopman W, Hendriks E, et al. Long-term effect of antibodies against infused alpha-galactosidase A in Fabry disease on plasma and urinary (lyso)Gb3 reduction and treatment outcome. PLoS One. 2012;7(10):e47805.

51. Lenders M, Stappers F, Brand E. In Vitro and In Vivo Amenability to Migalastat in Fabry Disease. Mol Ther Methods Clin Dev. 2020 Dec 11;19:24–34.

52. Lenders M, Brand E. Effects of Enzyme Replacement Therapy and Antidrug Antibodies in Patients with Fabry Disease. J Am Soc Nephrol. 2018 Sep;29(9):2265–78.

53. Abasolo I, Seras-Franzoso J, Moltó-Abad M, Díaz-Riascos V, Corchero JL, Pintos-Morell G, et al. Nanotechnology-based approaches for treating lysosomal storage disorders, a focus on Fabry disease. WIREs Nanomed Nanobiotechnol. 2021 May;13(3):e1684.

54. Kizhner T, Azulay Y, Hainrichson M, Tekoah Y, Arvatz G, Shulman A, et al. Characterization of a chemically modified plant cell culture expressed human α-Galactosidase-A enzyme for treatment of Fabry disease. Mol Genet Metab. 2015 Feb;114(2):259–67.

55. Pardridge WM. Kinetics of Blood-Brain Barrier Transport of Monoclonal Antibodies Targeting the Insulin Receptor and the Transferrin Receptor. Pharmaceuticals (Basel). 2021 Dec 21;15(1):3.

56. Pulgar VM. Transcytosis to Cross the Blood Brain Barrier, New Advancements and Challenges. Front Neurosci [Internet]. 2019 Jan 11 [cited 2024 Oct 29];12. Available from: https://www.frontiersin.org/journals/neuroscience/articles/10.3389/fnins.2018.01019/full

57. Sonoda H, Minami K. IZCARGO®: the world's first biological drug applied with brain drug delivery technology. Drug Delivery System. 2023;38(1):68–74.

58. Yamamoto R, Kawashima S. [Pharmacological property, mechanism of action and clinical study results of Pabinafusp Alfa (Genetical Recombination) (IZCARGO® I.V. Infusion 10 mg) as the therapeutic for Mucopolysaccharidosis type-II (Hunter syndrome)]. Nihon Yakurigaku Zasshi. 2022;157(1):62–75.

59. Fan JQ, Ishii S. Active-site-specific chaperone therapy for Fabry disease. Yin and Yang of enzyme inhibitors. FEBS J. 2007 Oct;274(19):4962–71.

60. Hughes DA, Nicholls K, Sunder-Plassmann G, Jovanovic A, Feldt-Rasmussen U, Schiffmann R, et al. Safety of switching to Migalastat from enzyme replacement therapy in Fabry disease: Experience from the Phase 3 ATTRACT study. Am J Med Genet A. 2019 Jun;179(6):1069–73.

61. Germain DP, Nicholls K, Giugliani R, Bichet DG, Hughes DA, Barisoni LM, et al. Efficacy of the pharmacologic chaperone migalastat in a subset of male patients with the classic phenotype of Fabry disease and migalastat-amenable variants: data from the phase 3 randomized, multicenter, double-blind clinical trial and extension study. Genet Med. 2019 Sep;21(9):1987–97.

62. Oommen S, Zhou Y, Meiyappan M, Gurevich A, Qiu Y. Inter-assay variability influences migalastat amenability assessments among Fabry disease variants. Molecular Genetics and Metabolism. 2019 May 1;127(1):74–85.

63. Flanagan JJ, Rossi B, Tang K, Wu X, Mascioli K, Donaudy F, et al. The pharmacological chaperone 1-deoxynojirimycin increases the activity and lysosomal trafficking of multiple mutant forms of acid alpha-glucosidase. Hum Mutat. 2009 Dec;30(12):1683–92.

64. Khanna R, Jr ACP, Lun Y, Soska R, Feng J, Dhulipala R, et al. The Pharmacological Chaperone AT2220 Increases the Specific Activity and Lysosomal Delivery of Mutant Acid Alpha-Glucosidase, and Promotes Glycogen Reduction in a Transgenic Mouse Model of Pompe Disease. PLOS ONE. 2014 Jul 18;9(7):e102092.

65. Shen JS, Edwards NJ, Hong YB, Murray GJ. Isofagomine increases lysosomal delivery of exogenous glucocerebrosidase. Biochem Biophys Res Commun. 2008 May 16;369(4):1071–5.

66. Warnock DG, Bichet DG, Holida M, Goker-Alpan O, Nicholls K, Thomas M, et al. Oral Migalastat HCl Leads to Greater Systemic Exposure and Tissue Levels of Active α-Galactosidase A in Fabry Patients when Co-Administered with Infused Agalsidase. PLoS One. 2015;10(8):e0134341.

67. Suzuki Y. Chaperone therapy: Stabilization and enhancement of endogenous and exogenous lysosomal enzymes. Brain and Development. 2025 Feb 1;47(1):104298.

68. Zheng W, Padia J, Urban DJ, Jadhav A, Goker-Alpan O, Simeonov A, et al. Three classes of glucocerebrosidase inhibitors identified by quantitative high-throughput screening are chaperone leads for Gaucher disease. Proc Natl Acad Sci U S A. 2007 Aug 7;104(32):13192–7.

69. Marugan JJ, Zheng W, Ferrer M, Motabar O, Southall N, Goldin E, et al. Discovery, SAR, and Biological Evaluation of a Non-Inhibitory Chaperone for Acid Alpha Glucosidase. In: Probe Reports from the NIH Molecular Libraries Program [Internet]. Bethesda (MD): National Center for Biotechnology Information (US); 2010 [cited 2025 Feb 8]. Available from: http://www.ncbi.nlm.nih.gov/books/NBK153221/

70. Guce AI, Clark NE, Salgado EN, Ivanen DR, Kulminskaya AA, Brumer H, et al. Catalytic mechanism of human alpha-galactosidase. J Biol Chem. 2010 Feb 5;285(6):3625–32.

71. Ortolano S. Small Molecules: Substrate Inhibitors, Chaperones, Stop-Codon Read Through, and Beyond. J inborn errors metab screen. 2019 May 30;4:e160038.

72. Patterson MC, Vecchio D, Jacklin E, Abel L, Chadha-Boreham H, Luzy C, et al. Long-term miglustat therapy in children with Niemann-Pick disease type C. J Child Neurol. 2010 Mar;25(3):300–5.

73. Byrne BJ, Parenti G, Schoser B, van der Ploeg AT, Do H, Fox B, et al. Cipaglucosidase alfa plus miglustat: linking mechanism of action to clinical outcomes in late-onset Pompe disease. Front Neurol. 2024;15:1451512.

74. Amiri M, Naim HY. Miglustat-induced intestinal carbohydrate malabsorption is due to the inhibition of α-glucosidases, but not β-galactosidases. J Inherit Metab Dis. 2012 Nov;35(6):949–54.

75. Cox TM, Drelichman G, Cravo R, Balwani M, Burrow TA, Martins AM, et al. Eliglustat compared with imiglucerase in patients with Gaucher's disease type 1 stabilised on enzyme replacement therapy: a phase 3, randomised, open-label, non-inferiority trial. Lancet. 2015 Jun 13;385(9985):2355–62.

76. Guérard N, Oder D, Nordbeck P, Zwingelstein C, Morand O, Welford RWD, et al. Lucerastat, an Iminosugar for Substrate Reduction Therapy: Tolerability, Pharmacodynamics, and Pharmacokinetics in Patients With Fabry Disease on Enzyme Replacement. Clin Pharmacol Ther. 2018 Apr;103(4):703–11.

77. Peterschmitt MJ, Crawford NPS, Gaemers SJM, Ji AJ, Sharma J, Pham TT. Pharmacokinetics, Pharmacodynamics, Safety, and Tolerability of Oral Venglustat in Healthy Volunteers. Clin Pharmacol Drug Dev. 2021 Jan;10(1):86–98.

78. Guérard N, Morand O, Dingemanse J. Lucerastat, an iminosugar with potential as substrate reduction therapy for glycolipid storage disorders: safety, tolerability, and pharmacokinetics in healthy subjects. Orphanet Journal of Rare Diseases. 2017 Jan 14;12(1):9.

79. Parenti G, Pignata C, Vajro P, Salerno M. New strategies for the treatment of lysosomal storage diseases (review). Int J Mol Med. 2013 Jan;31(1):11–20.

80. Valayannopoulos V, Wijburg FA. Therapy for the mucopolysaccharidoses. Rheumatology (Oxford). 2011 Dec;50 Suppl 5:v49-59.

81. Yoon IC, Bascou NA, Poe MD, Szabolcs P, Escolar ML. Long-term neurodevelopmental outcomes of hematopoietic stem cell transplantation for late-infantile Krabbe disease. Blood. 2021 Apr 1;137(13):1719–30.

82. Orchard PJ, Tolar J. Transplant outcomes in leukodystrophies. Semin Hematol. 2010 Jan;47(1):70–8.

83. Kido J, Sugawara K, Nakamura K. Gene therapy for lysosomal storage diseases: Current clinical trial prospects. Front Genet. 2023;14:1064924.

84. Wang D, Tai PWL, Gao G. Adeno-associated virus vector as a platform for gene therapy delivery. Nat Rev Drug Discov. 2019 May;18(5):358–78.

85. Manfredsson FP, Rising AC, Mandel RJ. AAV9: a potential blood-brain barrier buster. Mol Ther. 2009 Mar;17(3):403–5.

86. Biferi MG, Cohen-Tannoudji M, García-Silva A, Souto-Rodríguez O, Viéitez-González I, San-Millán-Tejado B, et al. Systemic Treatment of Fabry Disease Using a Novel AAV9 Vector Expressing α-Galactosidase A. Mol Ther Methods Clin Dev. 2021 Mar 12;20:1–17.

87. Nagree MS, Scalia S, McKillop WM, Medin JA. An update on gene therapy for lysosomal storage disorders. Expert Opinion on Biological Therapy. 2019 Jul 3;19(7):655–70.

88. Rastall DP, Amalfitano A. Recent advances in gene therapy for lysosomal storage disorders. The Application of Clinical Genetics. 2015 Jun 24;8:157–69.

89. Gregersen N, Bross P. Protein misfolding and cellular stress: an overview. Methods Mol Biol. 2010;648:3–23.

90. Almeida LM, Oliveira Â, Oliveira JMA, Pinho BR. Stress response mechanisms in protein misfolding diseases: Profiling a cellular model of Huntington's disease. Archives of Biochemistry and Biophysics. 2023 Sep 1;745:109711.

91. Gomez-Pastor R, Burchfiel ET, Thiele DJ. Regulation of heat shock transcription factors and their roles in physiology and disease. Nat Rev Mol Cell Biol. 2018 Jan;19(1):4–19.

92. Kirkegaard T, Roth AG, Petersen NHT, Mahalka AK, Olsen OD, Moilanen I, et al. Hsp70 stabilizes lysosomes and reverts Niemann-Pick disease-associated lysosomal pathology. Nature. 2010 Jan 28;463(7280):549–53.

93. Nylandsted J, Gyrd-Hansen M, Danielewicz A, Fehrenbacher N, Lademann U, Høyer-Hansen M, et al. Heat shock protein 70 promotes cell survival by inhibiting lysosomal membrane permeabilization. J Exp Med. 2004 Aug 16;200(4):425–35.

94. Petersen NHT, Kirkegaard T, Olsen OD, Jäättelä M. Connecting Hsp70, sphingolipid metabolism and lysosomal stability. Cell Cycle. 2010 Jun 15;9(12):2305–9.

95. Kirkegaard T, Gray J, Priestman DA, Wallom KL, Atkins J, Olsen OD, et al. Heat shock protein-based therapy as a potential candidate for treating the sphingolipidoses. Sci Transl Med. 2016 Sep 7;8(355):355ra118.

96. Mu TW, Ong DST, Wang YJ, Balch WE, Yates JR, Segatori L, et al. Chemical and biological approaches synergize to ameliorate protein-folding diseases. Cell. 2008 Sep 5;134(5):769–81.

97. Cudkowicz ME, Shefner JM, Simpson E, Grasso D, Yu H, Zhang H, et al. Arimoclomol at dosages up to 300 mg/day is well tolerated and safe in amyotrophic lateral sclerosis. Muscle Nerve. 2008 Jul;38(1):837–44.

98. Commissioner O of the. FDA. FDA; 2024 [cited 2025 Feb 8]. FDA Approves First Treatment for Niemann-Pick Disease, Type C. Available from: https://www.fda.gov/news-events/press-announcements/fda-approves-first-treatment-niemann-pick-disease-type-c

99. Nakasone N, Nakamura YS, Higaki K, Oumi N, Ohno K, Ninomiya H. Endoplasmic Reticulum-associated Degradation of Niemann-Pick C1. J Biol Chem. 2014 Jul 11;289(28):19714–25.

100. Kieran D, Kalmar B, Dick JRT, Riddoch-Contreras J, Burnstock G, Greensmith L. Treatment with arimoclomol, a coinducer of heat shock proteins, delays disease progression in ALS mice. Nat Med. 2004 Apr;10(4):402–5.

101. Ingemann L, Kirkegaard T. Lysosomal storage diseases and the heat shock response: convergences and therapeutic opportunities. J Lipid Res. 2014 Nov;55(11):2198–210.

102. Fog CK, Zago P, Malini E, Solanko LM, Peruzzo P, Bornaes C, et al. The heat shock protein amplifier arimoclomol improves refolding, maturation and lysosomal activity of glucocerebrosidase. EBioMedicine. 2018 Dec;38:142–53.

103. Medina DL, Fraldi A, Bouche V, Annunziata F, Mansueto G, Spampanato C, et al. Transcriptional activation of lysosomal exocytosis promotes cellular clearance. Dev Cell. 2011 Sep 13;21(3):421–30.

104. Song W, Wang F, Savini M, Ake A, di Ronza A, Sardiello M, et al. TFEB regulates lysosomal proteostasis. Hum Mol Genet. 2013 May 15;22(10):1994–2009.

105. Moskot M, Montefusco S, Jakóbkiewicz-Banecka J, Mozolewski P, Węgrzyn A, Di Bernardo D, et al. The phytoestrogen genistein modulates lysosomal metabolism and transcription factor EB (TFEB) activation. J Biol Chem. 2014 Jun 13;289(24):17054–69.

106. Ellison S, Parker H, Bigger B. Advances in therapies for neurological lysosomal storage disorders. J of Inher Metab Disea. 2023 Sep;46(5):874–905.

107. Schaefer RM, Tylki-Szymańska A, Hilz MJ. Enzyme replacement therapy for Fabry disease: a systematic review of available evidence. Drugs. 2009 Nov 12;69(16):2179–205.

108. Pisani A, Visciano B, Roux GD, Sabbatini M, Porto C, Parenti G, et al. Enzyme replacement therapy in patients with Fabry disease: state of the art and review of the literature. Mol Genet Metab. 2012 Nov;107(3):267–75.

109. West M, Nicholls K, Mehta A, Clarke JTR, Steiner R, Beck M, et al. Agalsidase alfa and kidney dysfunction in Fabry disease. J Am Soc Nephrol. 2009 May;20(5):1132–9.

110. Fernandez J, Sigurdsson G, Farivar RS. Cardiac surgery in patients with Fabry's disease: review of literature. J Card Surg. 2012 Jul;27(4):478–80.

111. Bersano A, Lanfranconi S, Valcarenghi C, Bresolin N, Micieli G, Baron P. Neurological features of Fabry disease: clinical, pathophysiological aspects and therapy. Acta Neurol Scand. 2012 Aug;126(2):77–97.

112. Grewal RP. Stroke in Fabry's disease. J Neurol. 1994 Mar 1;241(3):153–6.

113. Miller JJ, Kanack AJ, Dahms NM. Progress in the understanding and treatment of Fabry disease. Biochim Biophys Acta Gen Subj. 2020 Jan;1864(1):129437.

114. Lenders M, Brand E. Fabry Disease: The Current Treatment Landscape. Drugs. 2021 Apr 1;81(6):635–45.

115. Alipourfetrati S, Saeed A, Norris JM, Sheckley F, Rastogi A. A Review of Current and Future Treatment Strategies for Fabry Disease: A Model for Treating Lysosomal Storage Diseases. Journal of Pharmacology and Clinical Toxicology. 2015 May 11;3(3):1–8.

116. Lee K. A biochemical and pharmacological comparison of enzyme replacement therapies for the glycolipid storage disorder Fabry disease. Glycobiology. 2003 Apr 1;13(4):305–13.

117. Azevedo O, Gago MF, Miltenberger-Miltenyi G, Sousa N, Cunha D. Fabry Disease Therapy: State-of-the-Art and Current Challenges. Int J Mol Sci. 2020 Dec 28;22(1):206.

118. Hughes D, Gonzalez D, Maegawa G, Bernat JA, Holida M, Giraldo P, et al. Long-term safety and efficacy of pegunigalsidase alfa: A multicenter 6-year study in adult patients with Fabry disease. Genet Med. 2023 Dec;25(12):100968.

119. Lenders M, Pollmann S, Terlinden M, Brand E. Pre-existing anti-drug antibodies in Fabry disease show less affinity for pegunigalsidase alfa. Mol Ther Methods Clin Dev. 2022 Sep 8;26:323–30.

120. Fervenza FC, Torra R, Warnock DG. Safety and efficacy of enzyme replacement therapy in the nephropathy of Fabry disease. Biologics. 2008 Dec;2(4):823–43.

121. Nakamura K, Kawashima S, Tozawa H, Yamaoka M, Yamamoto T, Tanaka N, et al. Pharmacokinetics and pharmacodynamics of JR-051, a biosimilar of agalsidase beta, in healthy adults and patients with Fabry disease: Phase I and II/III clinical studies. Mol Genet Metab. 2020 Jul;130(3):215–24.

122. Tsukimura T, Shiga T, Togawa T, Sakuraba H. Comparative study on incorporation of three recombinant human α-galactosidase A drugs (agalsidases) into cultured fibroblasts and organs/tissues of Fabry mice. Mol Genet Metab Rep. 2024 Sep;40:101118.

123. Morimoto H, Ito Y, Yoden E, Horie M, Tanaka N, Komurasaki Y, et al. Non-clinical evaluation of JR-051 as a biosimilar to agalsidase beta for the treatment of Fabry disease. Mol Genet Metab. 2018 Sep;125(1–2):153–60.

124. Wallace EL, Goker-Alpan O, Wilcox WR, Holida M, Bernat J, Longo N, et al. Head-to-head trial of pegunigalsidase alfa versus agalsidase beta in patients with Fabry disease and deteriorating renal function: results from the 2-year randomised phase III BALANCE study. J Med Genet. 2024 Jun;61(6):520–30.

125. Medin JA, Khan A, Huang J, Barber D, Anthony Rupar C, Auray-Blais C, et al. FACTs Fabry gene therapy clinical trial: Two-year data. Molecular Genetics and Metabolism. 2019 Feb 1;126(2):S99.

126. Khan A, Barber DL, Huang J, Rupar CA, Rip JW, Auray-Blais C, et al. Lentivirus-mediated gene therapy for Fabry disease. Nat Commun. 2021 Feb 25;12(1):1178.

127. Khan A, Barber DL, McKillop WM, Rupar CA, Auray-Blais C, Fraser G, et al. Lentivirus-mediated gene therapy for Fabry disease: 5-year End-of-Study results from the Canadian FACTs trial. Clin Transl Med. 2025 Jan;15(1):e70073.

128. Jeyakumar JM, Kia A, Tam LCS, McIntosh J, Spiewak J, Mills K, et al. Preclinical evaluation of FLT190, a liver-directed AAV gene therapy for Fabry disease. Gene Ther. 2023 Jun;30(6):487–502.

129. Yasuda M, Huston MW, Pagant S, Gan L, St Martin S, Sproul S, et al. AAV2/6 Gene Therapy in a Murine Model of Fabry Disease Results in Supraphysiological Enzyme Activity and Effective Substrate Reduction. Mol Ther Methods Clin Dev. 2020 Sep 11;18:607–19.

130. Lu B, Ku J, Flojo R, Olson C, Bengford D, Marriott G. Exosome- and extracellular vesicle-based approaches for the treatment of lysosomal storage disorders. Advanced Drug Delivery Reviews. 2022 Sep;188:114465.

131. Pardridge WM. Blood-brain barrier delivery for lysosomal storage disorders with IgG-lysosomal enzyme fusion proteins. Adv Drug Deliv Rev. 2022 May;184:114234.

132. Seras-Franzoso J, Díaz-Riascos ZV, Corchero JL, González P, García-Aranda N, Mandaña M, et al. Extracellular vesicles from recombinant cell factories improve the activity and efficacy of enzymes defective in lysosomal storage disorders. J Extracell Vesicles. 2021 Mar;10(5):e12058.

133. Zeb A, Rana I, Choi HI, Lee CH, Baek SW, Lim CW, et al. Potential and Applications of Nanocarriers for Efficient Delivery of Biopharmaceuticals. Pharmaceutics. 2020 Dec 6;12(12):1184.

134. Bozzuto G, Molinari A. Liposomes as nanomedical devices. Int J Nanomedicine. 2015;10:975–99.

135. Wilczewska AZ, Niemirowicz K, Markiewicz KH, Car H. Nanoparticles as drug delivery systems. Pharmacol Rep. 2012;64(5):1020–37.

136. Yetisgin AA, Cetinel S, Zuvin M, Kosar A, Kutlu O. Therapeutic Nanoparticles and Their Targeted Delivery Applications. Molecules. 2020 May 8;25(9):2193.

137. Juszkiewicz K, Sikorski AF, Czogalla A. Building Blocks to Design Liposomal Delivery Systems. Int J Mol Sci. 2020 Dec 15;21(24):9559.

138. Torchilin VP. Recent advances with liposomes as pharmaceutical carriers. Nat Rev Drug Discov. 2005 Feb;4(2):145–60.

139. Glassman PM, Muzykantov VR. Pharmacokinetic and Pharmacodynamic Properties of Drug Delivery Systems. J Pharmacol Exp Ther. 2019 Sep;370(3):570–80.

140. Bashiri G, Padilla MS, Swingle KL, Shepherd SJ, Mitchell MJ, Wang K. Nanoparticle protein corona: from structure and function to therapeutic targeting. Lab Chip. 2023;23(6):1432–66.

141. Qin X, Yu C, Wei J, Li L, Zhang C, Wu Q, et al. Rational Design of Nanocarriers for Intracellular Protein Delivery. Adv Mater. 2019 Nov;31(46):e1902791.

142. Gu Z, Biswas A, Zhao M, Tang Y. Tailoring nanocarriers for intracellular protein delivery. Chem Soc Rev. 2011 Jun 20;40(7):3638–55.

143. Aminu N, Bello I, Umar NM, Tanko N, Aminu A, Audu MM. The influence of nanoparticulate drug delivery systems in drug therapy. Journal of Drug Delivery Science and Technology. 2020 Dec 1;60:101961.

144. Sercombe L, Veerati T, Moheimani F, Wu SY, Sood AK, Hua S. Advances and Challenges of Liposome Assisted Drug Delivery. Front Pharmacol. 2015;6:286.

145. Chang HI, Yeh MK. Clinical development of liposome-based drugs: formulation, characterization, and therapeutic efficacy. Int J Nanomedicine. 2012;7:49–60.

146. Inglut CT, Sorrin AJ, Kuruppu T, Vig S, Cicalo J, Ahmad H, et al. Immunological and Toxicological Considerations for the Design of Liposomes. Nanomaterials (Basel). 2020 Jan 22;10(2):190.

147. Petros RA, DeSimone JM. Strategies in the design of nanoparticles for therapeutic applications. Nat Rev Drug Discov. 2010 Aug;9(8):615–27.

148. Grimaldi N, Andrade F, Segovia N, Ferrer-Tasies L, Sala S, Veciana J, et al. Lipid-based nanovesicles for nanomedicine. Chem Soc Rev. 2016 Nov 21;45(23):6520–45.

149. Nosova AS, Koloskova OO, Nikonova AA, Simonova VA, Smirnov VV, Kudlay D, et al. Diversity of PEGylation methods of liposomes and their influence on RNA delivery. Medchemcomm. 2019 Feb 12;10(3):369–77.

150. Cattel L, Ceruti M, Dosio F. From conventional to stealth liposomes: a new frontier in cancer chemotherapy. Tumori. 2003;89(3):237–49.

151. Cruz MEM, Corvo ML, Martins MB, Simões S, Gaspar MM. Liposomes as Tools to Improve Therapeutic Enzyme Performance. Pharmaceutics. 2022 Feb 27;14(3):531.

152. Immordino ML, Dosio F, Cattel L. Stealth liposomes: review of the basic science, rationale, and clinical applications, existing and potential. Int J Nanomedicine. 2006;1(3):297–315.

153. Lamichhane N, Udayakumar TS, D'Souza WD, Simone CB, Raghavan SR, Polf J, et al. Liposomes: Clinical Applications and Potential for Image-Guided Drug Delivery. Molecules. 2018 Jan 30;23(2):288.

154. Nsairat H, Khater D, Sayed U, Odeh F, Al Bawab A, Alshaer W. Liposomes: structure, composition, types, and clinical applications. Heliyon. 2022 May;8(5):e09394.

155. Bulbake U, Doppalapudi S, Kommineni N, Khan W. Liposomal Formulations in Clinical Use: An Updated Review. Pharmaceutics. 2017 Mar 27;9(2):12.

156. Đorđević S, Gonzalez MM, Conejos-Sánchez I, Carreira B, Pozzi S, Acúrcio RC, et al. Current hurdles to the translation of nanomedicines from bench to the clinic. Drug Deliv Transl Res. 2022 Mar;12(3):500–25.

157. Kalluri R, LeBleu VS. The biology, function, and biomedical applications of exosomes. Science. 2020 Feb 7;367(6478):eaau6977.

158. Doyle LM, Wang MZ. Overview of Extracellular Vesicles, Their Origin, Composition, Purpose, and Methods for Exosome Isolation and Analysis. Cells. 2019 Jul 15;8(7):727.

159. Ståhl AL, Johansson K, Mossberg M, Kahn R, Karpman D. Exosomes and microvesicles in normal physiology, pathophysiology, and renal diseases. Pediatr Nephrol. 2019 Jan;34(1):11–30.

160. Sharma S, Masud MK, Kaneti YV, Rewatkar P, Koradia A, Hossain MSA, et al. Extracellular Vesicle Nanoarchitectonics for Novel Drug Delivery Applications. Small. 2021 Oct;17(42):e2102220.

161. Hessvik NP, Llorente A. Current knowledge on exosome biogenesis and release. Cell Mol Life Sci. 2018 Jan;75(2):193–208.

162. Leone DA, Rees AJ, Kain R. Dendritic cells and routing cargo into exosomes. Immunol Cell Biol. 2018 May 24;

163. Schulz-Siegmund M, Aigner A. Nucleic acid delivery with extracellular vesicles. Adv Drug Deliv Rev. 2021 Jun;173:89–111.

164. Teng F, Fussenegger M. Shedding Light on Extracellular Vesicle Biogenesis and Bioengineering. Adv Sci (Weinh). 2020 Jan;8(1):2003505.

165. Takahashi RU, Prieto-Vila M, Hironaka A, Ochiya T. The role of extracellular vesicle microRNAs in cancer biology. Clin Chem Lab Med. 2017 May 1;55(5):648–56.

166. Mathieu M, Martin-Jaular L, Lavieu G, Théry C. Specificities of secretion and uptake of exosomes and other extracellular vesicles for cell-to-cell communication. Nat Cell Biol. 2019 Jan;21(1):9–17.

167. Lane JD, Allan VJ, Woodman PG. Active relocation of chromatin and endoplasmic reticulum into blebs in late apoptotic cells. J Cell Sci. 2005 Sep 1;118(Pt 17):4059–71.

168. Du S, Guan Y, Xie A, Yan Z, Gao S, Li W, et al. Extracellular vesicles: a rising star for therapeutics and drug delivery. Journal of Nanobiotechnology. 2023 Jul 20;21(1):231.

169. Welsh JA, Goberdhan DCI, O'Driscoll L, Buzas EI, Blenkiron C, Bussolati B, et al. Minimal information for studies of extracellular vesicles (MISEV2023): From basic to advanced approaches. J Extracell Vesicles. 2024;13(2):e12404.

170. Lischnig A, Bergqvist M, Ochiya T, Lässer C. Quantitative Proteomics Identifies Proteins Enriched in Large and Small Extracellular Vesicles. Mol Cell Proteomics [Internet]. 2022 Sep 1 [cited 2024 Dec 12];21(9). Available from: https://www.mcponline.org/article/S1535-9476(22)00081-0/abstract

171. Carney RP, Mizenko RR, Bozkurt BT, Lowe N, Henson T, Arizzi A, et al. Harnessing extracellular vesicle heterogeneity for diagnostic and therapeutic applications. Nat Nanotechnol [Internet]. 2024 Oct 28 [cited 2024 Dec 12]; Available from: https://www.nature.com/articles/s41565-024-01774-3

172. Sahoo S, Adamiak M, Mathiyalagan P, Kenneweg F, Kafert-Kasting S, Thum T. Therapeutic and Diagnostic Translation of Extracellular Vesicles in Cardiovascular Diseases. Circulation. 2021 Apr 6;143(14):1426–49.

173. Abreu RC de, Fernandes H, Martins PA da C, Sahoo S, Emanueli C, Ferreira L. Native and engineered extracellular vesicles for cardiovascular therapeutics. Nature reviews Cardiology. 2020 Jun 1;17(11):685.

174. Anggraeni N, Vuong CK, Silvia P, Fukushige M, Yamashita T, Obata-Yasuoka M, et al. Mesenchymal stem cell-derived extracellular vesicles reduce inflammatory responses to SARS-CoV-2 and Influenza viral proteins via miR-146a/NF-κB pathway. Sci Rep. 2024 Nov 4;14(1):26649.

175. Katsuda T, Tsuchiya R, Kosaka N, Yoshioka Y, Takagaki K, Oki K, et al. Human adipose tissue-derived mesenchymal stem cells secrete functional neprilysin-bound exosomes. Sci Rep. 2013;3:1197.

176. Del Fattore A, Luciano R, Saracino R, Battafarano G, Rizzo C, Pascucci L, et al. Differential effects of extracellular vesicles secreted by mesenchymal stem cells from different sources on glioblastoma cells. Expert Opin Biol Ther. 2015 Apr;15(4):495–504.

177. Li SJ, Cheng RJ, Wei SX, Xia ZJ, Pu YY, Liu Y. Advances in mesenchymal stem cell-derived extracellular vesicles therapy for Sjogren's syndrome-related dry eye disease. Experimental Eye Research. 2023 Dec 1;237:109716.

178. Seras-Franzoso J, Díaz-Riascos ZV, Corchero JL, González P, García-Aranda N, Mandaña M, et al. Extracellular vesicles from recombinant cell factories improve the activity and efficacy of enzymes defective in lysosomal storage disorders. J Extracell Vesicles. 2021 Mar;10(5):e12058.

179. Cooper JM, Wiklander PBO, Nordin JZ, Al-Shawi R, Wood MJ, Vithlani M, et al. Systemic exosomal siRNA delivery reduced alpha-synuclein aggregates in brains of transgenic mice. Mov Disord. 2014 Oct;29(12):1476–85.

180. Ju Y, Hu Y, Yang P, Xie X, Fang B. Extracellular vesicle-loaded hydrogels for tissue repair and regeneration. Mater Today Bio. 2022 Dec 21;18:100522.

181. Li Y, Wu Y, Federzoni EA, Wang X, Dharmawan A, Hu X, et al. CD47 cross-dressing by extracellular vesicles expressing CD47 inhibits phagocytosis without transmitting cell death signals. Elife. 2022 Dec 1;11:e73677.

182. Meng W, Wang L, Du X, Xie M, Yang F, Li F, et al. Engineered mesenchymal stem cell-derived extracellular vesicles constitute a versatile platform for targeted drug delivery. J Control Release. 2023 Nov 1;363:235–52.

183. Alvarez-Erviti L, Seow Y, Yin H, Betts C, Lakhal S, Wood MJA. Delivery of siRNA to the mouse brain by systemic injection of targeted exosomes. Nat Biotechnol. 2011 Apr;29(4):341–5.

184. Kooijmans SAA, Gitz-Francois JJJM, Schiffelers RM, Vader P. Recombinant phosphatidylserine-binding nanobodies for targeting of extracellular vesicles to tumor cells: a plug-and-play approach †Electronic supplementary information (ESI) available. See DOI: 10.1039/c7nr06966a. Nanoscale. 2018 Feb 7;10(5):2413–26.

185. Gupta D, Wiklander OPB, Görgens A, Conceição M, Corso G, Liang X, et al. Amelioration of systemic inflammation via the display of two different decoy protein receptors on extracellular vesicles. Nat Biomed Eng. 2021 Sep;5(9):1084–98.

186. Sadeghi S, Tehrani FR, Tahmasebi S, Shafiee A, Hashemi SM. Exosome engineering in cell therapy and drug delivery. Inflammopharmacology. 2023;31(1):145–69.

187. Gangadaran P, Ahn BC. Extracellular Vesicle- and Extracellular Vesicle Mimetics-Based Drug Delivery Systems: New Perspectives, Challenges, and Clinical Developments. Pharmaceutics. 2020 May 11;12(5):442.

188. van der Meel R, Fens MHAM, Vader P, Van Solinge WW, Eniola-Adefeso O, Schiffelers RM. Extracellular vesicles as drug delivery systems: Lessons from the liposome field. J Control Release. 2014 Dec;195:72–85.

189. Murphy DE, de Jong OG, Evers MJW, Nurazizah M, Schiffelers RM, Vader P. Natural or Synthetic RNA Delivery: A Stoichiometric Comparison of Extracellular Vesicles and Synthetic Nanoparticles. Nano Lett. 2021 Feb 24;21(4):1888–95.

190. Abra RM, Hunt CA. Liposome disposition in vivo. III. Dose and vesicle-size effects. Biochim Biophys Acta. 1981 Dec 23;666(3):493–503.

191. Lai CP, Mardini O, Ericsson M, Prabhakar S, Maguire C, Chen JW, et al. Dynamic biodistribution of extracellular vesicles in vivo using a multimodal imaging reporter. ACS Nano. 2014 Jan 28;8(1):483–94.

192. Willekens FLA, Werre JM, Kruijt JK, Roerdinkholder-Stoelwinder B, Groenen-Döpp YAM, van den Bos AG, et al. Liver Kupffer cells rapidly remove red blood cell-derived vesicles from the circulation by scavenger receptors. Blood. 2005 Mar 1;105(5):2141–5.

193. Elsharkasy OM, Nordin JZ, Hagey DW, De Jong OG, Schiffelers RM, Andaloussi SE, et al. Extracellular vesicles as drug delivery systems: Why and how? Adv Drug Deliv Rev. 2020;159:332–43.

194. Kimiz-Gebologlu I, Oncel SS. Exosomes: Large-scale production, isolation, drug loading efficiency, and biodistribution and uptake. J Control Release. 2022 Jul 1;347:533–43.

195. Haney MJ, Zhao Y, Jin YS, Batrakova EV. Extracellular Vesicles as Drug Carriers for Enzyme Replacement Therapy to Treat CLN2 Batten Disease: Optimization of Drug Administration Routes. Cells. 2020 May 20;9(5):1273.

196. Alvarez-Erviti L, Seow Y, Yin H, Betts C, Lakhal S, Wood MJA. Delivery of siRNA to the mouse brain by systemic injection of targeted exosomes. Nat Biotechnol. 2011 Apr;29(4):341–5.

197. Xia Y, Zhang J, Liu G, Wolfram J. Immunogenicity of Extracellular Vesicles. Adv Mater. 2024 Aug;36(33):e2403199.

198. Komuro H, Aminova S, Lauro K, Harada M. Advances of engineered extracellular vesicles-based therapeutics strategy. Sci Technol Adv Mater. 23(1):655–81.

199. Zhang Y, Bi J, Huang J, Tang Y, Du S, Li P. Exosome: A Review of Its Classification, Isolation Techniques, Storage, Diagnostic and Targeted Therapy Applications. Int J Nanomedicine. 2020 Sep 22;15:6917–34.

200. Tomsen-Melero J, Moltó-Abad M, Merlo-Mas J, Díaz-Riascos ZV, Cristóbal-Lecina E, Soldevila A, et al. Targeted nanoliposomes to improve enzyme replacement therapy of Fabry disease. Sci Adv. 2024 Dec 13;10(50):eadq4738.

201. Cabrera I, Elizondo E, Esteban O, Corchero JL, Melgarejo M, Pulido D, et al. Multifunctional Nanovesicle-Bioactive Conjugates Prepared by a One-Step Scalable Method Using CO_2 -Expanded Solvents. Nano Lett. 2013 Aug 14;13(8):3766–74.

202. Cabrera I, Abasolo I, Corchero JL, Elizondo E, Gil PR, Moreno E, et al. α-Galactosidase-A Loaded-Nanoliposomes with Enhanced Enzymatic Activity and Intracellular Penetration. Adv Healthcare Materials. 2016 Apr;5(7):829–40.

203. Tomsen-Melero J. Study of New Liposomes for the Delivery of Enzymes through Biological Membranes [Internet]. 2021 [cited 2021 Oct 30]. Available from: http://hdl.handle.net/10803/673786

204. Schneider CA, Rasband WS, Eliceiri KW. NIH Image to ImageJ: 25 years of image analysis. Nat Methods. 2012 Jul;9(7):671–5.

205. Ramiro L, García-Berrocoso T, Briansó F, Goicoechea L, Simats A, Llombart V, et al. Integrative Multi-omics Analysis to Characterize Human Brain Ischemia. Mol Neurobiol. 2021 Aug 1;58(8):4107–21.

206. Garcia-Puig A, Mosquera JL, Jiménez-Delgado S, García-Pastor C, Jorba I, Navajas D, et al. Proteomics Analysis of Extracellular Matrix Remodeling During Zebrafish Heart Regeneration. Mol Cell Proteomics. 2019 Sep;18(9):1745–55.

207. Orsburn BC. Proteome Discoverer—A Community Enhanced Data Processing Suite for Protein Informatics. Proteomes. 2021 Mar 23;9(1):15.

208. Perkins DN, Pappin DJ, Creasy DM, Cottrell JS. Probability-based protein identification by searching sequence databases using mass spectrometry data. Electrophoresis. 1999 Dec;20(18):3551–67.

209. Chen C, Hou J, Tanner JJ, Cheng J. Bioinformatics Methods for Mass Spectrometry-Based Proteomics Data Analysis. IJMS. 2020 Apr 20;21(8):2873.

210. Corchero JL, Mendoza R, Lorenzo J, Rodríguez-Sureda V, Domínguez C, Vázquez E, et al. Integrated approach to produce a recombinant, His-tagged human α-galactosidase A in mammalian cells. Biotechnol Prog. 2011;27(5):1206–17.

211. Merlo-Mas J, Tomsen-Melero J, Corchero JL, González-Mira E, Font A, Pedersen JN, et al. Application of Quality by Design to the robust preparation of a liposomal GLA formulation by DELOS-susp method. J Supercrit Fluids. 2021 Jul;173:105204.

212. Luke JM, Vincent JM, Du SX, Gerdemann U, Leen AM, Whalen RG, et al. Improved antibiotic-free plasmid vector design by incorporation of transient expression enhancers. Gene Ther. 2011;18(4):334–43.

213. ORTEGA JS, Navarro SS, FRANZOSO JS, BARRIOCANAL ÁM, RAFAEL DFDS, ANDRADE FRDS. Cell-penetrating peptides [Internet]. US20230416334A1, 2023 [cited 2025 Feb 19]. Available from: https://patents.google.com/patent/US20230416334A1/en

214. Tan KL, Chia WC, How CW, Tor YS, Show PL, Looi QHD, et al. Benchtop Isolation and Characterisation of Small Extracellular Vesicles from Human Mesenchymal Stem Cells. Mol Biotechnol. 2021 Sep;63(9):780–91.

215. Desnick RJ, Allen KY, Desnick SJ, Raman MK, Bernlohr RW, Krivit W. Fabry's disease: enzymatic diagnosis of hemizygotes and heterozygotes. Alpha-galactosidase activities in plasma, serum, urine, and leukocytes. J Lab Clin Med. 1973 Feb;81(2):157–71.

216. Mayes JS, Scheerer JB, Sifers RN, Donaldson ML. Differential assay for lysosomal alpha-galactosidases in human tissues and its application to Fabry's disease. Clin Chim Acta. 1981 May 5;112(2):247–51.

217. Ohshima T, Murray GJ, Swaim WD, Longenecker G, Quirk JM, Cardarelli CO, et al. alpha-Galactosidase A deficient mice: a model of Fabry disease. Proc Natl Acad Sci U S A. 1997 Mar 18;94(6):2540–4.

218. Shu L, Murphy HS, Cooling L, Shayman JA. An in vitro model of Fabry disease. J Am Soc Nephrol. 2005 Sep;16(9):2636–45.

219. Giannotti MI, Abasolo I, Oliva M, Andrade F, García-Aranda N, Melgarejo M, et al. Highly Versatile Polyelectrolyte Complexes for Improving the Enzyme Replacement Therapy of Lysosomal Storage Disorders. ACS Appl Mater Interfaces. 2016 Oct 5;8(39):25741–52.

220. Nazarenus M, Abasolo I, García-Aranda N, Voccoli V, Rejman J, Cecchini M, et al. Polymer Capsules as a Theranostic Tool for a Universal In Vitro Screening Assay—The Case of Lysosomal Storage Diseases. Particle & Particle Systems Characterization. 2015;32(11):991–8.

221. Schindelin J, Arganda-Carreras I, Frise E, Kaynig V, Longair M, Pietzsch T, et al. Fiji: an open-source platform for biological-image analysis. Nat Methods. 2012 Jul;9(7):676–82.

222. Zhang XY, Dinh A, Cronin J, Li SC, Reiser J. Cellular uptake and lysosomal delivery of galactocerebrosidase tagged with the HIV Tat protein transduction domain. Journal of Neurochemistry. 2008;104(4):1055–64.

223. Orii KO, Grubb JH, Vogler C, Levy B, Tan Y, Markova K, et al. Defining the pathway for Tat-mediated delivery of beta-glucuronidase in cultured cells and MPS VII mice. Mol Ther. 2005 Aug;12(2):345–52.

224. Mehta A, Hughes DA. Fabry Disease. In: Adam MP, Feldman J, Mirzaa GM, Pagon RA, Wallace SE, Amemiya A, editors. GeneReviews® [Internet]. Seattle (WA): University of Washington, Seattle; 1993 [cited 2025 Feb 27]. Available from: http://www.ncbi.nlm.nih.gov/books/NBK1292/

225. Tsukimura T, Tayama Y, Shiga T, Hirai K, Togawa T, Sakuraba H. Anti-drug antibody formation in Japanese Fabry patients following enzyme replacement therapy. Mol Genet Metab Rep. 2020 Dec;25:100650.

226. Cabrera I, Abasolo I, Corchero JL, Elizondo E, Gil PR, Moreno E, et al. α-Galactosidase-A Loaded-Nanoliposomes with Enhanced Enzymatic Activity and Intracellular Penetration. Adv Healthc Mater. 2016 Apr 6;5(7):829–40.

227. Tomsen-Melero J, Passemard S, García-Aranda N, Díaz-Riascos ZV, González-Rioja R, Nedergaard Pedersen J, et al. Impact of Chemical Composition on the Nanostructure and Biological Activity of α-Galactosidase-Loaded Nanovesicles for Fabry Disease Treatment. ACS Appl Mater Interfaces. 2021 Feb 24;13(7):7825–38.

228. de la Fuente M, Lombardero L, Gómez-González A, Solari C, Angulo-Barturen I, Acera A, et al. Enzyme Therapy: Current Challenges and Future Perspectives. Int J Mol Sci. 2021 Aug 25;22(17):9181.

229. Poznansky MJ, Juliano RL. Biological approaches to the controlled delivery of drugs: a critical review. Pharmacol Rev. 1984 Dec;36(4):277–336.

230. Bosio VE, Islan GA, Martínez YN, Durán N, Castro GR. Nanodevices for the immobilization of therapeutic enzymes. Crit Rev Biotechnol. 2016;36(3):447–64.

231. Eloy JO, Claro de Souza M, Petrilli R, Barcellos JPA, Lee RJ, Marchetti JM. Liposomes as carriers of hydrophilic small molecule drugs: strategies to enhance encapsulation and delivery. Colloids Surf B Biointerfaces. 2014 Nov 1;123:345–63.

232. Kepczyński M, Nawalany K, Kumorek M, Kobierska A, Jachimska B, Nowakowska M. Which physical and structural factors of liposome carriers control their drug-loading efficiency? Chem Phys Lipids. 2008 Sep;155(1):7–15.

233. Girão LFC, Carvalheiro MC, Ferreira-Silva M, da Rocha SLG, Perales J, Martins MBF, et al. ASP-Enzymosomes with Saccharomyces cerevisiae Asparaginase II Expressed in Pichia pastoris: Formulation Design and In Vitro Studies of a Potential Antileukemic Drug. Int J Mol Sci. 2021 Oct 15;22(20):11120.

234. Jorge JC, Perez-Soler R, Morais JG, Cruz ME. Liposomal palmitoyl-L-asparaginase: characterization and biological activity. Cancer Chemother Pharmacol. 1994;34(3):230–4.

235. Gaspar MM, Perez-Soler R, Cruz ME. Biological characterization of L-asparaginase liposomal formulations. Cancer Chemother Pharmacol. 1996;38(4):373–7.

236. Do TT, Do TP, Nguyen TN, Nguyen TC, Vu TTP, Nguyen TGA. Nanoliposomal L-Asparaginase and Its Antitumor Activities in Lewis Lung Carcinoma Tumor-Induced BALB/c Mice. Advances in Materials Science and Engineering. 2019;2019(1):3534807.

237. Hei Y, Teng B, Zeng Z, Zhang S, Li Q, Pan J, et al. Multifunctional Immunoliposomes Combining Catalase and PD-L1 Antibodies Overcome Tumor Hypoxia and Enhance Immunotherapeutic Effects Against Melanoma. Int J Nanomedicine. 2020;15:1677–91.

238. Corvo ML, Martins MB, Francisco AP, Morais JG, Cruz MEM. Liposomal formulations of Cu,Zn-superoxide dismutase: physico-chemical characterization and activity assessment in an inflammation model. Journal of Controlled Release. 1997 Jan 3;43(1):1–8.

239. Costa C, Liu Z, Simões SI, Correia A, Rahikkala A, Seitsonen J, et al. One-step microfluidics production of enzyme-loaded liposomes for the treatment of inflammatory diseases. Colloids Surf B Biointerfaces. 2021 Mar;199:111556.

240. Vaidya B, Nayak MK, Dash D, Agrawal GP, Vyas SP. Development and characterization of highly selective target-sensitive liposomes for the delivery of streptokinase: in vitro/in vivo studies. Drug Deliv. 2016;23(3):801–7.

241. Kim IS, Choi HG, Choi HS, Kim BK, Kim CK. Prolonged systemic delivery of streptokinase using liposome. Arch Pharm Res. 1998 Jun;21(3):248–52.

242. Zhang N, Li C, Zhou D, Ding C, Jin Y, Tian Q, et al. Cyclic RGD functionalized liposomes encapsulating urokinase for thrombolysis. Acta Biomater. 2018 Apr 1;70:227–36.

243. Xiong H, Zhou Y, Zhou Q, He D, Wan S, Tan Q, et al. Nanosomal Microassemblies for Highly Efficient and Safe Delivery of Therapeutic Enzymes. ACS Appl Mater Interfaces. 2015 Sep 16;7(36):20255–63.

244. Dapergolas G, Neerunjun ED, Gregoriadis G. Penetration of target areas in the rat by liposome-associated bleomycin, glucose oxidase and insulin. FEBS Lett. 1976 Apr 1;63(2):235–9.

245. Sessa G, Weissmann G. Incorporation of Lysozyme into Liposomes: A MODEL FOR STRUCTURE-LINKED LATENCY. Journal of Biological Chemistry. 1970 Jul 10;245(13):3295–301.

246. Thekkedath R, Koshkaryev A, Torchilin VP. Lysosome-targeted octadecyl-rhodamine B-liposomes enhance lysosomal accumulation of glucocerebrosidase in Gaucher's cells in vitro. Nanomedicine (Lond). 2013 Jul;8(7):1055–65.

247. Sun Y, Liou B, Chu Z, Fannin V, Blackwood R, Peng Y, et al. Systemic enzyme delivery by blood-brain barrier-penetrating SapC-DOPS nanovesicles for treatment of neuronopathic Gaucher disease. EBioMedicine. 2020 May;55:102735.

248. Aldosari MH, de Vries RP, Rodriguez LR, Hesen NA, Beztsinna N, van Kuilenburg ABP, et al. Liposome-targeted recombinant human acid sphingomyelinase: Production, formulation, and in vitro evaluation. Eur J Pharm Biopharm. 2019 Apr;137:185–95.

249. Hamill KM, Wexselblatt E, Tong W, Esko JD, Tor Y. Delivery of an active lysosomal enzyme using GNeosomes. J Mater Chem B. 2016 Sep 21;4(35):5794–7.

250. Schneider JL, Dingman RK, Balu-Iyer SV. Lipidic Nanoparticles Comprising Phosphatidylinositol Mitigate Immunogenicity and Improve Efficacy of Recombinant Human Acid Alpha-Glucosidase in a Murine Model of Pompe Disease. J Pharm Sci. 2018 Mar;107(3):831–7.

251. Hayashi T, Shinagawa M, Kawano T, Iwasaki T. Drug delivery using polyhistidine peptide-modified liposomes that target endogenous lysosome. Biochem Biophys Res Commun. 2018 Jun 27;501(3):648–53.

252. Yamaguchi A, Katsuyama K, Suzuki K, Kosaka K, Aoki I, Yamanaka S. Plasmid-based gene transfer ameliorates visceral storage in a mouse model of Sandhoff disease. J Mol Med (Berl). 2003 Mar;81(3):185–93.

253. Zhang Y, Wang Y, Boado RJ, Pardridge WM. Lysosomal Enzyme Replacement of the Brain with Intravenous Non-Viral Gene Transfer. Pharm Res. 2008 Feb 1;25(2):400–6.

254. Schuh RS, Poletto É, Pasqualim G, Tavares AMV, Meyer FS, Gonzalez EA, et al. In vivo genome editing of mucopolysaccharidosis I mice using the CRISPR/Cas9 system. J Control Release. 2018 Oct 28;288:23–33.

255. Schuh RS, Gonzalez EA, Tavares AMV, Seolin BG, Elias L de S, Vera LNP, et al. Neonatal nonviral gene editing with the CRISPR/Cas9 system improves some cardiovascular, respiratory, and bone disease features of the mucopolysaccharidosis I phenotype in mice. Gene Ther. 2020 Feb;27(1–2):74–84.

256. Jiang D, Lee H, Pardridge WM. Plasmid DNA gene therapy of the Niemann-Pick C1 mouse with transferrin receptor-targeted Trojan horse liposomes. Sci Rep. 2020 Aug 7;10(1):13334.

257. Hamill KM, Wexselblatt E, Tong W, Esko JD, Tor Y. Delivery of Cargo to Lysosomes Using GNeosomes. Methods Mol Biol. 2017;1594:151–63.

258. Soh SH, Lee LY. Microencapsulation and Nanoencapsulation Using Supercritical Fluid (SCF) Techniques. Pharmaceutics. 2019 Jan 5;11(1):21.

259. Maja L, Željko K, Mateja P. Sustainable technologies for liposome preparation. The Journal of Supercritical Fluids. 2020 Nov 1;165:104984.

260. William B, Noémie P, Brigitte E, Géraldine P. Supercritical fluid methods: An alternative to conventional methods to prepare liposomes. Chemical Engineering Journal. 2020 Mar 1;383:123106.

261. Cano-Sarabia M, Ventosa N, Sala S, Patiño C, Arranz R, Veciana J. Preparation of uniform rich cholesterol unilamellar nanovesicles using CO2-expanded solvents. Langmuir. 2008 Mar 18;24(6):2433–7.

262. Elizondo E, Veciana J, Ventosa N. Nanostructuring molecular materials as particles and vesicles for drug delivery, using compressed and supercritical fluids. Nanomedicine (Lond). 2012 Sep;7(9):1391–408.

263. Cabrera I, Elizondo E, Esteban O, Corchero JL, Melgarejo M, Pulido D, et al. Multifunctional Nanovesicle-Bioactive Conjugates Prepared by a One-Step Scalable Method Using CO_2 -Expanded Solvents. Nano Lett. 2013 Aug 14;13(8):3766–74.

264. Ludwig BS, Kessler H, Kossatz S, Reuning U. RGD-Binding Integrins Revisited: How Recently Discovered Functions and Novel Synthetic Ligands (Re-)Shape an Ever-Evolving Field. Cancers. 2021 Apr 4;13(7):1711.

265. Trimarchi H, Ortiz A, Sánchez-Niño MD. Lyso-Gb3 Increases αvβ3 Integrin Gene Expression in Cultured Human Podocytes in Fabry Nephropathy. J Clin Med. 2020 Nov 13;9(11):3659.

266. Sajid M, Stouffer GA. The role of alpha(v)beta3 integrins in vascular healing. Thromb Haemost. 2002 Feb;87(2):187–93.

267. Utsumi K, Itoh K, Kase R, Shimmoto M, Yamamoto N, Katagiri Y, et al. Urinary excretion of the vitronectin receptor (integrin alpha V beta 3) in patients with Fabry disease. Clin Chim Acta. 1999 Jan;279(1–2):55–68.

268. Prabakaran T, Nielsen R, Satchell SC, Mathieson PW, Feldt-Rasmussen U, Sørensen SS, et al. Mannose 6-phosphate receptor and sortilin mediated endocytosis of α-galactosidase A in kidney endothelial cells. PLoS One. 2012;7(6):e39975.

269. Prabakaran T, Nielsen R, Larsen JV, Sørensen SS, Rasmussen UF, Saleem MA, et al. Receptor-Mediated Endocytosis of α-Galactosidase A in Human Podocytes in Fabry Disease. PLoS One. 2011 Sep 19;6(9):e25065.

270. Temming K, Schiffelers RM, Molema G, Kok RJ. RGD-based strategies for selective delivery of therapeutics and imaging agents to the tumour vasculature. Drug Resist Updat. 2005 Dec;8(6):381–402.

271. Kulhari H, Pooja D, Shrivastava S, Telukutala SR, Barui AK, Patra CR, et al. Cyclic-RGDfK peptide conjugated succinoyl-TPGS nanomicelles for targeted delivery of docetaxel to integrin receptor over-expressing angiogenic tumours. Nanomedicine. 2015 Aug;11(6):1511–20.

272. EU/3/20/2396 - orphan designation for treatment of Fabry disease | European Medicines Agency (EMA) [Internet]. 2021 [cited 2025 Jan 12]. Available from: https://www.ema.europa.eu/en/medicines/human/orphan-designations/eu-3-20-2396

273. Colletier JP, Chaize B, Winterhalter M, Fournier D. Protein encapsulation in liposomes: efficiency depends on interactions between protein and phospholipid bilayer. BMC Biotechnol. 2002 May 10;2:9.

274. Hwang SY, Kim HK, Choo J, Seong GH, Hien TBD, Lee EK. Effects of operating parameters on the efficiency of liposomal encapsulation of enzymes. Colloids Surf B Biointerfaces. 2012 Jun 1;94:296–303.

275. Shimizu T, Mori T, Tomita M, Tsumoto K. pH switching that crosses over the isoelectric point (pI) can improve the entrapment of proteins within giant liposomes by enhancing protein-membrane interaction. Langmuir. 2014 Jan 21;30(2):554–63.

276. Randolph TW. The two faces of His-tag: immune response versus ease of protein purification. Biotechnol J. 2012 Jan;7(1):18–9.

277. Khan F, Legler PM, Mease RM, Duncan EH, Bergmann-Leitner ES, Angov E. Histidine affinity tags affect MSP1(42) structural stability and immunodominance in mice. Biotechnol J. 2012 Jan;7(1):133–47.

278. Danaei M, Dehghankhold M, Ataei S, Hasanzadeh Davarani F, Javanmard R, Dokhani A, et al. Impact of Particle Size and Polydispersity Index on the Clinical Applications of Lipidic Nanocarrier Systems. Pharmaceutics. 2018 May 18;10(2):57.

279. Németh Z, Csóka I, Semnani Jazani R, Sipos B, Haspel H, Kozma G, et al. Quality by Design-Driven Zeta Potential Optimisation Study of Liposomes with Charge Imparting Membrane Additives. Pharmaceutics. 2022 Aug 26;14(9):1798.

280. Bohnsack RN, Misra SK, Liu J, Ishihara-Aoki M, Pereckas M, Aoki K, et al. Lysosomal enzyme binding to the cation-independent mannose 6-phosphate receptor is regulated allosterically by insulin-like growth factor 2. Sci Rep. 2024 Nov 6;14(1):26875.

281. Frustaci A, Verardo R, Scialla R, Bagnato G, Verardo M, Alfarano M, et al. Downregulation of Mannose-6-Phosphate Receptors in Fabry Disease Cardiomyopathy: A Potential Target for Enzyme Therapy Enhancement. Journal of Clinical Medicine. 2022 Jan;11(18):5440.

282. Braulke T, Tippmer S, Neher E, von Figura K. Regulation of the mannose 6-phosphate/IGF II receptor expression at the cell surface by mannose 6-phosphate, insulin like growth factors and epidermal growth factor. EMBO J. 1989 Mar;8(3):681–6.

283. Rom WN. Human mononuclear phagocytes express the insulin-like growth factor-II/mannose-6-phosphate receptor. Am J Respir Cell Mol Biol. 1991 Jun;4(6):555–9.

284. Braulke T, Tippmer S, Matzner U, Gartung C, von Figura K. Mannose 6-phosphate/insulin-like growth factor II receptor in I-cell disease fibroblasts: increased synthesis and defective regulation of cell surface expression. Biochim Biophys Acta. 1992 Apr 14;1138(4):334–42.

285. Covian-Nares JF, Smith RM, Vogel SS. Two independent forms of endocytosis maintain embryonic cell surface homeostasis during early development. Dev Biol. 2008 Apr 1;316(1):135–48.

286. Polychronakos C, Piscina R. Endocytosis of receptor-bound insulin-like growth factor II is enhanced by mannose-6-phosphate in IM9 cells. Endocrinology. 1988 Oct;123(4):2146–8.

287. Polychronakos C, Guyda HJ, Janthly U, Posner BI. Effects of mannose-6-phosphate on receptor-mediated endocytosis of insulin-like growth factor-II. Endocrinology. 1990 Oct;127(4):1861–6.

288. Preta G, Cronin JG, Sheldon IM. Dynasore - not just a dynamin inhibitor. Cell Communication and Signaling. 2015 Apr 10;13(1):24.

289. Lin H, Singla B, Ghoshal P, Faulkner JL, Cherian-Shaw M, O'Connor PM, et al. Identification of novel macropinocytosis inhibitors using a rational screen of Food and Drug Administration-approved drugs. Br J Pharmacol. 2018 Sep;175(18):3640–55.

290. Blot V, McGraw TE. GLUT4 is internalized by a cholesterol-dependent nystatin-sensitive mechanism inhibited by insulin. EMBO J. 2006 Dec 13;25(24):5648–58.

291. Chang CC, Wu M, Yuan F. Role of specific endocytic pathways in electrotransfection of cells. Molecular Therapy Methods & Clinical Development [Internet]. 2014 Jan 1 [cited 2025 Jan 8];1. Available from: https://www.cell.com/molecular-therapy-family/methods/abstract/S2329-0501(16)30125-5

292. Suemura M, Shibutani S, Iwata H. The endocytosis inhibitor dynasore induces a DNA damage response pathway that can be manipulated for enhanced apoptosis. Biochemical and Biophysical Research Communications. 2023 Feb 19;645:1–9.

293. Chan ET, Kural C. Targeting endocytosis to sensitize cancer cells to programmed cell death. Biochem Soc Trans. 2024 Aug 28;52(4):1703–13.

294. Sheikh A, Alhakamy NA, Md S, Kesharwani P. Recent Progress of RGD Modified Liposomes as Multistage Rocket Against Cancer. Front Pharmacol. 2022 Jan 25;12:803304.

295. Guo Z, He B, Jin H, Zhang H, Dai W, Zhang L, et al. Targeting efficiency of RGD-modified nanocarriers with different ligand intervals in response to integrin αvβ3 clustering. Biomaterials. 2014 Jul;35(23):6106–17.

296. Kibria G, Hatakeyama H, Ohga N, Hida K, Harashima H. Dual-ligand modification of PEGylated liposomes shows better cell selectivity and efficient gene delivery. J Control Release. 2011 Jul 30;153(2):141–8.

297. Ren Y, Yuan B, Hou S, Sui Y, Yang T, Lv M, et al. Delivery of RGD-modified liposome as a targeted colorectal carcinoma therapy and its autophagy mechanism. J Drug Target. 2021 Sep;29(8):863–74.

298. Rappaport J, Manthe RL, Solomon M, Garnacho C, Muro S. A Comparative Study on the Alterations of Endocytic Pathways in Multiple Lysosomal Storage Disorders. Mol Pharm. 2016 Feb 1;13(2):357–68.

299. Yoshimoto M, Hayakawa T, Yamaguchi M, Kimura S, Fujii H. αvβ3 integrin-targeted magnetic resonance imaging in a pancreatic cancer mouse model using RGD-modified liposomes encapsulated with Fe-deferoxamine. PLoS One. 2024;19(9):e0310984.

300. Rangger C, Helbok A, von Guggenberg E, Sosabowski J, Radolf T, Prassl R, et al. Influence of PEGylation and RGD loading on the targeting properties of radiolabeled liposomal nanoparticles. Int J Nanomedicine. 2012;7:5889–900.

301. Shuhendler AJ, Prasad P, Leung M, Rauth AM, Dacosta RS, Wu XY. A novel solid lipid nanoparticle formulation for active targeting to tumor α(v) β(3) integrin receptors reveals cyclic RGD as a double-edged sword. Adv Healthc Mater. 2012 Sep;1(5):600–8.

302. Yano A, Onozuka A, Matin K, Imai S, Hanada N, Nisizawa T. RGD motif enhances immunogenicity and adjuvanicity of peptide antigens following intranasal immunization. Vaccine. 2003 Dec 12;22(2):237–43.

303. Wang X, Meng N, Wang S, Lu L, Wang H, Zhan C, et al. Factors Influencing the Immunogenicity and Immunotoxicity of Cyclic RGD Peptide-Modified Nanodrug Delivery Systems. Mol Pharm. 2020 Sep 8;17(9):3281–90.

304. Wang X, Wang H, Jiang K, Zhang Y, Zhan C, Ying M, et al. Liposomes with cyclic RGD peptide motif triggers acute immune response in mice. J Control Release. 2019 Jan 10;293:201–14.

305. Deuker MFS, Mailänder V, Morsbach S, Landfester K. Anti-PEG antibodies enriched in the protein corona of PEGylated nanocarriers impact the cell uptake. Nanoscale Horiz. 2023;8(10):1377–85.

306. Qin L, Wang CZ, Fan HJ, Zhang CJ, Zhang HW, Lv MH, et al. A dual-targeting liposome conjugated with transferrin and arginine-glycine-aspartic acid peptide for glioma-targeting therapy. Oncol Lett. 2014 Nov;8(5):2000–6.

307. Liu Y, Ran R, Chen J, Kuang Q, Tang J, Mei L, et al. Paclitaxel loaded liposomes decorated with a multifunctional tandem peptide for glioma targeting. Biomaterials. 2014 Jun;35(17):4835–47.

308. Chen C, Duan Z, Yuan Y, Li R, Pang L, Liang J, et al. Peptide-22 and Cyclic RGD Functionalized Liposomes for Glioma Targeting Drug Delivery Overcoming BBB and BBTB. ACS Appl Mater Interfaces. 2017 Feb 22;9(7):5864–73.

309. Li XT, Tang W, Xie HJ, Liu S, Song XL, Xiao Y, et al. The efficacy of RGD modified liposomes loaded with vinorelbine plus tetrandrine in treating resistant brain glioma. Journal of Liposome Research. 2019 Jan 2;29(1):21–34.

310. Linthorst GE, Hollak CEM, Donker-Koopman WE, Strijland A, Aerts JMFG. Enzyme therapy for Fabry disease: Neutralizing antibodies toward agalsidase alpha and beta. Kidney International. 2004 Oct 1;66(4):1589–95.

311. Stappers F, Scharnetzki D, Schmitz B, Manikowski D, Brand SM, Grobe K, et al. Neutralising anti-drug antibodies in Fabry disease can inhibit endothelial enzyme uptake and activity. J Inherit Metab Dis. 2020 Mar;43(2):334–47.

312. Lenders M, Brand E. Mechanisms of Neutralizing Anti-drug Antibody Formation and Clinical Relevance on Therapeutic Efficacy of Enzyme Replacement Therapies in Fabry Disease. Drugs. 2021;81(17):1969–81.

313. Yin L, Li X, Wang R, Zeng Y, Zeng Z, Xie T. Recent Research Progress of RGD Peptide–Modified Nanodrug Delivery Systems in Tumor Therapy. Int J Pept Res Ther. 2023 May 16;29(4):53.

314. Moncelet D, Bouchaud V, Mellet P, Ribot E, Miraux S, Franconi JM, et al. Cellular Density Effect on RGD Ligand Internalization in Glioblastoma for MRI Application. PLOS ONE. 2013 Dec 27;8(12):e82777.

315. Hölig P, Bach M, Völkel T, Nahde T, Hoffmann S, Müller R, et al. Novel RGD lipopeptides for the targeting of liposomes to integrin-expressing endothelial and melanoma cells. Protein Eng Des Sel. 2004 May;17(5):433–41.

316. Lubitz LJ, Haffner MP, Rieger H, Leneweit G. Increased Cellular Uptake of ApoE3- or c(RGD)-Modified Liposomes for Glioblastoma Therapy Depending on the Target Cells. Pharmaceutics. 2024 Aug 23;16(9):1112.

317. Nierenberg D, Khaled AR, Flores O. Formation of a protein corona influences the biological identity of nanomaterials. Rep Pract Oncol Radiother. 2018;23(4):300–8.

318. Li H, Wang Y, Tang Q, Yin D, Tang C, He E, et al. The protein corona and its effects on nanoparticle-based drug delivery systems. Acta Biomaterialia. 2021 Jul;129:57–72.

319. Onishchenko N, Tretiakova D, Vodovozova E. Spotlight on the protein corona of liposomes. Acta Biomaterialia. 2021 Oct;134:57–78.

320. Nguyen VH, Lee BJ. Protein corona: a new approach for nanomedicine design. Int J Nanomedicine. 2017 Apr 18;12:3137–51.

321. Wang S, Zhang J, Zhou H, Lu YC, Jin X, Luo L, et al. The role of protein corona on nanodrugs for organ-targeting and its prospects of application. Journal of Controlled Release. 2023 Aug;360:15–43.

322. Tasciotti E, Molinaro R, Taraballi F, Toledano Furman N, Sherman M, Parodi A, et al. Effects of the protein corona on liposome-liposome and liposome-cell interactions. IJN. 2016 Jul;Volume 11:3049–63.

323. Caracciolo G, Cardarelli F, Pozzi D, Salomone F, Maccari G, Bardi G, et al. Selective targeting capability acquired with a protein corona adsorbed on the surface of 1,2-dioleoyl-3-trimethylammonium propane/DNA nanoparticles. ACS Appl Mater Interfaces. 2013 Dec 26;5(24):13171–9.

324. Papi M, Caputo D, Palmieri V, Coppola R, Palchetti S, Bugli F, et al. Clinically approved PEGylated nanoparticles are covered by a protein corona that boosts the uptake by cancer cells. Nanoscale. 2017 Jul 27;9(29):10327–34.

325. Arcella A, Palchetti S, Digiacomo L, Pozzi D, Capriotti AL, Frati L, et al. Brain Targeting by Liposome-Biomolecular Corona Boosts Anticancer Efficacy of Temozolomide in Glioblastoma Cells. ACS Chem Neurosci. 2018 Dec 19;9(12):3166–74.

326. Kim H, Röth D, Isoe Y, Hayashi K, Mochizuki C, Kalkum M, et al. Protein corona components of polyethylene glycol-conjugated organosilica nanoparticles modulates macrophage uptake. Colloids and Surfaces B: Biointerfaces. 2021 Mar;199:111527.

327. Walkey CD, Olsen JB, Guo H, Emili A, Chan WCW. Nanoparticle Size and Surface Chemistry Determine Serum Protein Adsorption and Macrophage Uptake. J Am Chem Soc. 2012 Feb 1;134(4):2139–47.

328. Cedervall T, Lynch I, Lindman S, Berggård T, Thulin E, Nilsson H, et al. Understanding the nanoparticle-protein corona using methods to quantify exchange rates and affinities of proteins for nanoparticles. Proc Natl Acad Sci U S A. 2007 Feb 13;104(7):2050–5.

329. Lynch I, Dawson KA, Linse S. Detecting cryptic epitopes created by nanoparticles. Sci STKE. 2006 Mar 21;2006(327):pe14.

330. Wheeler KE, Chetwynd AJ, Fahy KM, Hong BS, Tochihuitl JA, Foster LA, et al. Environmental dimensions of the protein corona. Nat Nanotechnol. 2021 Jun;16(6):617–29.

331. Vroman L, Adams AL, Fischer GC, Munoz PC. Interaction of high molecular weight kininogen, factor XII, and fibrinogen in plasma at interfaces. Blood. 1980 Jan;55(1):156–9.

332. Lundqvist M, Stigler J, Elia G, Lynch I, Cedervall T, Dawson KA. Nanoparticle size and surface properties determine the protein corona with possible implications for biological impacts. Proc Natl Acad Sci U S A. 2008 Sep 23;105(38):14265–70.

333. Richtering W, Alberg I, Zentel R. Nanoparticles in the Biological Context: Surface Morphology and Protein Corona Formation. Small. 2020 Oct;16(39):e2002162.

334. Treuel L, Docter D, Maskos M, Stauber RH. Protein corona - from molecular adsorption to physiological complexity. Beilstein J Nanotechnol. 2015;6:857–73.

335. Cedervall T, Lynch I, Foy M, Berggård T, Donnelly SC, Cagney G, et al. Detailed identification of plasma proteins adsorbed on copolymer nanoparticles. Angew Chem Int Ed Engl. 2007;46(30):5754–6.

336. Tenzer S, Docter D, Rosfa S, Wlodarski A, Kuharev J, Rekik A, et al. Nanoparticle size is a critical physicochemical determinant of the human blood plasma corona: a comprehensive quantitative proteomic analysis. ACS Nano. 2011 Sep 27;5(9):7155–67.

337. Madathiparambil Visalakshan R, González García LE, Benzigar MR, Ghazaryan A, Simon J, Mierczynska-Vasilev A, et al. The Influence of Nanoparticle Shape on Protein Corona Formation. Small. 2020 Jun;16(25):e2000285.

338. Johnstone SA, Masin D, Mayer L, Bally MB. Surface-associated serum proteins inhibit the uptake of phosphatidylserine and poly(ethylene glycol) liposomes by mouse macrophages. Biochim Biophys Acta. 2001 Jul 2;1513(1):25–37.

339. Schrade A, Mailänder V, Ritz S, Landfester K, Ziener U. Surface roughness and charge influence the uptake of nanoparticles: fluorescently labeled pickering-type versus surfactant-stabilized nanoparticles. Macromol Biosci. 2012 Nov;12(11):1459–71.

340. Mahmoudi M, Serpooshan V. Large Protein Absorptions from Small Changes on the Surface of Nanoparticles. J Phys Chem C. 2011 Sep 22;115(37):18275–83.

341. Yu Q, Zhao L, Guo C, Yan B, Su G. Regulating Protein Corona Formation and Dynamic Protein Exchange by Controlling Nanoparticle Hydrophobicity. Front Bioeng Biotechnol. 2020;8:210.

342. Podila R, Chen R, Ke PC, Brown JM, Rao AM. Effects of surface functional groups on the formation of nanoparticle-protein corona. Appl Phys Lett. 2012 Dec 24;101(26):263701.

343. Pinals RL, Chio L, Ledesma F, Landry MP. Engineering at the nano-bio interface: harnessing the protein corona towards nanoparticle design and function. Analyst. 2020;145(15):5090–112.

344. Walkey CD, Chan WCW. Understanding and controlling the interaction of nanomaterials with proteins in a physiological environment. Chem Soc Rev. 2012 Mar 12;41(7):2780–99.

345. Walczyk D, Bombelli FB, Monopoli MP, Lynch I, Dawson KA. What the cell 'sees' in bionanoscience. J Am Chem Soc. 2010 Apr 28;132(16):5761–8.

346. Winzen S, Schoettler S, Baier G, Rosenauer C, Mailaender V, Landfester K, et al. Complementary analysis of the hard and soft protein corona: sample preparation critically effects corona composition. Nanoscale. 2015 Feb 5;7(7):2992–3001.

347. Monopoli MP, Åberg C, Salvati A, Dawson KA. Biomolecular coronas provide the biological identity of nanosized materials. Nature Nanotech. 2012 Dec;7(12):779–86.

348. Han GS, Domaille DW. Protein Corona, with a Twist. ACS Cent Sci. 2020 Jan 22;6(1):14–5.

349. Zanganeh S, Spitler R, Erfanzadeh M, Alkilany AM, Mahmoudi M. Protein corona: Opportunities and challenges. Int J Biochem Cell Biol. 2016 Jun;75:143–7.

350. Mahmoudi M, Lynch I, Ejtehadi MR, Monopoli MP, Bombelli FB, Laurent S. Protein-nanoparticle interactions: opportunities and challenges. Chem Rev. 2011 Sep 14;111(9):5610–37.

351. Schöttler S, Landfester K, Mailänder V. Controlling the Stealth Effect of Nanocarriers through Understanding the Protein Corona. Angew Chem Int Ed Engl. 2016 Jul 25;55(31):8806–15.

352. Miclăuş T, Bochenkov VE, Ogaki R, Howard KA, Sutherland DS. Spatial mapping and quantification of soft and hard protein coronas at silver nanocubes. Nano Lett. 2014;14(4):2086–93.

353. Lundqvist M, Augustsson C, Lilja M, Lundkvist K, Dahlbäck B, Linse S, et al. The nanoparticle protein corona formed in human blood or human blood fractions. PLoS One. 2017;12(4):e0175871.

354. Hadjidemetriou M, Al-Ahmady Z, Mazza M, Collins RF, Dawson K, Kostarelos K. In Vivo Biomolecule Corona around Blood-Circulating, Clinically Used and Antibody-Targeted Lipid Bilayer Nanoscale Vesicles. ACS Nano. 2015 Aug 25;9(8):8142–56.

355. Gunawan C, Lim M, Marquis CP, Amal R. Nanoparticle–protein corona complexes govern the biological fates and functions of nanoparticles. J Mater Chem B. 2014 Mar 19;2(15):2060–83.

356. Weber C, Morsbach S, Landfester K. Possibilities and Limitations of Different Separation Techniques for the Analysis of the Protein Corona. Angew Chem Int Ed. 2019 Sep 9;58(37):12787–94.

357. Palchetti S, Colapicchioni V, Digiacomo L, Caracciolo G, Pozzi D, Capriotti AL, et al. The protein corona of circulating PEGylated liposomes. Biochimica et Biophysica Acta (BBA) - Biomembranes. 2016 Feb;1858(2):189–96.

358. Caracciolo G, Pozzi D, Capriotti AL, Cavaliere C, Piovesana S, Amenitsch H, et al. Lipid composition: a “key factor” for the rational manipulation of the liposome–protein corona by liposome design. RSC Adv. 2014 Dec 17;5(8):5967–75.

359. Zhang Z, Guan J, Jiang Z, Yang Y, Liu J, Hua W, et al. Brain-targeted drug delivery by manipulating protein corona functions. Nat Commun. 2019 Aug 8;10(1):3561.

360. Han L, Zhan H, Sun X, Zhang ZR, Deng L. A Density-Changing Centrifugation Method for Efficient Separation of Free Drugs from Drug-Loaded Particulate Delivery Systems. AAPS J. 2019 Feb 25;21(3):33.

361. Chen D, Ganesh S, Wang W, Amiji M. The role of surface chemistry in serum protein corona-mediated cellular delivery and gene silencing with lipid nanoparticles. Nanoscale. 2019 May 9;11(18):8760–75.

362. Yang K, Mesquita B, Horvatovich P, Salvati A. Tuning liposome composition to modulate corona formation in human serum and cellular uptake. Acta Biomater. 2020 Apr 1;106:314–27.

363. Münter R, Kristensen K, Pedersbæk D, Larsen JB, Simonsen JB, Andresen TL. Dissociation of fluorescently labeled lipids from liposomes in biological environments challenges the interpretation of uptake studies. Nanoscale. 2018 Dec 13;10(48):22720–4.

364. Docter D, Westmeier D, Markiewicz M, Stolte S, Knauer SK, Stauber RH. The nanoparticle biomolecule corona: lessons learned – challenge accepted? Chem Soc Rev. 2015 Aug 17;44(17):6094–121.

365. Digiacomo L, Giulimondi F, Laura Capriotti A, Piovesana S, Maria Montone C, Zenezini Chiozzi R, et al. Optimal centrifugal isolating of liposome–protein complexes from human plasma. Nanoscale Advances. 2021;3(13):3824–34.

366. Böhmert L, Voß L, Stock V, Braeuning A, Lampen A, Sieg H. Isolation methods for particle protein corona complexes from protein-rich matrices. Nanoscale Adv. 2020;2(2):563–82.

367. Simonsen JB, Münter R. Pay Attention to Biological Nanoparticles when Studying the Protein Corona on Nanomedicines. Angew Chem Int Ed Engl. 2020 Jul 27;59(31):12584–8.

368. Vlassov AV, Magdaleno S, Setterquist R, Conrad R. Exosomes: current knowledge of their composition, biological functions, and diagnostic and therapeutic potentials. Biochim Biophys Acta. 2012 Jul;1820(7):940–8.

369. von Zychlinski A, Kleffmann T. Dissecting the proteome of lipoproteins: New biomarkers for cardiovascular diseases? Translational Proteomics. 2015 Jun 1;7:30–9.

370. Kristensen K, Münter R, Kempen PJ, Thomsen ME, Stensballe A, Andresen TL. Isolation methods commonly used to study the liposomal protein corona suffer from contamination issues. Acta Biomater. 2021 Aug;130:460–72.

371. Botto M, Kirschfink M, Macor P, Pickering MC, Würzner R, Tedesco F. Complement in human diseases: Lessons from complement deficiencies. Mol Immunol. 2009 Sep;46(14):2774–83.

372. Macor P, Capolla S, Tedesco F. Complement as a Biological Tool to Control Tumor Growth. Front Immunol. 2018;9:2203.

373. Tavano R, Gabrielli L, Lubian E, Fedeli C, Visentin S, Polverino De Laureto P, et al. C1q-Mediated Complement Activation and C3 Opsonization Trigger Recognition of Stealth Poly(2-methyl-2-oxazoline)-Coated Silica Nanoparticles by Human Phagocytes. ACS Nano. 2018 Jun 26;12(6):5834–47.

374. Macor P, Tedesco F. Complement as effector system in cancer immunotherapy. Immunol Lett. 2007 Jul 31;111(1):6–13.

375. Merle NS, Church SE, Fremeaux-Bacchi V, Roumenina LT. Complement System Part I - Molecular Mechanisms of Activation and Regulation. Front Immunol. 2015;6:262.

376. Vu VP, Gifford GB, Chen F, Benasutti H, Wang G, Groman EV, et al. Immunoglobulin deposition on biomolecule corona determines complement opsonization efficiency of preclinical and clinical nanoparticles. Nat Nanotechnol. 2019 Mar;14(3):260–8.

377. Klapper Y, Hamad OA, Teramura Y, Leneweit G, Nienhaus GU, Ricklin D, et al. Mediation of a non-proteolytic activation of complement component C3 by phospholipid vesicles. Biomaterials. 2014 Apr;35(11):3688–96.

378. Panico S, Capolla S, Bozzer S, Toffoli G, Dal Bo M, Macor P. Biological Features of Nanoparticles: Protein Corona Formation and Interaction with the Immune System. Pharmaceutics. 2022 Nov 26;14(12):2605.

379. Pham CTN, Mitchell LM, Huang JL, Lubniewski CM, Schall OF, Killgore JK, et al. Variable antibody-dependent activation of complement by functionalized phospholipid nanoparticle surfaces. J Biol Chem. 2011 Jan 7;286(1):123–30.

380. La-Beck NM, Islam MdR, Markiewski MM. Nanoparticle-Induced Complement Activation: Implications for Cancer Nanomedicine. Front Immunol. 2021 Jan 8;11:603039.

381. Coty JB, Eleamen Oliveira E, Vauthier C. Tuning complement activation and pathway through controlled molecular architecture of dextran chains in nanoparticle corona. International Journal of Pharmaceutics. 2017 Nov 5;532(2):769–78.

382. Hamad I, Hunter AC, Szebeni J, Moghimi SM. Poly(ethylene glycol)s generate complement activation products in human serum through increased alternative pathway turnover and a MASP-2-dependent process. Mol Immunol. 2008 Dec;46(2):225–32.

383. Gabizon A, Martin F. Polyethylene glycol-coated (pegylated) liposomal doxorubicin. Rationale for use in solid tumours. Drugs. 1997;54 Suppl 4:15–21.

384. Szebeni J, Fontana JL, Wassef NM, Mongan PD, Morse DS, Dobbins DE, et al. Hemodynamic changes induced by liposomes and liposome-encapsulated hemoglobin in pigs: a model for pseudoallergic cardiopulmonary reactions to liposomes. Role of complement and inhibition by soluble CR1 and anti-C5a antibody. Circulation. 1999 May 4;99(17):2302–9.

385. Szebeni J. Complement activation-related pseudoallergy: a new class of drug-induced acute immune toxicity. Toxicology. 2005 Dec 15;216(2–3):106–21.

386. Szebeni J, Muggia F, Gabizon A, Barenholz Y. Activation of complement by therapeutic liposomes and other lipid excipient-based therapeutic products: prediction and prevention. Adv Drug Deliv Rev. 2011 Sep 16;63(12):1020–30.

387. Szebeni J, Bedőcs P, Urbanics R, Bünger R, Rosivall L, Tóth M, et al. Prevention of infusion reactions to PEGylated liposomal doxorubicin via tachyphylaxis induction by placebo vesicles: a porcine model. J Control Release. 2012 Jun 10;160(2):382–7.

388. Pedersen MB, Zhou X, Larsen EKU, Sørensen US, Kjems J, Nygaard JV, et al. Curvature of synthetic and natural surfaces is an important target feature in classical pathway complement activation. J Immunol. 2010 Feb 15;184(4):1931–45.

389. Szebeni J, Bedőcs P, Rozsnyay Z, Weiszhár Z, Urbanics R, Rosivall L, et al. Liposome-induced complement activation and related cardiopulmonary distress in pigs: factors promoting reactogenicity of Doxil and AmBisome. Nanomedicine: Nanotechnology, Biology and Medicine. 2012 Feb 1;8(2):176–84.

390. Matsumura Y, Gotoh M, Muro K, Yamada Y, Shirao K, Shimada Y, et al. Phase I and pharmacokinetic study of MCC-465, a doxorubicin (DXR) encapsulated in PEG immunoliposome, in patients with metastatic stomach cancer. Ann Oncol. 2004 Mar;15(3):517–25.

391. Fridman WH. Fc receptors and immunoglobulin binding factors. FASEB J. 1991 Sep;5(12):2684–90.

392. Amara U, Flierl MA, Rittirsch D, Klos A, Chen H, Acker B, et al. Molecular intercommunication between the complement and coagulation systems. J Immunol. 2010 Nov 1;185(9):5628–36.

393. Lee YK, Choi EJ, Webster TJ, Kim SH, Khang D. Effect of the protein corona on nanoparticles for modulating cytotoxicity and immunotoxicity. Int J Nanomedicine. 2015;10:97–113.

394. Deng ZJ, Liang M, Monteiro M, Toth I, Minchin RF. Nanoparticle-induced unfolding of fibrinogen promotes Mac-1 receptor activation and inflammation. Nat Nanotechnol. 2011 Jan;6(1):39–44.

395. Papini E, Tavano R, Mancin F. Opsonins and Dysopsonins of Nanoparticles: Facts, Concepts, and Methodological Guidelines. Front Immunol. 2020 Oct 12;11:567365.

396. Hamilton KK, Zhao J, Sims PJ. Interaction between apolipoproteins A-I and A-II and the membrane attack complex of complement. Affinity of the apoproteins for polymeric C9. J Biol Chem. 1993 Feb 15;268(5):3632–8.

397. Aoyama M, Hata K, Higashisaka K, Nagano K, Yoshioka Y, Tsutsumi Y. Clusterin in the protein corona plays a key role in the stealth effect of nanoparticles against phagocytes. Biochem Biophys Res Commun. 2016 Nov 25;480(4):690–5.

398. Thiele L, Diederichs JE, Reszka R, Merkle HP, Walter E. Competitive adsorption of serum proteins at microparticles affects phagocytosis by dendritic cells. Biomaterials. 2003 Apr;24(8):1409–18.

399. Ogawara K ichi, Furumoto K, Nagayama S, Minato K, Higaki K, Kai T, et al. Pre-coating with serum albumin reduces receptor-mediated hepatic disposition of polystyrene nanosphere: implications for rational design of nanoparticles. J Control Release. 2004 Dec 10;100(3):451–5.

400. Schöttler S, Becker G, Winzen S, Steinbach T, Mohr K, Landfester K, et al. Protein adsorption is required for stealth effect of poly(ethylene glycol)- and poly(phosphoester)-coated nanocarriers. Nature Nanotech. 2016 Apr;11(4):372–7.

401. Yang K, Reker-Smit C, Stuart MCA, Salvati A. Effects of Protein Source on Liposome Uptake by Cells: Corona Composition and Impact of the Excess Free Proteins. Adv Healthcare Materials. 2021 Jul;10(14):2100370.

402. Van der Sanden N, Paun RA, Yitayew MY, Boyadjian O, Tabrizian M. An investigation of the effect of the protein corona on the cellular uptake of nanoliposomes under flow conditions using quartz crystal microgravimetry with dissipation. Nanoscale Adv. 7(1):169–84.

403. Caracciolo G. Liposome–protein corona in a physiological environment: Challenges and opportunities for targeted delivery of nanomedicines. Nanomedicine: Nanotechnology, Biology and Medicine. 2015 Apr;11(3):543–57.

404. Nguyen VH, Lee BJ. Protein corona: a new approach for nanomedicine design. Int J Nanomedicine. 2017 Apr 18;12:3137–51.

405. Mahmoudi M, Landry MP, Moore A, Coreas R. The protein corona from nanomedicine to environmental science. Nat Rev Mater. 2023 Mar 24;8(7):422–38.

406. Yu Y, Luan Y, Dai W. Dynamic process, mechanisms, influencing factors and study methods of protein corona formation. International Journal of Biological Macromolecules. 2022 Apr 30;205:731–9.

407. Wolfram J, Suri K, Yang Y, Shen J, Celia C, Fresta M, et al. Shrinkage of pegylated and non-pegylated liposomes in serum. Colloids Surf B Biointerfaces. 2014 Feb 1;114:294–300.

408. Tan X, Welsher K. Particle-by-particle in situ characterization of the protein corona via real-time 3D single-particle tracking spectroscopy. Angew Chem Int Ed Engl. 2021 Oct 4;60(41):22359–67.

409. Hadjidemetriou M, McAdam S, Garner G, Thackeray C, Knight D, Smith D, et al. The Human In Vivo Biomolecule Corona onto PEGylated Liposomes: A Proof-of-Concept Clinical Study. Adv Mater. 2019 Jan;31(4):e1803335.

410. Palchetti S, Colapicchioni V, Digiacomo L, Caracciolo G, Pozzi D, Capriotti AL, et al. The protein corona of circulating PEGylated liposomes. Biochimica et Biophysica Acta (BBA) - Biomembranes. 2016 Feb;1858(2):189–96.

411. Palchetti S, Caputo D, Digiacomo L, Capriotti AL, Coppola R, Pozzi D, et al. Protein Corona Fingerprints of Liposomes: New Opportunities for Targeted Drug Delivery and Early Detection in Pancreatic Cancer. Pharmaceutics. 2019 Jan 15;11(1):31.

412. Chou CY, Chiang PC, Li CC, Chang JW, Lu PH, Hsu WF, et al. Improving the Purity of Extracellular Vesicles by Removal of Lipoproteins from Size Exclusion Chromatography- and Ultracentrifugation-Processed Samples Using Glycosaminoglycan-Functionalized Magnetic Beads. ACS Appl Mater Interfaces. 2024 Aug 28;16(34):44386–98.

413. Benayas B, Morales J, Egea C, Armisén P, Yáñez-Mó M. Optimization of extracellular vesicle isolation and their separation from lipoproteins by size exclusion chromatography. Journal of Extracellular Biology. 2023;2(7):e100.

414. Onishchenko N, Tretiakova D, Vodovozova E. Spotlight on the protein corona of liposomes. Acta Biomaterialia. 2021 Oct;134:57–78.

415. Hadjidemetriou M, McAdam S, Garner G, Thackeray C, Knight D, Smith D, et al. The Human In Vivo Biomolecule Corona onto PEGylated Liposomes: A Proof-of-Concept Clinical Study. Adv Mater. 2019 Jan;31(4):e1803335.

416. Tran TT, Roffler SR. Interactions between nanoparticle corona proteins and the immune system. Current Opinion in Biotechnology. 2023 Dec 1;84:103010.

417. Caracciolo G, Pozzi D, Capriotti AL, Cavaliere C, Piovesana S, La Barbera G, et al. The liposome–protein corona in mice and humans and its implications for in vivo delivery. J Mater Chem B. 2014 Sep 5;2(42):7419–28.

418. Bai X, Wang J, Mu Q, Su G. In vivo Protein Corona Formation: Characterizations, Effects on Engineered Nanoparticles' Biobehaviors, and Applications. Front Bioeng Biotechnol. 2021 Mar 31;9:646708.

419. Serpina3k serine (or cysteine) peptidase inhibitor, clade A, member 3K [Mus musculus (house mouse)] - Gene - NCBI [Internet]. [cited 2025 Jan 2]. Available from: https://www.ncbi.nlm.nih.gov/gene/20714

420. Serpina1b serine (or cysteine) preptidase inhibitor, clade A, member 1B [Mus musculus (house mouse)] - Gene - NCBI [Internet]. [cited 2025 Jan 2]. Available from: https://www.ncbi.nlm.nih.gov/gene/20701

421. Serpina1d serine (or cysteine) peptidase inhibitor, clade A, member 1D [Mus musculus (house mouse)] - Gene - NCBI [Internet]. [cited 2025 Jan 2]. Available from: https://www.ncbi.nlm.nih.gov/gene/20703

422. Kng1 kininogen 1 [Mus musculus (house mouse)] - Gene - NCBI [Internet]. [cited 2025 Jan 2]. Available from: https://www.ncbi.nlm.nih.gov/gene?Db=gene&Cmd=DetailsSearch&Term=16644

423. Ces1c carboxylesterase 1C [Mus musculus (house mouse)] - Gene - NCBI [Internet]. [cited 2025 Jan 2]. Available from: https://www.ncbi.nlm.nih.gov/gene/13884

424. Hpx hemopexin [Mus musculus (house mouse)] - Gene - NCBI [Internet]. [cited 2025 Jan 2]. Available from: https://www.ncbi.nlm.nih.gov/gene?Db=gene&Cmd=DetailsSearch&Term=15458#bibliography

425. Mug1 murinoglobulin 1 [Mus musculus (house mouse)] - Gene - NCBI [Internet]. [cited 2025 Jan 2]. Available from: https://www.ncbi.nlm.nih.gov/gene?Db=gene&Cmd=DetailsSearch&Term=17836

426. Wilson ZS, Raya-Sandino A, Miranda J, Fan S, Brazil JC, Quiros M, et al. Critical role of thrombospondin-1 in promoting intestinal mucosal wound repair. JCI Insight. 2024 Jul 30;9(17):e180608.

427. Cpn1 carboxypeptidase N, polypeptide 1 [Mus musculus (house mouse)] - Gene - NCBI [Internet]. [cited 2025 Jan 2]. Available from: https://www.ncbi.nlm.nih.gov/gene/93721

428. Gpld1 glycosylphosphatidylinositol specific phospholipase D1 [Mus musculus (house mouse)] - Gene - NCBI [Internet]. [cited 2025 Jan 2]. Available from: https://www.ncbi.nlm.nih.gov/gene/14756

429. He J, Wang C, Fang X, Li J, Shen X, Zhang J, et al. Tuning the fluidity and protein corona of ultrasound-responsive liposomal nanovaccines to program T cell immunity in mice. Nat Commun. 2024 Sep 16;15:8121.

430. Javid H, Oryani MA, Rezagholinejad N, Esparham A, Tajaldini M, Karimi-Shahri M. RGD peptide in cancer targeting: Benefits, challenges, solutions, and possible integrin–RGD interactions. Cancer Med. 2024 Feb 1;13(2):e6800.

431. Mata E, Igartua M, Patarroyo ME, Pedraz JL, Hernández RM. Enhancing immunogenicity to PLGA microparticulate systems by incorporation of alginate and RGD-modified alginate. European Journal of Pharmaceutical Sciences. 2011 Sep 18;44(1):32–40.

432. Deuker MFS, Mailänder V, Morsbach S, Landfester K. Anti-PEG antibodies enriched in the protein corona of PEGylated nanocarriers impact the cell uptake. Nanoscale Horiz. 2023;8(10):1377–85.

433. Papini E, Tavano R, Mancin F. Opsonins and Dysopsonins of Nanoparticles: Facts, Concepts, and Methodological Guidelines. Front Immunol. 2020 Oct 12;11:567365.

434. Moghimi SM, Simberg D. Complement activation turnover on surfaces of nanoparticles. Nano Today. 2017 Aug;15:8–10.

435. Gifford G, Vu VP, Banda NK, Holers VM, Wang G, Groman E, et al. Complement therapeutics meets nanomedicine: overcoming human complement activation and leukocyte uptake of nanomedicines with soluble domains of CD55. J Control Release. 2019 May 28;302:181–9.

436. Struijf EM, De La O Becerra KI, Ruyken M, De Haas CJC, Van Oosterom F, Siere DY, et al. Inhibition of cleavage of human complement component C5 and the R885H C5 variant by two distinct high affinity anti-C5 nanobodies. Journal of Biological Chemistry. 2023 Aug;299(8):104956.

437. Nilsson SC, Sim RB, Lea SM, Fremeaux-Bacchi V, Blom AM. Complement factor I in health and disease. Mol Immunol. 2011 Aug;48(14):1611–20.

438. Scharnetzki D, Stappers F, Lenders M, Brand E. Detailed epitope mapping of neutralizing anti-drug antibodies against recombinant α-galactosidase A in patients with Fabry disease. Mol Genet Metab. 2020;131(1–2):229–34.

439. Sroda K, Rydlewski J, Langner M, Kozubek A, Grzybek M, Sikorski AF. Repeated injections of PEG-PE liposomes generate anti-PEG antibodies. Cell Mol Biol Lett. 2005;10(1):37–47.

440. Nevskaya KV, Krivoshchekov SV, Zima AP, Baikov AN, Gur'ev AM, Pershina AG. The Level of Anti-Polyethylene Glycol (PEG) Immunoglobulin G Antibodies in Human Serum Does Not Correlate with Efficiency of PEGylated Nanoparticle Uptake by Monocytes. Bull Exp Biol Med. 2023 Jun;175(2):270–4.

441. Dal Magro R, Ornaghi F, Cambianica I, Beretta S, Re F, Musicanti C, et al. ApoE-modified solid lipid nanoparticles: A feasible strategy to cross the blood-brain barrier. Journal of Controlled Release. 2017 Mar 10;249:103–10.

442. Kreuter J, Shamenkov D, Petrov V, Ramge P, Cychutek K, Koch-Brandt C, et al. Apolipoprotein-mediated transport of nanoparticle-bound drugs across the blood-brain barrier. J Drug Target. 2002 Jun;10(4):317–25.

443. Pozzi D, Colapicchioni V, Caracciolo G, Piovesana S, Capriotti AL, Palchetti S, et al. Effect of polyethyleneglycol (PEG) chain length on the bio-nano-interactions between PEGylated lipid nanoparticles and biological fluids: from nanostructure to uptake in cancer cells. Nanoscale. 2014 Mar 7;6(5):2782–92.

444. Pattipeiluhu R, Crielaard S, Klein-Schiphorst I, Florea BI, Kros A, Campbell F. Unbiased Identification of the Liposome Protein Corona using Photoaffinity-based Chemoproteomics. ACS Cent Sci. 2020 Apr 22;6(4):535–45.

445. Digiacomo L, Cardarelli F, Pozzi D, Palchetti S, Digman MA, Gratton E, et al. An apolipoprotein-enriched biomolecular corona switches the cellular uptake mechanism and trafficking pathway of lipid nanoparticles. Nanoscale. 2017 Nov 16;9(44):17254–62.

446. Vogt LM, Kwasniewicz E, Talens S, Scavenius C, Bielecka E, Ekdahl KN, et al. Apolipoprotein E Triggers Complement Activation in Joint Synovial Fluid of Rheumatoid Arthritis Patients by Binding C1q. J Immunol. 2020 May 15;204(10):2779–90.

447. Bisgaier CL, Siebenkas MV, Williams KJ. Effects of apolipoproteins A-IV and A-I on the uptake of phospholipid liposomes by hepatocytes. J Biol Chem. 1989 Jan 15;264(2):862–6.

448. Schäffler M, Sousa F, Wenk A, Sitia L, Hirn S, Schleh C, et al. Blood protein coating of gold nanoparticles as potential tool for organ targeting. Biomaterials. 2014 Mar;35(10):3455–66.

449. Marques C, Hajipour MJ, Marets C, Oudot A, Safavi-Sohi R, Guillemin M, et al. Identification of the Proteins Determining the Blood Circulation Time of Nanoparticles. ACS Nano. 2023 Jul 11;17(13):12458–70.

450. Fedeli C, Segat D, Tavano R, Bubacco L, Franceschi GD, Laureto PP de, et al. The functional dissection of the plasma corona of SiO2-NPs spots histidine rich glycoprotein as a major player able to hamper nanoparticle capture by macrophages. Nanoscale. 2015 Oct 22;7(42):17710–28.

451. Ritz S, Schöttler S, Kotman N, Baier G, Musyanovych A, Kuharev J, et al. Protein Corona of Nanoparticles: Distinct Proteins Regulate the Cellular Uptake. Biomacromolecules. 2015 Apr 13;16(4):1311–21.

452. Taguchi K, Okamoto Y, Matsumoto K, Otagiri M, Chuang VTG. When Albumin Meets Liposomes: A Feasible Drug Carrier for Biomedical Applications. Pharmaceuticals (Basel). 2021 Mar 26;14(4):296.

453. Schöttler S, Becker G, Winzen S, Steinbach T, Mohr K, Landfester K, et al. Protein adsorption is required for stealth effect of poly(ethylene glycol)- and poly(phosphoester)-coated nanocarriers. Nature Nanotech. 2016 Apr;11(4):372–7.

454. Capriotti AL, Caracciolo G, Cavaliere C, Foglia P, Pozzi D, Samperi R, et al. Do plasma proteins distinguish between liposomes of varying charge density? J Proteomics. 2012 Mar 16;75(6):1924–32.

455. Kawanishi M, Hashimoto Y, Shimizu T, Sagawa I, Ishida T, Kiwada H. Comprehensive analysis of PEGylated liposome-associated proteins relating to the accelerated blood clearance phenomenon by combination with shotgun analysis and conventional methods. Biotechnol Appl Biochem. 2015;62(4):547–55.

456. Caracciolo G, Pozzi D, Capriotti AL, Cavaliere C, Foglia P, Amenitsch H, et al. Evolution of the protein corona of lipid gene vectors as a function of plasma concentration. Langmuir. 2011 Dec 20;27(24):15048–53.

457. Caracciolo G, Palchetti S, Colapicchioni V, Digiacomo L, Pozzi D, Capriotti AL, et al. Stealth effect of biomolecular corona on nanoparticle uptake by immune cells. Langmuir. 2015 Oct 6;31(39):10764–73.

458. Mosesson MW, Siebenlist KR, Meh DA. The structure and biological features of fibrinogen and fibrin. Ann N Y Acad Sci. 2001;936:11–30.

459. Price ME, Cornelius RM, Brash JL. Protein adsorption to polyethylene glycol modified liposomes from fibrinogen solution and from plasma. Biochim Biophys Acta. 2001 Jun 6;1512(2):191–205.

460. Amici A, Caracciolo G, Digiacomo L, Gambini V, Marchini C, Tilio M, et al. In vivo protein corona patterns of lipid nanoparticles. RSC Adv. 2017 Jan 3;7(2):1137–45.

461. Terstappen GC, Meyer AH, Bell RD, Zhang W. Strategies for delivering therapeutics across the blood-brain barrier. Nat Rev Drug Discov. 2021 May;20(5):362–83.

462. Naidu PSR, Gavriel N, Gray CGG, Bartlett CA, Toomey LM, Kretzmann JA, et al. Elucidating the Inability of Functionalized Nanoparticles to Cross the Blood-Brain Barrier and Target Specific Cells in Vivo. ACS Applied Materials and Interfaces [Internet]. 2019 May 31 [cited 2025 Jan 4];11(25). Available from: https://research.monash.edu/en/publications/elucidating-the-inability-of-functionalized-nanoparticles-to-cros

463. Sobczynski DJ, Eniola-Adefeso O. IgA and IgM protein primarily drive plasma corona-induced adhesion reduction of PLGA nanoparticles in human blood flow. Bioeng Transl Med. 2017 Jun;2(2):180–90.

464. Sobczynski DJ, Charoenphol P, Heslinga MJ, Onyskiw PJ, Namdee K, Thompson AJ, et al. Plasma protein corona modulates the vascular wall interaction of drug carriers in a material and donor specific manner. PLoS One. 2014;9(9):e107408.

465. Halter M, Antia M, Vogel V. Fibronectin conformational changes induced by adsorption to liposomes. Journal of Controlled Release. 2005 Jan;101(1–3):209–22.

466. Aramaki Y, Akiyama K, Hara T, Tsuchiya S. Recognition of charged liposomes by rat peritoneal and splenic macrophages: effects of fibronectin on the uptake of charged liposomes. European Journal of Pharmaceutical Sciences. 1995 Apr 1;3(2):63–70.

467. Gailit J, Ruoslahti E. Regulation of the fibronectin receptor affinity by divalent cations. J Biol Chem. 1988 Sep 15;263(26):12927–32.

468. Pytela R, Pierschbacher MD, Ruoslahti E. A 125/115-kDa cell surface receptor specific for vitronectin interacts with the arginine-glycine-aspartic acid adhesion sequence derived from fibronectin. Proceedings of the National Academy of Sciences. 1985 Sep;82(17):5766–70.

469. Turner MW. The role of mannose-binding lectin in health and disease. Mol Immunol. 2003 Nov;40(7):423–9.

470. Hazarika Z, Nath Jha A. Structural and functional premise of transport protein transthyretin in the sight of silver and zinc oxide nanoparticles through atomistic simulations. Inorganica Chimica Acta. 2024 Apr 1;563:121923.

471. Yang K, Reker-Smit C, Stuart MCA, Salvati A. Effects of Protein Source on Liposome Uptake by Cells: Corona Composition and Impact of the Excess Free Proteins. Adv Healthcare Materials. 2021 Jul;10(14):2100370.

472. Tasciotti E, Molinaro R, Taraballi F, Toledano Furman N, Sherman M, Parodi A, et al. Effects of the protein corona on liposome-liposome and liposome-cell interactions. IJN. 2016 Jul;Volume 11:3049–63.

473. Dai Q, Yan Y, Guo J, Björnmalm M, Cui J, Sun H, et al. Targeting Ability of Affibody-Functionalized Particles Is Enhanced by Albumin but Inhibited by Serum Coronas. ACS Macro Lett. 2015 Nov 17;4(11):1259–63.

474. Gangadaran P, Ahn BC. Extracellular Vesicle- and Extracellular Vesicle Mimetics-Based Drug Delivery Systems: New Perspectives, Challenges, and Clinical Developments. Pharmaceutics. 2020 May 11;12(5):442.

475. Luo R, Liu M, Tan T, Yang Q, Wang Y, Men L, et al. Emerging Significance and Therapeutic Potential of Extracellular vesicles. Int J Biol Sci. 2021 Jun 16;17(10):2476–86.

476. Ramos-Zaldívar HM, Polakovicova I, Salas-Huenuleo E, Corvalán AH, Kogan MJ, Yefi CP, et al. Extracellular vesicles through the blood–brain barrier: a review. Fluids Barriers CNS. 2022 Jul 25;19(1):60.

477. Nawaz M, Tangruksa B, Heydarkhan-Hagvall S, Kohl F, Garibotti HGK, Jing Y, et al. Targeted delivery of mRNA to the heart via extracellular vesicles or lipid nanoparticles [Internet]. bioRxiv; 2025 [cited 2025 Feb 23]. p. 2025.01.25.634881. Available from: https://www.biorxiv.org/content/10.1101/2025.01.25.634881v1

478. Andriolo G, Provasi E, Lo Cicero V, Brambilla A, Soncin S, Torre T, et al. Exosomes From Human Cardiac Progenitor Cells for Therapeutic Applications: Development of a GMP-Grade Manufacturing Method. Front Physiol [Internet]. 2018 Aug 24 [cited 2024 Nov 8];9. Available from: https://www.frontiersin.org/journals/physiology/articles/10.3389/fphys.2018.01169/full

479. de Almeida Fuzeta M, Bernardes N, Oliveira FD, Costa AC, Fernandes-Platzgummer A, Farinha JP, et al. Scalable Production of Human Mesenchymal Stromal Cell-Derived Extracellular Vesicles Under Serum-/Xeno-Free Conditions in a Microcarrier-Based Bioreactor Culture System. Front Cell Dev Biol [Internet]. 2020 Nov 3 [cited 2024 Nov 8];8. Available from: https://www.frontiersin.org/journals/cell-and-developmental-biology/articles/10.3389/fcell.2020.553444/full

480. Wiklander OPB, Brennan MÁ, Lötvall J, Breakefield XO, EL Andaloussi S. Advances in therapeutic applications of extracellular vesicles. Sci Transl Medel. 2019 May 15;11(492):eaav8521.

481. Hettich BF, Bader JJ, Leroux JC. Encapsulation of Hydrophilic Compounds in Small Extracellular Vesicles: Loading Capacity and Impact on Vesicle Functions. Adv Healthc Mater. 2021 May 5;11(5):2100047.

482. Li G, Chen T, Dahlman J, Eniola-Adefeso L, Ghiran IC, Kurre P, et al. Current challenges and future directions for engineering extracellular vesicles for heart, lung, blood and sleep diseases. J Extracell Vesicles. 2023 Feb;12(2):e12305.

483. Haney MJ, Klyachko NL, Zhao Y, Gupta R, Plotnikova EG, He Z, et al. Exosomes as Drug Delivery Vehicles for Parkinson's Disease Therapy. J Control Release. 2015 Jun 10;207:18–30.

484. Rankin-Turner S, Vader P, O'Driscoll L, Giebel B, Heaney LM, Davies OG. A call for the standardised reporting of factors affecting the exogenous loading of extracellular vesicles with therapeutic cargos. Adv Drug Deliv Rev. 2021 Jun;173:479–91.

485. Pham TC, Jayasinghe MK, Pham TT, Yang Y, Wei L, Usman WM, et al. Covalent conjugation of extracellular vesicles with peptides and nanobodies for targeted therapeutic delivery. J Extracell Vesicles. 2021 Feb 16;10(4):e12057.

486. Rädler J, Gupta D, Zickler A, Andaloussi SE. Exploiting the biogenesis of extracellular vesicles for bioengineering and therapeutic cargo loading. Mol Ther. 2023 May 3;31(5):1231–50.

487. Inano S, Kitano T. A modified CD9 tag for efficient protein delivery via extracellular vesicles. PLoS One. 2024 Oct 17;19(10):e0310083.

488. Zheng W, Rädler J, Sork H, Niu Z, Roudi S, Bost JP, et al. Identification of scaffold proteins for improved endogenous engineering of extracellular vesicles. Nat Commun. 2023 Aug 7;14:4734.

489. Peruzzi JA, Gunnels TF, Edelstein HI, Lu P, Baker D, Leonard JN, et al. Enhancing extracellular vesicle cargo loading and functional delivery by engineering protein-lipid interactions. Nat Commun. 2024 Jul 4;15(1):5618.

490. Silva AM, Lázaro-Ibáñez E, Gunnarsson A, Dhande A, Daaboul G, Peacock B, et al. Quantification of protein cargo loading into engineered extracellular vesicles at single-vesicle and single-molecule resolution. J Extracell Vesicles. 2021 Aug;10(10):e12130.

491. Lundberg P, Langel Ü. A brief introduction to cell-penetrating peptides. Journal of Molecular Recognition. 2003;16(5):227–33.

492. Patel SG, Sayers EJ, He L, Narayan R, Williams TL, Mills EM, et al. Cell-penetrating peptide sequence and modification dependent uptake and subcellular distribution of green florescent protein in different cell lines. Sci Rep. 2019 Apr 18;9(1):6298.

493. Gori A, Lodigiani G, Colombarolli SG, Bergamaschi G, Vitali A. Cell Penetrating Peptides: Classification, Mechanisms, Methods of Study, and Applications. ChemMedChem. 2023;18(17):e202300236.

494. Lindgren M, Hällbrink M, Prochiantz A, Langel Ü, Lindgren M, Hällbrink M, et al. Cell-penetrating peptides. Trends in Pharmacological Sciences. 2000 Mar 1;21(3):99–103.

495. Guidotti G, Brambilla L, Rossi D. Cell-Penetrating Peptides: From Basic Research to Clinics. Trends in Pharmacological Sciences. 2017 Apr 1;38(4):406–24.

496. Swanson WB, Zhang Z, Xiu K, Gong T, Eberle M, Wang Z, et al. Scaffolds with Controlled Release of Pro-Mineralization Exosomes to Promote Craniofacial Bone Healing without Cell Transplantation. Acta Biomater. 2020 Oct 13;118:215.

497. Wei X, Liu S, Cao Y, Wang Z, Chen S. Polymers in Engineering Extracellular Vesicle Mimetics: Current Status and Prospective. Pharmaceutics. 2023 May 14;15(5):1496.

498. Flanagan M, Pathak I, Gan Q, Winter L, Emnet R, Akel S, et al. Umbilical mesenchymal stem cell-derived extracellular vesicles as enzyme delivery vehicle to treat Morquio A fibroblasts. Stem Cell Res Ther. 2021 May 6;12(1):276.

499. Iglesias DM, El-Kares R, Taranta A, Bellomo F, Emma F, Besouw M, et al. Stem Cell Microvesicles Transfer Cystinosin to Human Cystinotic Cells and Reduce Cystine Accumulation In Vitro. PLoS ONE. 2012 Aug 13;7(8):e42840.

500. Thomas VJC, Caterson B, Kao WWY. Transplantation of human umbilical mesenchymal stem cells cures the corneal defects of Mucopolysaccharidosis VII mice. Stem Cells. 2013 Oct;31(10):10.1002/stem.1481.

501. Haney MJ, Klyachko NL, Harrison EB, Zhao Y, Kabanov AV, Batrakova EV. TPP1 Delivery to Lysosomes with Extracellular Vesicles and their Enhanced Brain Distribution in the Animal Model of Batten Disease. Adv Healthc Mater. 2019 Jun;8(11):e1801271.

502. El-Hage N, Haney MJ, Zhao Y, Rodriguez M, Wu Z, Liu M, et al. Extracellular Vesicles Released by Genetically Modified Macrophages Activate Autophagy and Produce Potent Neuroprotection in Mouse Model of Lysosomal Storage Disorder, Batten Disease. Cells. 2023 Jan;12(11):1497.

503. Calzoni E, Cerrotti G, Sagini K, Delo F, Buratta S, Pellegrino RM, et al. Evidence of Lysosomal β-Hexosaminidase Enzymatic Activity Associated with Extracellular Vesicles: Potential Applications for the Correction of Sandhoff Disease. J Funct Biomater. 2024 Jun 4;15(6):153.

504. Do MA, Levy D, Brown A, Marriott G, Lu B. Targeted delivery of lysosomal enzymes to the endocytic compartment in human cells using engineered extracellular vesicles. Sci Rep. 2019 Nov 21;9(1):17274.

505. Thoene J, Goss T, Witcher M, Mullet J, N'Kuli F, Van Der Smissen P, et al. In vitro correction of disorders of lysosomal transport by microvesicles derived from baculovirus-infected Spodoptera cells. Mol Genet Metab. 2013 May;109(1):77–85.

506. Van Hoecke L, Van Cauwenberghe C, Börger V, Bruggeman A, Castelein J, Van Imschoot G, et al. Anti-Inflammatory Mesenchymal Stromal Cell-Derived Extracellular Vesicles Improve Pathology in Niemann–Pick Type C Disease. Biomedicines. 2021 Dec;9(12):1864.

507. Hean J, Lundin, Görgens A. Protein engineered extracellular vesicles. Oxford Science Park, Medawar Centre - 2nd Floor East Building, Robert Robinson Avenue, Oxford Oxfordshire OX4 4HG (GB).; WO 2019/092287 Al, 2019. p. 41.

508. He M, Zhou X, Wang X. Glycosylation: mechanisms, biological functions and clinical implications. Sig Transduct Target Ther. 2024 Aug 5;9(1):1–33.

509. Walsh G, Walsh E. Biopharmaceutical benchmarks 2022. Nat Biotechnol. 2022 Dec;40(12):1722–60.

510. Sarkar A, Wintrode PL. Effects of glycosylation on the stability and flexibility of a metastable protein: the human serpin α1-antitrypsin. Int J Mass Spectrom. 2011 Apr;302(1–3):69–75.

511. Bekri S. Importance of glycosylation in enzyme replacement therapy. In: Mehta A, Beck M, Sunder-Plassmann G, editors. Fabry Disease: Perspectives from 5 Years of FOS [Internet]. Oxford: Oxford PharmaGenesis; 2006 [cited 2024 Dec 17]. Available from: http://www.ncbi.nlm.nih.gov/books/NBK11598/

512. Kim TK, Eberwine JH. Mammalian cell transfection: the present and the future. Anal Bioanal Chem. 2010 Aug;397(8):3173–8.

513. Pham PL, Kamen A, Durocher Y. Large-Scale Transfection of Mammalian Cells for the Fast Production of Recombinant Protein. MB. 2006;34(2):225–38.

514. Wade-Martins R, Frampton J, James MR. Long-term stability of large insert genomic DNA episomal shuttle vectors in human cells. Nucleic Acids Res. 1999 Apr 1;27(7):1674–82.

515. Tan E, Chin CSH, Lim ZFS, Ng SK. HEK293 Cell Line as a Platform to Produce Recombinant Proteins and Viral Vectors. Front Bioeng Biotechnol. 2021;9:796991.

516. Boeckle S, von Gersdorff K, van der Piepen S, Culmsee C, Wagner E, Ogris M. Purification of polyethylenimine polyplexes highlights the role of free polycations in gene transfer. J Gene Med. 2004 Oct;6(10):1102–11.

517. Choi YJ, Kang SJ, Kim YJ, Lim YB, Chung HW. Comparative studies on the genotoxicity and cytotoxicity of polymeric gene carriers polyethylenimine (PEI) and polyamidoamine (PAMAM) dendrimer in Jurkat T-cells. Drug Chem Toxicol. 2010 Oct;33(4):357–66.

518. Kircheis R, Wightman L, Wagner E. Design and gene delivery activity of modified polyethylenimines. Adv Drug Deliv Rev. 2001 Dec 31;53(3):341–58.

519. Bieber T, Meissner W, Kostin S, Niemann A, Elsasser HP. Intracellular route and transcriptional competence of polyethylenimine-DNA complexes. J Control Release. 2002 Aug 21;82(2–3):441–54.

520. Kazemi Oskuee R, Dabbaghi M, Gholami L, Taheri-Bojd S, Balali-Mood M, Mousavi SH, et al. Investigating the influence of polyplex size on toxicity properties of polyethylenimine mediated gene delivery. Life Sci. 2018 Mar 15;197:101–8.

521. Wurm FM. Production of recombinant protein therapeutics in cultivated mammalian cells. Nat Biotechnol. 2004 Nov;22(11):1393–8.

522. Balasubramanian S, Wurm FM, Hacker DL. Multigene expression in stable CHO cell pools generated with the piggyBac transposon system. Biotechnol Prog. 2016 Sep;32(5):1308–17.

523. Maltais JS, Lord-Dufour S, Morasse A, Stuible M, Loignon M, Durocher Y. Repressing expression of difficult-to-express recombinant proteins during the selection process increases productivity of CHO stable pools. Biotechnol Bioeng. 2023 Oct;120(10):2840–52.

524. Baldi L, Hacker DL, Adam M, Wurm FM. Recombinant protein production by large-scale transient gene expression in mammalian cells: state of the art and future perspectives. Biotechnol Lett. 2007 May;29(5):677–84.

525. Croset A, Delafosse L, Gaudry JP, Arod C, Glez L, Losberger C, et al. Differences in the glycosylation of recombinant proteins expressed in HEK and CHO cells. Journal of Biotechnology. 2012 Oct;161(3):336–48.

526. Abaandou L, Quan D, Shiloach J. Affecting HEK293 Cell Growth and Production Performance by Modifying the Expression of Specific Genes. Cells. 2021 Jul 2;10(7):1667.

527. Meng W, He C, Hao Y, Wang L, Li L, Zhu G. Prospects and challenges of extracellular vesicle-based drug delivery system: considering cell source. Drug Delivery. 2020 Jan 1;27(1):585–98.

528. Taylor DD, Shah S. Methods of isolating extracellular vesicles impact down-stream analyses of their cargoes. Methods. 2015 Oct 1;87:3–10.

529. Kurian TK, Banik S, Gopal D, Chakrabarti S, Mazumder N. Elucidating Methods for Isolation and Quantification of Exosomes: A Review. Mol Biotechnol. 2021 Apr;63(4):249–66.

530. Yang D, Zhang W, Zhang H, Zhang F, Chen L, Ma L, et al. Progress, opportunity, and perspective on exosome isolation - efforts for efficient exosome-based theranostics. Theranostics. 2020;10(8):3684–707.

531. Alzhrani GN, Alanazi ST, Alsharif SY, Albalawi AM, Alsharif AA, Abdel-Maksoud MS, et al. Exosomes: Isolation, characterization, and biomedical applications. Cell Biol Int. 2021 Sep;45(9):1807–31.

532. Liu J, Chen Y, Pei F, Zeng C, Yao Y, Liao W, et al. Extracellular Vesicles in Liquid Biopsies: Potential for Disease Diagnosis. Biomed Res Int. 2021;2021:6611244.

533. Chen J, Li P, Zhang T, Xu Z, Huang X, Wang R, et al. Review on Strategies and Technologies for Exosome Isolation and Purification. Front Bioeng Biotechnol. 2021;9:811971.

534. Monguió-Tortajada M, Gálvez-Montón C, Bayes-Genis A, Roura S, Borràs FE. Extracellular vesicle isolation methods: rising impact of size-exclusion chromatography. Cell Mol Life Sci. 2019 Jun;76(12):2369–82.

535. Willms E, Johansson HJ, Mäger I, Lee Y, Blomberg KEM, Sadik M, et al. Cells release subpopulations of exosomes with distinct molecular and biological properties. Sci Rep. 2016 Mar 2;6:22519.

536. Bobrie A, Colombo M, Krumeich S, Raposo G, Théry C. Diverse subpopulations of vesicles secreted by different intracellular mechanisms are present in exosome preparations obtained by differential ultracentrifugation. J Extracell Vesicles. 2012;1.

537. Aalberts M, van Dissel-Emiliani FMF, van Adrichem NPH, van Wijnen M, Wauben MHM, Stout TAE, et al. Identification of distinct populations of prostasomes that differentially express prostate stem cell antigen, annexin A1, and GLIPR2 in humans. Biol Reprod. 2012 Mar;86(3):82.

538. Jeppesen DK, Hvam ML, Primdahl-Bengtson B, Boysen AT, Whitehead B, Dyrskjøt L, et al. Comparative analysis of discrete exosome fractions obtained by differential centrifugation. J Extracell Vesicles. 2014;3:25011.

539. Webber J, Clayton A. How pure are your vesicles? J Extracell Vesicles. 2013;2.

540. Goss DM, Vasilescu SA, Sacks G, Gardner DK, Warkiani ME. Microfluidics facilitating the use of small extracellular vesicles in innovative approaches to male infertility. Nat Rev Urol. 2023 Feb;20(2):66–95.

541. Lattmann E, Lapaire V, Levesque MP. Isolation and detection of extracellular vesicles from melanoma cells and liquid biopsies using size-exclusion chromatography and nano-flow cytometry. STAR Protoc. 2023 Sep 15;4(3):102365.

542. Konoshenko MYu, Lekchnov EA, Vlassov AV, Laktionov PP. Isolation of Extracellular Vesicles: General Methodologies and Latest Trends. BioMed Research International. 2018;2018(1):8545347.

543. Lobb RJ, Becker M, Wen SW, Wong CSF, Wiegmans AP, Leimgruber A, et al. Optimized exosome isolation protocol for cell culture supernatant and human plasma. J Extracell Vesicles. 2015;4:27031.

544. Gámez-Valero A, Monguió-Tortajada M, Carreras-Planella L, Franquesa M, Beyer K, Borràs FE. Size-Exclusion Chromatography-based isolation minimally alters Extracellular Vesicles' characteristics compared to precipitating agents. Sci Rep. 2016 Sep 19;6(1):33641.

545. Helwa I, Cai J, Drewry MD, Zimmerman A, Dinkins MB, Khaled ML, et al. A Comparative Study of Serum Exosome Isolation Using Differential Ultracentrifugation and Three Commercial Reagents. PLoS One. 2017;12(1):e0170628.

546. Tang YT, Huang YY, Zheng L, Qin SH, Xu XP, An TX, et al. Comparison of isolation methods of exosomes and exosomal RNA from cell culture medium and serum. Int J Mol Med. 2017 Sep;40(3):834–44.

547. Koliha N, Wiencek Y, Heider U, Jüngst C, Kladt N, Krauthäuser S, et al. A novel multiplex bead-based platform highlights the diversity of extracellular vesicles. J Extracell Vesicles. 2016;5:29975.

548. van der Pol E, Sturk A, van Leeuwen T, Nieuwland R, Coumans F, ISTH-SSC-VB Working group. Standardization of extracellular vesicle measurements by flow cytometry through vesicle diameter approximation. J Thromb Haemost. 2018 Jun;16(6):1236–45.

549. Libregts SFWM, Arkesteijn GJA, Németh A, Nolte-'t Hoen ENM, Wauben MHM. Flow cytometric analysis of extracellular vesicle subsets in plasma: impact of swarm by particles of non-interest. J Thromb Haemost. 2018 Jul;16(7):1423–36.

550. Ronquist GK, Larsson A, Stavreus-Evers A, Ronquist G. Prostasomes are heterogeneous regarding size and appearance but affiliated to one DNA-containing exosome family. Prostate. 2012 Dec 1;72(16):1736–45.

551. Lane RE, Korbie D, Trau M, Hill MM. Optimizing Size Exclusion Chromatography for Extracellular Vesicle Enrichment and Proteomic Analysis from Clinically Relevant Samples. Proteomics. 2019 Apr;19(8):e1800156.

552. Baranyai T, Herczeg K, Onódi Z, Voszka I, Módos K, Marton N, et al. Isolation of Exosomes from Blood Plasma: Qualitative and Quantitative Comparison of Ultracentrifugation and Size Exclusion Chromatography Methods. PLoS One. 2015;10(12):e0145686.

553. Böing AN, van der Pol E, Grootemaat AE, Coumans FAW, Sturk A, Nieuwland R. Single-step isolation of extracellular vesicles by size-exclusion chromatography. J Extracell Vesicles. 2014;3.

554. Muller L, Hong CS, Stolz DB, Watkins SC, Whiteside TL. Isolation of biologically-active exosomes from human plasma. J Immunol Methods. 2014 Sep;411:55–65.

555. Wiklander OPB, Bostancioglu RB, Welsh JA, Zickler AM, Murke F, Corso G, et al. Systematic Methodological Evaluation of a Multiplex Bead-Based Flow Cytometry Assay for Detection of Extracellular Vesicle Surface Signatures. Front Immunol. 2018;9:1326.

556. Sódar BW, Kittel Á, Pálóczi K, Vukman KV, Osteikoetxea X, Szabó-Taylor K, et al. Low-density lipoprotein mimics blood plasma-derived exosomes and microvesicles during isolation and detection. Sci Rep. 2016 Apr 18;6(1):24316.

557. Karimi N, Cvjetkovic A, Jang SC, Crescitelli R, Hosseinpour Feizi MA, Nieuwland R, et al. Detailed analysis of the plasma extracellular vesicle proteome after separation from lipoproteins. Cell Mol Life Sci. 2018 Aug;75(15):2873–86.

558. Zhang P, Yeo JC, Lim CT. Advances in Technologies for Purification and Enrichment of Extracellular Vesicles. SLAS Technol. 2019 Oct;24(5):477–88.

559. Zhang H, Lyden D. Asymmetric-flow field-flow fractionation technology for exomere and small extracellular vesicle separation and characterization. Nat Protoc. 2019 Apr;14(4):1027–53.

560. Gholizadeh S, Shehata Draz M, Zarghooni M, Sanati-Nezhad A, Ghavami S, Shafiee H, et al. Microfluidic approaches for isolation, detection, and characterization of extracellular vesicles: Current status and future directions. Biosens Bioelectron. 2017 May 15;91:588–605.

561. Guo SC, Tao SC, Dawn H. Microfluidics-based on-a-chip systems for isolating and analysing extracellular vesicles. J Extracell Vesicles. 2018;7(1):1508271.

562. Kanwar SS, Dunlay CJ, Simeone DM, Nagrath S. Microfluidic device (ExoChip) for On-Chip isolation, quantification and characterization of circulating exosomes. Lab Chip. 2014 Jun 7;14(11):1891–900.

563. Visan KS, Lobb RJ, Ham S, Lima LG, Palma C, Edna CPZ, et al. Comparative analysis of tangential flow filtration and ultracentrifugation, both combined with subsequent size exclusion chromatography, for the isolation of small extracellular vesicles. Journal of Extracellular Vesicles. 2022;11(9):12266.

564. Kawai-Harada Y, Nimmagadda V, Harada M. Scalable isolation of surface-engineered extracellular vesicles and separation of free proteins via tangential flow filtration and size exclusion chromatography (TFF-SEC). BMC Methods. 2024 Aug 1;1(1):9.

565. Gurriaran-Rodriguez U, De Repentigny Y, Kothary R, Rudnicki MA. Isolation of small extracellular vesicles from regenerating muscle tissue using tangential flow filtration and size exclusion chromatography. Skelet Muscle. 2024 Oct 11;14(1):22.

566. Benedikter BJ, Bouwman FG, Vajen T, Heinzmann ACA, Grauls G, Mariman EC, et al. Ultrafiltration combined with size exclusion chromatography efficiently isolates extracellular vesicles from cell culture media for compositional and functional studies. Sci Rep. 2017 Nov 10;7(1):15297.

567. Nordin JZ, Lee Y, Vader P, Mäger I, Johansson HJ, Heusermann W, et al. Ultrafiltration with size-exclusion liquid chromatography for high yield isolation of extracellular vesicles preserving intact biophysical and functional properties. Nanomedicine. 2015 May;11(4):879–83.

568. Guerreiro EM, Vestad B, Steffensen LA, Aass HCD, Saeed M, Øvstebø R, et al. Efficient extracellular vesicle isolation by combining cell media modifications, ultrafiltration, and size-exclusion chromatography. PLOS ONE. 2018 Sep 27;13(9):e0204276.

569. Oeyen E, Van Mol K, Baggerman G, Willems H, Boonen K, Rolfo C, et al. Ultrafiltration and size exclusion chromatography combined with asymmetrical-flow field-flow fractionation for the isolation and characterisation of extracellular vesicles from urine. Journal of Extracellular Vesicles. 2018 Dec 1;7(1):1490143.

570. Monguió-Tortajada M, Gálvez-Montón C, Bayes-Genis A, Roura S, Borràs FE. Extracellular vesicle isolation methods: rising impact of size-exclusion chromatography. Cell Mol Life Sci. 2019 Jun;76(12):2369–82.

571. Dong L, Zieren RC, Horie K, Kim C, Mallick E, Jing Y, et al. Comprehensive evaluation of methods for small extracellular vesicles separation from human plasma, urine and cell culture medium. J of Extracellular Vesicle. 2020 Dec;10(2):e12044.

572. Sidhom K, Obi PO, Saleem A. A Review of Exosomal Isolation Methods: Is Size Exclusion Chromatography the Best Option? IJMS. 2020 Sep 4;21(18):6466.

573. Yáñez-Mó M, Siljander PR -M., Andreu Z, Bedina Zavec A, Borràs FE, Buzas EI, et al. Biological properties of extracellular vesicles and their physiological functions. J of Extracellular Vesicle. 2015 Jan;4(1):27066.

574. Welsh JA, Goberdhan DCI, O'Driscoll L, Buzas EI, Blenkiron C, Bussolati B, et al. Minimal information for studies of extracellular vesicles (MISEV2023): From basic to advanced approaches. J of Extracellular Vesicle. 2024 Feb;13(2):e12404.

575. Carney RP, Mizenko RR, Bozkurt BT, Lowe N, Henson T, Arizzi A, et al. Harnessing extracellular vesicle heterogeneity for diagnostic and therapeutic applications. Nat Nanotechnol [Internet]. 2024 Oct 28 [cited 2024 Dec 12]; Available from: https://www.nature.com/articles/s41565-024-01774-3

576. Lange S. Extracellular Vesicles in Phylogeny. Int J Mol Sci. 2023 Jun 21;24(13):10466.

577. Fais S, O'Driscoll L, Borras FE, Buzas E, Camussi G, Cappello F, et al. Evidence-Based Clinical Use of Nanoscale Extracellular Vesicles in Nanomedicine. ACS Nano. 2016 Apr 26;10(4):3886–99.

578. van Niel G, Porto-Carreiro I, Simoes S, Raposo G. Exosomes: a common pathway for a specialized function. J Biochem. 2006 Jul;140(1):13–21.

579. Kim YB, Lee GB, Moon MH. Size Separation of Exosomes and Microvesicles Using Flow Field-Flow Fractionation/Multiangle Light Scattering and Lipidomic Comparison. Anal Chem. 2022 Jun 28;94(25):8958–65.

580. Kim K, Park J, Jung JH, Lee R, Park JH, Yuk JM, et al. Cyclic tangential flow filtration system for isolation of extracellular vesicles. APL Bioeng. 2021 Mar;5(1):016103.

581. Watson DC, Yung BC, Bergamaschi C, Chowdhury B, Bear J, Stellas D, et al. Scalable, cGMP-compatible purification of extracellular vesicles carrying bioactive human heterodimeric IL-15/lactadherin complexes. J Extracell Vesicles. 2018;7(1):1442088.

582. Vergauwen G, Dhondt B, Van Deun J, De Smedt E, Berx G, Timmerman E, et al. Confounding factors of ultrafiltration and protein analysis in extracellular vesicle research. Sci Rep. 2017 Jun 2;7(1):2704.

583. Boeckle S, von Gersdorff K, van der Piepen S, Culmsee C, Wagner E, Ogris M. Purification of polyethylenimine polyplexes highlights the role of free polycations in gene transfer. J Gene Med. 2004 Oct;6(10):1102–11.

584. Ketola TM, Hanzlikova M, Urtti A, Lemmetyinen H, Yliperttula M, Vuorimaa E. Role of Polyplex Intermediate Species on Gene Transfer Efficiency: Polyethylenimine-DNA Complexes and Time-Resolved Fluorescence Spectroscopy. Journal of Physical Chemistry Part B. 2011;115(8):1895–902.

585. Modrego A, Amaranto M, Godino A, Mendoza R, Barra JL, Corchero JL. Human α-Galactosidase A Mutants: Priceless Tools to Develop Novel Therapies for Fabry Disease. International Journal of Molecular Sciences. 2021 Jan;22(12):6518.

586. Frank J, Richter M, De Rossi C, Lehr CM, Fuhrmann K, Fuhrmann G. Extracellular vesicles protect glucuronidase model enzymes during freeze-drying. Sci Rep. 2018 Aug 17;8(1):12377.

587. Bajgelman MC, Costanzi-Strauss E, Strauss BE. Exploration of critical parameters for transient retrovirus production. Journal of Biotechnology. 2003 Jun;103(2):97–106.

588. Li Z, Zhou X, Gao X, Bai D, Dong Y, Sun W, et al. Fusion protein engineered exosomes for targeted degradation of specific RNAs in lysosomes: a proof-of-concept study. J of Extracellular Vesicle. 2020 Sep;9(1):1816710.

589. Cao Y, Ao T, Wang X, Wei W, Fan J, Tian X. CD300a and CD300f molecules regulate the function of leukocytes. Int Immunopharmacol. 2021 Apr;93:107373.

590. Andrews JM, Newbound GC, Lairmore MD. Transcriptional modulation of viral reporter gene constructs following induction of the cellular stress response. Nucleic Acids Res. 1997 Mar 1;25(5):1082–4.

591. Benedikter BJ, Bouwman FG, Vajen T, Heinzmann ACA, Grauls G, Mariman EC, et al. Ultrafiltration combined with size exclusion chromatography efficiently isolates extracellular vesicles from cell culture media for compositional and functional studies. Sci Rep. 2017 Nov 10;7(1):15297.

592. Zhao S, Xiu G, Wang J, Wen Y, Lu J, Wu B, et al. Engineering exosomes derived from subcutaneous fat MSCs specially promote cartilage repair as miR-199a-3p delivery vehicles in Osteoarthritis. J Nanobiotechnol. 2023 Sep 22;21(1):341.

593. Chen F, Cen H, Mao D, Feng R. Placental homing peptide guides HIF1α-silenced exosomes conjugates for targeted enhancement of invasion of trophoblast cells. Mol Med Rep. 2023 May 24;28(1):135.

594. Ibane Abasolo, Diana Rafael, Águeda Martínez-Barriocanal, Marc Moltó-Abad, Vincenzo Montanarella, Júlia German Cortés, et al. CD300f derived F7 peptide: a powerful tool to facilitate drug delivery systems to cross biological barriers. In: CD300f derived F7 peptide: a powerful tool to facilitate drug delivery systems to cross biological barriers [Internet]. Barcelona; 2024. Available from: https://premc.org/conferences/iconan-nanomedicine-nanobiotechnology/

595. Costa Verdera H, Gitz-Francois JJ, Schiffelers RM, Vader P. Cellular uptake of extracellular vesicles is mediated by clathrin-independent endocytosis and macropinocytosis. Journal of Controlled Release. 2017 Nov;266:100–8.

596. Tu C, Du Z, Zhang H, Feng Y, Qi Y, Zheng Y, et al. Endocytic pathway inhibition attenuates extracellular vesicle-induced reduction of chemosensitivity to bortezomib in multiple myeloma cells. Theranostics. 2021;11(5):2364–80.

597. Rappaport J, Manthe RL, Solomon M, Garnacho C, Muro S. A Comparative Study on the Alterations of Endocytic Pathways in Multiple Lysosomal Storage Disorders. Mol Pharm. 2016 Feb 1;13(2):357–68.

598. Rossowska J, Anger N, Wegierek K, Szczygieł A, Mierzejewska J, Milczarek M, et al. Antitumor Potential of Extracellular Vesicles Released by Genetically Modified Murine Colon Carcinoma Cells With Overexpression of Interleukin-12 and shRNA for TGF-β1. Front Immunol. 2019;10:211.

599. Salazar-Puerta AI, Rincon-Benavides MA, Cuellar-Gaviria TZ, Aldana J, Vasquez Martinez G, Ortega-Pineda L, et al. Engineered Extracellular Vesicles Derived from Dermal Fibroblasts Attenuate Inflammation in a Murine Model of Acute Lung Injury. Advanced Materials. 2023;35(28):2210579.

600. Tang TT, Wang B, Wu M, Li ZL, Feng Y, Cao JY, et al. Extracellular vesicle-encapsulated IL-10 as novel nanotherapeutics against ischemic AKI. Sci Adv. 2020 Aug;6(33):eaaz0748.

601. Chen L, Wang Y, Li S, Zuo B, Zhang X, Wang F, et al. Exosomes derived from GDNF-modified human adipose mesenchymal stem cells ameliorate peritubular capillary loss in tubulointerstitial fibrosis by activating the SIRT1/eNOS signaling pathway. Theranostics. 2020;10(20):9425–42.

602. Zhou X, Deng X, Liu M, He M, Long W, Xu Z, et al. Intranasal delivery of BDNF-loaded small extracellular vesicles for cerebral ischemia therapy. Journal of Controlled Release. 2023 May 1;357:1–19.

603. Zhao Z, Shuang T, Gao Y, Lu F, Zhang J, He W, et al. Targeted delivery of exosomal miR-484 reprograms tumor vasculature for chemotherapy sensitization. Cancer Lett. 2022 Apr 1;530:45–58.

604. Ren X, Zhao Y, Xue F, Zheng Y, Huang H, Wang W, et al. Exosomal DNA Aptamer Targeting α-Synuclein Aggregates Reduced Neuropathological Deficits in a Mouse Parkinson's Disease Model. Mol Ther Nucleic Acids. 2019 Sep 6;17:726–40.

605. Yang J, Wu S, Hou L, Zhu D, Yin S, Yang G, et al. Therapeutic Effects of Simultaneous Delivery of Nerve Growth Factor mRNA and Protein via Exosomes on Cerebral Ischemia. Mol Ther Nucleic Acids. 2020 Sep 4;21:512–22.

606. Hao S, Bai O, Li F, Yuan J, Laferte S, Xiang J. Mature dendritic cells pulsed with exosomes stimulate efficient cytotoxic T-lymphocyte responses and antitumour immunity. Immunology. 2007 Jan;120(1):90–102.

607. Xu X, Liang Y, Li X, Ouyang K, Wang M, Cao T, et al. Exosome-mediated delivery of kartogenin for chondrogenesis of synovial fluid-derived mesenchymal stem cells and cartilage regeneration. Biomaterials. 2021 Feb;269:120539.

608. Muro S. New biotechnological and nanomedicine strategies for treatment of lysosomal storage disorders. Wiley Interdiscip Rev Nanomed Nanobiotechnol. 2010;2(2):189–204.

609. Hsu J, Serrano D, Bhowmick T, Kumar K, Shen Y, Kuo YC, et al. Enhanced endothelial delivery and biochemical effects of α-galactosidase by ICAM-1-targeted nanocarriers for Fabry disease. J Control Release. 2011 Feb 10;149(3):323–31.

610. Hsu J, Northrup L, Bhowmick T, Muro S. Enhanced delivery of α-glucosidase for Pompe disease by ICAM-1-targeted nanocarriers: comparative performance of a strategy for three distinct lysosomal storage disorders. Nanomedicine. 2012 Jul;8(5):731–9.

611. Rappaport J, Manthe RL, Garnacho C, Muro S. Altered Clathrin-Independent Endocytosis in Type A Niemann-Pick Disease Cells and Rescue by ICAM-1-Targeted Enzyme Delivery. Mol Pharm. 2015 May 4;12(5):1366–76.

612. Manthe RL, Loeck M, Bhowmick T, Solomon M, Muro S. Intertwined mechanisms define transport of anti-ICAM nanocarriers across the endothelium and brain delivery of a therapeutic enzyme. J Control Release. 2020 Aug 10;324:181–93.

613. Tancini B, Tosi G, Bortot B, Dolcetta D, Magini A, De Martino E, et al. Use of Polylactide-Co-Glycolide-Nanoparticles for Lysosomal Delivery of a Therapeutic Enzyme in Glycogenosis Type II Fibroblasts. J Nanosci Nanotechnol. 2015 Apr;15(4):2657–66.

614. Salvalaio M, Rigon L, Belletti D, D'Avanzo F, Pederzoli F, Ruozi B, et al. Targeted Polymeric Nanoparticles for Brain Delivery of High Molecular Weight Molecules in Lysosomal Storage Disorders. PLoS One. 2016 May 26;11(5):e0156452.

615. Haney MJ, Klyachko NL, Harrison EB, Zhao Y, Kabanov AV, Batrakova EV. TPP1 Delivery to Lysosomes with Extracellular Vesicles and their Enhanced Brain Distribution in the Animal Model of Batten Disease. Adv Healthc Mater. 2019 Jun;8(11):1801271.

616. Spada M, Pagliardini V, Ricci F, Biamino E, Mongini T, Porta F. Early higher dosage of alglucosidase alpha in classic Pompe disease. J Pediatr Endocrinol Metab. 2018 Dec 19;31(12):1343–7.

617. Bonam SR, Wang F, Muller S. Lysosomes as a therapeutic target. Nat Rev Drug Discov. 2019 Dec;18(12):923–48.

618. Willenborg M, Schmidt CK, Braun P, Landgrebe J, von Figura K, Saftig P, et al. Mannose 6-phosphate receptors, Niemann-Pick C2 protein, and lysosomal cholesterol accumulation. J Lipid Res. 2005 Dec;46(12):2559–69.

619. Funk B, Kessler U, Eisenmenger W, Hansmann A, Kolb HJ, Kiess W. Expression of the insulin-like growth factor-II/mannose-6-phosphate receptor in multiple human tissues during fetal life and early infancy. J Clin Endocrinol Metab. 1992 Aug;75(2):424–31.

620. Martin-Kleiner I, Gall Troselj K. Mannose-6-phosphate/insulin-like growth factor 2 receptor (M6P/IGF2R) in carcinogenesis. Cancer Lett. 2010 Mar 1;289(1):11–22.

621. Song G, Wu H, Yoshino K, Zamboni WC. Factors affecting the pharmacokinetics and pharmacodynamics of liposomal drugs. J Liposome Res. 2012 Sep;22(3):177–92.

622. Aimaletdinov AM, Gomzikova MO. Tracking of Extracellular Vesicles' Biodistribution: New Methods and Approaches. Int J Mol Sci. 2022 Sep 25;23(19):11312.

623. Gupta D, Wiklander OPB, Wood MJA, El-Andaloussi S. Biodistribution of therapeutic extracellular vesicles. Extracell Vesicles Circ Nucl Acids. 2023;4(2):170–90.

624. Panico S, Capolla S, Bozzer S, Toffoli G, Dal Bo M, Macor P. Biological Features of Nanoparticles: Protein Corona Formation and Interaction with the Immune System. Pharmaceutics. 2022 Nov 26;14(12):2605.

625. Li H, Yin D, Liao J, Wang Y, Gou R, Tang C, et al. Regulation of protein corona on liposomes using albumin-binding peptide for targeted tumor therapy. Journal of Controlled Release. 2023 Mar 1;355:593–603.

626. Zheng H, Guan S, Wang X, Zhao J, Gao M, Zhang X. Deconstruction of Heterogeneity of Size-Dependent Exosome Subpopulations from Human Urine by Profiling N-Glycoproteomics and Phosphoproteomics Simultaneously. Anal Chem. 2020 Jul 7;92(13):9239–46.

627. Haraszti RA, Didiot MC, Sapp E, Leszyk J, Shaffer SA, Rockwell HE, et al. High-resolution proteomic and lipidomic analysis of exosomes and microvesicles from different cell sources. J Extracell Vesicles. 2016;5:32570.

628. Yang H, Ma Q, Wang Y, Tang Z. Clinical application of exosomes and circulating microRNAs in the diagnosis of pregnancy complications and foetal abnormalities. J Transl Med. 2020 Jan 22;18(1):32.

629. Arrighetti N, Corbo C, Evangelopoulos M, Pastò A, Zuco V, Tasciotti E. Exosome-like Nanovectors for Drug Delivery in Cancer. Curr Med Chem. 2019;26(33):6132–48.

630. Kim Y, Mok H. Citraconylated exosomes for improved internalization into macrophages. Applied Biological Chemistry. 2019 May 2;62(1):26.

631. Tóth EÁ, Turiák L, Visnovitz T, Cserép C, Mázló A, Sódar BW, et al. Formation of a protein corona on the surface of extracellular vesicles in blood plasma. J Extracell Vesicles. 2021 Sep;10(11):e12140.

632. Shimizu A, Sawada K, Kobayashi M, Yamamoto M, Yagi T, Kinose Y, et al. Exosomal CD47 Plays an Essential Role in Immune Evasion in Ovarian Cancer. Mol Cancer Res. 2021 Sep;19(9):1583–95.

633. Liu Q, Li D, Pan X, Liang Y. Targeted therapy using engineered extracellular vesicles: principles and strategies for membrane modification. Journal of Nanobiotechnology. 2023 Sep 16;21(1):334.

634. Gatto MS, Johnson MP, Najahi-Missaoui W. Targeted Liposomal Drug Delivery: Overview of the Current Applications and Challenges. Life. 2024 Jun;14(6):672.

635. Marques AC, Costa PJ, Velho S, Amaral MH. Functionalizing nanoparticles with cancer-targeting antibodies: A comparison of strategies. J Control Release. 2020 Apr 10;320:180–200.

636. Cho H, Huh KM, Shim MS, Cho YY, Lee JY, Lee HS, et al. Beyond Nanoparticle-Based Intracellular Drug Delivery: Cytosol/Organelle-Targeted Drug Release and Therapeutic Synergism. Macromol Biosci. 2024 Jul;24(7):e2300590.

637. Sanna V, Sechi M. Therapeutic Potential of Targeted Nanoparticles and Perspective on Nanotherapies. ACS Med Chem Lett. 2020 Jun 11;11(6):1069–73.

638. Pearce AK, O'Reilly RK. Insights into Active Targeting of Nanoparticles in Drug Delivery: Advances in Clinical Studies and Design Considerations for Cancer Nanomedicine. Bioconjugate Chem. 2019 Sep 18;30(9):2300–11.

639. Elbayoumi TA, Torchilin VP. Tumor-specific anti-nucleosome antibody improves therapeutic efficacy of doxorubicin-loaded long-circulating liposomes against primary and metastatic tumor in mice. Mol Pharm. 2009;6(1):246–54.

640. Steichen SD, Caldorera-Moore M, Peppas NA. A review of current nanoparticle and targeting moieties for the delivery of cancer therapeutics. Eur J Pharm Sci. 2013 Feb 14;48(3):416–27.

641. Ohradanova-Repic A, Nogueira E, Hartl I, Gomes AC, Preto A, Steinhuber E, et al. Fab antibody fragment-functionalized liposomes for specific targeting of antigen-positive cells. Nanomedicine. 2018 Jan;14(1):123–30.

642. Moase EH, Qi W, Ishida T, Gabos Z, Longenecker BM, Zimmermann GL, et al. Anti-MUC-1 immunoliposomal doxorubicin in the treatment of murine models of metastatic breast cancer. Biochim Biophys Acta. 2001 Feb 9;1510(1–2):43–55.

643. Laginha KM, Verwoert S, Charrois GJR, Allen TM. Determination of doxorubicin levels in whole tumor and tumor nuclei in murine breast cancer tumors. Clin Cancer Res. 2005 Oct 1;11(19 Pt 1):6944–9.

644. Micklus M, Greig N, Rapoport S. Targeting of liposomes to the blood-brain barrier [Internet]. US20020025313A1, 2002 [cited 2025 Feb 22]. Available from: https://patents.google.com/patent/US20020025313A1/en

645. Drummond DC, KAMOUN W. Treating ephrin receptor a2 (epha2) positive cancer with targeted docetaxel-generating nano-liposome compositions [Internet]. WO2017161071A1, 2017 [cited 2025 Feb 22]. Available from: https://patents.google.com/patent/WO2017161071A1/en?oq=US2017022629W

646. Tie Y, Zheng H, He Z, Yang J, Shao B, Liu L, et al. Targeting folate receptor β positive tumor-associated macrophages in lung cancer with a folate-modified liposomal complex. Signal Transduct Target Ther. 2020 Jan 22;5(1):6.

647. Moghimipour E, Handali S. Functionalized liposomes as a potential drug delivery systems for colon cancer treatment: A systematic review. Int J Biol Macromol. 2024 Jun;269(Pt 1):132023.

648. Choi SW, Mason JB. Folate and carcinogenesis: an integrated scheme. J Nutr. 2000 Feb;130(2):129–32.

649. Kelemen LE. The role of folate receptor alpha in cancer development, progression and treatment: cause, consequence or innocent bystander? Int J Cancer. 2006 Jul 15;119(2):243–50.

650. Kabilova TO, Shmendel EV, Gladkikh DV, Chernolovskaya EL, Markov OV, Morozova NG, et al. Targeted delivery of nucleic acids into xenograft tumors mediated by novel folate-equipped liposomes. Eur J Pharm Biopharm. 2018 Feb;123:59–70.

651. Patil Y, Amitay Y, Ohana P, Shmeeda H, Gabizon A. Targeting of pegylated liposomal mitomycin-C prodrug to the folate receptor of cancer cells: Intracellular activation and enhanced cytotoxicity. J Control Release. 2016 Mar 10;225:87–95.

652. Wang L, Evans JC, Ahmed L, Allen C. Folate receptor targeted nanoparticles containing niraparib and doxorubicin as a potential candidate for the treatment of high grade serous ovarian cancer. Sci Rep. 2023 Feb 24;13(1):3226.

653. Xia W, Low PS. Folate-targeted therapies for cancer. J Med Chem. 2010 Oct 14;53(19):6811–24.

654. Gabizon A, Horowitz AT, Goren D, Tzemach D, Shmeeda H, Zalipsky S. In vivo fate of folate-targeted polyethylene-glycol liposomes in tumor-bearing mice. Clin Cancer Res. 2003 Dec 15;9(17):6551–9.

655. Leamon CP, Cooper SR, Hardee GE. Folate-liposome-mediated antisense oligodeoxynucleotide targeting to cancer cells: evaluation in vitro and in vivo. Bioconjug Chem. 2003;14(4):738–47.

656. Tombelli S, Minunni M, Mascini M. Analytical applications of aptamers. Biosens Bioelectron. 2005 Jun 15;20(12):2424–34.

657. Keefe AD, Pai S, Ellington A. Aptamers as therapeutics. Nat Rev Drug Discov. 2010 Jul;9(7):537–50.

658. Mashreghi M, Zamani P, Karimi M, Mehrabian A, Arabsalmani M, Zarqi J, et al. Anti-epithelial cell adhesion molecule RNA aptamer-conjugated liposomal doxorubicin as an efficient targeted therapy in mice bearing colon carcinoma tumor model. Biotechnol Prog. 2021 May;37(3):e3116.

659. Shakib Z, Mahmoudi A, Moosavian SA, Malaekeh-Nikouei B. PEGylated solid lipid nanoparticles functionalized by aptamer for targeted delivery of docetaxel in mice bearing C26 tumor. Drug Dev Ind Pharm. 2022 Feb;48(2):69–78.

660. Kim M, Lee JS, Kim W, Lee JH, Jun BH, Kim KS, et al. Aptamer-conjugated nano-liposome for immunogenic chemotherapy with reversal of immunosuppression. J Control Release. 2022 Aug;348:893–910.

661. Ding Z, Wang D, Shi W, Yang X, Duan S, Mo F, et al. In vivo Targeting of Liver Cancer with Tissue- and Nuclei-Specific Mesoporous Silica Nanoparticle-Based Nanocarriers in mice. Int J Nanomedicine. 2020;15:8383–400.

662. Wong KY, Liu Y, Zhou L, Wong MS, Liu J. Mucin-targeting-aptamer functionalized liposomes for delivery of cyclosporin A for dry eye diseases. J Mater Chem B. 2023 May 31;11(21):4684–94.

663. Sun S, Liu H, Hu Y, Wang Y, Zhao M, Yuan Y, et al. Selection and identification of a novel ssDNA aptamer targeting human skeletal muscle. Bioact Mater. 2023 Feb;20:166–78.

664. He Y, Huang Y, Xu H, Yang X, Liu N, Xu Y, et al. Aptamer-modified M cell targeting liposomes for oral delivery of macromolecules. Colloids Surf B Biointerfaces. 2023 Feb;222:113109.

665. Mahmoudian F, Ahmari A, Shabani S, Sadeghi B, Fahimirad S, Fattahi F. Aptamers as an approach to targeted cancer therapy. Cancer Cell International. 2024 Mar 16;24(1):108.

666. Khan MSA, Park J, Lee S, Hwang JE, Oh C, Kim M, et al. Aptamer-conjugated liposome system for targeting MUC1-positive cancer: an in silico screening approach. Health Nanotechnology. 2025 Jan 28;1(1):2.

667. Baig MH, Ahmad K, Saeed M, Alharbi AM, Barreto GE, Ashraf GM, et al. Peptide based therapeutics and their use for the treatment of neurodegenerative and other diseases. Biomed Pharmacother. 2018 Jul;103:574–81.

668. Meers PR, Pak C, Ali S, Janoff A, Franklin JC, Erukulla RK, et al. Peptide-lipid conjugates, liposomes and lipsomal drug delivery [Internet]. US6339069B1, 2002 [cited 2025 Feb 22]. Available from: https://patents.google.com/patent/US6339069B1/en?oq=US6339069B1

669. Kim IS, Lee BH, Lu MJM, Liang HF, Ko YJ, Lo YC, et al. Target-aiming drug delivery system for diagnosis and treatment of cancer containing liposome labeled with peptides which specifically targets interleukin-4 receptors, and manufacturing method thereof [Internet]. US9833464B2, 2017 [cited 2025 Feb 22]. Available from: https://patents.google.com/patent/US9833464B2/en?oq=US9833464B2

670. Kato N, Sato T, Fuchigami Y, Suga T, Geng L, Tsurumaru M, et al. Synthesis and evaluation of a novel adapter lipid derivative for preparation of cyclic peptide-modified PEGylated liposomes: Application of cyclic RGD peptide. Eur J Pharm Sci. 2022 Sep 1;176:106239.

671. Sonju JJ, Dahal A, Jois SD. Liposome Nanocarriers for Peptide Drug Delivery. In: Jois SD, editor. Peptide Therapeutics: Fundamentals of Design, Development, and Delivery [Internet]. Cham: Springer International Publishing; 2022 [cited 2025 Apr 16]. p. 203–35. Available from: https://doi.org/10.1007/978-3-031-04544-8_6

672. Wang S, Chen Y, Guo J, Huang Q. Liposomes for Tumor Targeted Therapy: A Review. Int J Mol Sci. 2023 Jan 31;24(3):2643.

673. Davoodi Z, Shafiee F. Internalizing RGD, a great motif for targeted peptide and protein delivery: a review article. Drug Deliv Transl Res. 2022 Oct;12(10):2261–74.

674. Arzani H, Rafii-Tabar H, Ramezani F. The investigation into the effect of the length of RGD peptides and temperature on the interaction with the αIIbβ3 integrin: a molecular dynamic study. J Biomol Struct Dyn. 2022;40(20):9701–12.

675. Lindemann WR, Mijalis AJ, Alonso JL, Borbat PP, Freed JH, Arnaout MA, et al. Conformational Dynamics in Extended RGD-Containing Peptides. Biomacromolecules. 2020 Jul 13;21(7):2786–94.

676. Del Gatto A, De Simone M, de Paola I, Saviano M, Zaccaro L. Investigation of the Best Conditions to Obtain c(RGDfK) Peptide on Solid Phase. Int J Pept Res Ther. 2011 Mar 1;17(1):39–45.

677. Partridge AW, Kaan HYK, Juang YC, Sadruddin A, Lim S, Brown CJ, et al. Incorporation of Putative Helix-Breaking Amino Acids in the Design of Novel Stapled Peptides: Exploring Biophysical and Cellular Permeability Properties. Molecules. 2019 Jun 20;24(12):2292.

678. Pollmann S, Scharnetzki D, Manikowski D, Lenders M, Brand E. Endothelial Dysfunction in Fabry Disease Is Related to Glycocalyx Degradation. Front Immunol. 2021;12:789142.

679. Stamerra CA, Del Pinto R, di Giosia P, Ferri C, Sahebkar A. Anderson–Fabry Disease: From Endothelial Dysfunction to Emerging Therapies. Adv Pharmacol Pharm Sci. 2021 May 13;2021:5548445.

680. Wang F, Chen L, Zhang R, Chen Z, Zhu L. RGD peptide conjugated liposomal drug delivery system for enhance therapeutic efficacy in treating bone metastasis from prostate cancer. J Control Release. 2014 Dec 28;196:222–33.

681. Vakhshiteh F, Khabazian E, Atyabi F, Ostad SN, Madjd Z, Dinarvand R. Peptide-conjugated liposomes for targeted miR-34a delivery to suppress breast cancer and cancer stem-like population. Journal of Drug Delivery Science and Technology. 2020 Jun 1;57:101687.

682. Belfiore L, Saunders DN, Ranson M, Thurecht KJ, Storm G, Vine KL. Towards clinical translation of ligand-functionalized liposomes in targeted cancer therapy: Challenges and opportunities. J Control Release. 2018 May 10;277:1–13.

683. Juliano RL, Stamp D. The effect of particle size and charge on the clearance rates of liposomes and liposome encapsulated drugs. Biochem Biophys Res Commun. 1975 Apr 7;63(3):651–8.

684. Ge L, You X, Huang K, Kang Y, Chen Y, Zhu Y, et al. Screening of novel RGD peptides to modify nanoparticles for targeted cancer therapy. Biomater Sci. 2017 Dec 19;6(1):125–35.

685. Iwasaki T, Tokuda Y, Kotake A, Okada H, Takeda S, Kawano T, et al. Cellular uptake and in vivo distribution of polyhistidine peptides. J Control Release. 2015 Jul 28;210:115–24.

686. Kumar MA, Baba SK, Sadida HQ, Marzooqi SA, Jerobin J, Altemani FH, et al. Extracellular vesicles as tools and targets in therapy for diseases. Sig Transduct Target Ther. 2024 Feb 5;9(1):1–41.

687. Zhao S, Di Y, Fan H, Xu C, Li H, Wang Y, et al. Targeted delivery of extracellular vesicles: the mechanisms, techniques and therapeutic applications. Mol Biomed. 2024 Nov 21;5(1):60.

688. Choi W, Park DJ, Eliceiri BP. Defining tropism and activity of natural and engineered extracellular vesicles. Front Immunol. 2024 Apr 10;15:1363185.

689. Wiklander OPB, Nordin JZ, O'Loughlin A, Gustafsson Y, Corso G, Mäger I, et al. Extracellular vesicle in vivo biodistribution is determined by cell source, route of administration and targeting. J Extracell Vesicles. 2015;4:26316.

690. Tian T, Zhang HX, He CP, Fan S, Zhu YL, Qi C, et al. Surface functionalized exosomes as targeted drug delivery vehicles for cerebral ischemia therapy. Biomaterials. 2018 Jan;150:137–49.

691. Zhang H, Wu J, Wu J, Fan Q, Zhou J, Wu J, et al. Exosome-mediated targeted delivery of miR-210 for angiogenic therapy after cerebral ischemia in mice. J Nanobiotechnology. 2019 Feb 19;17(1):29.

692. Wang J, Li W, Lu Z, Zhang L, Hu Y, Li Q, et al. The use of RGD-engineered exosomes for enhanced targeting ability and synergistic therapy toward angiogenesis. Nanoscale. 2017 Oct 19;9(40):15598–605.

693. Kim MS, Haney MJ, Zhao Y, Yuan D, Deygen I, Klyachko NL, et al. Engineering macrophage-derived exosomes for targeted paclitaxel delivery to pulmonary metastases: in vitro and in vivo evaluations. Nanomedicine. 2018 Jan;14(1):195–204.

694. Liang SF, Zuo FF, Yin BC, Ye BC. Delivery of siRNA based on engineered exosomes for glioblastoma therapy by targeting STAT3. Biomater Sci. 2022 Mar 15;10(6):1582–90.

695. Cui G hong, Guo H dong, Li H, Zhai Y, Gong Z bin, Wu J, et al. RVG-modified exosomes derived from mesenchymal stem cells rescue memory deficits by regulating inflammatory responses in a mouse model of Alzheimer's disease. Immun Ageing. 2019 May 13;16:10.

696. Pi F, Binzel DW, Lee TJ, Li Z, Sun M, Rychahou P, et al. Nanoparticle orientation to control RNA loading and ligand display on extracellular vesicles for cancer regression. Nat Nanotechnol. 2018 Jan;13(1):82–9.

697. Wang Y, Chen X, Tian B, Liu J, Yang L, Zeng L, et al. Nucleolin-targeted Extracellular Vesicles as a Versatile Platform for Biologics Delivery to Breast Cancer. Theranostics. 2017;7(5):1360–72.

698. Wan Y, Wang L, Zhu C, Zheng Q, Wang G, Tong J, et al. Aptamer-Conjugated Extracellular Nanovesicles for Targeted Drug Delivery. Cancer Res. 2018 Feb 1;78(3):798–808.

699. Kojima R, Bojar D, Rizzi G, Hamri GCE, El-Baba MD, Saxena P, et al. Designer exosomes produced by implanted cells intracerebrally deliver therapeutic cargo for Parkinson's disease treatment. Nat Commun. 2018 Apr 3;9(1):1305.

700. Kim M, Kim G, Hwang DW, Lee M. Delivery of High Mobility Group Box-1 siRNA Using Brain-Targeting Exosomes for Ischemic Stroke Therapy. J Biomed Nanotechnol. 2019 Dec 1;15(12):2401–12.

701. Liu Y, Li D, Liu Z, Zhou Y, Chu D, Li X, et al. Targeted exosome-mediated delivery of opioid receptor Mu siRNA for the treatment of morphine relapse. Sci Rep. 2015 Dec 3;5:17543.

702. Yang J, Zhang X, Chen X, Wang L, Yang G. Exosome Mediated Delivery of miR-124 Promotes Neurogenesis after Ischemia. Mol Ther Nucleic Acids. 2017 Jun 16;7:278–87.

703. Yu X, Bai Y, Han B, Ju M, Tang T, Shen L, et al. Extracellular vesicle-mediated delivery of circDYM alleviates CUS-induced depressive-like behaviours. J Extracell Vesicles. 2022 Jan;11(1):e12185.

704. Yang L, Han B, Zhang Z, Wang S, Bai Y, Zhang Y, et al. Extracellular Vesicle-Mediated Delivery of Circular RNA SCMH1 Promotes Functional Recovery in Rodent and Nonhuman Primate Ischemic Stroke Models. Circulation. 2020 Aug 11;142(6):556–74.

705. Bai J, Duan J, Liu R, Du Y, Luo Q, Cui Y, et al. Engineered targeting tLyp-1 exosomes as gene therapy vectors for efficient delivery of siRNA into lung cancer cells. Asian J Pharm Sci. 2020 Jul;15(4):461–71.

706. Li X, Yu Q, Zhao R, Guo X, Liu C, Zhang K, et al. Designer Exosomes for Targeted Delivery of a Novel Therapeutic Cargo to Enhance Sorafenib-Mediated Ferroptosis in Hepatocellular Carcinoma. Front Oncol. 2022;12:898156.

707. Liang Y, Xu X, Li X, Xiong J, Li B, Duan L, et al. Chondrocyte-Targeted MicroRNA Delivery by Engineered Exosomes toward a Cell-Free Osteoarthritis Therapy. ACS Appl Mater Interfaces. 2020 Aug 19;12(33):36938–47.

708. Kim G, Kim M, Lee Y, Byun JW, Hwang DW, Lee M. Systemic delivery of microRNA-21 antisense oligonucleotides to the brain using T7-peptide decorated exosomes. J Control Release. 2020 Jan 10;317:273–81.

709. Gečys D, Kazlauskas A, Gečytė E, Paužienė N, Kulakauskienė D, Lukminaitė I, et al. Internalisation of RGD-Engineered Extracellular Vesicles by Glioblastoma Cells. Biology (Basel). 2022 Oct 10;11(10):1483.

710. Liang G, Kan S, Zhu Y, Feng S, Feng W, Gao S. Engineered exosome-mediated delivery of functionally active miR-26a and its enhanced suppression effect in HepG2 cells. Int J Nanomedicine. 2018;13:585–99.

711. Liang G, Zhu Y, Ali DJ, Tian T, Xu H, Si K, et al. Engineered exosomes for targeted co-delivery of miR-21 inhibitor and chemotherapeutics to reverse drug resistance in colon cancer. J Nanobiotechnology. 2020 Jan 9;18(1):10.

712. Choi H, Choi K, Kim DH, Oh BK, Yim H, Jo S, et al. Strategies for Targeted Delivery of Exosomes to the Brain: Advantages and Challenges. Pharmaceutics. 2022 Mar 18;14(3):672.

713. Lewis ND, Sia CL, Kirwin K, Haupt S, Mahimkar G, Zi T, et al. Exosome Surface Display of IL12 Results in Tumor-Retained Pharmacology with Superior Potency and Limited Systemic Exposure Compared with Recombinant IL12. Mol Cancer Ther. 2021 Mar;20(3):523–34.

714. Cheng Q, Shi X, Han M, Smbatyan G, Lenz HJ, Zhang Y. Reprogramming Exosomes as Nanoscale Controllers of Cellular Immunity. J Am Chem Soc. 2018 Dec 5;140(48):16413–7.

715. Ho M, Nagata S, Pastan I. Isolation of anti-CD22 Fv with high affinity by Fv display on human cells. Proc Natl Acad Sci U S A. 2006 Jun 20;103(25):9637–42.

716. Cheng Q, Dai Z, Smbatyan G, Epstein AL, Lenz HJ, Zhang Y. Eliciting anti-cancer immunity by genetically engineered multifunctional exosomes. Mol Ther. 2022 Sep 7;30(9):3066–77.

717. Liu M, Hu Y, Chen G. The Antitumor Effect of Gene-Engineered Exosomes in the Treatment of Brain Metastasis of Breast Cancer. Front Oncol. 2020;10:1453.

718. Welsh JA, Arkesteijn GJA, Bremer M, Cimorelli M, Dignat-George F, Giebel B, et al. A compendium of single extracellular vesicle flow cytometry. J Extracell Vesicles. 2023 Feb;12(2):e12299.

719. Breitwieser K, Koch LF, Tertel T, Proestler E, Burgers LD, Lipps C, et al. Detailed Characterization of Small Extracellular Vesicles from Different Cell Types Based on Tetraspanin Composition by ExoView R100 Platform. Int J Mol Sci. 2022 Aug 1;23(15):8544.

720. Chaize B, Colletier JP, Winterhalter M, Fournier D. Encapsulation of enzymes in liposomes: high encapsulation efficiency and control of substrate permeability. Artif Cells Blood Substit Immobil Biotechnol. 2004 Feb;32(1):67–75.

721. Galzigna L, Garbin L, Burlina A. Liposome-incorporated enzymes: Studies on amylase. Clinical Biochemistry. 1979 Dec 1;12(6):267–9.

722. Kumar M, Kulkarni P, Liu S, Chemuturi N, Shah DK. Nanoparticle biodistribution coefficients: A quantitative approach for understanding the tissue distribution of nanoparticles. Advanced Drug Delivery Reviews. 2023 Mar 1;194:114708.

723. Nik ME, Malaekeh-Nikouei B, Amin M, Hatamipour M, Teymouri M, Sadeghnia HR, et al. Liposomal formulation of Galbanic acid improved therapeutic efficacy of pegylated liposomal Doxorubicin in mouse colon carcinoma. Sci Rep. 2019 Jul 2;9(1):9527.

724. Ruan H, Chen X, Xie C, Li B, Ying M, Liu Y, et al. Stapled RGD Peptide Enables Glioma-Targeted Drug Delivery by Overcoming Multiple Barriers. ACS Appl Mater Interfaces. 2017 May 31;9(21):17745–56.

725. Li AJ, Zheng YH, Liu GD, Liu WS, Cao PC, Bu ZF. Efficient delivery of docetaxel for the treatment of brain tumors by cyclic RGD-tagged polymeric micelles. Molecular Medicine Reports. 2015 Apr 1;11(4):3078–86.

726. Sonali, Singh RP, Sharma G, Kumari L, Koch B, Singh S, et al. RGD-TPGS decorated theranostic liposomes for brain targeted delivery. Colloids and Surfaces B: Biointerfaces. 2016 Nov 1;147:129–41.

727. Sidhom K, Obi PO, Saleem A. A Review of Exosomal Isolation Methods: Is Size Exclusion Chromatography the Best Option? IJMS. 2020 Sep 4;21(18):6466.

728. Matei AC, Antounians L, Zani A. Extracellular Vesicles as a Potential Therapy for Neonatal Conditions: State of the Art and Challenges in Clinical Translation. Pharmaceutics. 2019 Aug 11;11(8):404.

729. Shao J, Zaro J, Shen Y. Advances in Exosome-Based Drug Delivery and Tumor Targeting: From Tissue Distribution to Intracellular Fate. Int J Nanomedicine. 2020;15:9355–71.

730. Anselmo AC, Mitragotri S. Nanoparticles in the clinic: An update post COVID-19 vaccines. Bioeng Transl Med. 2021 Sep;6(3):e10246.

731. Large DE, Abdelmessih RG, Fink EA, Auguste DT. Liposome composition in drug delivery design, synthesis, characterization, and clinical application. Adv Drug Deliv Rev. 2021 Sep;176:113851.

732. Al-Jipouri A, Almurisi SH, Al-Japairai K, Bakar LM, Doolaanea AA. Liposomes or Extracellular Vesicles: A Comprehensive Comparison of Both Lipid Bilayer Vesicles for Pulmonary Drug Delivery. Polymers. 2023 Jan 7;15(2):318.

733. Johnsen KB, Gudbergsson JM, Duroux M, Moos T, Andresen TL, Simonsen JB. On the use of liposome controls in studies investigating the clinical potential of extracellular vesicle-based drug delivery systems - A commentary. J Control Release. 2018 Jan 10;269:10–4.

734. Van Deun J, Mestdagh P, Agostinis P, Akay Ö, Anand S, Anckaert J, et al. EV-TRACK: transparent reporting and centralizing knowledge in extracellular vesicle research. Nat Methods. 2017 Mar;14(3):228–32.

735. Aguilar-Pérez KM, Avilés-Castrillo JI, Medina DI, Parra-Saldivar R, Iqbal HMN. Insight Into Nanoliposomes as Smart Nanocarriers for Greening the Twenty-First Century Biomedical Settings. Front Bioeng Biotechnol. 2020;8:579536.

736. Lu X, Fan S, Cao M, Liu D, Xuan K, Liu A. Extracellular vesicles as drug delivery systems in therapeutics: current strategies and future challenges. J Pharm Investig. 2024 Nov 1;54(6):785–802.

737. Pande S. Liposomes for drug delivery: review of vesicular composition, factors affecting drug release and drug loading in liposomes. Artif Cells Nanomed Biotechnol. 2023 Dec;51(1):428–40.

738. Benzalkonium chloride | European Medicines Agency (EMA) [Internet]. 2017 [cited 2025 Apr 15]. Available from: https://www.ema.europa.eu/en/benzalkonium-chloride

739. van der Koog L, Gandek TB, Nagelkerke A. Liposomes and Extracellular Vesicles as Drug Delivery Systems: A Comparison of Composition, Pharmacokinetics, and Functionalization. Adv Healthc Mater. 2022 Mar 2;11(5):2100639.

740. Kooijmans S a. A, Fliervoet L a. L, van der Meel R, Fens MH a. M, Heijnen HFG, van Bergen En Henegouwen PMP, et al. PEGylated and targeted extracellular vesicles display enhanced cell specificity and circulation time. J Control Release. 2016 Feb 28;224:77–85.

741. Rahiman N. Updates and current states on liposomal vehicles for tumor targeting: precision therapy in the spotlight. Cancer Nanotechnology. 2025 Mar 10;16(1):12.

742. Cheng Z, Huang H, Yin M, Liu H. Applications of liposomes and lipid nanoparticles in cancer therapy: current advances and prospects. Exp Hematol Oncol. 2025 Jan 31;14(1):11.

Annex